RELAXIN REGULATES SYSTEMIC HEMODYNAMICS AND ARTERIAL WALL MECHANICAL PROPERTIES

by

Dan Onwona Debrah

B.S., Bioengineering, University of Pittsburgh, 2004

Submitted to the Graduate Faculty of

Swanson School of Engineering in partial fulfillment

of the requirements for the degree of

Doctor of Philosophy

University of Pittsburgh

2008

UNIVERSITY OF PITTSBURGH

SWANSON SCHOOL OF ENGINEERING

This dissertation was presented

by

Dan Onwona Debrah

It was defended on

May 12, 2008

and approved by

Kirk P. Conrad, M.D.
Professor, Departments of Physiology, Functional Genomics, and Obstetrics Gynecology, University of Florida College of Medicine

Pamela A. Moalli, M.D., Ph.D.
Assistant Professor, Department of Obstetrics, Gynecology and Reproductive Sciences

Michael S. Sacks, Ph.D.
William Kepler Whiteford Professor, Department of Bioengineering

David A. Vorp, Ph.D.
Associate Professor, Departments of Surgery and Bioengineering

Dissertation Director: Sanjeev G. Shroff, Ph.D.
Professor and Gerald McGinnis Chair in Bioengineering; Department of Bioengineering

RELAXIN REGULATES SYSTEMIC HEMODYNAMICS AND ARTERIAL MECHANICAL PROPERTIES

Dan Onwona Debrah, Ph.D.

University of Pittsburgh, 2008

Relaxin is a peptide hormone emanating from the corpus luteum of the ovary which circulates during pregnancy. Although traditionally associated with female reproductive processes, recent evidence has suggested relaxin may play a vital role in regulating renal and cardiovascular function. Analogous to pregnancy, chronic administration of recombinant human relaxin (rhRLX) to nonpregnant female or male rats induces renal vasodilation and reduces the myogenic reactivity of small renal arteries (SRA). Additionally, elimination of circulating relaxin in pregnant rats with specific antibodies prevents the pregnancy associated changes in the renal circulation.

Based on these findings we postulated that relaxin exerts similar vasodilatory effects in the systemic circulation and examined its role in modulating systemic hemodynamics and vascular wall mechanical properties. Analogous to pregnancy, administration of rhRLX to nonpregnant female or male rats elicited increases in cardiac output and global arterial compliance, as well decreases in systemic vascular resistance. Additionally, neutralizing circulating relaxin in midpregnant rats eliminated the pregnancy associated changes in the systemic circulation.

In order to understand the mechanistic bases for the relaxin-induced increase in global arterial compliance, we examined the hormone's effects on vascular wall remodeling. From a geometric perspective, SRA isolated from rhRLX-treated rats and mice were characterized by larger wall area resulting from relaxin-mediated smooth muscle cell (SMC) hyperplasia, and not

hypertrophy. From a compositional perspective, these arteries were characterized by decreased collagen. Opposite results were obtained with removal of endogeneous relaxin: SRA from relaxin knock-out mice exhibited increased collagen content and decreased SMC density compared to wild-type mice. Finally, from a tissue mechanics perspective, SRA from rhRlx-treated mice exhibited strain-dependent reductions in tissue strain energy such that the greatest reduction was observed at the highest circumferential and axial strains.

We conclude that relaxin exerts systemic vasodilatory effects in both pregnant and nonpregnant states and in a gender-independent manner. Our findings indicate that the relaxin-induced increase in global arterial compliance is, at least in part, due to vascular wall compositional and geometric remodeling. Finally, our data indicate that the relaxin-induced compositional remodeling of SRA contributes to tissue mechanical properties under conditions of high circumferential and axial loads.

TABLE OF CONTENTS

LIST OF TABLES

LIST OF FIGURES

ACKNOWLEDGEMENTS

I would like to thank my co-advisors, Sanjeev Shroff and Kirk Conrad, for their unwavering support and guidance over the years. I believe that I have grown tremendously both on a professional and personal level over the last 6 years from observing and learning from how you both handle situations in and out of the lab. I have also learned a lot about the dedication and work ethic required to be a good scientist. I could not have asked for better teachers than the two of you and I will forever regard you both with the utmost respect and admiration. I would also like to express my gratitude to the rest of my committee: Michael Sacks, Pamela Moalli, and David Vorp, for their invaluable time and guidance over the years. Special thanks go to Michael Sacks for his help with the biaxial analysis portion of my dissertation.

I would like to express my sincerest admiration and appreciation to all of my lab mates in the Cardiovascular Systems Lab over the years: Caroline, Lauren, Jonathan, Steve, Yong, Andrej, Nick and Eric. It has been an honor and a tremendous pleasure to work with you over the years. I can say with an absolute certainty that I always looked forward to coming to work and spending time with you guys. Each of you, in your own way, holds a special place in my heart and you have all had a positive impact in my life in one way or another. I will forever be appreciative for everything each of you has done for me both on a professional level and on a personal level. I consider each of you as a dear friend. I would also like to thank all the high school and undergraduate students that have helped my throughout the years: Adam, Andrew, Brad, Janelle, Trent and Will.

I would like to thank the Magee Womens Research Institute for their support over the years. I would especially like to express my gratitude to Robin Gandley, Jackie Novak and JJ Ramirez for their help and guidance with the isolated artery work. Special thanks go to Jennifer Rohland for being a wonderful lab mate and an even better friend. My appreciation also goes to the Center for Biologic Imaging, with special thanks to Jason Devlin. My sincerest gratitude goes to Rachelle Prantil-Baun for her help with the Biochemical Assays. I would also like to thank Harvey Borovetz and all the faculty and staff of the Bioengineering Department for their help and support over the years.

I would also like to thank Robert Kormos, Steve Winowich all my co-workers at the Artificial Heart Program. It has been a joy to work with such a wonderful group of people and I have learned a great deal about compassion and selflessness from my experiences with the Artificial Heart Program.

I would like to acknowledge the sources of funding that allowed me to pursue and complete my doctorate: the Beckman Foundation, the McGinnis Chair Endowment, and the National Institutes of Health.

Finally, I would like to express my deepest gratitude to my family and wife. To my wonderful parents: thank you for showing me the true meaning of perseverance and for instilling in me the strong work ethic needed to succeed. I have learned a lot from watching you overcome many trials and tribulations over the years and I believe I am a stronger person for it today. To my sister, Lily: thank you for showing me what it takes to achieve your dreams in the face of tremendous odds. I am so proud of the person you grown to be. Who would have thought we would have made it this far when we began our journey. To my brother Edbert: thank you for showing me what it means to be truly independent and be fully accountable for yourself. I would

like to dedicate this work to the memory of my brother Steve. You always looked after and protected me when we were growing up and I know you continue to do so. I wish you could have been here to see your little brother grow up and I hope you are still proud of me. To my extended family: thank you all for your love and support over the years. Finally, to my amazing wife: words cannot express my gratitude for all your support and understanding throughout this process. From cooking dinner and cleaning the house to helping me with all my experiments, I cannot thank you enough for everything you have sacrificed for me. You are truly an incredible woman and I cannot wait to spend the rest of our lives together.

1.0 INTRODUCTION AND BACKGROUND

Systemic arterial load is defined as the mechanical opposition to movement of blood flow out of the left ventricle [1]. It is described by two components. One is the steady arterial load commonly known as systemic vascular resistance (SVR). This is quantified as the ratio of mean arterial pressure (MAP)-to-cardiac output (CO) and results mainly from arteriolar properties. The other component is pulsatile arterial load, which arises solely as a consequence of the inherently pulsatile nature of the cardiac pump. It is determined by the following: vessel geometry and wall visco-elasticity, the branching property of the vasculature that gives rise to wave propagations and reflections, and the mechanical properties of blood. Global arterial compliance (AC) is one measure of pulsatile arterial load, and is typically derived from CO and the diastolic decay of the aortic pressure waveform [2].

Increased arterial stiffness (or decreased compliance) is observed in many physiological (normal aging, post-menopausal state) and pathological (accelerated aging, chronic hypertension, diabetes, diastolic heart failure) conditions, typically resulting in an increase in arterial load and modifications of systemic hemodynamics that negatively impact both the heart and the vessels. For example, increased arterial stiffness results in a reduction in diastolic pressures, which can compromise coronary perfusion. With the reduction in diastolic pressure (and increase in systolic pressure), pulse pressure increases. There is considerable evidence linking increased pulse pressures to various cardiovascular pathologies including myocardial and vascular

hypertrophy [3]. Increased pulse pressure also results in an increase in pulsatile shear stress on the endothelium which promotes formations of reactive oxygen species rather than nitric oxide [4]. This process neutralizes the beneficial effects of nitric oxide and results in endothelial dysfunction.

Conversely, there are certain physiological phenomena which result in an acute or chronic reduction in arterial load. Understanding the mechanistic basis for such conditions may provide some insight into developing therapeutic agents for treating cardiovascular pathologies wherein an increase in arterial load is a major underlying cause. One such condition is pregnancy, during which there are significant reductions in both the steady and pulsatile components of arterial load. These changes result primarily from significant vasodilation of the systemic circulation as well as alterations in vascular wall mechanical properties and structure.

1.1 MATERNAL CARDIOVASCULAR ADAPTATIONS TO PREGNANCY

The serial changes in systemic hemodynamics and arterial properties that occur during pregnancy are believed to be a necessary adaptation to ensure adequate uteroplacental perfusion for fetal development. These alterations in cardiovascular function are believed to result from the actions of the nervous system and circulating humoral factors, as well as functional and structural modifications within the heart and vascular tissue. These changes include an increase in heart rate and stroke volume, yielding a significant increase in cardiac output (CO) that is maximum by the end of the first or beginning of the second trimester. Additionally, SVR (the steady component of arterial load) is significantly decreased during pregnancy, reaching a nadir by the end of the first or beginning of the second trimester. This combined with the increase in

CO results in a slight decrease in mean arterial pressure [5]. Also during pregnancy, global AC (the pulsatile component of arterial load) reaches a peak by the end of the first trimester just as SVR reaches a nadir [6]. At least in theory, the rise in global AC is critical to the maintenance of cardiovascular homeostasis during pregnancy for several reasons: (1) it prevents excessive decline in diastolic pressure which otherwise would fall to precariously low levels due to the significant decline in SVR; (2) it minimizes the pulsatile or oscillatory work wasted by the heart which otherwise would increase in disproportion to the rise in total work required of and expended by the heart during pregnancy; and (3) it preserves steady shear-type (or prevents oscillatory shear-type) stress at the blood-endothelial interface despite the hyperdynamic circulation of pregnancy, thereby favoring production of nitric oxide rather than superoxide and other damaging reactive oxygen species by the endothelium.

The increase in global AC observed during pregnancy most likely result from a decrease in smooth muscle tone, maternal angiogenesis, or alterations in the passive mechanical properties and vascular wall stiffness of systemic arteries. To this end, several works examining passive mechanical behavior of various arteries from pregnant species showed an increase passive compliance of these arteries when compared to nonpregnant counterparts. Initially, many studies focused on examining the changes in the uterine vasculature during pregnancy. These studies reported that uterine arteries and veins from different pregnant species exhibit significant vasodilation (as measured by an increase in lumen diameter) and increased passive compliance [7-11] when compared with those from respective, nonpregnant controls. Other works focused on the effects of pregnancy on passive mechanical properties of arteries associated with non-reproductive organs. Specifically, mesenteric arteries from late pregnant rats have been shown to exhibit increased passive compliance [12] whereas carotid arteries from late pregnant sheep

exhibited no changes in passive compliance [7]. To determine the mechanisms underlying this pregnancy-induced increase in passive compliance, some studies examined the changes in the biochemical constituents of the vascular wall (i.e., collagen and elastin) during pregnancy. As expected, uterine arteries and veins from pregnant animals were characterized by reduced collagen content when compared to nonpregnant animals [7], while elastin content was decreased or remained unaltered during pregnancy [7, 9]. Similarly, collagen and elastin content were both significantly reduced in mesenteric arteries from late pregnant rats [12].

To summarize, pregnancy is a physiological condition characterized by significant systemic vasodilation (reduced SVR) resulting in an increase in CO. Additionally, there is a significant increase in global AC during pregnancy most likely resulting from a decrease in smooth muscle tone, maternal angiogenesis, and alterations in the passive mechanical properties and vascular wall stiffness of systemic resistance arteries. Of note, the systemic vasodilation observed during early pregnancy is believed to be a result of vasodilation of mainly non-reproductive vascular beds such as the renal circulation. At the onset of the present work, the factor(s) mediating these changes in systemic hemodynamics and global arterial compliance during pregnancy was(were) not completely understood. Traditionally, sex hormones have been postulated to mediate these changes in cardiovascular function during pregnancy [5, 13-15]. However, recently a role for the ovarian hormone, relaxin, has been advanced [16-20].

1.2 RELAXIN

Most investigations conducted by reproductive biologists have dealt with relaxin in the context of pregnancy. The traditional sources of relaxin have been reproductive tissues such as

the corpus luteum of the ovary from which the hormone emanates and circulates during the luteal phase of the menstrual cycle and during pregnancy in women [21]. The concept that relaxin can affect cardiovascular function and, more specifically, blood vessel structure and function has gained considerable support. Much of our recently gained knowledge of relaxin in this new light has arisen from studies of maternal renal and cardiovascular function in the gravid rat model where relaxin has emerged as a prominent modulator of cardiovascular function.

1.3 PREGNANCY-INDUCED RENAL VASODILATION: A ROLE FOR RELAXIN

The renal circulation during pregnancy is characterized by profound vasodilation and hyperfiltration. This results in an increase in effective renal plasma flow and glomerular filtration rate while renal vascular resistance is reduced. In addition, the myogenic reactivity of small renal arteries is significantly reduced during pregnancy. Similar to the changes in overall cardiovascular function during pregnancy, it was initially believed sex hormones mediated these pregnancy-associated changes in renal function. However, numerous studies revealed little or no influence of estrogen on the renal circulation, while progesterone showed only a modest effect [22]. Recent investigation implicated relaxin as the mediator of renal vasodilation and hyperfiltration during pregnancy [16, 23].

Conrad and colleagues reported that prolonged administration of porcine relaxin or recombinant human relaxin (rhRLX) to chronically instrumented, conscious, nonpregnant female rats increased both effective renal plasma flow and glomerular filtration rate to levels observed during midterm pregnancy when renal function peaks in this species [16]. This response to relaxin was also observed in both male and overiectomized female rats [16, 24] suggesting other

reproductive hormones such as estrogen and progesterone are not necessary for these relaxin-mediated changes in the renal circulation. In addition, the pregnancy-associated osmoregulatory changes (i.e. reductions in plasma sodium concentration and osmolality) were reproduced by chronic relaxin infusion in these studies [16, 24]. Chronic relaxin administration also attenuated the renal vasoconstrictor response to angiotensin II infusion comparable to pregnancy [25-27]. Furthermore, the myogenic reactivity of small renal arteries isolated from relaxin-treated rats was reduced [28], comparable to the reductions observed in small renal arteries isolated from midterm pregnant rats [23].

Using relaxin neutralizing antibodies or removing circulating relaxin from midpregnant rats by ovariectomy, Conrad and colleagues showed the gestational renal vasodilation, hyperfiltration and reduced myogenic reactivity of small renal arteries were totally abolished in the absence of relaxin [23]. Additionally, the osmoregulatory adaptations of pregnancy at midterm were prevented [23]. In short, these studies demonstrated relaxin is essential for the renal circulatory and osmoregulatory changes of pregnancy in the gravid rat model.

1.4 MOLECULAR MECHANISMS OF RELAXIN

Through the use of nitric oxide (NO) synthase inhibitors, Conrad and colleagues demonstrated an essential role for NO in the renal vasodilation, hyperfiltration and reduced myogenic reactivity of small renal arteries from pregnant and relaxin-treated nonpregnant rats [16, 27-29]. Further, they showed endogenous endothelin (ET) acting through the endothelial ET_B receptor subtype plays an essential role in the pregnant and relaxin-mediated changes in the renal circulation [24, 25, 28-30]. Comparable to the findings using inhibitors of nitric oxide

synthase, acute administration of the endothelial ET_B receptor antagonist, RES-701-1, inhibited the gestational renal vasodilation and hyperfiltration, thereby resulting in a convergence of glomerular filtration rate, effective renal plasma flow, and effective renal vascular resistance in conscious gravid and virgin rats [30]. Furthermore, there was a reversal of the reduced myogenic reactivity of small renal arteries isolated from gravid rats [29].

Combining these findings with the ability of relaxin to upregulate matrix metalloproteinase (MMP) activity, at least in fibroblasts, and the potential for vascular MMPs, such as the gelatinases, MMP-2 and MMP-9, to process big ET to yield ET_{1-32}, with the latter being capable of activating endothelin receptors [31, 32], Conrad and colleagues postulated that during pregnancy, relaxin may alter one or more of the steps in the vasodilatory pathway depicted in **Figure 1**. Using chronically instrumented conscious rats, they demonstrated that a specific gelatinase inhibitor and a general inhibitor of MMPs both reversed the renal vascular changes induced by relaxin administration to nonpregnant rats. Further, the typical reduction in myogenic reactivity of small renal arteries from relaxin-treated, nonpregnant rats and from pregnant rats was reversed by 4 different inhibitors of MMPs in vitro including an MMP-2-neutralizing antibody. Finally, small renal arteries from relaxin-treated, nonpregnant, ET_B-receptor deficient rats, did not exhibit a reduction in myogenic reactivity despite an increase in vascular MMP-2 activity. These results indicate an essential role for vascular gelatinase, which is in series with, and upstream of, the endothelial ET_B/NO signaling pathway in the renal vasodilatory response to relaxin and pregnancy [25].

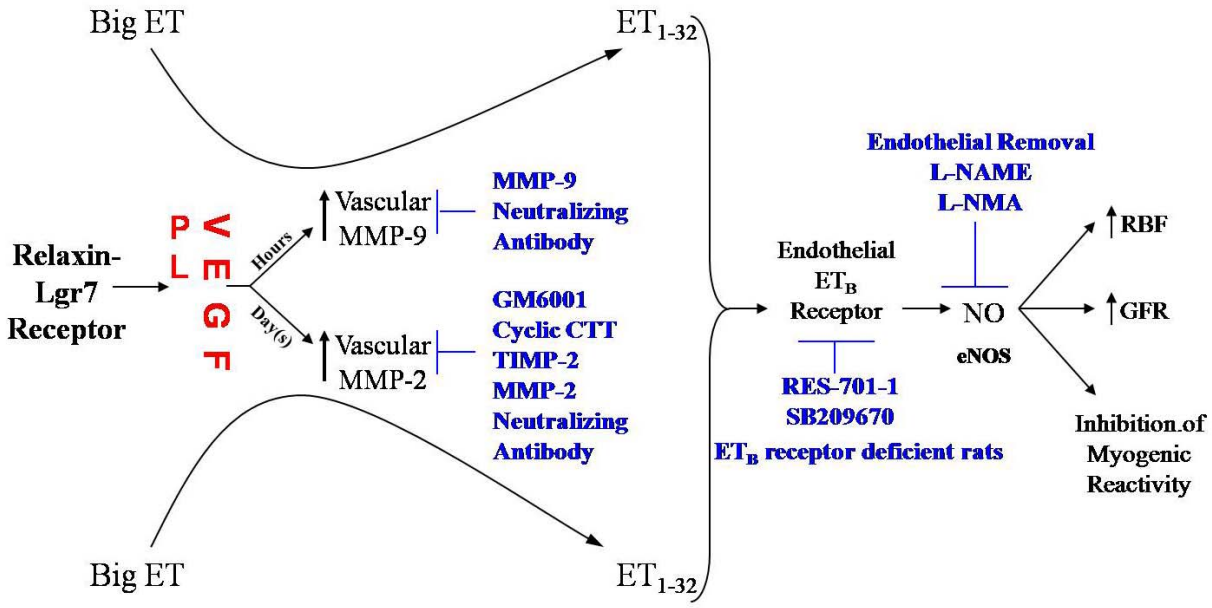

Figure 1. Working model for the slow vasodilatory actions of relaxin.

┤, indicates inhibitors of relaxin vasodilation. **VEGF and PlGF**, vascular endothelial and placental growth factor activities, respectively; ET, endothelin; MMP, matrix metalloproteinase; RBF, renal blood flow; GFR, glomerular filtration rate; **GM6001**, a general MMP inhibitor; **cyclic CTT**, a specific peptide inhibitor of MMP-2; **TIMP-2**, tissue inhibitor of metalloproteinase; **RES-701-1**, a specific ET_B receptor antagonist; **SB209670,** a mixed ET_A and ET_B receptor antagonist; **L-NAME**, nitro-L-arginine methyl ester; **L-NMA,** NG-monomethyl-L-arginine. Note that phosphoramidon (an inhibitor of the classical endothelin converting enzyme), STT (control peptide for cyclic CTT); heat inactivated TIMP-2, BQ-123 (a specific ET_A receptor antagonist), D-NAME and IgGs (control antibodies for MMP neutralizing antibodies) did not affect the slow vasodilatory actions of relaxin. Modified from Jeyabalan A et al. *Adv Exp Med Biol*. 2007 [33].

2.0 HYPOTHESES

Circulating relaxin mediates maternal renal vasodilation, hyperfiltration and reduced myogenic reactivity of small renal arteries in rats [23]. Based on this observation and because serum levels of relaxin in rats increase early in pregnancy concurrent with the changes in cardiovascular function [15, 21, 34], we postulate that this hormone might also contribute to the broader cardiovascular changes of pregnancy, i.e., the increases in CO and global AC, as well as the reduction in SVR. In addition, because the effects of relaxin on the renal circulation were observed in male rats, we believe relaxin's ability to regulate cardiovascular function is not limited to the female sex or to the pregnancy state. Finally, we postulate that similar to pregnancy, the increase in global AC observed with relaxin administration is a result of altered arterial passive mechanical properties through vascular wall remodeling. Based on these postulates, we developed the following specific aims to determine the role of relaxin in regulating cardiovascular function in the presence or absence of pregnancy, with particular emphasis on the hormone's effects on arterial passive mechanical properties and vascular wall remodeling.

3.0 SPECIFIC AIMS

Hypothesis 1. **Exogenous administration** of recombinant human relaxin (rhRLX) to *nonpregnant animals* elicits dose-dependent alterations in systemic hemodynamics and arterial mechanical properties that are comparable to those seen in normal pregnancy.

Specific Aim 1A. To determine systemic hemodynamics and arterial load in conscious, *nonpregnant female rats* administered rhRLX.

Specific Aim 1B. To determine the dose-response of systemic hemodynamics and arterial load in conscious, *nonpregnant female rats* administered rhRLX.

Hypothesis 2. Effects of **exogenous administration** of rhRLX on systemic hemodynamics and arterial mechanical properties are gender independent.

Specific Aim 2. To determine systemic hemodynamics and arterial load in conscious, *male rats* administered rhRLX and compare these responses to those observed in female rats.

Hypothesis 3. **Endogenous (circulating)** relaxin mediates the alterations in systemic hemodynamics and arterial properties that occurs during normal pregnancy.

Specific Aim 3. To determine systemic hemodynamics and arterial load in conscious, *mid and late-pregnant rats* administered control or relaxin neutralizing antibodies.

Hypothesis 4. The relaxin-mediated increase global arterial compliance in pregnant and nonpregnant animals is a result altered arterial passive mechanical properties.

Specific Aim 4A. To evaluate the passive mechanical properties of small renal and external iliac arteries isolated from rhRLX-treated, *nonpregnant female rats and mice*.

Specific Aim 4B. To evaluate the passive mechanical properties of small renal and messenteric arteries isolated from *mid-pregnant rats* administered control or relaxin neutralizing antibodies.

Hypothesis 5. Vascular wall remodeling contributes to the relaxin-mediated alterations in arterial passive mechanical properties.

Specific Aim 5A. To analyze smooth muscle cell characteristics (size and count) in small renal and external iliac arteries isolated from rhRLX-treated *mice*.

Specific Aim 5B. To determine elastin and collagen content in small renal and external iliac arteries isolated from rhRLX-treated *mice*.

Hypothesis 6. **Locally-produced endogenous** relaxin regulates arterial passive mechanical properties through vascular wall remodeling.

Specific Aim 6A. To evaluate the passive mechanical properties of small renal arteries isolated from $Rlx^{+/+}$ *and* $Rlx^{-/-}$ *mice*.

Specific Aim 6B. To analyze smooth muscle cell characteristics (size and count) in small renal and external iliac arteries isolated from $Rlx^{+/+}$ *and* $Rlx^{-/-}$ *mice*.

Specific Aim 6C. To determine elastin and collagen content in small renal and external iliac arteries isolated from $Rlx^{+/+}$ *and* $Rlx^{-/-}$ *mice*.

4.0 MATERIALS AND METHODS

4.1 SYSTEMIC HEMODYNAMICS AND ARTERIAL PROPTERTIES IN RELAXIN-TREATED RATS

4.1.1 Animals

Long-Evans male and female rats of 12-14 weeks old were purchased from Harlan Sprague-Dawley (Frederick, Maryland USA). They were provided PROLAB RMH 2000 diet containing 0.48% sodium (PME Feeds Inc., St. Louis, MO USA) and water *ad libitum*. The rats were maintained on a 12 h light/dark cycle. The Institutional Animal Care and Use Committee of the Magee-Womens Research Institute approved all animal procedures. The rats were habituated to Nalgene metabolism cages for one week (VWR Scientific Products), followed by another week in a harness/7.5 cm spring assembly (Harvard Apparatus, Holliston, MA USA).

4.1.2 Animal Instrumentation

After the habituation period, the rats were anesthetized with 60 mg/kg ketamine i.m. and 21 mg/kg pentobarbital i.p., and placed in the prone position on a heating pad. After application of 70 % ethanol and betadine to all exposed skin areas, ampicillin was administered s.c. (0.2 ml

of a 125 mg/ml solution) and atropine was also administered s.c. (0.075 ml of a 0.4 mg/ml solution).

Next, a sterile tygon catheter (18 in long, 0.015 in ID, 0.030 OD) connected to a syringe containing Ringer's solution, as well as a sterile thermodilution microprobe (22 cm long, F #1.5; Columbus Instruments, Columbus, OH USA) were threaded through the spring. The tygon catheter was subsequently threaded through the hole in the harness and then tunneled subcutaneously from the midpoint between the shoulder blades out the small incision behind the ear using an 18-gauge trocar. The thermodilution catheter was also threaded through the harness assembly and then tunneled subcutaneously from the midpoint between the scapulae out the skin incision in the left costal margin. The spring was then reattached to the harness.

The rat was repositioned on the back. A 1.0 cm skin incision was made in the left inguinal region. The external iliac artery was isolated and prepared for catheterization. The thermocouple was then tunneled subcutaneously exiting at the inguinal incision. The thermocouple was next inserted into the external iliac artery being directed rostrally, so that it passed easily into the internal iliac artery and subsequently into the aorta. After it was advanced 4.0 cm, the thermocouple lay approximately 1.0 cm below the left renal artery.

Next, a horizontal 2.0 cm incision was made over the trachea, 1.0 cm above the cricoid notch. Through this incision, a large subcutaneous pocket was dissected in the neck and above the left shoulder. The right jugular vein and carotid artery were then isolated and prepared for catheterization, the latter facilitated by placing a small roll of gauze under the neck to elevate this deep structure. Using the 18-gauge trocar, the tygon catheter was tunneled subcutaneously from the small incision behind the right ear out the incision in the neck. The tygon catheter was implanted in the right jugular vein and advanced 3.0 cm, thereby placing the catheter tip at the

confluence of the anterior vena cava and the right atrial appendage. The battery/transmitter of a sterile mouse pressure catheter (TA11PA-C20; ca. F #1.2; Data Sciences International, St. Paul, MN USA) was inserted in the subcutaneous pocket. The mouse pressure catheter was then implanted in the right carotid artery 2.8 cm, thereby placing the catheter tip at the confluence of the right carotid artery and aortic arch. All wounds were closed with 4-0 silk or autoclips. After instilling 0.05 ml of a heparin solution into the jugular catheter and plugging it with a straight pin, the rat was placed in the metabolism cage and given ampicillin by drinking water for 2 days (100 mg/50 ml with 2 tablespoons of dextrose). The spring and catheters that exit the cage top were secured. Terbutrol was given s.c. for post-operative analgesia as soon as the rats were recovered sufficiently from the anesthesia.

After completion of the measurement for the last time point, the rat was anesthetized with 60 mg/kg pentobarbital i.v. and the position of the jugular catheter relative to the right atrium, the placement of the pressure catheter relative to the aortic arch, and the position of the thermocouple relative to the left renal artery were recorded.

4.1.3 **Administration of Recombinant Human Relaxin (rhRLX)**

We used three different doses of rhRLX intended to yield concentrations of circulating relaxin that ranged from levels seen during the early stages of pregnancy to those observed during the late stages [21, 24, 25, 35]. For chronic administration of low dose rhRLX (1.0-4.0 μg/h), two Alzet model 2002 or one model 1002 osmotic minipumps (Durect Corporation, Curpertino, CA USA) was inserted subcutaneously in the back of the animal under isoflurane anesthesia. For medium (25 μg/h) or high (50 μg/h) dose administration, one Alzet model 2ML2

osmotic minipump was implanted. The rhRLX (Connetics, Palo Alto, California USA) was provided as a 5.0 mg/ml solution in 20 mM sodium acetate, pH 5.0 and was diluted in the same buffer.

4.1.4 **Experimental Protocol**

Time control studies were first performed in 5 rats, in order to document the stability of systemic hemodynamics over a 17 day period after surgery. In these animals, measurements were recorded on days 4-5, 7-8, 9-10, 13-14, and 16-17 after surgery.

The low, medium, and high dose rhRLX protocols entailed 6, 7 and 9 rats, respectively. In addition, the vehicle for rhRLX (20mM sodium acetate, pH 5.0) was administered to another 6 rats. After 2 baseline measurements of systemic hemodynamics on days 5 and 7 after surgery, either low, medium, or high dose rhRLX or vehicle was administered by osmotic minipump. Systemic hemodynamics were again assessed on days 3, 6, 8 and 10 after initiation of low or medium dose rhRLX or vehicle infusion. Systemic hemodynamics were assessed on days 3 and 6 after initiation of high dose rhRLX.

Each measurement consisted of 4 to 6 recordings of cardiac output and blood pressure waveforms obtained when the rat was either sleeping or resting. At least 10 min was allowed between recordings. These measurements were obtained between 9am and 3pm.

4.1.5 **Measurement of Cardiac Output**

To measure cardiac output, we used the thermodilution technique [36]. Ringer's solution of known volume and temperature was injected into the anterior vena cava using the Micro

Injector 400 (Columbus Instruments). The cardiac output was calculated from the change in blood temperature (Cardiotherm 400R, Columbus Instruments). The cardiac output as determined by the Cardiotherm 400R was calculated as:

$$CO = \frac{[(B_T - I_T) * V_I]}{\int B_T(t)}$$

where, B_T is the blood temperature (recorded by the thermocouple implanted in the abdominal aorta), I_T is the injectate temperature (room temperature), V_I is the injectate volume (150 μL), and $B_T(t)$ is the blood temperature as a function of time.

4.1.6 **Measurement of Instantaneous Aortic Pressure Waveforms**

Instantaneous aortic pressure was recorded using a blood pressure telemetry system (Data Sciences International, St. Paul, MN USA) [37]. The aortic pressure was recorded by a pressure catheter implanted in the aortic arch via the right carotid artery and transmitted to an external receiver. Steady-state aortic pressure was digitized online using a PC-based data acquisition system with 16 bit resolution and 2000 Hz sampling rate and stored as text files for off-line analysis. Each measurement consisted of a 30 second sampling duration.

4.1.7 **Aortic Pressure Analysis**

Analysis of the acquired data and calculation of global AC was performed by a custom computer program developed using MATLAB software (MathWorks Inc., Natick, MA USA). Briefly, individual beats were selected (3 – 15 cycles) from the 10 seconds of the aortic pressure recording, immediately preceding the measurement of cardiac output. The ensemble was

averaged as described by Burattini *et al*. [38] to yield a single representative beat for each trial. The mean arterial pressure (MAP), peak systolic pressure (P_s), and end diastolic pressure (P_d) were calculated from this averaged beat. Pulse pressure (PP) was calculated as $P_s - P_d$. Systemic vascular resistance (SVR) was calculated by dividing the MAP by CO.

4.1.8 **Global Arterial Compliance**

Two measures of global arterial compliance were calculated. The first, AC_{area}, was calculated from the diastolic decay of the aortic pressure waveform [P(t)] using the area method [2]:

$$AC_{area} = \frac{A_d}{[SVR * (P_1 - P_2)]}$$

where P_1 and P_2 are the pressures at the beginning and end of the diastolic decay curve, respectively, and Ad is the area under the P(t) waveform over this region.

The second measure of global arterial compliance was calculated as the stroke volume (SV)-to-pulse pressure (PP) ratio [39]:

$$AC = \frac{SV}{PP}$$

Stroke volume was defined as:

$$SV = \frac{CO}{HR}$$

4.2 SYSTEMIC HEMODYNAMICS AND ARTERIAL PROPERTIES IN MID AND LATE-PREGNANT RATS

4.2.1 **Animals**

See **Section 4.1.1** above. After being habituated to the experimental conditions, rats were either housed with males or remained as virgin controls. The presence of spermatozoa in the vaginal lavage was considered day 0 of gestation.

4.2.2 **Animal Instrumentation**

See **Section 4.1.2** above for details regarding the surgical procedure used. Of note, pregnant rats studied at mid-gestation were instrumented between days 4 and 6 of gestation while rats studied at late-gestation were instrumented between days 8-10.

4.2.3 **Administration of relaxin-neutralizing antibodies**

Neutralizing antibodies against rat relaxin (MCA1) or control antibodies against fluorescein (MCAF) were administered via daily i.v. injection between 12 and 4 PM for up to 8 days beginning on day 8 of gestation. Each injection containing 5.0 mg of antibody in 0.5 ml of phosphate buffered saline (PBS) was infused over 5 minutes into the femoral venous catheter [23, 40, 41]. Other pregnant rats were administered PBS vehicle to serve as a second untreated-pregnant control group.

4.2.4 **Measurements of Hemodynamics and Determination of Arterial Mechanical Properties**

See **Section 4.1.5 – 4.1.8** above for experimental procedures used. Of note, systemic hemodynamics and arterial properties were assessed on two separate days between gestational days 11 and 15 in rats studied at mid-gestation and days 18 and 21 in rats studied at late-gestation. The average values of each given variable assessed on the two separate days from each animal was taken to be the representative value of that variable for that animal.

4.3 PASSIVE ARTERIAL MECHANICAL PROPERTIES

4.3.1 **Animals**

Table 1 below lists the different animal models and arteries used in this work. The protocols used for administration of relaxin and vehicle or relaxin neutralizing and control antibodies are described in **Sections 4.1.3 and 4.2.3** above.

Table 1. Animal Models Utilized to Study Effects of Relaxin on Passive Arterial Mechanical Properties

Species	Gender	Stage of Pregnancy	Treatment or Genotype	Artery	Mechanical Test
Rat	Female	Nonpregnant	Relaxin/Vehicle	Small Renal	Uniaxial
Rat	Female	Midpregnant	MCA1/MCAF	Small Renal	Uniaxial
Rat	Female	Midpregnant	MCA1/MCAF	Mesenteric	Uniaxial
Mouse	Female	Nonpregnant	Relaxin/Vehicle	Small Renal	Uniaxial
Mouse	Female	Nonpregnant	Relaxin/Vehicle	Ext. Iliac	Uniaxial
Mouse	Female	Nonpregnant	Relaxin/Vehicle	Small Renal	Biaxial
Mouse	Female	Nonpregnant	Relaxin/Vehicle	Ext. Iliac	Biaxial
Mouse	Male	N/A	$Rlx^{+/+}$	Small Renal	Uniaxial
Mouse	Male	N/A	$Rlx^{-/-}$	Ext. Iliac	Uniaxial

4.3.2 **Isolation and Preparation of Arterial Segments**

For isolation of small renal arteries, a kidney was removed and placed in ice-cold HEPES buffered physiological saline solution (PSS, a modified Kreb's buffer). The HEPES PSS was composed of (in mmol/L): sodium chloride 142, potassium chloride 4.7, magnesium sulfate 1.17, calcium chloride 2.5, potassium phosphate 1.18, HEPES 10, glucose 5.5, and was pH 7.4 at 37^{o}C. A stereo dissecting microscope, fine forceps and iridectomy scissors were used to isolate interlobar arteries as described by Gandley et al. [29]. Briefly, the arteries were exposed by carefully dissecting the overlying tissue. The main renal artery is typically divided into three branches in each half of the kidney which then further bifurcates to form two smaller arteries that give rise to the arcuate arteries. Segments of these smaller arterial branches were dissected free from surrounding medullary tissue. For isolation of mesenteric arteries, the mesenteric arcade

was removed and placed in ice-cold HEPES buffered PSS. Segments of first-order mesenteric arteries were then carefully dissected free from the surrounding fatty tissue. Finally, for isolation of external iliac arteries the animals were placed in the supine position and an incision was made along the both hind legs to expose the iliac arteries. Segments of the external iliac arteries along with the surrounding tissue were then removed and placed in ice-cold HEPES buffered PSS. The arterial segments were then carefully dissected free from the surrounding tissue.

Following isolation, arterial segments were then transferred to an isobaric arteriograph (Living Systems Instrumentation, Burlington, VT USA) and mounted on two glass micro-cannulae suspended in the chamber. After the residual blood was flushed from the lumen of the artery, the distal cannula was occluded to prevent flow. Of note, for biaxial mechanical testing the distal cannula was replaced with a metal hook that was attached to a force transducer (Aurora Scientific, Model 400A) which enabled us to measure axial force (see **Appendix A**). In this configuration, the artery was occluded with a suture and then tied to the metal hook. In both configurations, the proximal cannula was attached to a pressure transducer, a pressure servo-controller and a peristaltic pump. The servo-controller maintained a selected intraluminal pressure that can be changed in a stepwise manner. An electronic dimension analyzing system obtained arterial diameter measures. Prior to experimentation, the vessels were heated to 37^{o}C (the arteriograph chamber was maintained at this temperature for the duration of the experiment) and incubated in the bath with 0.01 M papaverine and 0.01 M EGTA in calcium-free HEPES PSS.

4.3.3 **Pressure-Diameter Data at Fixed Axial Load**

4.3.3.1 Experimental Protocol

After a 30 min equilibration period, transmural pressure was increased in up to 14 steps from at 0 to 120 mmHg. Inner and outer diameters as well as wall thickness were measured following each pressure step when the vessel had reached a steady state. These measurements were used to compute uniaxial stiffness parameters as described by Cholley et al [42].

4.3.3.2 Uniaxial (Circumferential) Stress-Strain Analysis

Measurements of the inner (D_{i0}) and outer diameters (D_{o0}) and wall thickness (H_0) in the unloaded configuration (typically occurred at transmural pressures between 0 and 5 mmHg) were used to compute the unstressed muscle area (A_{M0}):

$$A_{M0} = \pi * H_0 * (D_{i0} + H_0)$$

Assuming an incompressible arterial wall, wall thickness was calculated at each given pressure step (H_I) using the calculated unloaded muscle area and the lumen area (A_i) for that given pressure:

$$H_I = \sqrt{\frac{A_{M0} + A_i}{\pi}} - \sqrt{\frac{A_i}{\pi}}$$

From this inner (R_i), outer (R_o), and midwall radii (R_m) was calculated as:

$$R_i = \sqrt{\frac{A_i}{\pi}}$$

$$R_o = \sqrt{\frac{A_{M0} + A_i}{\pi}}$$

$$R_m = \frac{R_i + R_o}{2}$$

and midwall strain (ε_m) was calculated as:

$$\varepsilon_m = \frac{R_m}{R_{m0}}$$

where R_{m0} represents the midwall radius in the unloaded state. Circumferential wall stress (σ) was calculated from the intraluminal pressure (P) as:

$$\sigma = 2 * P * \left(\frac{R_i * R_o}{R_m}\right)^2 * \left({R_o}^2 - {R_i}^2\right)^{-1}$$

Finally, the σ–R_m and σ–ε_m relationships were fitted to a third-order polynomial function:

$$\sigma = A_0 + (A_1 * R_m) + \left(A_2 * {R_m}^2\right) + \left(A_3 * {R_m}^3\right), \text{ or}$$

$$\sigma = A_0 + (A_1 * \varepsilon_m) + (A_2 * {\varepsilon_m}^2) + (A_3 * {\varepsilon_m}^3)$$

where A_0, A_1, A_2 and A_3 are constants. These derived constants were then used to compute average values of σ at prescribed values of R_m and ε_m for each given artery.

4.3.4 **Pressure-Diameter Data at Varying Axial Loads**

4.3.4.1 Experimental Protocol

As stated above (see **section 4.3.2**), for biaxial mechanical testing the proximal end of the arterial segment was tied to a force transducer thus enabling us to measure axial force. Simultaneously, pressure-diameter and force-length data were attained using this setup. Transmural pressure was increased in up to 12 steps from at 0 to 120 mmHg at a given axial length; each cycle was then repeated at incrementing axial stretches. Inner (D_i) and outer (D_o) diameters, wall thickness (H), axial length (L) and force (F) were measured following each

pressure step when the vessel had reached a steady state. These measurements were then used compute biaxial stiffness parameters as described by Schulze-Bauer et al. [43].

4.3.4.2 Biaxial Stretches and Cauchy Stresses

Circumferential (λ_θ) and axial (λ_z) stretches were calculated as:

$$\lambda_\theta = \frac{R_o}{R_{o0}}$$

$$\lambda_z = \frac{L}{L_0}$$

where R_{o0} and L_0 represent the vessel outer radius and axial length in the load-free configuration. Circumferential ($\sigma_{\theta\theta}$) and axial (σ_{zz}) Cauchy stresses were calculated from the collected data as:

$$\sigma_{\theta\theta} = P * \left(\frac{R_o * {\lambda_\theta}^2}{H} - 1\right)$$

$$\sigma_{zz} = \frac{F}{\pi * H * (2 * R_o - H)} + \frac{\sigma_{\theta\theta}}{2}$$

where, H_0 represents wall thickness in the load-free configuration and P represents the intraluminal pressure.

4.3.4.3 Second Piola-Kirchhoff Stresses and Green Lagrange Strains

The second Piola-Kirchhoff stresses, $S_{\theta\theta}$ and S_{zz}, were defined as:

$$S_{\theta\theta} = \frac{\sigma_{\theta\theta}}{{\lambda_\theta}^2}$$

$$S_{zz} = \frac{\sigma_{zz}}{{\lambda_z}^2}$$

From the circumferential and axial stretches, the Green-Lagrange strains are calculated as:

$$E_{\theta\theta} = \frac{{\lambda_\theta}^2 - 1}{2}$$

$$E_{zz} = \frac{{\lambda_z}^2 - 1}{2}$$

where, $E_{\theta\theta}$ and E_{zz} represent Green-Lagrange circumferential and axial strains, respectively.

4.3.4.4 Strain Energy Function

Circuferential and axial stresses can also be expressed as derivatives of a given strain-energy function (Ψ) as follows:

$$S_{\theta\theta}^{\psi} = \frac{\partial \psi}{\partial E_{\theta\theta}}$$

$$S_{zz}^{\psi} = \frac{\partial \psi}{\partial E_{zz}}$$

We tested several different strain-energy functions to determine which one best described our data. The 7-parameter polynomial model [44]:

$$\psi = \left(C_1 * {E_{\theta\theta}}^2\right) + \left(C_2 * E_{\theta\theta} * E_{zz}\right) + \left(C_3 * {E_{zz}}^2\right) + \left(C_4 * {E_{\theta\theta}}^3\right) + \left(C_5 * {E_{\theta\theta}}^2 * E_{zz}\right) + \left(C_6 * E_{\theta\theta} * {E_{zz}}^2\right) + \left(C_7 * {E_{zz}}^3\right),$$

the 4-parameter exponential model [45]:

$$\psi = C_1 * \left[\exp\left(C_2 * {E_{\theta\theta}}^2 + C_3 * E_{\theta\theta} * E_{zz} + C_4 * {E_{zz}}^2\right) - 1\right],$$

and the 7-paramter mixed polynomial-exponential model [46]:

$$\psi = \left(C_1 * {E_{\theta\theta}}^2\right) + \left(C_2 * E_{\theta\theta} * E_{zz}\right) + \left(C_3 * {E_{zz}}^2\right) + C_4 * \left[\exp\left(C_5 * {E_{\theta\theta}}^2 + C_6 * E_{\theta\theta} * E_{zz} + C_7 * {E_{zz}}^2\right) - 1\right].$$

Of these three, we found that the mixed polynomial-exponential model best described our data. Using this model, we derived the 7 constitutive parameters (C_1, C_2, C_3, C_4, C_5, C_6, and C_7) that best-fit each vessel using the Levenberg-Marquardt algorithm in Matlab. From these

parameters we computed the 2-dimensional behavior of strain energy (i.e. the magnitude of strain energy at simultaneously varying levels of axial and circumferential strain) for each vessel.

4.4 SMOOTH MUSCLE CELL CHARACTERISTICS

4.4.1 **Animals**

This work was done in vehicle and relaxin treated female C57-BL/6J mice 6-8 weeks of age, male wild-type ($Rlx^{+/+}$) and relaxin knock-out ($Rlx^{-/-}$) mice 8-12 weeks old (provided by Dr. Laura J. Parry, Department of Zoology, Univeristy of Melbourne, Parkville, Victoria, Australia). For this work, we studied external iliac, and small renal arteries in both sets of mice.

4.4.2 **Arterial Cross-Sections**

Isolated external iliac arteries were fixed in 2% Paraformaldehyde-PBS at 4ºC for 4 hours after which they were rinsed in PBS and cryoprotected in 30% sucrose at 4ºC for at least 24 hours. These arteries were then embedded in OCT and cut into several 6μm thick sections and collected on Superfrost Plus microscope slides. To obtain cross-sections of small renal arteries, an entire kidney was fixed in Paraformaldehyde, and cryoprotected in sucrose after which it was embedded in OCT in a configuration that ensured that the cut was in the cross sectional direction of small renal arteries. The slides were stored in a freezer (-80^{o}C) until the sections were ready to be stained at which point each section was rehydrated with PBS and stained using the techniques described below (see **Section 4.4.4**).

4.4.3 **Smooth Muscle Cell Isolation**

Small renal arteries were isolated from vehicle or rhRLX-treated mice as described above (see **Section 4.3.2**). Arterial segments were then cut into smaller pieces and placed in a small eppendorf tube. An enzyme solution containing 2 mg/ml collagenase (Worthingon Corp., Lakewood, NJ) and 0.8 mg/ml elastase (Sigma-Aldrich, St. Louis, MO) in DMEM culture medium (Invitrogen/Gibco, Carlsbad, California) was poured into the tube. The tube was then closed with a cap and incubated at 37^{o}C for 1-2 hours. The enzyme solution was gently triturated periodically during this incubation period to help with tissue dispersion. Following digestion, the solution was centrifuged at 300 RPM. The pellet was resuspended in culture medium. The cells were then seeded on collagen-coated Superfrost Plus microscope slides and incubated for another hour after which cells were stained and imaged using the techniques described below.

4.4.4 **Immunofluorescence Staining**

Each slide (both arterial cross-sections and seeded cells) was permeabilized with 0.1% triton X for 15 min after which they were rehydrated with 3 washes of PBS followed by 5 washes of 0.5% BSA. The slides were then treated with blocking solution (2% BSA) for 1 hour at room temperature followed by 5 washes with 0.5% BSA. They were then incubated with a primary antibody for smooth muscle actin (Sigma-Aldrich, St. Louis, MO) at room temperature followed by an additional 5 washes with 0.5% BSA. Next the slides were stained with a FITC-conjugated secondary antibody for another hour (Sigma-Aldrich, St. Louis, MO) at room temperature followed by 5 washes with 0.5% BSA and 5 more washes with PBS. Of note, some

samples were stained directly with a Cy3-conjugated smooth muscle actin antibody (Sigma-Aldrich, St. Louis, MO) followed by 5 washes with 0.5% BSA and 5 more washes with PBS. Finally the nuclei were stained with Hoescht or DAPI (Sigma-Aldrich, St. Louis, MO) for 30 seconds followed by 2 washes with PBS. The slides were then cover-slipped with gelvatol mounting media and stored at 4^{o}C in the dark. The slides were imaged with an Olympus Provis fluorescence microscope.

4.4.5 **Arterial Smooth Muscle Cell Density and Size**

Fluorescent images were analyzed using ImageJ software (Wayne Rashband, National Institutes of Health, USA). **Figure 2A** represents a sample image obtained after a cross-section of a small renal artery was stained for smooth muscle actin and nuclei. The arterial wall was identified as the area of the artery stained positive for smooth muscle actin (red) while nuclei stained with Hoescht (or DAPI) appeared as blue. Nuclei belonging to smooth muscle cells (SMC) were designated as those that lay within the smooth muscle actin-positive region of the arterial wall. Smooth muscle cell density for each arterial cross-section was quantified as the ratio of number of SMC to arterial wall area. Each individual, discernable SMC within a cross-section was outlined and the average SMC size per cross-section was measured. The mean SMC density and size for each artery was determined by analyzing at least 4 non-consecutive cross-sections of that artery. Of note, each field of view contained a single arterial cross-section as shown in Figure 2A. **Figure 2B** represents a sample image obtained after cells isolated from a small renal artery were stained for smooth muscle actin and nuclei. Smooth muscle cells were identified as the cells stained positive for smooth muscle actin (red). Individual cell sizes were measured and the average cell size per artery was computed.

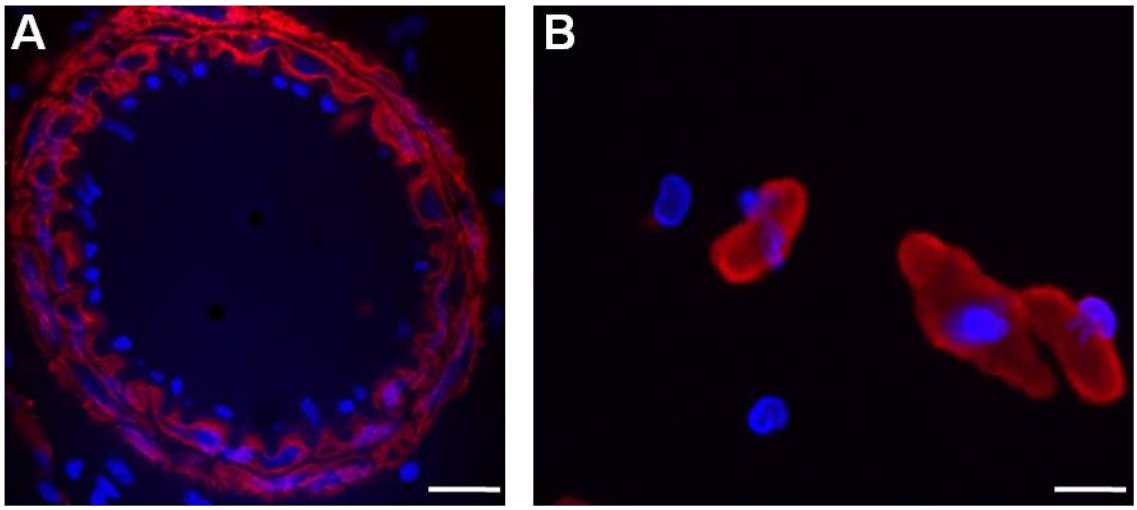

Figure 2. Arterial Cross-Section Stained for α-SMA and Nuclei.

(A) Mouse kidneys were sectioned at 6 μm thickness. Small renal arteries were identified by positive staining for smooth muscle actin. Smooth muscle actin was stained as red, while nuclei were stained as blue. The scale bar equals 10 μm. **(B)** Isolated small renal arteries were enzymatically digested and cells were seeded on a collagen-coated Superfrost Plus microscope slide. Smooth muscle actin was stained as red, while nuclei were stained as blue. The scale bar equals 10 μm.

4.5 ARTERIAL WALL BIOCHEMICAL COMPOSITION

4.5.1 **Animals**

This work was done in conjunction with our work examining the effects of relaxin on vascular smooth muscle cell characteristics. Accordingly, we used the same animal models. See **Section 4.4.1** above.

4.5.2 **Total Protein Content**

Total protein content was determined using the Pierce BCA Protein Assay Kit (Pierce, Rockford IL) per instructions provided by the manufacturer. Briefly, the arteries were cleaned of any extraneous tissue, lyophilized, minced and digested for 48 hours in a pepsin-HCL solution (0.05 g of pepsin in 50 ml of 0.01N HCL; 100 μl per 0.001 g of tissue). Following the digestion, the solution was vortexed and a 25 μl sample was added to 100 μl of the BCA Working Reagent. This solution was incubated at 37^{o}C for 30 minutes and then allowed to cool to room temperature. Absorbance was determined at 550nm on a spectrophotometer (Kinetic Microplate Reader; Molecular Devices, Sunnyvale, CA).

4.5.3 **Collagen Content**

Isolated arteries were assayed for total collagen levels using the Sircol collagen dye binding assay (Biocolor Ltd., Northern Ireland) according to the manufacturer's instructions. Briefly, the arteries were be cleaned of any extraneous tissue, lyophilized, minced and digested for 48 hours in a pepsin-HCL solution (0.05 g of pepsin in 50 ml of 0.01N HCL; 100 μl per 0.001 g of tissue). Following the digestion, the solution was vortexed and a 50 μl sample was collected. One milliliter of Sirius red dye was then added to this sample and mixed on a rocking platform for 1 hour. The samples were then centrifuged (10,000 RPM for 10 min) and the precipitate was digested in 1 ml of acetic acid solution included in the kit. Absorbance was determined at 550 nm (Kinetic Microplate Reader; Molecular Devices, Sunnyvale, CA). Relative collagen content was quantified as the ratio of collagen concentration to total protein concentration.

4.5.4 **Elastin Content**

Elastin levels were determined using the Fastin Elastin assay kit and protocol provided by the same manufacturer (Biocolor Ltd., Northern Ireland). Briefly, arteries were lyophilized overnight and tissues dry weight was recorded. Each artery was then placed into 0.25 M oxalic acid (2ml of oxalic acid solution per 0.1g of tissue). The samples were then heated to 90°C for 1 hour, and centrifuged (3000 RPM @ 4^{o}C for 10 min). The supernatant was collected. The same volume of oxalic acid as before was added to the remaining pellet and the above procedure of heating and centrifugation was repeated four additional times. Each of the collected precipitates was pooled and added to 1 ml of elastin precipitating reagent. The samples were then placed in the refrigerator (4^{o}C) overnight. After 24 hours the extracts were spun down (2000 RPM @ 4^{o}C for 10 min) and the supernatants were poured off. One milliliter of elastin dye reagent and 100µl of 90% ammonium sulfate was added to the extracts. The solution was mixed on a rocking platform for 1 hour after which the samples were spun down again (12000 RPM for 10min at room temperature) and the supernatant discarded. Finally, 1 ml of destaining agent was added to the extracts. Absorbance was determined at 550nm on a spectrophotometer (Kinetic Microplate Reader; Molecular Devices, Sunnyvale, CA). Relative elastin content was quantified as the ratio of the mass of elastin to tissue dry weight.

4.6 STATISTICAL ANALYSES

Data are presented as means ± SEM and $P < 0.05$ was taken to be significant.

4.6.1 Systemic Hemodynamics and Arterial Mechanical Properties

4.6.1.1 Vehicle and rhRLX-Treated Conscious Female and Male Rats

Two-factor repeated-measures ANOVA was used to compare mean values of systemic hemodynamics and arterial mechanical properties among vehicle and rhRLX-treated rats. The same analysis was used to compare mean values between low dose male and female rats at various time points. If significant main effects or interactions were observed, comparisons between groups were performed using Fisher's LSD or Dunnett's test. Student's unpaired 't' test was used to compare the composite mean values during infusion of rhRLX (i.e., values averaged over all time points during rhRLX or vehicle infusion) with baseline.

4.6.1.2 Conscious Mid and Late-Pregnant Rats

One-factor randomized block ANOVA was used with 3 levels corresponding to the MCA1 and MCAF-treated mid or late-pregnant rats, and the virgin controls. If a significant main effect was observed, then comparisons among groups were performed using Fisher's least significant difference (LSD) test.

4.6.2 **Arterial Passive Mechanics**

4.6.2.1 Uniaxial Analysis

Least squares regression analysis was performed on stress-midwall radius relationships. Analysis of excess variance (or extra sum of squares) [47] was used to compare these relationships between vehicle and relaxin-treated groups.

4.6.2.2 Biaxial Analysis

Student's unpaired 't' test was used to compare the mean values of maximum strain energies of small renal arteries isolated from vehicle and rhRLX-treated mice.

4.6.3 **Smooth Muscle Cell Characteristics and Arterial Wall Biochemical Composition**

Student's unpaired 't' test was used to compare the mean values of SMC density and size, arterial collagen content, and arterial elastin content of rhRLX-treated animals versus vehicle control. Similarly, Student's unpaired 't' test was used to compare the corresponding data from $Rlx^{-/-}$ and $Rlx^{+/+}$ mice.

5.0 RESULTS

5.1 SYSTEMIC HEMODYNAMICS AND ARTERIAL PROPERTIES IN CONSCIOUS FEMALE RATS

Specific Aim 1A. To determine systemic hemodynamics and arterial load in conscious, *nonpregnant female rats* administered rhRLX.

Specific Aim 1B. To determine the dose-response of systemic hemodynamics and arterial load in conscious, *nonpregnant female rats* administered rhRLX.

5.1.1 *Female* Time Control Rats

Portions of this work have been previously published elsewhere [48]. In order to determine the stability of systemic hemodynamics and arterial load using our conscious rat technique we studied control rats over a 17-day period after surgery (**Table 2**). Heart rate (HR) declined significantly due to a training effect as has been previously reported [49]. Stroke volume (SV) reciprocally increased such that cardiac output (CO) was unchanged. All other variables did not change significantly over the 17-day period after surgery, thus this conscious rat model can be used to obtain meaningful data under experimental conditions.

Table 2. Absolute Values of Systemic Hemodynamics and Arterial Properties in *Female*, Time Control Rats

Days After Surgery	Δ_T (^oC)	CO (mL/min)	HR* (bpm)	SV* (mL)	AC_{area} (μl/mmHg)	SVR (mmHg.s/mL)	MAP (mmHg)
4-5	0.37±0.01	119±3	428±7	0.28±0.01	6.8±0.3	57±2	107.6±0.8
7-8	0.37±0.01	121±3	378±8	0.32±0.01	7.2±0.3	55±2	107.3±1.5
9-10	0.38±0.01	120±4	382±8	0.31±0.01	6.9±0.3	55±2	108.1±1.5
13-14	0.35±0.01	115±4	354±5	0.32±0.01	7.3±0.3	58±2	107.0±1.5
16-17	0.32±0.02	122±3	349±7	0.36±0.01	8.0±0.4	52±2	103.7±2.2

Mean±SEM. N=5 rats (longitudinal measurements were made in each animal at the time-points specified above). Δ_T, change in blood temperature after injection of Ringer's solution into the right heart; CO, cardiac output; HR, heart rate; SV, stroke volume; AC_{area}, global arterial compliance calculated using area method; SVR, systemic vascular resistance; MAP, mean arterial pressure. *$P < 0.05$ by single factor repeated measures ANOVA.

5.1.2 *Female Rats* Administered Vehicle (Control)

Portions of this work have been previously published elsewhere [48]. These results were derived from 3 rats administered the vehicle for rhRLX at the infusion rate of 4 μg/h, and from another 3 rats administered the vehicle for rhRLX at the infusion rate of 25 μg/h for 10 days (these correspond to the infusion rates for the low and medium dose administration of rhRLX, respectively). The results were comparable, and therefore, combined. **Figures 3 and 4** depict the percent change from baseline of systemic hemodynamics and arterial properties. Similar to the time control studies, there was a significant decrease in heart rate, which was offset by an insignificant rise in stroke volume, such that CO remained unchanged. All other variables remained relatively constant. Combining all of the time points during administration of vehicle yielded overall changes in CO, global AC, and SVR of -1.4 $\pm$ 1.3, 2.2 $\pm$ 4.6, and 0.4 $\pm$ 3.4 % of

baseline, respectively (all *P* NS vs. baseline). As expected, there was no measurable rhRLX in the serum, and the osmolality was 309 $\pm$ 6 mOsm/kg water.

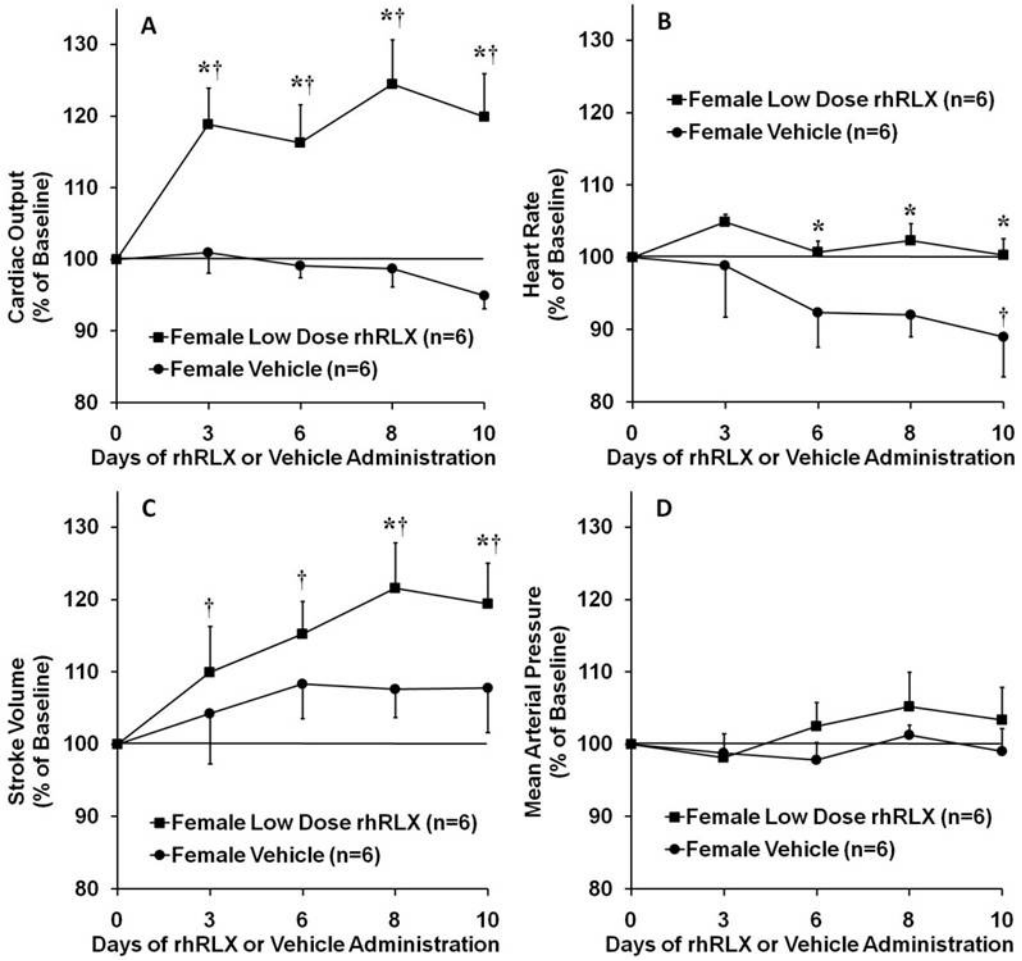

Figure 3. Temporal Pattern of Changes in Systemic Hemodynamics in Conscious *Female Rats* Administered Low Dose rhRLX

Percent change from baseline for (**A**) cardiac output, (**B**) heart rate, (**C**) stroke volume, and (**D**) mean arterial pressure in female rats administered low dose recombinant human relaxin (rhRLX; 4 μg/h) or vehicle. † $P < 0.05$ vs. baseline, * $P < 0.05$ vs. vehicle at the same time point by Fisher's or Dunnett's posthoc tests.

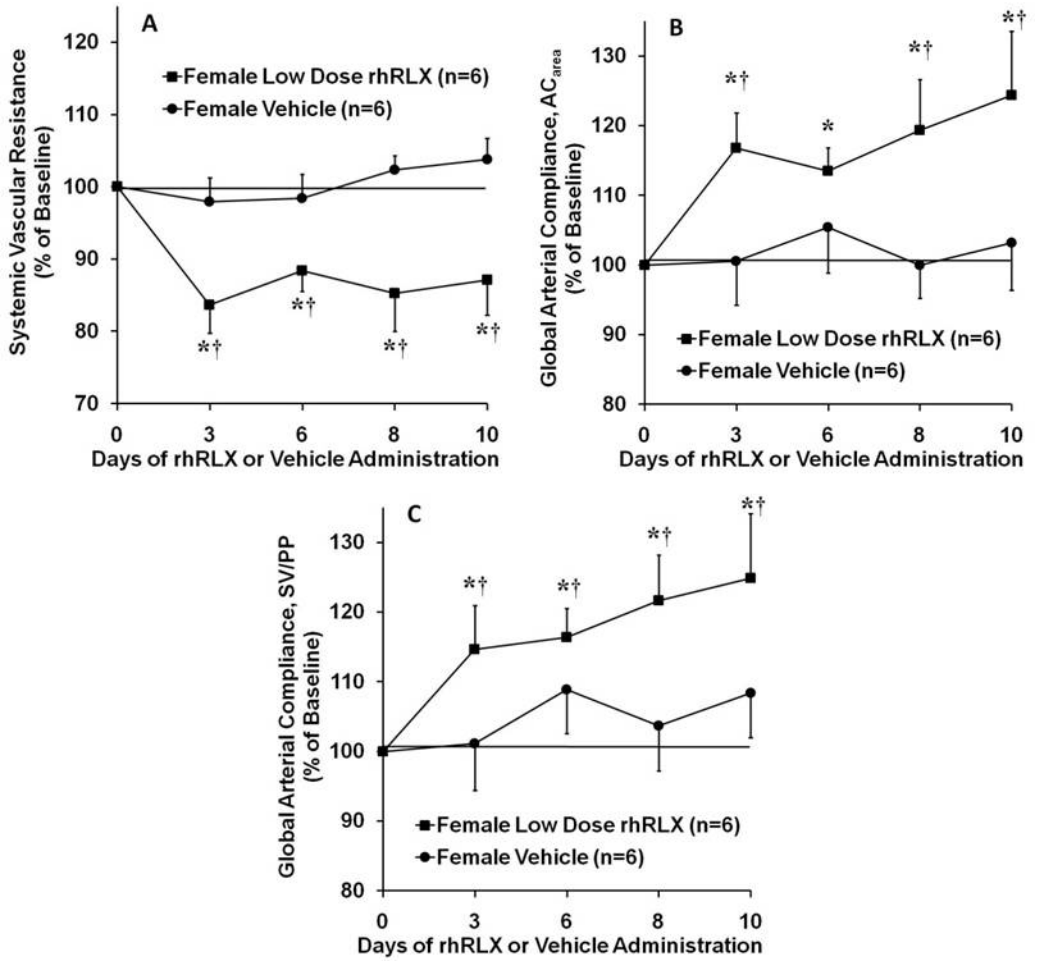

Figure 4. Temporal Pattern of Changes in Systemic Arterial Properties in Conscious *Female Rats* Administered Low Dose rhRLX

Percent change from baseline for (**A**) systemic vascular resistance, (**B**) global arterial compliance (AC_{area}), and **(C)** ratio of stroke volume-to-pulse pressure in female rats administered low dose recombinant human relaxin (rhRLX; 4 μg/h), or vehicle. † $P < 0.05$ vs. baseline, * $P < 0.05$ vs. vehicle at the same time point by Fisher's or Dunnett's posthoc tests.

5.1.3 *Female Rats* Administered Low Dose rhRLX (4 μg/h)

Portions of this work have been previously published elsewhere [48]. The absolute values for systemic hemodynamics and arterial properties from female rats administered low dose rhRLX are shown in **Table 3**, while Figs. 3 and 4 show the temporal pattern of percentage change from baseline. Low dose rhRLX significantly increased CO relative to baseline and to vehicle infusion (Fig. 3A). The infusion of rhRLX prevented the decline normally observed in HR (c.f. vehicle, Fig. 3B), and the hormone significantly increased SV (Fig. 3C). Thus, increases in both SV, and to a lesser degree, HR combined to raise the CO relative to vehicle-infused rats. Systemic vascular resistance fell significantly relative to baseline and to vehicle infusion (Fig. 4A), while MAP remained unchanged (Fig. 3D). Global AC as measured by the area method significantly increased relative to baseline and to vehicle infusion (Fig. 4B). There was no significant change in pulse pressure; however, the ratio of stroke volume-to-pulse pressure, another index of arterial compliance, increased significantly during the infusion of low dose rhRLX relative to baseline and to vehicle infusion (Fig. 4C).

For variables that showed a significant change with low dose rhRLX administration (i.e., significant *P* value for relaxin and/or interaction), we further examined the time course of these changes. This was accomplished by *post hoc* pairwise comparisons of data at different time points (Fisher's LSD). Both CO and SV were significantly higher than baseline at day 3. While SV continued to increase until day 8 ($P < 0.05$, day 8 vs. day 3) (Fig. 3C), there were no significant changes with time in CO beyond day 3 (Fig. 3A). This was partly a result of a small, but insignificant, fall in HR from day 3 to day 8 (Fig. 3B). SVR and both measures of global AC were significantly altered at day 3; thereafter there were no further significant changes (Fig. 4). In general, maximal changes in systemic hemodynamics and arterial properties following low

dose rhRLX administration were observed at the earliest time point examined (day 3), with no further temporal alterations.

Combining all of the time points during administration of low dose rhRLX yielded an overall increase in CO and global AC of 19.2 $\pm$ 4.8 and 21.4 $\pm$ 3.6 % above baseline, respectively, and an overall decrease in SVR of 15.5 $\pm$ 2.4 % below baseline (all $P < 0.01$ vs. baseline). Serum rhRLX and osmolality were 14 $\pm$ 2 ng/ml and 284 $\pm$ 2 mOsm/kg water, respectively. The latter significantly decreased compared to vehicle infusion ($P < 0.05$ by Student's "t" test).

Table 3. Absolute Values of Systemic Hemodynamics and Arterial Properties in *Female Rats* Administered Low Dose rhRLX

Days After Minipump	Δ_T (^oC)	CO* (mL/min)	HR (bpm)	SV* (mL)	AC_{area}* (μl/mmHg)	SVR* (mmHg·s/mL)	MAP (mmHg)
Baseline	0.34±0.02	128±2	417±6	0.31±0.01	6.2±0.3	51±2	108.9±3.4
2-3	0.31±0.01	151±6	436±9	0.35±0.01	7.2±0.3	43±3	107.3±3.1
6	0.31±0.01	149±7	419±6	0.36±0.02	7.1±0.5	46±3	111.3±3.2
8	0.31±0.01	159±7	427±11	0.37±0.02	7.4±0.5	44±2	114.1±3.6
10	0.31±0.01	153±5	418±10	0.37±0.01	7.7±0.5	44±2	112.1±3.8

Mean±SEM. N=6 rats (longitudinal measurements were made in each animal at the time-points specified above). Two baseline measurements were made on days 5 and 7 after surgery. These results were averaged for each rat. Δ_T, change in blood temperature after injection of Ringer's solution into the right heart; CO, cardiac output; HR, heart rate; SV, stroke volume; AC_{area}, global arterial compliance calculated using area method; SVR, systemic vascular resistance; MAP, mean arterial pressure. *$P < 0.05$ by single factor repeated measures ANOVA.

5.1.4 *Female Rats* Administered Medium Dose rhRLX (25 μg/h)

Portions of this work have been previously published elsewhere [50]. The absolute values for systemic hemodynamics and arterial properties from female rats administered medium dose rhRLX are shown in **Table 4**. The results for the medium dose infusion were comparable to the low dose administration in direction, but were somewhat less, although not significantly so, in magnitude. The temporal analysis of changes in individual variables with medium dose rhRLX was performed in a manner similar to that for the low dose rhRLX. Once again, CO (**Figure 5A**), SV (**Figure 5C**), SVR (**Figure 6A**), and global AC (SV/PP method) (**Figure 6C**) were maximally altered by the earliest time point examined (day 3), with no further significant changes thereafter. The temporal response of global AC as calculated by the area method (**Figure 6B**) deviated slightly from this general pattern as AC_{area} at day 6 was not significantly different from that at baseline. Although we do not have a specific explanation, we believe this to be an aberration. This belief is based on the observations that the second measure of global AC at all time points (Fig. 6C) and AC_{area} at day 3 (Fig. 6B) were significantly higher than baseline.

Combining all of the time points during administration of medium dose rhRLX yielded an overall increase in CO and global AC of 14.1 $\pm$ 3.2 and 15.6 $\pm$ 4.7 % above baseline, respectively, and an overall decrease in SVR of 9.7 $\pm$ 2.4 % below baseline (all $P < 0.02$). Serum relaxin and osmolality were 36 $\pm$ 3 ng/ml and 287 $\pm$ 1 mOsm/kg water, respectively. The latter significantly decreased compared to vehicle infusion ($P < 0.05$ by Student's "t" test).

Table 4. Absolute Values of Systemic Hemodynamics and Arterial Properties in *Female Rats* Administered Medium Dose rhRLX

Days After Minipump	Δ_T (^oC)	CO* (mL/min)	HR (bpm)	SV (mL)	AC_{area}* (μl/mmHg)	SVR* (mmHg.s/mL)	MAP (mmHg)
Baseline	0.37±0.02	129±6	438±10	0.30±0.02	7.7±0.7	53±3	111.6±3.7
2-3	0.33±0.02	141±7	454±13	0.31±0.02	8.5±0.8	49±4	110.2±4.9
6	0.35±0.02	147±4	432±10	0.34±0.01	8.1±0.4	48±2	116.9±3.8
8	0.35±0.03	150±5	451±9	0.33±0.01	9.4±0.7	45±2	112.1±2.8
10	0.34±0.02	146±9	442±6	0.33±0.02	9.2±1.0	48±3	115.2±5.8

Mean±SEM. N=7 rats (longitudinal measurements were made in each animal at the time-points specified above). Two baseline measurements were made on days 5 and 7 after surgery. These results were averaged for each rat. Δ_T, change in blood temperature after injection of Ringer's solution into the right heart; CO, cardiac output; HR, heart rate; SV, stroke volume; AC_{area}, global arterial compliance calculated using area method; SVR, systemic vascular resistance; MAP, mean arterial pressure. *$P < 0.05$ by single factor repeated measures ANOVA.

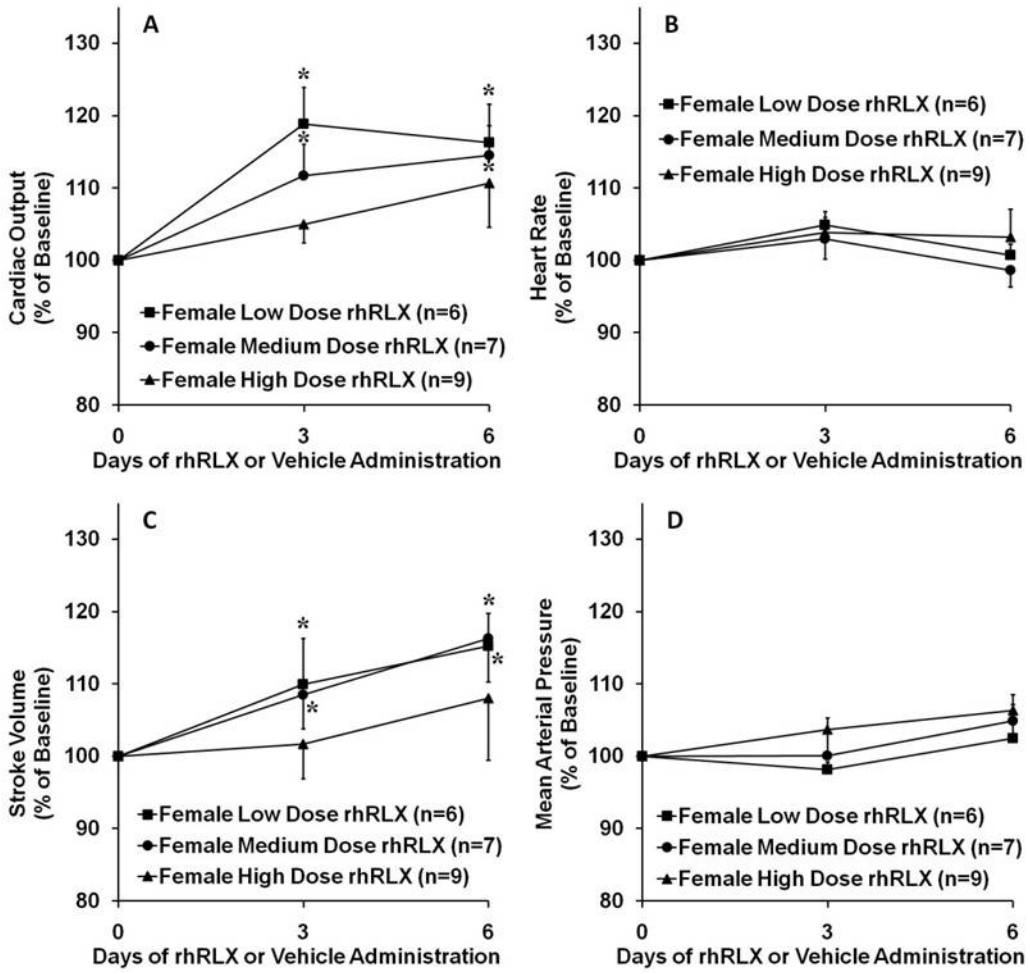

Figure 5. Systemic Hemodynamics in Conscious *Female Rats*: Dose Response

Temporal changes in systemic hemodynamics in response to three doses of recombinant human relaxin administration in female rats: low (4 μg/h), medium (25 μg/h), and high (50 μg/h). cardiac output (**A**), heart rate (**B**), stroke volume (**C**), and mean arterial pressure (**D**) data are presented as percentages of baseline. * $P < 0.05$ *vs*. baseline (post-hoc Fisher's LSD).

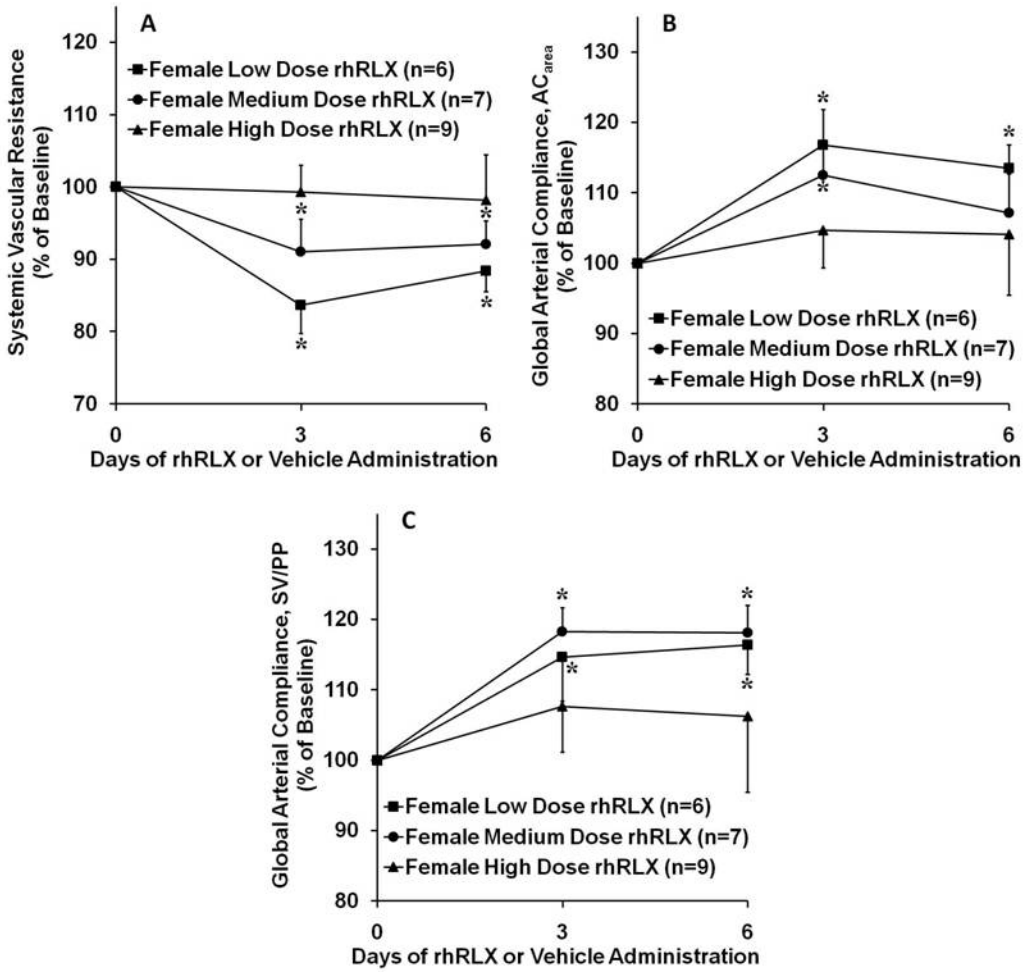

Figure 6. Systemic Arterial Properties in Conscious *Female Rats*: Dose Response.

Temporal changes in systemic arterial properties in response to three doses of recombinant human relaxin administration in female rats: low (4 μg/h), medium (25 μg/h), and high (50 μg/h). Systemic vascular resistance (**A**) and two measures of global arterial compliance, AC_{area} (**B**) and SV/PP (**C**), data are presented as percentages of baseline. * $P < 0.05$ *vs*. baseline (post-hoc Fisher's LSD).

5.1.5 *Female Rats* Administered High Dose rhRLX (50 μg/h)

Portions of this work have been previously published elsewhere [50]. Absolute values of systemic hemodynamics and arterial properties from female rats administered high dose rhRLX are listed in **Table 5** and their temporal patterns following the initiation of rhRLX infusion are depicted in Figs. 5 and 6. Serum rhRLX concentration for the high dose infusion (71.5 $\pm$ 1.6 ng/ml) was much greater than that of low (14 $\pm$ 2 ng/ml) and medium (36 $\pm$ 3 ng/ml) dose infusion. However, there was no change from baseline in any of the systemic hemodynamics (Fig. 5) or arterial properties (Fig. 6). Thus, the effects of rhRLX on systemic hemodynamics and arterial properties are apparently biphasic whereby, low (4 μg/ml) and medium (25 μg/ml) doses are effective, but high doses are not (50 μg/ml).

Table 5. Absolute Values of Systemic Hemodynamics and Arterial Properties in *Female Rats* Administered High Dose rhRLX

Days after minipump	Δ_T (^oC)	CO (mL/min)	HR (bpm)	SV (mL)	AC_{area} (μl/mmHg)	SVR (mmHg.s/mL)	MAP* (mmHg)
Baseline	0.34±0.02	134±5	425±14	0.32±0.02	7.0±0.4	53±2	115.9±2.7
3	0.32±0.02	141±6	438±6	0.32±0.01	7.2±0.3	52±2	120.2±3.3
6	0.31±0.01	146±6	437±8	0.33±0.02	7.4±0.4	51±3	121.1±2.8

Mean±SEM. N=8 rats (longitudinal measurements were made in each animal at the time-points specified above). Two baseline measurements were made on days 5 and 7 after surgery. These results were averaged for each rat. Δ_T, change in blood temperature after injection of Ringer's solution into the right heart; CO, cardiac output; HR, heart rate; SV, stroke volume; AC_{area}, global arterial compliance calculated using area method; SVR, systemic vascular resistance; MAP, mean arterial pressure. *$P < 0.05$ by single factor repeated measures ANOVA.

5.1.6 **Summary**

Our data to this point indicate that chronic administration of rhRLX to nonpregnant female rats results in an increase in CO and a reduction in systemic arterial load in a biphasic manner. Previous work indicated that the vasodilatory effects of relaxin in female rats were also observed in male rats [24]. Accordingly, we next examined the effects of relaxin on systemic hemodynamics and arterial properties in male rats.

5.2 SYSTEMIC HEMODYNAMICS AND ARTERIAL PROPERTIES IN CONSCIOUS MALE RATS

Specific Aim 2. To determine systemic hemodynamics and arterial load in conscious, *male rats* administered rhRLX and compare these responses to those observed in female rats.

5.2.1 ***Male Rats*** **Administered Low Dose rhRLX (4 μg/h)**

Portions of this work have been previously published elsewhere [50]. The temporal patterns of systemic hemodynamic variables, expressed as a percentage of baseline values, are illustrated in **Figure 7** and absolute values of these variables are presented in **Table 6**. For the purpose of comparison, the data from female rats administered low dose rhRLX are also presented in Fig. 7. Low dose rhRLX significantly increased CO relative to baseline in male rats (Fig. 7A). There was a slight (~6%), but statistically insignificant, rise in HR in the relaxin-treated male rats (Fig. 7B). However, there was a greater rise in SV (Fig. 7C) indicating that the

elevation in CO resulted primarily from an increase in SV and, to a lesser degree, from a rise in HR. Mean arterial pressure was not significantly changed during rhRLX infusion (Fig. 7D). At the final time point (i.e., day 10 after the onset of rhRLX infusion), there was no statistically significant difference between the effects of rhRLX administration on systemic hemodynamics in the male and female rats.

The temporal effects of rhRLX infusion on systemic arterial properties in male rats, expressed as a percentage of baseline values, are depicted in **Figure 8**. Once again data from female rats are also shown for comparison. Systemic vascular resistance fell significantly relative to baseline (Fig. 8A), while both measures of arterial compliance (AC_{area} and SV/PP) were significantly increased (Figs. 8B and 8C). At the final time point (i.e., day 10 after the onset of rhRLX infusion), the changes in systemic arterial properties were not statistically different between male and female rats.

Although the final (peak) responses were similar, relaxin-induced changes in male rats tended to be delayed, especially for SVR (Fig. 8A) and AC_{area} (Fig. 8B). We expected the two-way analysis of variance to yield a significant interaction effect. However this was not the case because the difference between male and female responses was typically confined to the first time point following the initiation of rhRLX infusion (i.e., day 3) and we do not have sufficient power to detect this single time point difference. In some instances, the interaction effect did come close to being significant, e.g., interaction for HR and SVR had *P* values of 0.09 and 0.14, respectively.

Combining all of the time points during administration of rhRLX yielded overall increases in CO and global AC of 20.5 $\pm$ 4.2 and 19.4 $\pm$ 6.9% from baseline, respectively, and an overall decrease in SVR of 12.7 $\pm$ 3.9% from baseline (all $P < 0.05$ *vs*. baseline). There was no

statistical difference between these results in male rats and those we observed in female rats. Serum rhRLX was 17.7 $\pm$ 1.1 ng/ml, a value similar to that observed in female rats administered the same rhRLX regimen, 14.0 $\pm$ 2.0 ng/ml.

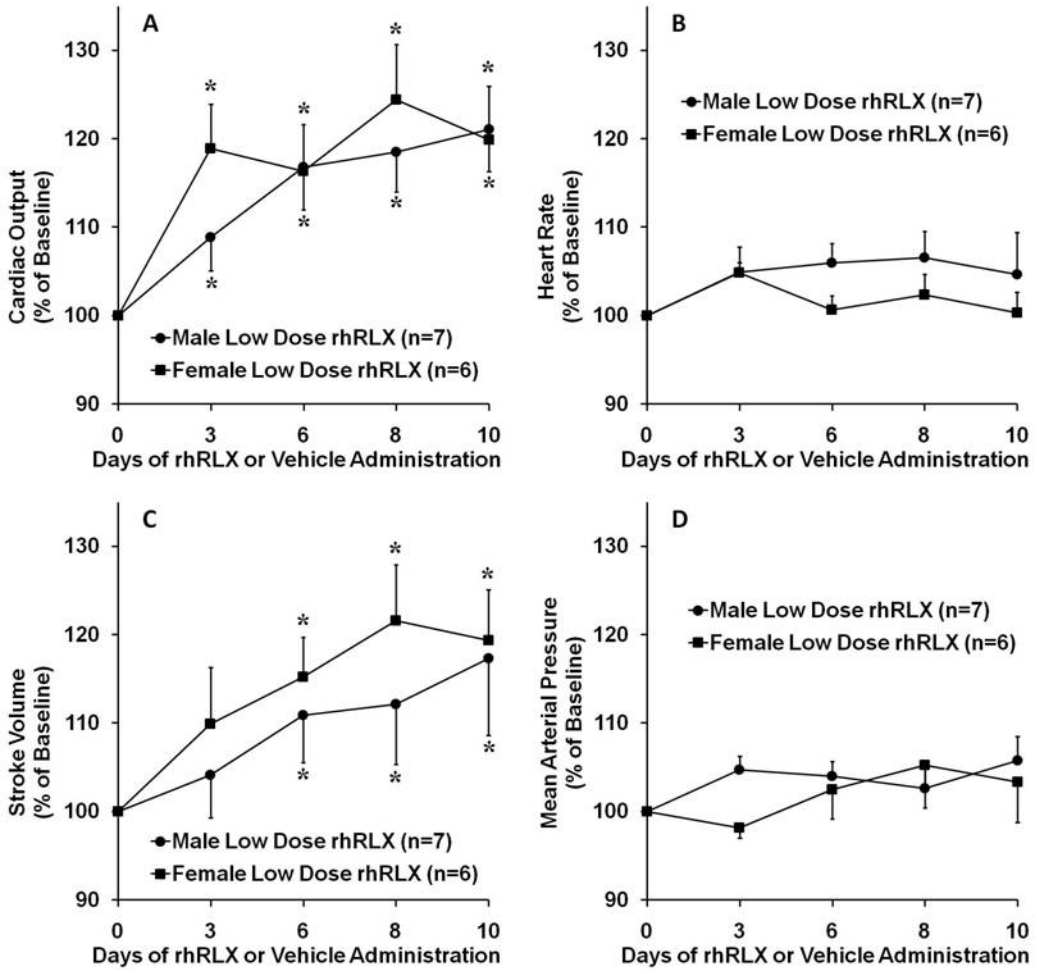

Figure 7. Systemic Hemodynamics in Conscious *Male Rats* Administered Low Dose rhRLX.

Temporal changes in systemic hemodynamics in response to low dose (4 μg/h) recombinant human relaxin administration in male and female rats. cardiac output (**A**), heart rate (**B**), stroke volume (**C**), and mean arterial pressure (**D**) data are presented as percentages of baseline. * $P <$ 0.05 *vs*. baseline (post-hoc Fisher's LSD). Although our previous analysis (Figure 3) of SV response in female rats alone indicated a significant increase at day 3, the simultaneous analysis of male and female responses did not yield a significant interaction term. Therefore, significant increments in SV are shown only for days 6, 8, and 10.

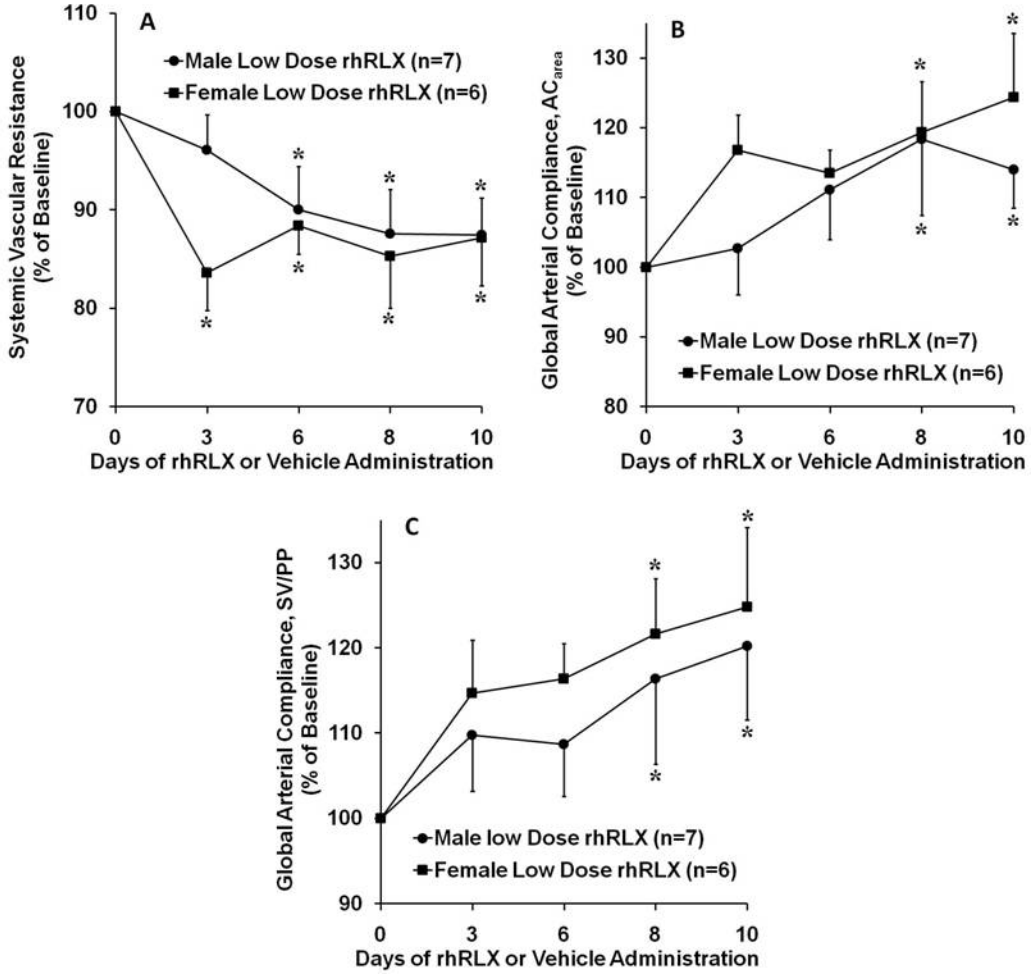

Figure 8. Systemic Arterial Properties in Conscious *Male Rats* Administered Low Dose rhRLX

Temporal changes in systemic arterial properties in response to low dose (4 μg/h) recombinant human relaxin administration in male and female rats. Systemic vascular resistance (**A**) and two measures of global arterial compliance, AC_{area} (**B**) and SV/PP (**C**), data are presented as percentages of baseline. * $P < 0.05$ *vs*. baseline (post-hoc Fisher's LSD). Although our previous analysis (Figure 4) of AC_{area} and SV/PP responses in female rats alone indicated significant increases at days 3 and 6, the simultaneous analyses of male and female responses did not yield significant interaction terms. Therefore, significant increments in AC_{area} and SV/PP are shown only for days 8 and 10.

Table 6. Absolute Values of Systemic Hemodynamics and Arterial Properties in *Male Rats* Administered Low Dose rhRLX

Days after minipump	Δ_T (^oC)	CO* (mL/min)	HR* (bpm)	SV* (mL)	AC_{area}* (μl/mmHg)	SVR* (mmHg.s/mL)	MAP (mmHg)
Baseline	0.32±0.03	148±9	416±12	0.36±0.03	7.5±0.6	49±3	115.8±2.4
3	0.31±0.01	160±6	440±8	0.36±0.01	7.6±0.5	46±1	121.3±3.6
6	0.29±0.02	169±4	441±6	0.38±0.01	7.9±0.3	43±1	119.9±1.7
8	0.27±0.02	178±6	445±4	0.40±0.01	8.7±0.4	41±1	118.8±2.0
10	0.28±0.02	183±11	442±5	0.41±0.02	8.8±0.5	41±2	121.6±2.6

Mean±SEM. N=7 rats (longitudinal measurements were made in each animal at the time-points specified above). Two baseline measurements were made on days 5 and 7 after surgery. These results were averaged for each rat. Δ_T, change in blood temperature after injection of Ringer's solution into the right heart; CO, cardiac output; HR, heart rate; SV, stroke volume; AC_{area}, global arterial compliance calculated using area method; SVR, systemic vascular resistance; MAP, mean arterial pressure. *$P < 0.05$ by single factor repeated measures ANOVA.

5.2.2 **Summary**

Chronic administration of low dose rhRLX to conscious male rats results in an increase in CO and a reduction in systemic arterial load comparable to female rats. This finding in combination with our other data (see **Section 5.1**) indicate that administration of rhRLX to nonpregnant rats elicits pregnancy-like changes in the systemic circulation. We next examined the role of relaxin in mediating the cardiovascular adaptations to pregnancy.

5.3 SYSTEMIC HEMODYNAMICS AND ARTERIAL PROPERTIES IN CONSCIOUS PREGNANT RATS

Specific Aim 3. To determine systemic hemodynamics and arterial load in conscious, *mid and late-pregnant rats* administered control or relaxin neutralizing antibodies.

5.3.1 *Mid-Pregnant Rats* Administered Relaxin Neutralizing Antibodies

Portions of this work have been previously published elsewhere [51]. Systemic hemodynamic variables for midterm pregnant and virgin rats are illustrated in **Figure 9**. There was no statistically significant difference in HR or MAP among the virgin rats, the rats administered relaxin neutralizing antibodies (MCA1), and those administered the control antibodies (MCAF; Fig. 9B & 9D). Stroke volume (Fig. 9C) and CO (Fig. 9A) were both significantly increased in midterm pregnant rats administered the irrelevant MCAF antibody against fluorescein compared to virgin controls (both $P < 0.05$). Importantly, the SV (0.38±0.02 ml) and CO (165±5 ml/min) of the midterm pregnant rats administered the PBS vehicle/diluent for the antibodies were comparable to the values observed in the control MCAF antibody-treated gravid rats (both P = NS). In contrast, both SV and CO were significantly decreased in midterm pregnant rats treated with rat relaxin neutralizing antibodies compared to the gravid animals administered MCAF antibody (both $P < 0.05$) and comparable to virgin levels (both P = NS).

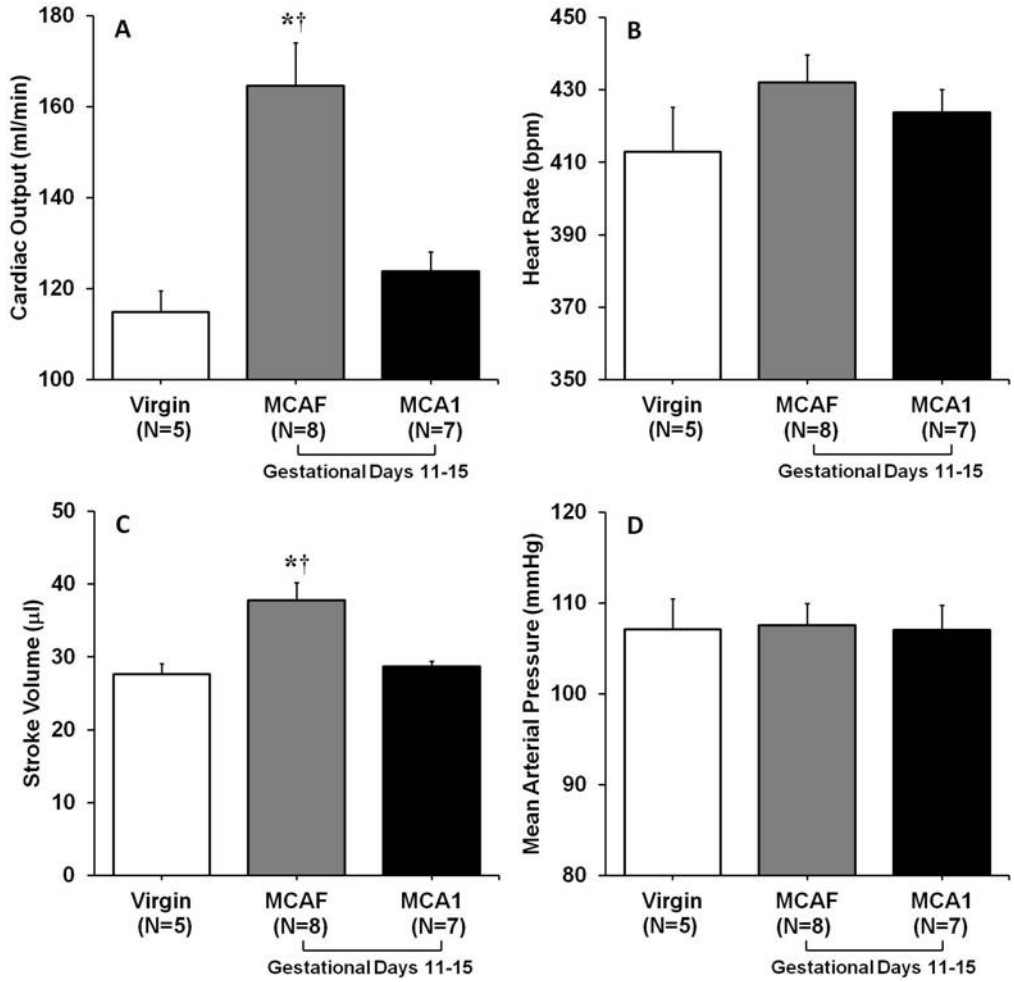

Figure 9. Systemic Hemodynamics in *Mid-Pregnant Rats* Administered Relaxin Neutralizing Antibodies

Systemic hemodynamics in mid-pregnant rats administered relaxin-neutralizing antibody (MCA1) or control antibody (MCAF), and virgin rats. Mid-pregnant rats were administered daily injections of antibodies beginning on gestational day 8. (**A**) Cardiac output, (**B**) heart rate, (**C**) stroke volume, and (**D**) mean arterial pressure. * $P < 0.05$ *vs*. MCA1 (post-hoc Fisher's LSD). † $P < 0.05$ *vs*. Virgin (post-hoc Fisher's LSD).

Systemic arterial properties for midterm pregnant and virgin rats are illustrated in **Figure 10**. Systemic vascular resistance in the MCAF-treated midterm pregnant rats was significantly lower compared to the virgin controls. Treatment with relaxin-neutralizing antibodies completely eliminated this pregnancy-associated reduction in SVR (Fig. 10A). Global AC as measured by AC_{area} and SV/PP was significantly increased in the MCAF-treated pregnant rats as compared to the virgin control group. Again, treatment with relaxin neutralizing antibodies completely abolished this pregnancy-associated increase in global AC (Figs. 10B & 10C). Systemic vascular resistance and global AC for the MCAF-treated rats were similar to levels observed in the control pregnant rats administered PBS (SVR: 39.4±1.7 mmHg.s/ml; AC_{area}: 9.7±0.5 μl/mmHg; SV/PP: 11.6±0.7 μl/mmHg; both P = NS).

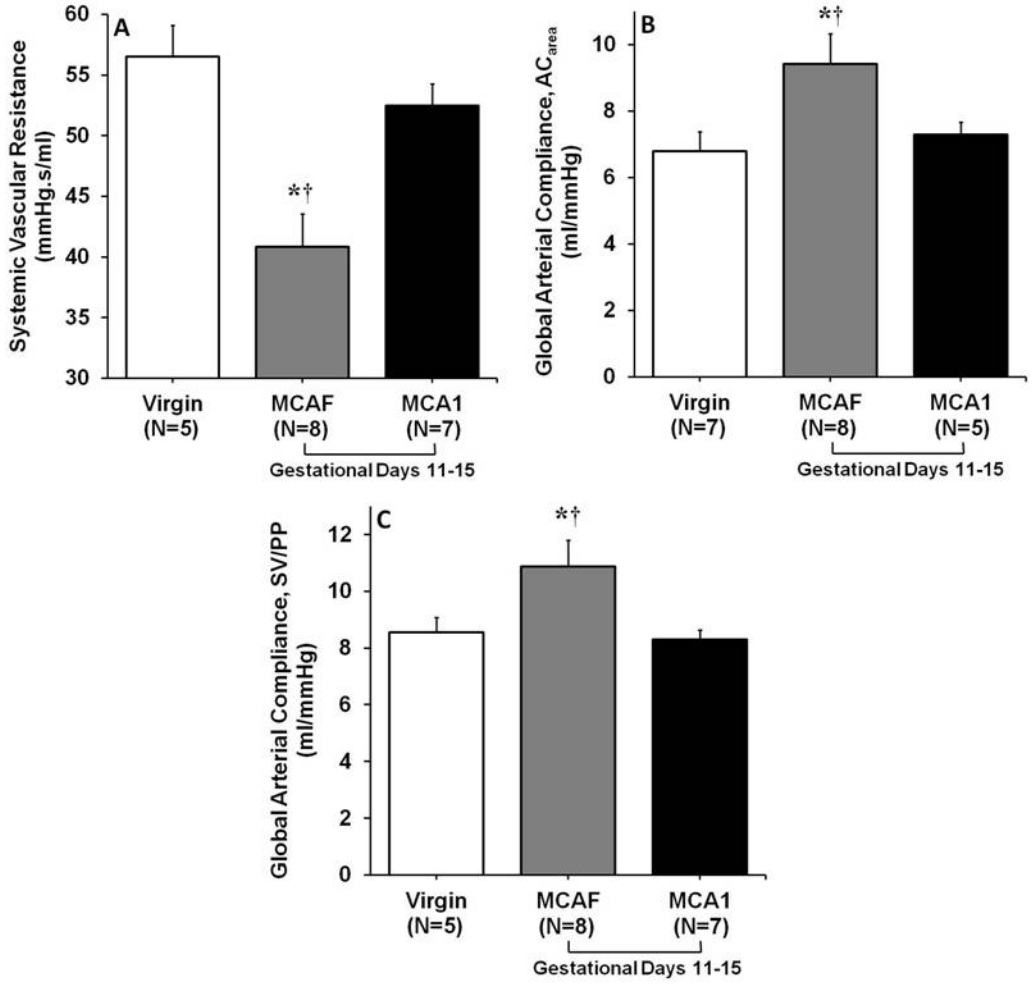

Figure 10. Systemic Arterial Properties in *Mid-Pregnant Rats* Administered Relaxin Neutralizing Antibodies

Systemic arterial properties in mid-pregnant rats administered relaxin-neutralizing antibody (MCA1) or control antibody (MCAF), and virgin rats. Mid-pregnant rats were administered daily injections of antibodies beginning on gestational day 8. (**A**) Systemic vascular resistance, and two measures of global arterial compliance, (**B**) AC_{area} and (**C**) SV/PP. * $P < 0.05$ *vs*. MCA1 (post-hoc Fisher's LSD). † $P < 0.05$ *vs*. Virgin (post-hoc Fisher's LSD).

5.3.2 *Late-Pregnant Rats* Administered Relaxin Neutralizing Antibodies

We began investigating the role of relaxin in maintaining the cardiovascular adaptations to pregnancy during the late stages of gestation by assessing systemic hemodynamics and arterial properties from late pregnant rats administered relaxin neutralizing antibodies. It is important to note the data presented here are results from our preliminary work on this subject and will represent only a subset of the final study. Due to time constraints, we were only able to study a few animals in the antibody-treated groups (3 MCA1-treated rats and 1 MCAF-treated rat; antibodies were administered beginning on day 8 of gestation) prior to the preparation of this document. Of note, data from 1 MCAF-treated rat was combined with data from 6 control late pregnant rats administered the PBS vehicle as our previous work has shown that MCAF antibody does not alter hemodynamics or arterial properties (see **Section 5.1.7**).

Systemic hemodynamic variables for late-pregnant and virgin rats are illustrated in **Figure 11**. Similar to mid-pregnant rats there was no statistically significant difference in MAP among the control, virgin and MCA1 antibody-treated pregnant groups (Fig. 11D). Also similar to mid-pregnant rats, CO (Fig. 11A) was significantly increased in control late-pregnant rats compared to virgin rats. Further, CO was significantly lower in late-pregnant rats treated with MCA1 relaxin neutralizing antibodies compared to the control late-pregnant animals. However, unlike midterm pregnant rats, the relaxin-neutralizing antibody did not completely eliminate the pregnancy-associated increase in CO as there was still a significant increase in CO from virgin levels in the MCA1-treated rats. Also unlike midterm pregnant rats, HR was significantly elevated in control late-pregnant rats compared to MCA1-treated and virgin rats and, although not statistically significant, the MCA1-treated rats exhibited a slightly higher HR than the virgin

animals (Fig. 11B). Finally, a similar pattern was observed for SV although this pattern did not prove to be statistically significant (Fig. 11C).

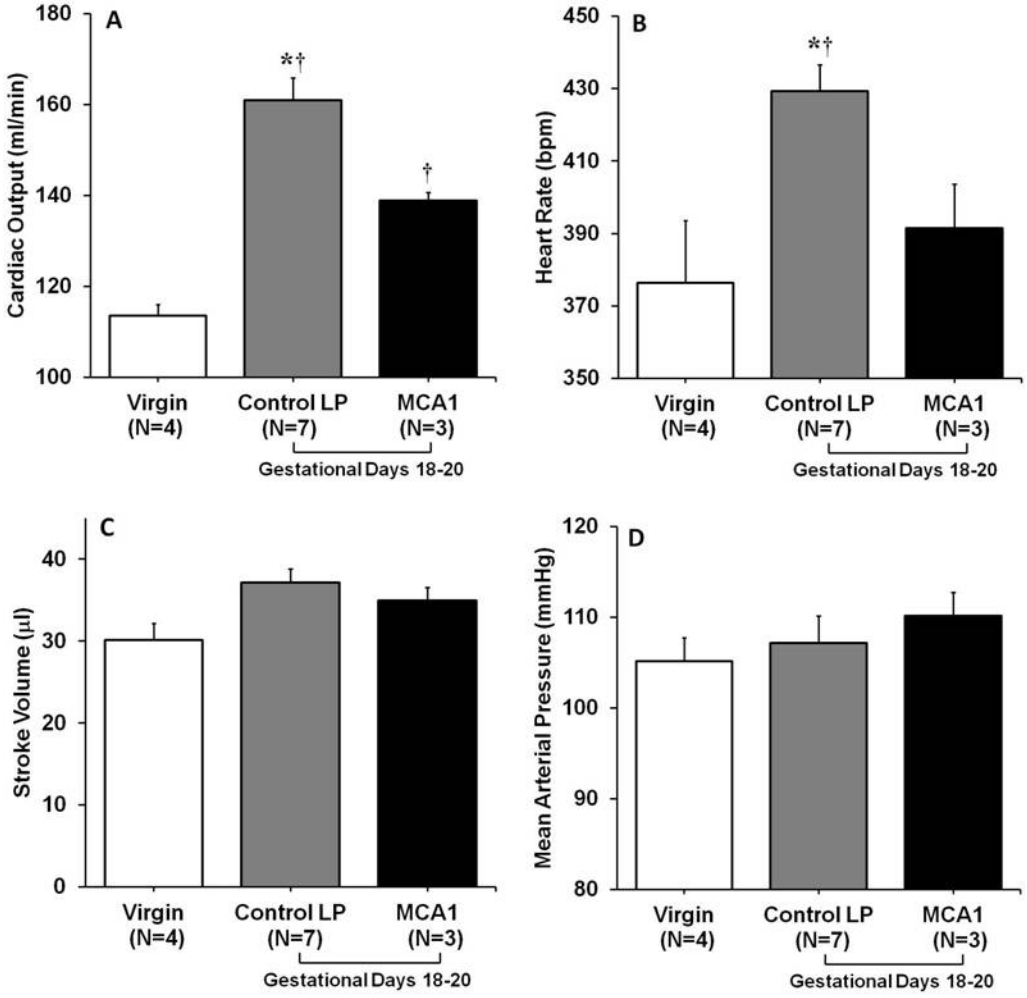

Figure 11. Systemic Hemodynamics in *Late-Pregnant Rats* Administered Relaxin Neutralizing Antibodies

Systemic hemodynamics in late-pregnant rats administered relaxin-neutralizing antibody (MCA1) or control antibody (MCAF), and virgin rats. Late-pregnant rats were administered daily injections of antibodies beginning on gestational day 8. (**A**) Cardiac output, (**B**) heart rate, (**C**) stroke volume, and (**D**) mean arterial pressure. * $P < 0.05$ *vs*. MCA1 (post-hoc Fisher's LSD). † $P < 0.05$ *vs*. Virgin (post-hoc Fisher's LSD).

Systemic arterial properties for late-pregnant and virgin rats are illustrated in **Figure 12**. As expected, SVR in the control late-pregnant rats was significantly lower compared to the virgin rats. However, treatment with relaxin-neutralizing antibodies only partially eliminated this pregnancy-associated reduction in SVR. Thus, SVR in the MCA1-treated late-pregnant rats was higher than the control late pregnant animals yet still significantly reduced from the virgin group (Fig. 12A). Similarly, global AC as measured by AC_{area}, was significantly increased in the control late-pregnant rats as compared to the virgin group and treatment with relaxin neutralizing antibodies abolished this pregnancy-associated increase (Figs. 12B). Although global AC in the MCA1-treated group was slightly elevated from virgin levels, this increase did not reach statistical significance. A similar pattern was observed in SV/PP although there were no statistically significant differences among the three groups (Fig. 12C).

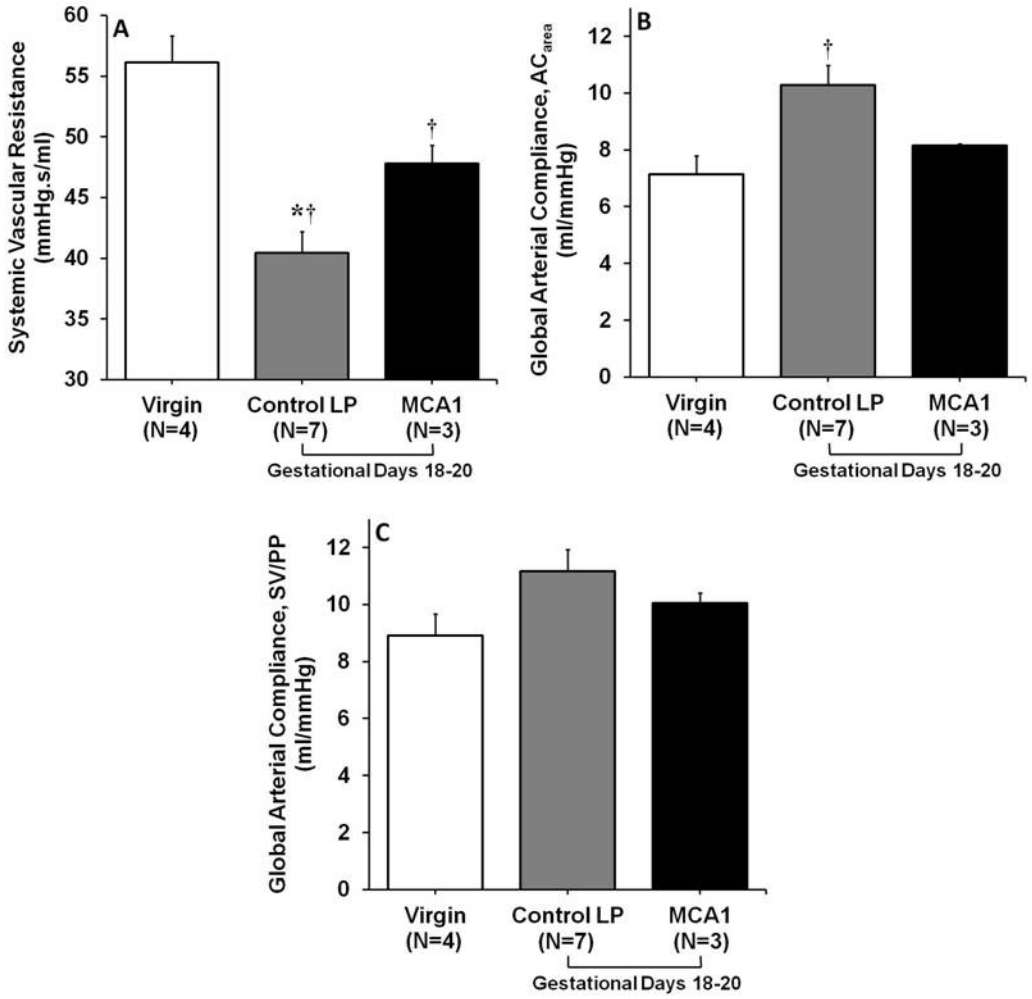

Figure 12. Systemic Arterial Properties in *Late-Pregnant Rats* Administered Relaxin Neutralizing Antibodies

Systemic arterial properties in late-pregnant rats administered relaxin-neutralizing antibody (MCA1) or control antibody (MCAF), and virgin rats. Late-pregnant rats were administered daily injections of antibodies beginning on gestational day 8. (**A**) Systemic vascular resistance, and two measures of global arterial compliance, (**B**) AC_{area} and (**C**) SV/PP. * $P < 0.05$ *vs*. MCA1 (post-hoc Fisher's LSD). † $P < 0.05$ *vs*. Virgin (post-hoc Fisher's LSD).

5.3.3 **Summary**

Our data here indicate that relaxin triggers the adaptations in the systemic circulation during the early stages of pregnancy. Our work in late pregnant rats suggest that although relaxin still plays a role in maintaining these adaptations during the late stages of pregnancy, it is most likely not the only mediator. Next, we examined whether the relaxin-mediated increase in global AC is a result of altered passive arterial mechanical properties.

5.4 PASSIVE ARTERIAL MECHANICAL PROPERTIES

Specific Aim 4A. To evaluate the passive mechanical properties of small renal and external iliac arteries isolated from rhRLX-treated, *nonpregnant female rats and mice*.

Specific Aim 4B. To evaluate the passive mechanical properties of small renal and messenteric arteries isolated from *mid-pregnant rats* administered control or relaxin neutralizing antibodies.

5.4.1 **Uniaxial (Circumferential) Stress-Strain Analysis**

These *in vitro* experiments were performed to examine the effects of relaxin on passive (i.e., in the absence of active smooth muscle tone) mechanical properties of the isolated arteries. As mentioned before, primary measurements consisted of vessel inner and outer diameters at various levels of intraluminal pressure (see **Section 4.3.3**). Circumferential wall stress (σ) along with midwall radius (R_m) and strain (ε_m) were calculated from these primary measurements and the relationships between these variables were used to quantify vessel wall elastic behavior.

5.4.1.1 Small Renal Arteries from *Female Rats* Administered Low Dose rhRLX (4 μg/h)

Portions of this work have been previously published elsewhere [48]. **Figure 13** illustrates the average σ-R_m and σ-ε_m relationships for small renal arteries isolated from female rats administered low dose rhRLX or vehicle. The σ-R_m relationship (Fig. 13A) was significantly different between the two groups ($P < 0.001$ by analysis of excess variance) such that σ was smaller for a given R_m in the relaxin-treated group. In contrast, there was no difference in the σ-ε_m relationships of these groups (Fig. 13B). Finally, arteries from rhRLX-treated rats were characterized by significantly increased unstressed muscle area (A_{M0}) when compared to arteries from control rats (**Figure 14**).

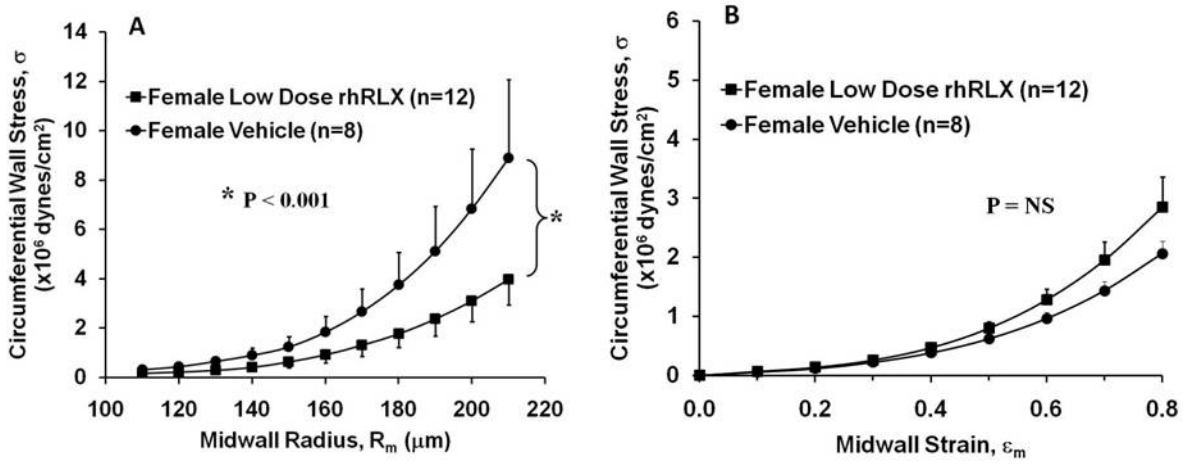

Figure 13. Stress-Midwall Radius and Stress-Midwall Strain Relationships of Small Renal Arteries from *Female Rats* Administered Low Dose rhRLX.

(A) Circumferential stress (σ)-midwall radius (R_m) and **(B)** σ-strain (ε_m) relationships for small renal arteries isolated from rats treated with low dose rhRLX (4 μg/h) or vehicle for 5 days. Original data from each animal were first fitted to a 3rd order polynomial, which was then used to obtain interpolated data (i.e., σ values for a given R_m or ε_m). Interpolated σ data at a common value of R_m or ε_m were averaged over all animals within a group to yield the relationships shown here. * $P < 0.001$ by analysis of excess variance using the original data.

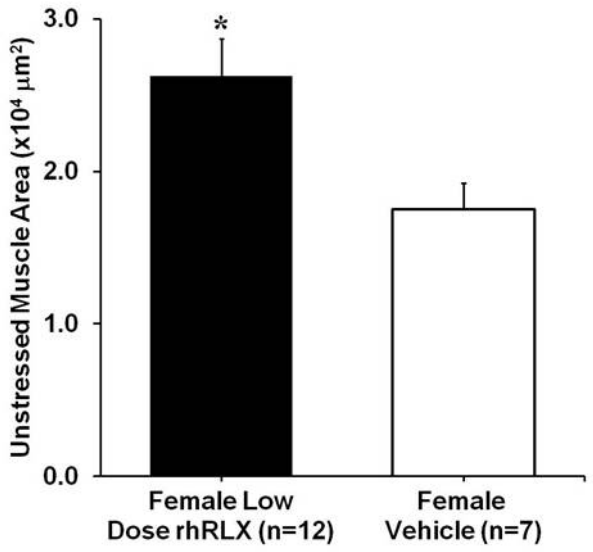

Figure 14. Unstressed Muscle Area of Small Renal Arteries from *Female Rats* Administered Low Dose rhRLX

Unstressed muscle area (A_{M0}) of small renal arteries isolated from rats treated with low dose rhRLX (4 μg/h) or vehicle for 5 days. A_{M0} computed from measurements of the inner and outer diameters, and wall thickness in the unloaded configuration. * $P < 0.05$ *vs*. vehicle group.

5.4.1.2 Small Renal Arteries from *Female Mice* Administered Low Dose rhRLX (1 μg/h)

Portions of this work have been previously published elsewhere [52]. We found comparable results in small renal arteries isolated from rhRLX-treated and vehicle-administered (control) mice (**Figures 15 and 16**). Specifically, arteries from rhRLX-treated mice were characterized by significantly lesser magnitudes of σ for a given R_m when compared to control mice (Figs. 15A). In addition, there were no differences between the σ-ε_m relationships of small renal arteries from rhRLX-treated versus control mice. Of note, although rhRLX-treated mice exhibited slightly increase A_{M0} compared to control mice, this increase was not statistically significant (**Figure 16**).

5.4.1.3 Small Renal Arteries *Male Untreated $Rlx^{-/-}$ Mice*

Small renal arteries from $Rlx^{+/+}$ mice were characterized by significantly lesser magnitudes of σ for a given R_m when compared to control and $Rlx^{-/-}$ mice with no differences between the σ-ε_m relationships (**Figure 17**). Analogous to our findings in rats, arteries from $Rlx^{+/+}$ mice were also characterized by significantly increased A_{M0} when compared to $Rlx^{-/-}$ mice (**Figure 18**).

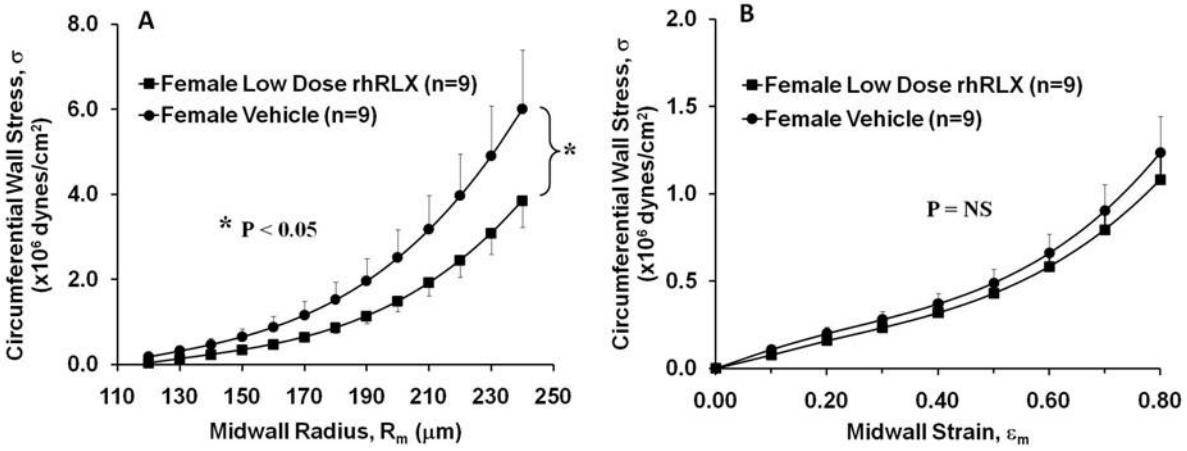

Figure 15. Stress-Midwall Radius and Stress-Midwall Strain Relationships of Small Renal Arteries from *Female Mice* Administered Low Dose rhRLX

(A) Circumferential stress (σ)-midwall radius (R_m) and **(B)** σ-strain (ε_m) relationships for small renal arteries isolated from mice treated with low dose rhRLX (1 μg/h) or vehicle for 5 days. Original data from each animal were first fitted to a 3rd order polynomial, which was then used to obtain interpolated data (i.e., σ values for a given R_m or ε_m). Interpolated σ data at a common value of R_m or ε_m were averaged over all animals within a group to yield the relationships shown here. * $P < 0.05$ by analysis of excess variance using the original data.

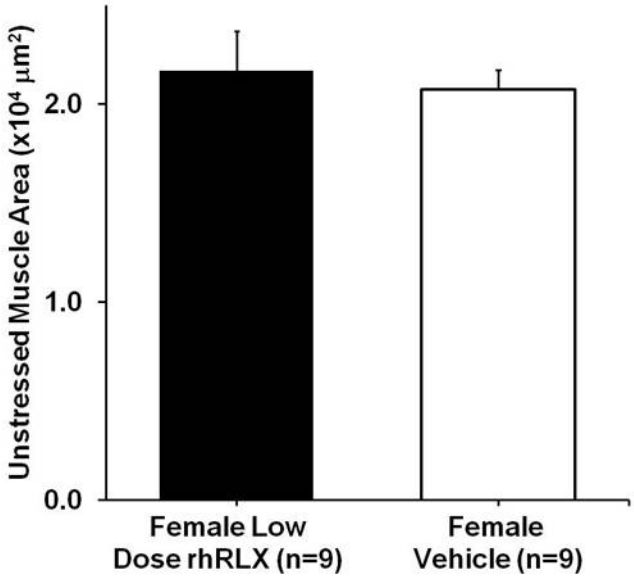

Figure 16. Unstressed Muscle Area of Small Renal Arteries from *Female Mice* Administered Low Dose rhRLX

Unstressed muscle area (A_{M0}) of small renal arteries isolated from mice treated with low dose rhRLX (1 μg/h) or vehicle for 5 days. A_{M0} computed from measurements of the inner and outer diameters, and wall thickness in the unloaded configuration.

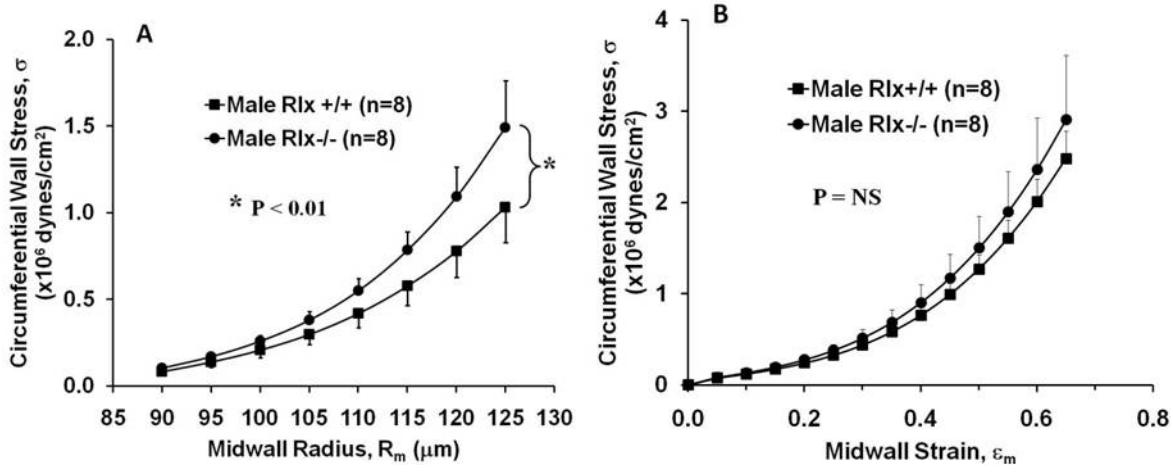

Figure 17. Stress-Midwall Radius and Stress-Midwall Strain Relationships of Small Renal Arteries from *Male $Rlx^{+/+}$ and $Rlx^{-/-}$ Mice*

(A) Circumferential stress (σ)-midwall radius (R_m) and **(B)** σ-strain (ε_m**)** relationships for small renal arteries isolated from $Rlx^{+/+}$ and $Rlx^{-/-}$, untreated mice. Original data from each animal were first fitted to a 3rd order polynomial, which was then used to obtain interpolated data (i.e., σ values for a given R_m or ε_m). Interpolated σ data at a common value of R_m or ε_m were averaged over all animals within a group to yield the relationships shown here. * $P < 0.01$ by analysis of excess variance using the original data.

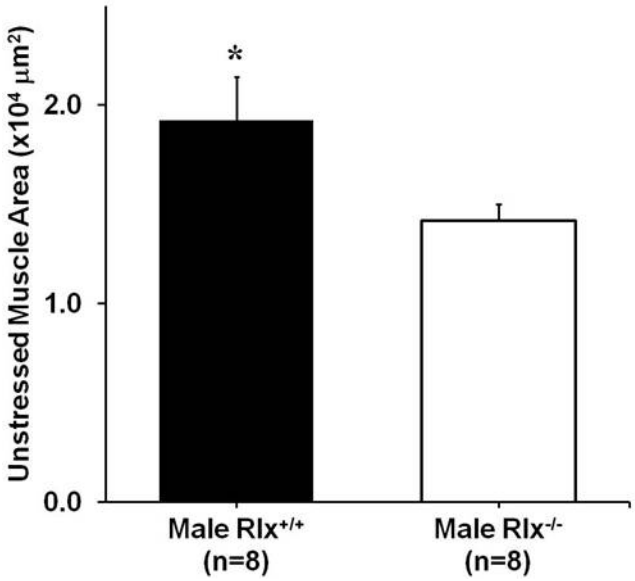

Figure 18. Unstressed Muscle Area of Small Renal Arteries from *Male $Rlx^{+/+}$ and $Rlx^{-/-}$ Mice*

Unstressed muscle area (A_{M0}) of small renal arteries isolated from $Rlx^{+/+}$ and $Rlx^{-/-}$, untreated mice. A_{M0} computed from measurements of the inner and outer diameters, and wall thickness in the unloaded configuration. * $P < 0.05$ *vs*. $Rlx^{-/-}$ group.

5.4.1.4 External Iliac Arteries from *Female Mice* Administered Low Dose rhRLX (1 μg/h)

To determine if these effects of relaxin on passive mechanical properties were evident in other arteries we examined external iliac arteries from rhRLX-treated mice. Interestingly, we found relaxin's effects on passive mechanical properties were in fact artery-type specific. i.e. external iliac arteries from rhRLX-treated mice were not characterized by any significant alterations in σ-R_m or σ-ε_m (**Figure 19**) relationships. Additionally, A_{M0} was unaltered in these arteries when compared to arteries from control mice (**Figure 20**).

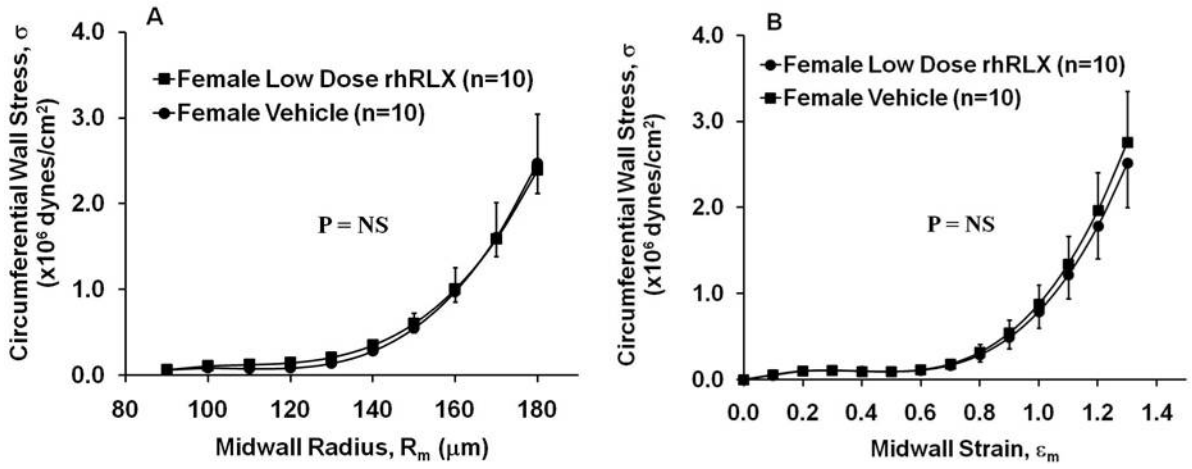

Figure 19. Stress-Midwall Radius and Stress-Midwall Strain Relationships of External Iliac Arteries from *Female Mice* Administered Low Dose rhRLX

(A) Circumferential stress (σ)-midwall radius (R_m) and **(B)** σ-strain (ε_m) relationships for external iliac arteries isolated from mice treated with low dose rhRLX (1 μg/h) or vehicle for 5 days. Original data from each animal were first fitted to a 3rd order polynomial, which was then used to obtain interpolated data (i.e., σ values for a given R_m or ε_m). Interpolated σ data at a common value of R_m or ε_m were averaged over all animals within a group to yield the relationships shown here. *P* = NS by analysis of excess variance using the original data.

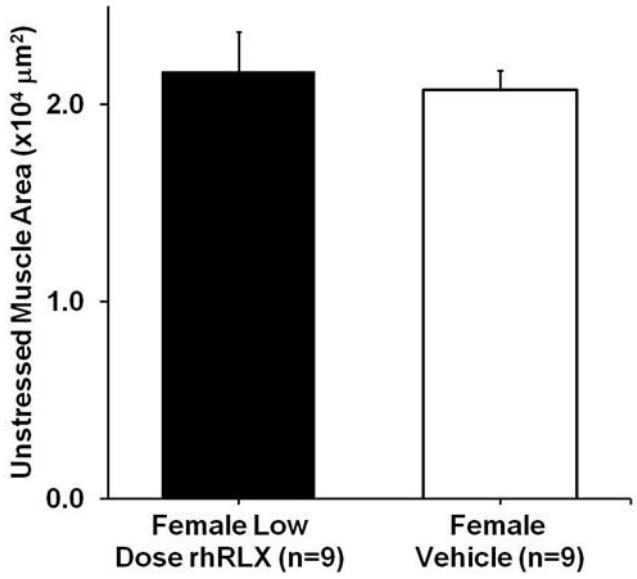

Figure 20. Unstressed Muscle Area of External Iliac Arteries from *Female Mice* Administered Low Dose rhRLX

Unstressed muscle area (A_{M0}) of external iliac arteries isolated from mice treated with low dose rhRLX (1 μg/h) or vehicle for 5 days. A_{M0} computed from measurements of the inner and outer diameters, and wall thickness in the unloaded configuration.

5.4.1.5 Small Renal and Mesenteric Arteries from *Mid-Pregnant Rats* Administered Relaxin Neutralizing Antibodies

Portions of this work have been previously published elsewhere [51]. Since mid-pregnant rats were characterized by a relaxin-mediated increase in global AC, we expected to observe relaxin-mediated alterations in arterial passive mechanical properties as well. To examine this, we assessed the passive mechanical properties of small renal and mesenteric arteries isolated from mid-pregnant rats using the same techniques described above (see **Section 4.3.3**). Contrary to our expectations, both small renal and mesenteric arteries from mid-pregnant rats administered the control antibody (MCAF) did not exhibit any significant changes in σ-R_m or σ-ε_m relationships compared to arteries from virgin rats (**Figures 21 and 22**). Furthermore, these relationships were not altered by administration of relaxin neutralizing antibodies (MCA1) to mid-pregnant rats. There were no significant alterations in A_{M0} of both artery types from the pregnant (MCAF or MCA1) rats and virgin controls (**Figure 23**).

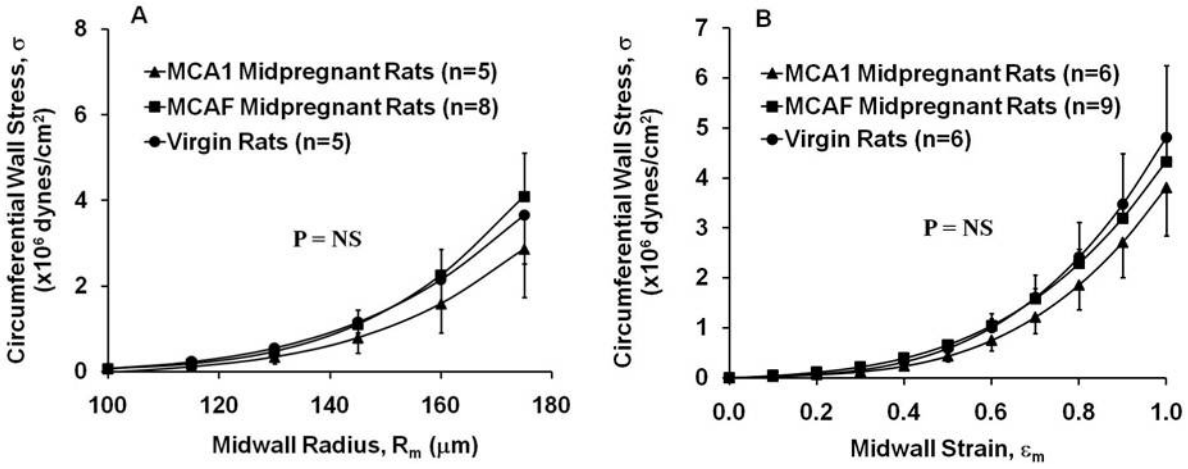

Figure 21. Stress-Midwall Radius and Stress-Midwall Strain Relationships of Small Renal Arteries from MCA1 or MCAF-Treated *Mid-Pregnant Rats*

(A) Circumferential wall stress (σ)-midwall radius (R_m) and **(B)** σ-strain (ε_m) relationships for small renal arteries isolated from MCA1 or MCAF-treated mid-pregnant rats and virgin controls. Original data from each animal were first fitted to a 3rd order polynomial, which was then used to obtain interpolated data (i.e., σ values for a given R_m or ε_m). Interpolated σ data at a common value of R_m or ε_m were averaged over all animals within a group to yield the relationships shown here. *P* = NS by analysis of excess variance using the original data.

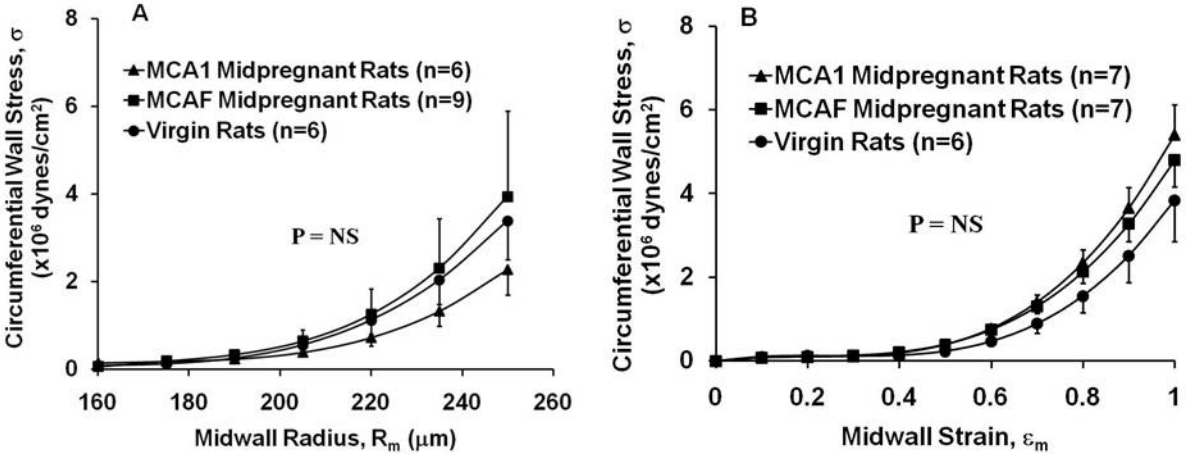

Figure 22. Stress-Midwall Radius and Stress-Midwall Strain Relationships of Mesenteric Arteries from MCA1 or MCAF-Treated *Mid-Pregnant Rats*

(A) Circumferential wall stress (σ)-midwall radius (R_m) and **(B)** σ-strain (ε_m) relationships for mesenteric arteries isolated from MCA1 or MCAF-treated mid-pregnant rats and virgin controls. Original data from each animal were first fitted to a 3rd order polynomial, which was then used to obtain interpolated data (i.e., σ values for a given R_m or ε_m). Interpolated σ data at a common value of R_m or ε_m were averaged over all animals within a group to yield the relationships shown here. *P* = NS by analysis of excess variance using the original data.

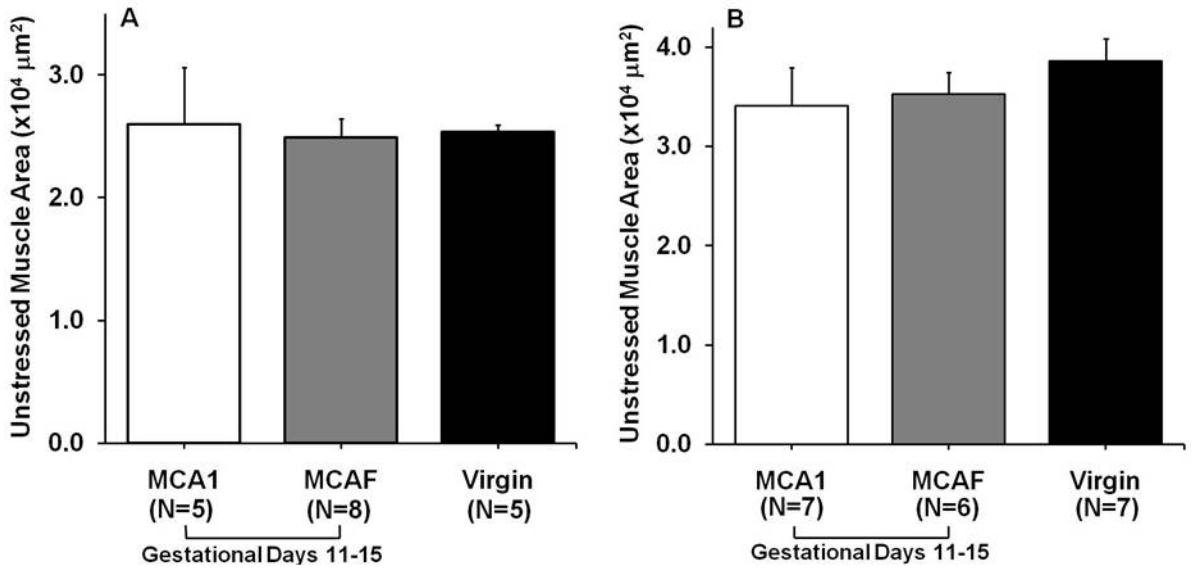

Figure 23. Unstressed Muscle Area of Small Renal and Mesenteric Arteries from MCA1 or MCAF-Treated *Mid-Pregnant Rats*

Unstressed muscle area (A_{M0}) of small renal and mesenteric arteries isolated from MCA1 or MCAF-treated mid-pregnant rats and virgin controls. A_{M0} computed from measurements of the inner and outer diameters, and wall thickness in the unloaded configuration.

5.4.1.6 Summary

Relaxin (both exogenously administered and locally produced) induces an increase in the passive compliance of small renal arteries from nonpregnant rats and mice. In addition, there is a relaxin-mediated geometric modification of the vascular wall of these arteries (i.e. A_{M0} was increased in small renal arteries from rhRLX-treated mice and decreased in those from $Rlx^{-/-}$ mice). Contrary to our expectations, small renal and mesenteric arteries from mid-pregnant rats did not exhibit any relaxin or pregnancy-mediated alterations in passive compliance or geometric properties. Finally, there were no relaxin-induced alterations in the stiffness properties of small renal arteries as quantified by their uniaxial (circumferential) σ-ε_m behavior. Since arterial wall properties are known to vary with direction, we considered the possibility that we were limited in

our approach by only characterizing arterial mechanical behavior in the circumferential direction. Thus, we next examined the vascular wall stiffness properties of small renal and external iliac arteries using a biaxial constitutive model.

5.4.2 **Biaxial (Circumferential and Axial) Stress-Strain Analysis**

We modified our testing apparatus to enable us to characterize the biaxial mechanical behavior of isolated arteries. These arteries were subjected to pressure cycles from 0 to 120 mmHg at various axial stretches and vascular wall mechanical properties were quantified in terms of tissue strain energy as discussed above (see **Section 4.3.4**). A representative mechanical response of an artery under multi-dimensional loading conditions is illustrated in **Figure 24**.

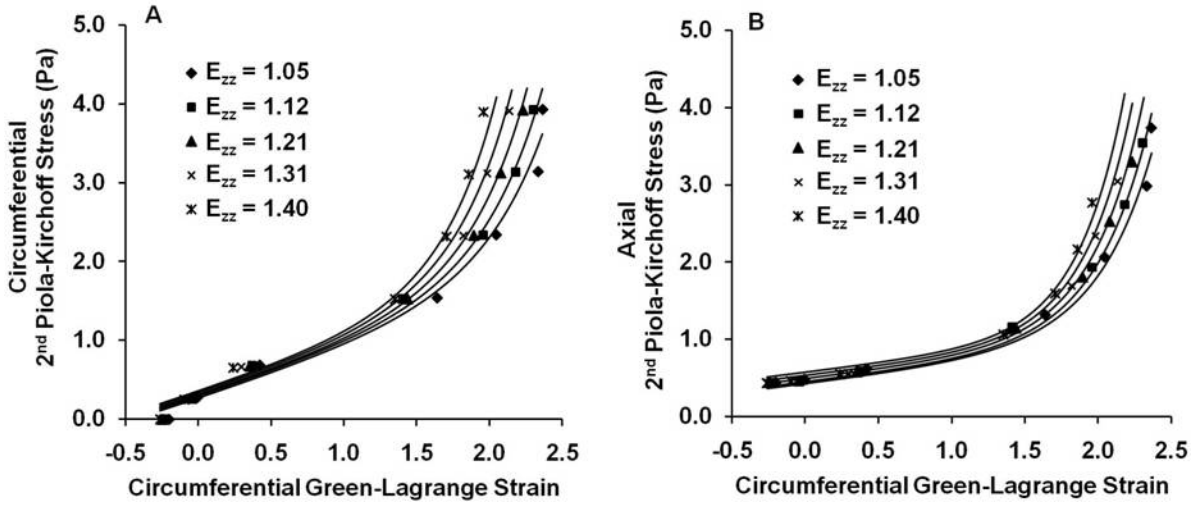

Figure 24. Representative Biaxial Stress-Strain Behavior of an Artery under Multi-Dimensional Loading Conditions

(A) Circumferential 2nd Piola-Kirchhoff stress ($S_{\theta\theta}$)-circumferential Green-Lagrange strain ($E_{\theta\theta}$) and **(B)** axial 2nd Piola-Kirchhoff stress (S_{zz})-$E_{\theta\theta}$ relationships from a mouse external iliac artery. Each curve is generated from pressure-diameter measurements made under a given axial Green-Lagrange strain (E_{zz}). Original data (symbols) were fitted to a 7 parameter mixed polynomial-exponential model of biaxial strain energy using the Levenberg-Marquardt algorithm. Solid lines represent computed $S_{\theta\theta}$ and S_{zz} data at given values of $E_{\theta\theta}$.

5.4.2.1 Small Renal Arteries from rhRLX-Treated Mice

As discussed before, we tested several different strain-energy functions and found the mixed polynomial-exponential model best described our data as it yielded the highest correlation coefficients. **Tables 7 and 8** lists the best fit constitutive parameters yielded using this model for each small renal artery sample along with the 95% confidence intervals for each predicted parameter and the correlation coefficients of the 2nd Piola-Kirchhoff stresses. Interestingly, 95% confidence intervals for certain parameters indicate that these parameters may not be significantly different from zero. This suggests that not all the parameters in this model may be needed to adequately predict strain energy as a function of biaxial Green-Lagrange strains. It is important to note, however, that in our subsequent analysis of these data we do not make any

interpretations based on absolute parameter values. Instead, our primary goal was to accurately predict the relationship between biaxial Green-Lagrange strains and 2nd Piola Kirchoff stresses. We believe that we were able to achieve this goal as indicated by the high correlation coefficients. Accordingly, the mixed polynomial-exponential model can be applied to our data to determine 2nd Piola Kirchoff stresses, and the resulting strain energy, for given biaxial Green-Lagrange strains.

From the best fit constitutive parameters we initially computed the tissue strain energy under equibiaxial strain (i.e. $E_{\theta\theta} = E_{zz}$) as a scalar index of overall tissue stiffness at varying levels of strain [53]. As shown in **Figure 25**, small renal arteries from rhRLX-treated mice compared to those from control counterparts exhibited slightly reduced magnitudes of equibiaxial strain energy especially at higher levels of strain although this small trend was not statistically significant. This suggested that under such loading conditions, relaxin treatment did not yield any significant alterations in the vascular wall mechanical behavior of these arteries.

Table 7. Best Fit Constitutive Parameters of Small Renal Arteries Isolated from Control Mice

Vessel	C_1	C_2	C_3	C_4	C_5	C_6	C_7	$R^2(S_{\theta\theta})$	$R^2(S_{zz})$
SRA #1	11097 (1184, 21509)	9178 (-16149, 34699)	12694 (3063, 22244)	8193 (-29855, 45725)	0.18 (-0.07, 0.41)	1.3 (-1.76, 4.35)	-0.57 (-2.16, 1.00)	0.93	0.91
SRA #2	12313 (8624, 17889)	6364 (-5969, 23465)	12456 (7029, 16639)	7913 (-11382, 21244)	0.09 (-0.27, 0.37)	1.4 (-1.10, 4.58)	-0.51 (-2.04, 0.67)	0.96	0.95
SRA #3	7822 (2272, 13263)	3426 (-12732, 19653)	8398 (2080, 14702)	9031 (-18833, 36872)	0.08 (-0.07, 0.23)	1.1 (-0.57, 2.83)	-0.50 (-1.36, 0.36)	0.92	0.94
SRA #4	10541 (7170, 14367)	3149 (-14322, 21030)	7184 (1143, 13084)	7375 (-18112, 32075)	-0.04 (-0.41, 0.30)	1.3 (-1.08, 3.85)	-0.52 (-1.66, 0.58)	0.95	0.96
SRA #5	7649 (1248, 13741)	7203 (-4070, 25057)	12844 (2971, 19882)	7832 (-12672, 21832)	0.16 (-0.01, 0.46)	1.4 (-1.33, 4.60)	-0.84 (-3.26, 1.09)	0.91	0.94
SRA #6	10320 (6579, 15042)	7830 (2505, 24847)	13452 (4927, 16693)	7767 (-5818, 10747)	0.10 (-0.16, 0.42)	1.6 (-1.26, 6.34)	-0.88 (-4.23, 1.11)	0.94	0.98
SRA #7	13289 (7258, 20691)	4572 (-19964, 29782)	8374 (600, 15910)	8902 (-29864, 45997)	-0.01 (-0.58, 0.49)	1.2 (-1.81, 4.45)	-0.43 (-1.68, 0.77)	0.92	0.92
Mean	10433	5960	10772	8145	0.08	1.3	-0.61	0.93	0.94
SE	798	870	1003	231	0.03	0.1	0.07	0.01	0.01

C_1-C_7, best-fit constitutive parameters for each artery computed by fitting original pressure-diameter and force-length data to a 7 parameter mixed polynomial-exponential model of biaxial strain energy using the Levenberg-Marquardt algorithm; values in parentheses represent 95% confidence intervals for each estimated parameter; $R^2(S_{\theta\theta})$ and $R^2(S_{zz})$, correlation coefficients calculated for circumferential and axial second Piola-Kirchoff stresses.

Table 8. Best Fit Constitutive Parameters of Small Renal Arteries Isolated from rhRLX-treated Mice

Vessel	C_1	C_2	C_3	C_4	C_5	C_6	C_7	R^2 ($S_{\theta\theta}$)	R^2 (S_{zz})
SRA #8	8532 (3672, 13146)	5289 (-10326, 21487)	11846 (5229, 18284)	7867 (-14645, 29865)	0.09 (-0.04, 0.25)	1.4 (-0.58, 3.30)	-0.65 (-1.76, 0.44)	0.93	0.95
SRA #9	6559 (1556, 11391)	1782 (-8135, 15680)	7252 (2567, 10884)	7921 (-12608, 23058)	0.12 (0.00, 0.24)	1.1 (-0.83, 3.38)	-0.42 (-1.54, 0.49)	0.94	0.92
SRA #10	7585 (4289, 11122)	6896 (-1501, 20730)	14069 (6289, 19204)	7439 (-6860, 16467)	0.10 (0.00, 0.25)	1.5 (-0.24, 3.79)	-0.97 (-2.77, 0.37)	0.96	0.98
SRA #11	6242 (4400, 8919)	9801 (9951, 20756)	19687 (11640, 20611)	7974 (-2975, 6819)	0.11 (0.01, 0.25)	1.2 (-0.43, 4.61)	-1.04 (-5.14, 0.75)	0.92	0.96
SRA #12	10905 (6470, 16003)	2601 (-13083, 18573)	4939 (1671, 8147)	8045 (-19514, 34812)	0.02 (-0.27, 0.28)	1.1 (-0.74, 2.93)	-0.25 (-0.79, 0.28)	0.95	0.94
SRA #13	12256 (7212, 17301)	7190 (-5836, 20216)	8320 (5035, 11604)	5176 (-9319, 19671)	0.16 (-0.03, 0.34)	1.7 (-0.46, 3.75)	-0.49 (-1.26, 0.28)	0.96	0.97
SRA #14	6743 (1491, 11994)	8255 (1614, 14896)	9761 (7455, 12067)	2118 (-4768, 9004)	0.46 (0.11, 0.081)	1.7 (-0.58, 3.94)	-0.68 (-1.75, 0.40)	0.94	0.94
Mean	8403	5973	10839	6649	0.15	1.4	-0.64	0.94	0.95
SE	881	1108	1858	847	0.05	0.1	0.11	0.01	0.01

C_1-C_7, best-fit constitutive parameters for each artery computed by fitting original pressure-diameter and force-length data to a 7 parameter mixed polynomial-exponential model of biaxial strain energy using the Levenberg-Marquardt algorithm; values in parentheses represent 95% confidence intervals for each estimated parameter; $R^2(S_{\theta\theta})$ and $R^2(S_{zz})$, correlation coefficients calculated for circumferential and axial second Piola-Kirchoff stresses.

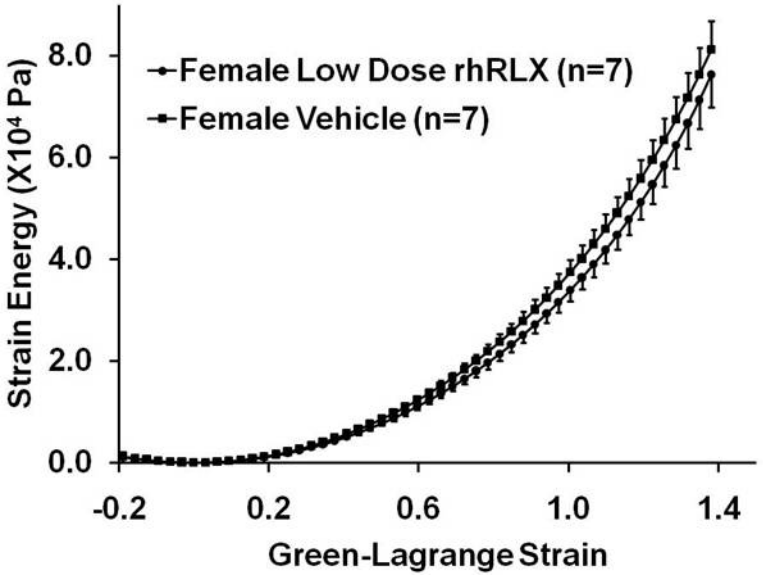

Figure 25. Equibiaxial Strain Energy of Small Renal Arteries from *Female Mice* Administered Low Dose rhRLX

Equibiaxial strain energy-Green-Lagrange strain relationships of small renal arteries isolated from mice treated with low dose rhRLX (1 μg/h) or vehicle for 5 days. Original pressure-diameter and force-length data were fitted to a 7 parameter mixed polynomial-exponential model of biaxial strain energy using the Levenberg-Marquardt algorithm. Best-fit constitutive parameters were then used to obtain strain energy values for a given equibiaxial Green-Lagrange strain (i.e. $E_{\theta\theta} = E_{zz}$). Computed strain energy data at a common value of strain were averaged over all animals within a group to yield the relationships shown here.

We still felt, however, that using equibiaxial strain energy as a measure of vascular wall stiffness confined us to a very specific and perhaps limited strain space. Instead, in order to get a more accurate representation of the biaxial mechanical behavior of these arteries, we needed to consider strain energy as a function of varying (and not necessarily equal) levels of circumferential and axial strain. Thus, we computed the strain energies of small renal arteries isolated from vehicle and rhRLX-treated mice at various levels of circumferential and axial strain. Of note, we used a strain space that was representative of our experimental conditions. **Figure 26** illustrates the difference in strain energy between the two groups. Comparing arteries from rhRLX-treated mice to those from control mice, we found that under conditions of low

circumferential strain there is little-to-no difference in strain energy regardless of the level axial strain. However, as circumferential strain increases, there is a trend of increasingly lower levels of strain energy in the arteries from the rhRLX-treated mice compared to the vehicle group. This trend becomes more pronounced at higher levels of axial strain and ultimately the maximum difference in strain energy between small renal arteries from rhRLX-treated mice and those from vehicle-administered mice occurs at maximum circumferential and axial strains. In fact, we computed tissue strain energy for each artery under maximum loading conditions ($E_{\sigma\sigma}$: 1.38, E_{zz}: 0.88) and found a strong trend, albeit statistically insignificant ($P = 0.09$), that the relaxin group exhibited lower magnitudes of strain energy under these loading conditions (**Figure 27**). Thus, our data suggest that under conditions of high circumferential and axial loads, small renal arteries isolated from rhRLX-treated mice exhibit some degree of reduced wall stiffness when compared to arteries from control mice.

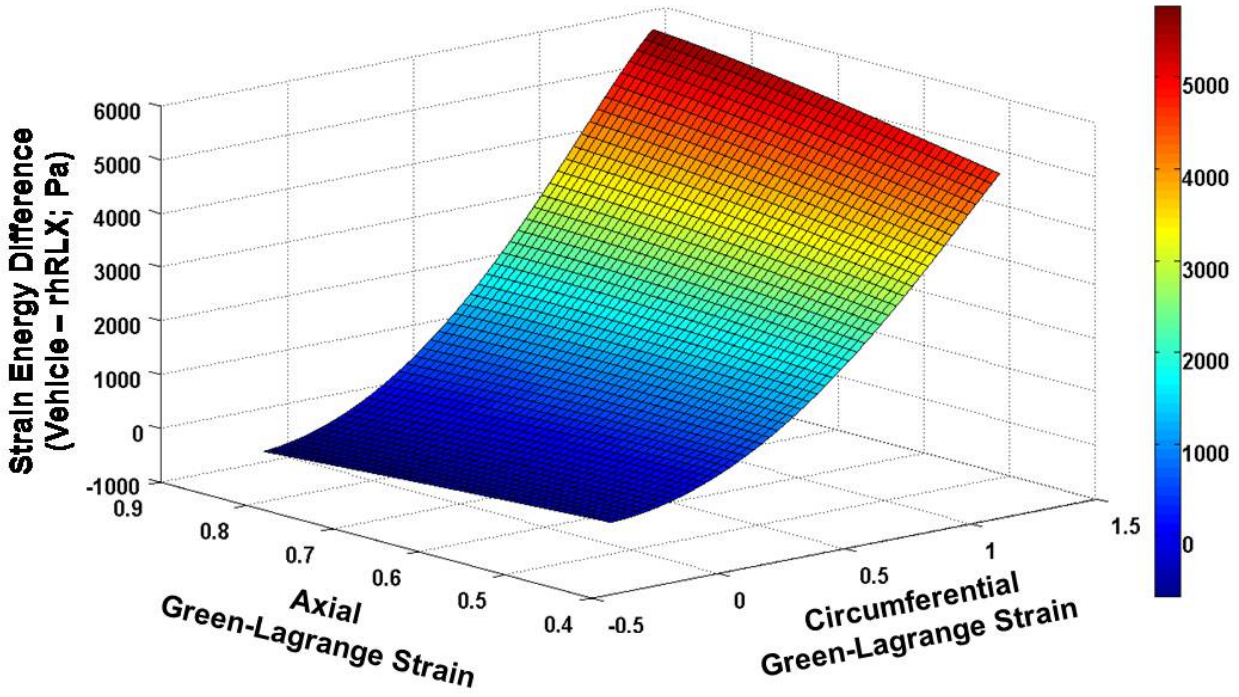

Figure 26. Two Dimensional Behavior of Tissue Strain Energy of Small Renal Arteries from *Female Mice* Administered Low Dose rhRLX

Difference in strain energy-Green-Lagrange strain relationships of small renal arteries isolated from mice treated with low dose rhRLX (1 μg/h) or vehicle for 5 days. Original pressure-diameter and force-length data were fitted to a 7 parameter mixed polynomial-exponential model of biaxial strain energy using the Levenberg-Marquardt algorithm. Best-fit constitutive parameters were then used to compute strain energy values for varying levels of circumferential and axial Green-Lagrange strains. Computed strain energy data at a common value of biaxial strain were averaged over all animals within a group. The average values of strain energy for the relaxin group were then subtracted from those of the vehicle group to yield the relationships shown here.

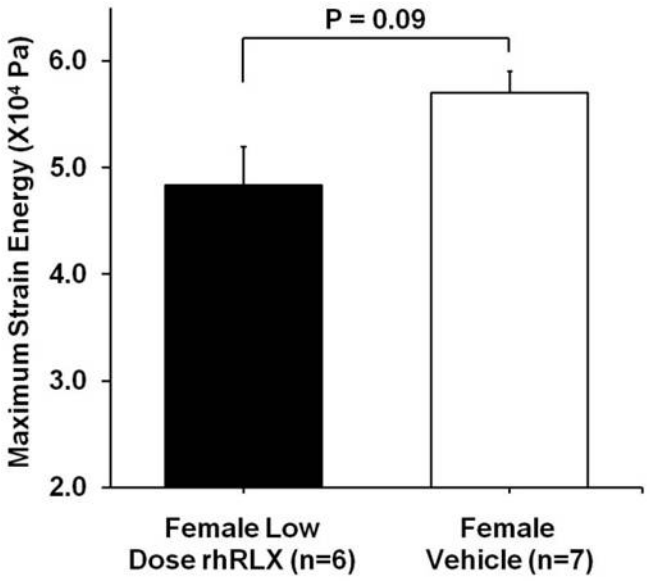

Figure 27. Strain Energy under Maximum Loading Conditions of Small Renal Arteries from *Female Mice* Administered Low Dose rhRLX

Tissue strain energy under maximum axial and circumferential Green-Lagrange strains of small renal arteries isolated from mice treated with low dose rhRLX (1 μg/h) or vehicle for 5 days. Original pressure-diameter and force-length data were fitted to a 7 parameter mixed polynomial-exponential model of biaxial strain energy using the Levenberg-Marquardt algorithm. Best-fit constitutive parameters were then used to obtain tissue strain energy under maximum loading conditions. Maximum strain energy data were averaged for all animals within a group to yield the data illustrated here. The difference in maximum strain energy was not quite significant between the two groups (P = 0.09 by Student's "t" test).

5.4.2.2 External Iliac Arteries from rhRLX-Treated Mice

Although relaxin did not induce any significant geometric modification of the vascular wall of external iliac arteries (i.e. A_{M0} was unchanged in external iliac arteries from rhRLX-treated mice compared to control mice) we still wanted to verify that our inability to detect any difference in the vascular wall mechanical properties of these arteries was not a result of limited approach; as it seemed to be the case in small renal arteries. Thus, we examined the biaxial mechanical behavior of external iliac arteries isolated from rhRLX-treated and control mice using similar techniques as above.

Tables 9 and 10 lists the best fit constitutive parameters were yielded using the mixed polynomial-exponential model of strain energy for each external iliac artery along with the 95% confidence intervals for each predicted parameter and the correlation coefficients of the second Piola-Kirchhoff stresses. Similar to our results from small renal arteries, 95% confidence intervals for the predicted parameters indicated that certain parameters might not be significantly different from zero. However, for reasons discussed above (see **Section 5.2.2.1**), we believe that we can accurately predict 2nd Piola-Kirchoff stresses, and the resulting strain energy, as a function of biaxial Green-Lagrange strains based on goodness of fit of the stress-strain behavior.

External iliac arteries from rhRLX-treated mice did not exhibit any significant changes in equibiaxial strain energy at varying levels of strain (**Figure 28**). However, unlike small renal arteries, when we computed the average strain energies of external iliac arteries from the two groups at various levels of circumferential and axial strain, we found that under any loading conditions there was no relaxin-induced change in tissue strain energy (**Figure 29**). Accordingly, there was no difference between the two groups in tissue strain energy under maximum loading conditions as there was for small renal arteries. Therefore, our data suggest that under varying conditions of circumferential and axial loads, external iliac arteries from rhRLX-treated mice do not exhibit a change in tissue stiffness when compared to arteries from control mice.

Table 9. Best Fit Constitutive Parameters of External Iliac Arteries Isolated from Control Mice

Vessel	C_1	C_2	C_3	C_4	C_5	C_6	C_7	R^2 ($S_{\theta\theta}$)	R^2 (S_{zz})
EIA #1	-872 (-6337, 4593)	2081 (-2330, 6491)	3109 (1894, 4323)	3201 (-6233, 12635)	0.35 (0.09, 0.61)	0.66 (-0.06, 1.37)	-0.17 (-0.42, 0.09)	0.93	0.87
EIA #2	2971 (2517, 3425)	2418 (1802, 3034)	2072 (1800, 3034)	178 (-8,364)	0.16 (0.09, 0.23)	1.35 (0.96,1.75)	-0.27 (-0.48, -0.06)	0.99	0.99
EIA #3	1333 (455, 2210)	4032 (3008, 5057)	3832 (3338, 4326)	179 (-103, 406)	0.29 (0.20, 0.37)	1.14 (0.66, 1.62)	-0.41 (-0.71, -0.11)	0.96	0.97
EIA #4	-208 (-914, 498)	3561 (1972, 5151)	3674 (2374, 4975)	1374 (-920, 3668)	0.09 (0.05, 0.12)	0.60 (0.24, 0.95)	-0.68 (-1.17, -0.19)	0.87	0.97
Mean	806	3023	3172	1233	0.22	0.94	-0.38	0.94	0.95
SE	1212	654	563	1010	0.06	0.18	0.11	0.04	0.04

C_1-C_7, best-fit constitutive parameters for each artery computed by fitting original pressure-diameter and force-length data to a 7 parameter mixed polynomial-exponential model of biaxial strain energy using the Levenberg-Marquardt algorithm; values in parentheses represent 95% confidence intervals for each estimated parameter; $R^2(S_{\theta\theta})$ and $R^2(S_{zz})$, correlation coefficients calculated for circumferential and axial second Piola-Kirchoff stresses.

Table 10. Best Fit Constitutive Parameters of External Iliac Arteries Isolated from rhRLX-Treated Mice

Vessel	C_1	C_2	C_3	C_4	C_5	C_6	C_7	$R^2(S_{\theta\theta})$	$R^2(S_{zz})$
EIA #5	1556 (447, 2665)	4437 (3205, 5669)	3421 (2772, 4070)	37 (-45, 117)	0.60 (0.37, 0.83)	2.27 (1.05, 3.48)	-0.82 (-1.63, -0.01)	0.96	0.97
EIA #6	4116 (2164, 6068)	2342.3 (200, 4485)	2640 (1669, 3611)	120 (-302, 541)	0.25 (-0.15, 0.65)	1.54 (0.02, 3.07)	-0.06 (-0.82, 0.69)	0.92	0.93
EIA #7	603 (-1006, 2212)	2639 (-29, 5307)	5097 (4166, 6020)	1390 (-1036, 3816)	0.27 (0.16, 0.38)	0.89 (0.34, 1.43)	-0.21 (-0.54, 0.12)	0.96	0.96
EIA #8	2551 (1843, 3259)	3331 (2659, 4002)	2922 (2571, 3273)	14 (-12, 39)	0.55 (0.37, 0.73)	1.92 (1.18, 2.65)	-0.30 (-0.75, -0.04)	0.97	0.97
Mean	2207	3187	3520	390	0.42	1.65	-0.37	0.95	0.96
SE	1062	658	778	473	0.09	0.29	0.16	0.02	0.01

C_1-C_7, best-fit constitutive parameters for each artery computed by fitting original pressure-diameter and force-length data to a 7 parameter mixed polynomial-exponential model of biaxial strain energy using the Levenberg-Marquardt algorithm; values in parentheses represent 95% confidence intervals for each estimated parameter; $R^2(S_{\theta\theta})$ and $R^2(S_{zz})$, correlation coefficients calculated for circumferential and axial second Piola-Kirchoff stresses.

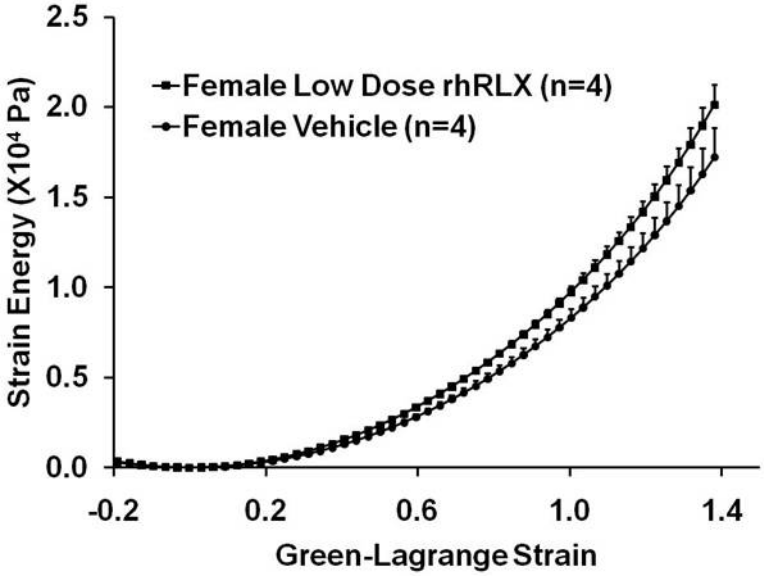

Figure 28. Equibiaxial Strain Energy of External Iliac Arteries from *Female Mice* Administered Low Dose rhRLX

Equibiaxial strain energy-Green-Lagrange strain relationships of external iliac arteries isolated from mice treated with low dose rhRLX (1 μg/h) or vehicle for 5 days. Original pressure-diameter and force-length data were fitted to a 7 parameter mixed polynomial-exponential model of biaxial strain energy using the Levenberg-Marquardt algorithm. Best-fit constitutive parameters were then used to obtain strain energy values for a given equibiaxial Green-Lagrange strain (i.e. $E_{\theta\theta} = E_{zz}$). Computed strain energy data at a common value of strain were averaged over all animals within a group to yield the relationships shown here.

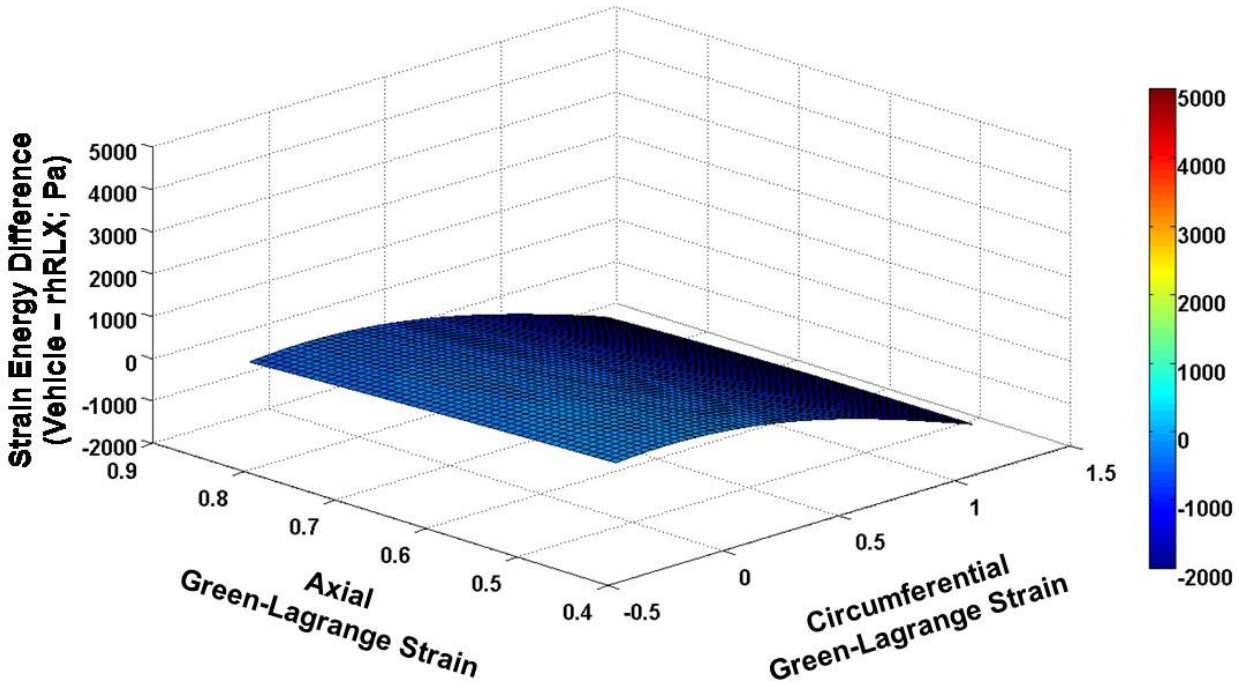

Figure 29. Two Dimensional Behavior of Tissue Strain Energy of External Iliac Arteries *Female Mice* Administered Low Dose rhRLX

Difference in strain energy-Green-Lagrange strain relationships of external iliac arteries isolated from mice treated with low dose rhRLX (1 μg/h) or vehicle for 5 days. Original pressure-diameter and force-length data were fitted to a 7 parameter mixed polynomial-exponential model of biaxial strain energy using the Levenberg-Marquardt algorithm. Best-fit constitutive parameters were then used to obtain strain energy values for varying levels of circumferential and axial Green-Lagrange strains. Computed strain energy data at a common value of biaxial strain were averaged over all animals within a group. The average values of strain energy for the relaxin group were then subtracted from those of the vehicle group to yield the relationships shown here.

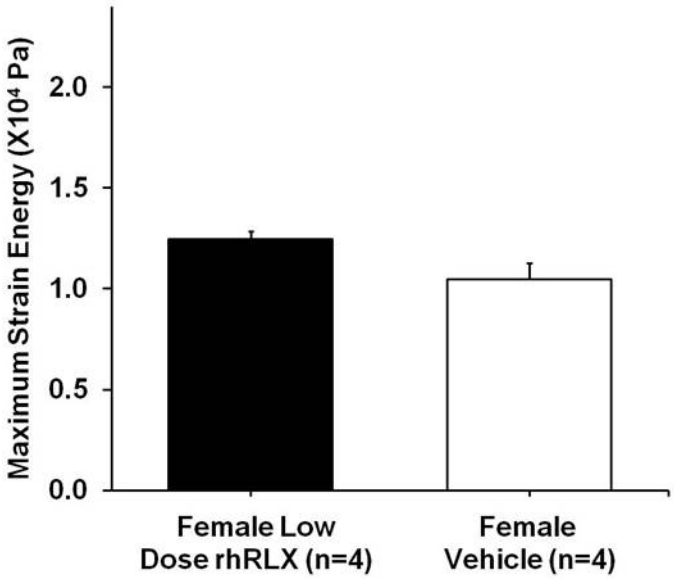

Figure 30. Strain Energy under Maximum Loading Conditions of External Iliac Arteries from *Female Mice* Administered Low Dose rhRLX

Tissue strain energy under maximum axial and circumferential Green-Lagrange strains of external iliac arteries isolated from mice treated with low dose rhRLX (1 μg/h) or vehicle for 5 days. Original pressure-diameter and force-length data were fitted to a 7 parameter mixed polynomial-exponential model of biaxial strain energy using the Levenberg-Marquardt algorithm. Best-fit constitutive parameters were then used to obtain tissue strain energy under maximum loading conditions. Maximum strain energy data were averaged for all animals within a group to yield the data illustrated here. The difference in maximum strain energy was not quite significant between the two groups ($P = 0.09$ by Student's "t" test).

5.4.2.3 Summary

Under conditions of low axial and circumferential loads, there are no relaxin-induced changes in vascular wall stiffness properties as quantified by tissue strain energy. However, under conditions of high biaxial loads small renal (and not external iliac) arteries from rhRLX-treated mice exhibit reduced wall stiffness. This finding suggests that there may be relaxin-mediated alterations in vascular wall biochemical composition of small renal arteries. Thus, we next examined the effects of relaxin on vascular wall collagen and elastin content. In addition, to

determine the mechanistic basis of the relaxin-mediated vascular wall geometric remodeling, we examined the hormone's effects on vascular smooth muscle cell hypertrophy and hyperplasia.

Of note, to determine whether our current data are comparable to previously published works, we compared the strain energy from our mouse external iliac arteries to that reported by Schulze-Bauer et al. for human external iliac arteries [43]. Interestingly, they observed much lower magnitudes of circumferential and axial stretches in human iliac arteries than we report here for mouse iliac arteries. Thus, we only compared strain energies from their study and ours in a region of circumferential and axial strains that was common between the two groups. We found that within this common strain domain, strain energies were generally similar in magnitude under conditions high circumferential strain irrespective of the level of axial strain, and under conditions low circumferential and axial strains. However, under conditions of high axial strain and low circumferential strain, the magnitude of strain energy reported for the human iliac arteries were much higher than what we report here for mouse iliac arteries.

5.5 ARTERIAL BIOCHEMICAL COMPOSITION AND STRUCTURE IN FEMALE RELAXIN-TREATED MICE

Specific Aim 5A. To analyze smooth muscle cell characteristics (size and count) in small renal and external iliac arteries isolated from rhRLX-treated *mice*.

Specific Aim 5B. To determine elastin and collagen content in small renal and external iliac arteries isolated from rhRLX-treated *mice*.

Specific Aim 6B. To analyze smooth muscle cell characteristics (size and count) in small renal and external iliac arteries isolated from $Rlx^{+/+}$ *and* $Rlx^{-/-}$ *mice*.

Specific Aim 6C. To determine elastin and collagen content in small renal and external iliac arteries isolated from *$Rlx^{+/+}$ and $Rlx^{-/-}$ mice*.

To determine the structural basis for the relaxin-induced increase in unstressed arterial muscle area and decrease in vascular wall stiffness, we examined smooth muscle cell (SMC) size and density, as well as collagen and elastin content in small renal and external iliac arteries isolated from rhRLX-treated and control mice, as well as, $Rlx^{+/+}$ and $Rlx^{-/-}$ mice.

5.5.1 **Smooth Muscle Cell Characteristics**

We measured SMC size in these arteries using two different techniques described above (see **Section 4.4**). Average SMC sizes measured from arterial cross-sections of small renal arteries isolated from vehicle and rhRLX-treated mice, as well as $Rlx^{+/+}$ and $Rlx^{-/-}$ mice, are illustrated in **Figure 31**. Arteries from mice administered rhRLX did not exhibit significant changes in SMC size when compared to those from mice administered the vehicle control (111.3±4.3 vs 105.0±3.1 μm^2; P=NS; Fig. 31A). Isolated SMCs from enzymatically digested, rhRLX-treated small renal arteries were also similar in size to SMCs isolated from control arteries (145.5±4.2 vs 143.2±6.4 μm^2; P=NS; Fig. 31B). Finally, SMC size measured from arterial cross-sections of small renal arteries isolated from $Rlx^{-/-}$ mice were not significantly different from those from $Rlx^{+/+}$ mice (110.2±3.1 vs 112.6±2.8μm^2; P=NS; Fig. 31C). These findings indicate the relaxin mediated increase unstressed muscle area of small renal arteries is not attributable to SMC hypertrophy.

Of note, SMCs isolated from enzymatically digested arteries appeared to be larger in size when compared to SMCs within arterial cross-sections. We believe that this difference in cell

size may be a result of some level of residual smooth muscle tone within the intact arteries. Importantly, there was no difference in SMC size between rhRLX-treated small renal arteries and control arteries irrespective of the method used to quantify cell size.

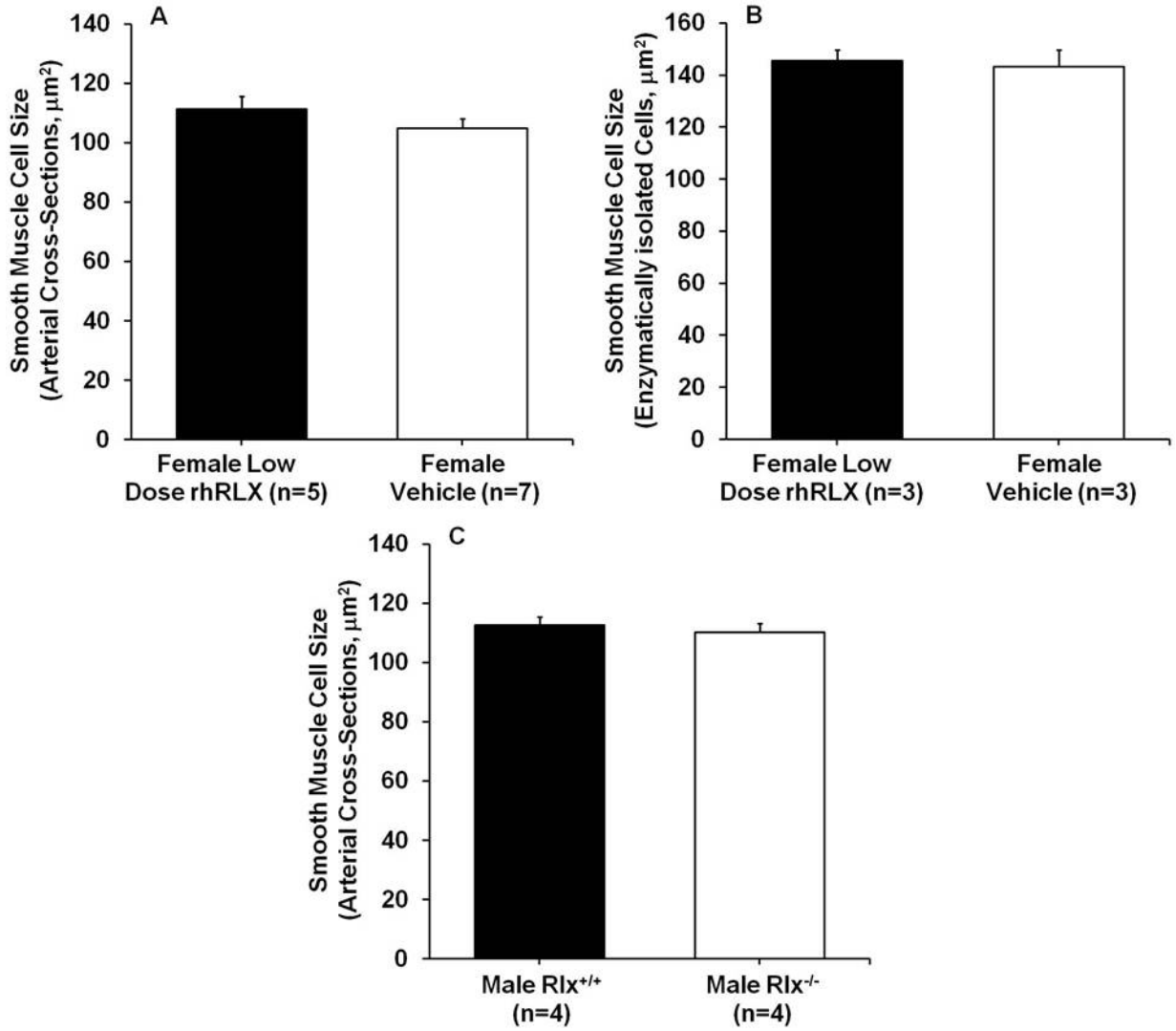

Figure 31. Smooth Muscle Cell Size of Small Renal Arteries from *Female Mice* Administered Low Dose rhRLX, and *Male* $Rlx^{+/+}$ and $Rlx^{-/-}$ *mice*.

Average smooth muscle cell (SMC) size of small renal arteries isolated from **(A&B)** mice treated with low dose rhRLX (1 μg/h) or vehicle for 5 days, and **(B)** $Rlx^{+/+}$ and $Rlx^{-/-}$ mice. (A) Isolated small renal arteries were enzymatically digested or (B) intact kidneys were sectioned at 6 μm thickness and stained for smooth muscle actin. Smooth muscle cells were identified by positive staining for smooth muscle actin. The sizes of individual islolated SMCs or SMCs within an arterial cross-section were determined. Representative SMC size of a given arterial cross-section was computed as the average SMC size of all discernable SMCs within 4-10 serial cross-sections of that artery. Data presented here are the composite average representative SMC size of each treatment group or genotype.

Figure 32 illustrates SMC density in small renal arteries isolated from rhRLX-treated, and vehicle-administered mice (**Fig. 32A**), as well as $Rlx^{+/+}$ and $Rlx^{-/-}$ mice (**Fig. 32B**). Arteries from rhRLX-treated mice were characterized by a significant increase in SMC density when compared to those from control mice (6.1±0.1 vs 5.0±0.1 cells/1000 μm^2; mean±SEM; $P<0.001$). Of note, although wall area was increased in the arteries from rhRLX-treated mice, there was an even larger increase the number of smooth muscle cells thus resulting in the increase in SMC density. Conversely, arteries from $Rlx^{-/-}$ mice were characterized by a significant decrease in smooth muscle cell density when compared to those from $Rlx^{+/+}$ mice (3.7±0.1 vs 4.4 ±0.1 cells/1000 μm^2; $P<0.05$).

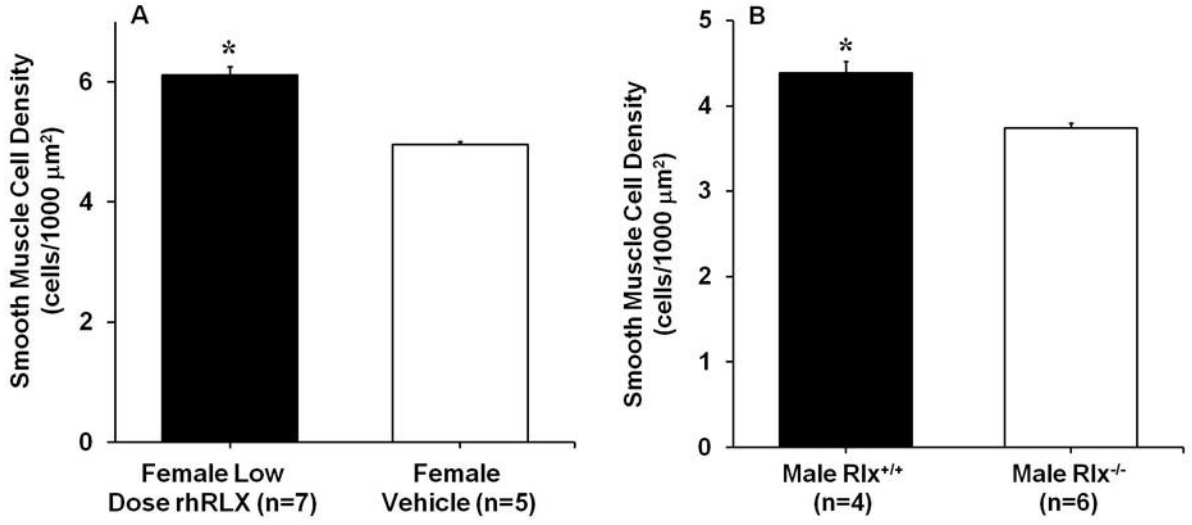

Figure 32. Smooth Muscle Cell Density of Small Renal Arteries from *Female Mice* Administered Low Dose rhRLX, and *Male* $Rlx^{+/+}$ and $Rlx^{-/-}$ *mice*.

Average smooth muscle cell (SMC) density of small renal arteries isolated from **(A)** mice treated with low dose rhRLX (1 μg/h) or vehicle for 5 days, and **(B)** $Rlx^{+/+}$ and $Rlx^{-/-}$ mice. Kidneys were sectioned at 6 μm thickness and stained for smooth muscle actin and nuclei. Small renal arteries were identified by positive staining for smooth muscle actin. Smooth muscle cell density for each arterial cross-section was quantified as the ratio of number of SMC (determined by counting DAPI-stained nuclei) to arterial wall area. Representative SMC density of a given artery was computed as the average SMC density of 4-10 serial cross-sections of that artery. Data presented here are the composite average representative SMC density of each treatment group or genotype. * $P < 0.05$ *vs* vehicle or *vs* $Rlx^{-/-}$.

With respect to external iliac arteries, we did not observe any significant differences in wall area between arteries from rhRLX-treated and control mice; nor were there differences in the number of smooth muscle cells. Consequently, SMC density was not significantly altered in external iliac arteries from rhRLX-treated mice compared to control mice (3.9±0.2 vs 4.0±0.2 cells/1000 μm^2; P=NS; **Fig. 33A**). As expected, we observed similar results in external iliac arteries from the $Rlx^{-/-}$ and $Rlx^{+/+}$ mice (3.6±0.4 vs 3.8±0.7 cells/1000 μm^2; P=NS; **Fig. 33B**).

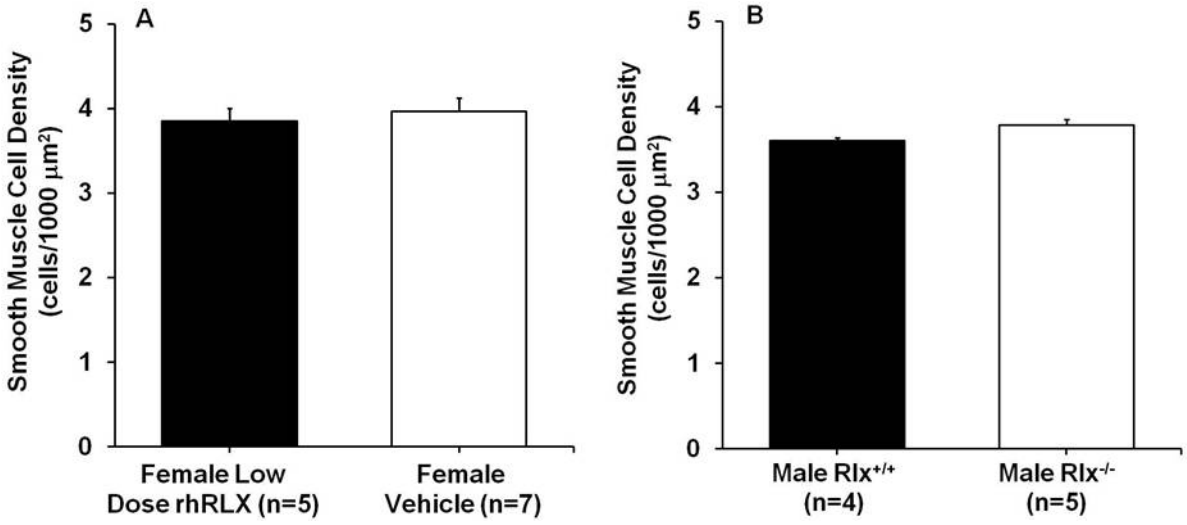

Figure 33. Smooth Muscle Cell Density of External Iliac Arteries from *Female Mice* Administered Low Dose rhRLX, and *Male* $Rlx^{+/+}$ and $Rlx^{-/-}$ *mice*.

Average smooth muscle cell (SMC) density of external iliac arteries isolated from **(A)** mice treated with low dose rhRLX (1 μg/h) or vehicle for 5 days, and **(B)** $Rlx^{+/+}$ and $Rlx^{-/-}$ mice. External iliac arteries were sectioned at 6 μm thickness and stained for smooth muscle actin and nuclei. Smooth muscle cell density for each arterial cross-section was quantified as the ratio of number of SMC (determined by counting DAPI-stained nuclei) to arterial wall area. Representative SMC density of a given artery was computed as the average SMC density of 4-10 serial cross-sections of that artery. Data presented here are the composite average representative SMC density of each treatment group or genotype.

5.5.2 **Collagen and Elastin Content**

As discussed before (see **Section 4.5**), relative collagen content was quantified as the ratio of collagen concentration to total protein concentration and relative elastin content was quantified as the ratio of the mass of elastin to tissue dry weight. Small renal arteries isolated from rhRLX-treated mice were characterized by a significant reduction in relative collagen content (0.13±0.01 vs 0.19±0.01 μg collagen/μg protein; mean±SEM; $P<0.02$) compared to control mice (**Fig. 34A**) with no significant change in elastin content (104±4 vs 97±14 μg elastin/mg dry weight; **Fig. 34B**). In contrast, there were no significant changes in collagen content (0.25±0.02 vs 0.28±0.04 μg collagen/μg protein; **Fig. 34C**) or elastin content (89±12 vs 83±5 μg elastin/mg dry weight; **Fig. 34D**) in external iliac arteries from the rhRLX-treated mice compared to control mice.

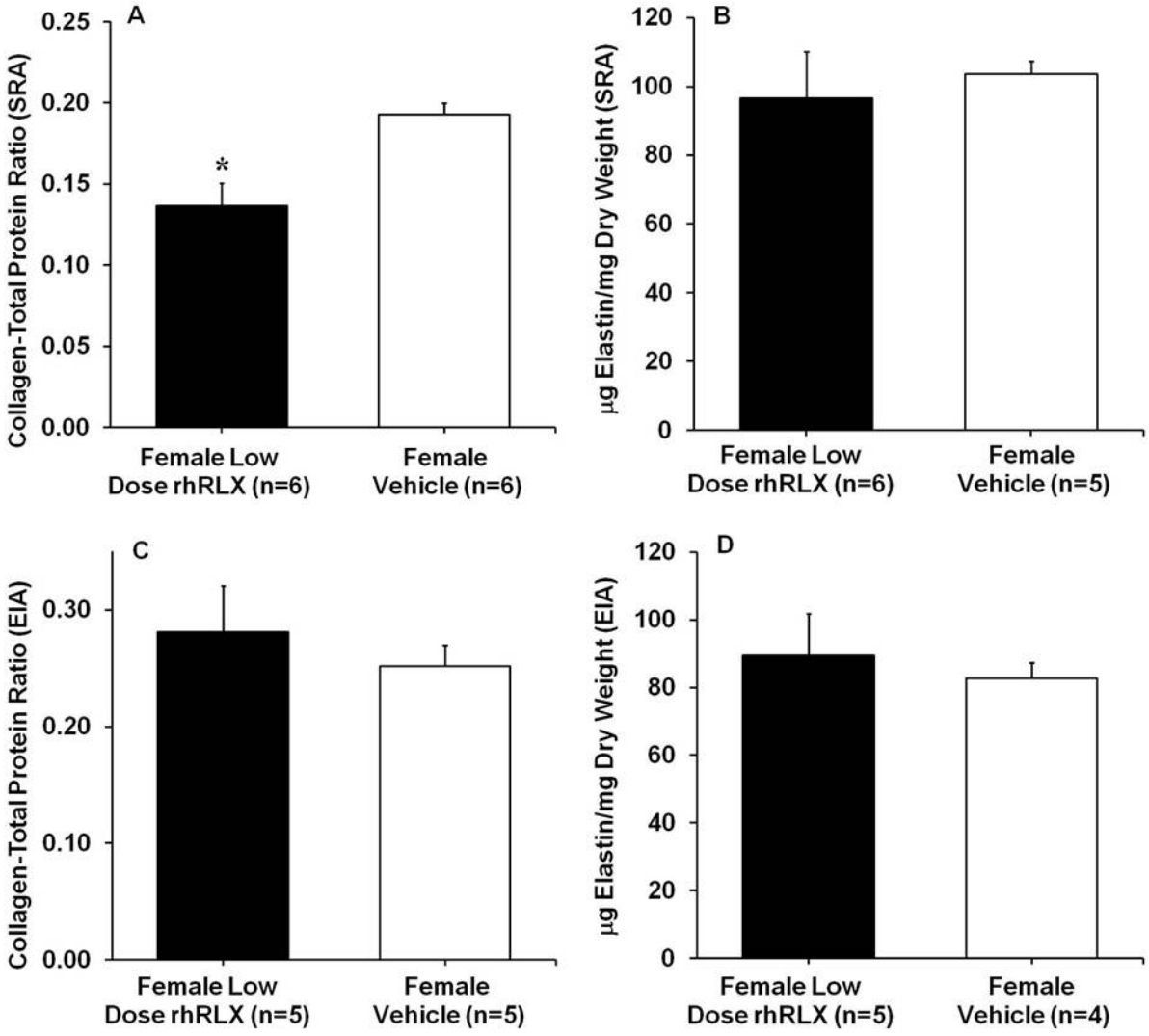

Figure 34. Relative Collagen and Elastin Content in Small Renal and External Iliac Arteries from *Female Mice* Administered Low Dose rhRLX.

Relative collagen **(A&C)** and elastin **(B&D)** content of small renal and external iliac arteries isolated from mice treated with low dose rhRLX (1 µg/h) or vehicle for 5 days. Collagen and total protein concentrations were determined using the Sircol Collagen Assay and the Pierce BCA Protein Assay, respectively. Elastin amount was determined using the Fastin Elastin Assay. Data presented here represents relative collagen content expressed as the ratio of collagen to total protein concentration and relative elastin content expressed as the amount of elastin per tissue dry weight. * $P < 0.05$ *vs* vehicle group. SRA: small renal arteries; EIA: external iliac arteries.

Small renal arteries isolated from $Rlx^{-/-}$ mice exhibited significantly increased collagen to total protein ratio (0.27±0.02 vs 0.19±0.03 μg collagen/μg protein; mean±SEM; $P<0.05$) compared to $Rlx^{+/+}$ mice (**Fig. 35A**). There were no significant changes in collagen to total protein ratio (0.41±0.05 vs 0.30±0.04 μg collagen/μg protein; **Fig. 35B**) in external iliac arteries from the $Rlx^{-/-}$ mice compared to $Rlx^{+/+}$ mice. Due to the limited availability of samples, we were unable to assess elastin content in these arteries. However, based on our other work, we do not anticipate there will be a relaxin-mediated alteration in elastin content in these arteries.

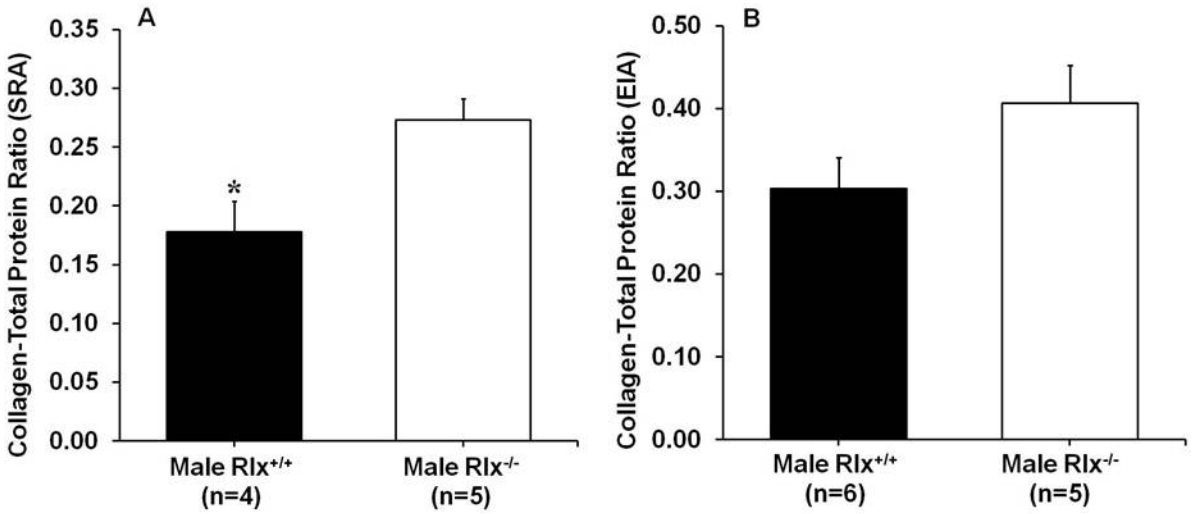

Figure 35. Relative Collagen Content in Small Renal and External Iliac Arteries from *Male* $Rlx^{-/-}$ and $Rlx^{+/+}$ *mice*

Relative collagen content of small renal **(A)** and external iliac **(B)** arteries isolated from $Rlx^{+/+}$ and $Rlx^{-/-}$ mice. Collagen and total protein concentrations were determined using the Sircol Collagen Assay and the Pierce BCA Protein Assay, respectively. Data presented here represents relative collagen content expressed as the ratio of collagen to total protein concentration. * $P <$ 0.05 *vs* $Rlx^{-/-}$ group. SRA: small renal arteries; EIA: external iliac arteries.

5.5.3 **Summary**

Relaxin induces both geometric and compositional vascular wall remodeling. The relaxin-induced geometric remodeling results in an increase in vascular wall area attributable to smooth muscle cell hyperplasia and not hypertrophy. The relaxin induced compositional remodeling is a result of decreased collagen content with no change in elastin content.

6.0 DISCUSSION

6.1 EFFECTS OF RELAXIN ON SYSTEMIC HEMODYNAMICS AND ARTERIAL PROPERTIES

6.1.1 **Relaxin: A Systemic Vasodilator**

Because relaxin is a potent renal vasodilator when administered to conscious, nonpregnant rats [16], and mediates renal vasodilation and hyperfiltration during pregnancy in conscious, gravid rats [23], we reasoned that the hormone might affect systemic hemodynamics and arterial load as well. Thus, one of the major objectives of this work was to determine whether relaxin administration to conscious, nonpregnant rats modifies both the steady and pulsatile components of arterial load. To this end, we found chronic administration of rhRLX to conscious, nonpregnant, female rats reduces steady arterial load by decreasing SVR, and reduces pulsatile arterial load by increasing global AC.

Analogous to previous work on relaxin in the renal circulation [16, 24, 25, 35], the hormone proved to be a general vasodilator reducing SVR and increasing CO each by approximately 20%, thereby maintaining MAP. As in pregnancy, this increase in CO was due primarily to an increase in stroke volume with a lesser contribution from heart rate [15, 54]. Although the renal circulation clearly participated in this systemic vasodilatory response, other

peripheral circulations undoubtedly contributed as well, but their relative contributions remain to be identified. Because relaxin administration reduced the myogenic reactivity of small mesenteric, and small renal arteries [28], we speculate that the hormone also vasodilates the mesenteric circulation. Others have shown that relaxin is most likely vasodilatory in several organ beds including heart, uterus, breast, liver and mesentery [20]. Therefore, these organ beds are likely to have contributed to the overall reduction in SVR and reciprocal rise in CO.

Concurrently with the decline in SVR, the pulsatile arterial load also fell. Global AC increased by approximately 20% during infusion of rhRLX. The magnitude of this change is comparable to the rise in global AC observed in human pregnancy (and rat pregnancy as indicated by our data; see **Section 5.1.7**) which peaks at about 30% above nonpregnant values during the first trimester [6] and coincides with the rise in circulating relaxin [21]. The increase in global AC observed here is similar to the rise in the compliance coefficient of the descending thoracic aorta measured in conscious pregnant rats that begins to increase with the rise in circulating relaxin [55]. Finally, consistent with an increase in global AC, pulse pressure remained unchanged in spite of a ~20% increase in stroke volume.

6.1.2 **Potential Mechanisms of Action of Relaxin**

Although the precise mechanisms for the relaxin-induced reduction in steady and pulsatile arterial loads are currently unknown, we propose three possible pathways (as reviewed in [33]). First, the hormone has been shown to exert renal vasodilation by increasing vascular gelatinase activity which, in turn, processes big endothelin to $ET_{1\text{-}32}$ [25, 32]. Subsequently, $ET_{1\text{-}32}$ stimulates the production of endothelial nitric oxide via the endothelial ET_B receptor subtype. This vasodilatory pathway may also be activated in other organ circulations during relaxin

infusion, thereby contributing to the reduction is SVR and increase in global AC. Second, vascular gelatinase and other matrix metalloproteinases can remodel extracellular matrix, as well, thereby contributing to the increase in global AC (along with the decrease in arterial tone). In fact, we found evidence of this remodeling process in this work as indicated by small renal arteries from rhRLX-treated mice exhibiting significantly reduced collagen content (see **Section 5.5.2**). Third, there is the possibility that relaxin induces the formation of new blood vessels and/or increases branching of existing vasculature [20, 56], which can contribute to the reduction in SVR and/or the increase in global AC. Interestingly, this process of angiogenesis may also require the participation of vascular gelatinase activity [57], the endothelial ET_B receptor, and NO [58]. Of note, increased skin capillary density has been reported in normal pregnancy [59] but it is not known whether relaxin is responsible for this pregnancy-associated angiogenesis.

6.1.3 **Dose Response to Relaxin**

Previous work demonstrated that the influence of relaxin on the renal circulation is biphasic in nature [24, 35]. Our initial work examining the effects of relaxin on systemic hemodynamics and arterial properties involved the administration of low doses of rhRLX to rats that yielded serum levels comparable to that observed in early gestation (~15 ng/ml) [21]. At this stage of pregnancy, CO is approximately 25% above nonpregnant values [15, 34]. However, during the late stages of pregnancy in rats, at which point serum relaxin levels are much higher (~80 ng/ml), some works have shown that CO is further increased to 50% above nonpregnant values [34] while others have shown that there is no further increase in CO ([15] and our current work). We administered higher doses of rhRLX to yield serum concentrations corresponding to mid and late-pregnancy, in order to determine whether systemic hemodynamics and arterial

properties would be further augmented. Analogous to relaxin's influence in the renal circulation and on osmoregulation [35], the effects of relaxin on systemic hemodynamics and arterial properties were biphasic. In contrast to our expectations, higher infusion rates of relaxin administered for 6 days yielding serum concentrations corresponding to late pregnancy in the rat, when CO is highest and SVR lowest [15], had no statistically significant effects on systemic hemodynamics and arterial properties. This finding suggests relaxin alone is unlikely to be responsible for the alterations in systemic hemodynamics and arterial properties during the later stages of pregnancy. Alternatively, during late gestation, increasing serum concentrations of relaxin may require other pregnancy factors to further augment and maintain the increase in CO and decrease in arterial load. Therefore, high dose relaxin infusion alone, in the absence of these other factors, is incapable of reproducing these changes.

There are several other possible explanations for this observation: (1) high dose relaxin infusion, may lead to classical downregulation of the LGR7 relaxin receptor in the vasculature especially if a rapid (hours) rather than gradual (days) increase in relaxin levels in blood is achieved [60]; (2) high dose relaxin infusion, may also lead to inactivation of this receptor through proteolytic cleavage at a glycine-leucine bond in the extracellular domain by gelatinases or other matrix metalloproteinases that relaxin stimulates [25]; and (3) high levels of circulating relaxin leads to excessive production of ET_{1-32} via proteolytic cleavage of big ET at a glycine-leucine bond to the active peptide, ET_{1-32} [25, 32]. Too much ET_{1-32} may then interact not only with the endothelial ET_B receptor to produce nitric oxide, but also with the vascular smooth muscle ET_A and ET_B receptors, thereby neutralizing the vasodilatory action of the endothelial ET_B receptor.

6.1.4 **Gender-Independence of Relaxin's Effects**

Analogous to previous work on relaxin in the renal circulation [24], this hormone elicited similar effects on systemic hemodynamics and arterial properties in both male and female rats even though relaxin is traditionally considered to be a female hormone and is not believed to circulate in male rats [21]. Of note, the renal effects of relaxin were observed in ovariectomized rats suggesting female sex steroids play little or no intermediary role [16]. Other studies have demonstrated relaxin increases coronary blood flow in male rats and guinea-pigs [19], and exerts chronotropic effects on the heart in male rats [61]. Recombinant human relaxin has also been shown to induce a significant increase in renal plasma flow in male human subjects comparable to observations made in females [62]. Additionally, the relaxin-1 and LGR7 gene and mRNA have been shown to be expressed by several arteries in male mice [52], while male mice deficient in the relaxin-1 gene exhibit fibrosis in several organs attributed to the absence of locally produced relaxin [63-65]; and in some cases, fibrosis is reversed with exogenous relaxin administration [64, 65]. Interestingly, although not statistically significant, results from our work examining the effects of relaxin on systemic hemodynamics and arterial properties tended to show a delay in the response to relaxin treatment in males when compared to females. This finding suggests there may be a reduced efficacy of the relaxin/relaxin receptor system in males. Although this issue needs to be explored further in order to elucidate any potential mechanisms for this seemingly delayed response in male rats, it is interesting to note that previous work showed that small renal arteries from male mice may be characterized by lower expression levels of the LGR7 receptor mRNA compared to female mice [52]. In addition, the three potential pathways for relaxin-induced changes in systemic arterial properties discussed above (see **Section 6.1.2**) are likely to exhibit different temporal patterns, with the reduction in tone being

the fastest and angiogenesis being the slowest. It is possible, therefore, that there is a difference in the relative contributions of these three pathways between males and females.

6.1.5 **Role of Relaxin in Mediating the Cardiovascular Adaptations to Pregnancy**

Our work with nonpregnant rats clearly shows that exogenously administered relaxin yielding serum concentrations in nonpregnant female rats comparable to those observed in early to mid-pregnant rats elicits alterations in systemic hemodynamics and arterial properties that mimic pregnancy. Next, we directly tested whether endogenous, circulating relaxin mediates the cardiovascular adaptations of pregnancy. This was accomplished by neutralizing circulating relaxin with specific antibodies. Using this technique, we were able to show that relaxin mediates the increase in CO and global AC, as well as the decrease in SVR during midterm pregnancy in rats.

Our current findings are consistent with earlier work which showed that either neutralization of circulating relaxin by antibodies or elimination by ovariectomy, abolished renal and osmoregulatory adaptations in midterm pregnant rats [23]. In both the renal and systemic circulations, there was total abrogation of the gestational changes by neutralization or elimination of circulating relaxin indicating the absence of other contributing or compensatory mechanisms at this stage of pregnancy. In addition, the osmoregulatory changes were either totally or largely prevented.

The decline in SVR and increase in global AC during pregnancy can be attributed, at least in part, to a reduction in vascular smooth muscle tone [5]. Another contribution may come from maternal angiogenesis [59] and, as discussed above, relaxin has been shown to exhibit angiogenic attributes [20, 56]. We believe that the same mechanisms involving upregulation of

vascular gelatinase by relaxin which acts through the endothelial ET_B receptor/nitric oxide vasodilatory pathway to trigger the gestational decline in renal vascular resistance, likely contributes to the decline in SVR during pregnancy; although different mechanisms in other circulatory beds are also likely to contribute [66, 67].

The findings from the present study indicate that circulating relaxin alone, without any other contributing or compensatory agents, mediates the transition of the systemic circulation from the virgin to the pregnant state in the gravid rat model. To determine whether relaxin alone maintains these adaptations in the systemic circulation through the late stages of pregnancy, we examined the effects of neutralizing circulating relaxin in late-pregnant rats on systemic hemodynamics and arterial properties. As discussed above this is still work in progress and the data presented here are preliminary (see **Section 5.1.8**). However, even with this preliminary data certain trends are evident. First, it appears that unlike during midgestation when the increase in CO was primarily a result of an increase in SV with little change in HR, the increase in CO in late pregnant rats appears to be governed by an increase in HR with little change in SV. This apparent difference in the mechanisms for the increase in CO during mid and late gestation needs to be explored further. Second, our data strongly suggest that although relaxin still plays a role in maintaining the adaptations in hemodynamics and arterial properties during the late stages of pregnancy, it is most likely not the only mediator. In contrast to during mid-pregnancy when eliminating circulating relaxin completely abolished the increase in CO and global AC and decrease in SVR, neutralizing circulating relaxin in late pregnant rats only partially eliminated these changes. It is likely that as pregnancy progresses other factors are recruited that act in concert with relaxin to maintain the changes in hemodynamics and arterial properties. Another possible reason for the partial response to the MCA1 antibody in late pregnant rats may be the

efficacy of the antibody during this stage of pregnancy. It is possible that during the late stages of pregnancy when circulating relaxin levels are at the highest, the MCA1 antibody only partially neutralizes the hormone. In that case there may still be low concentrations of relaxin circulating in the MCA1-treated late-pregnant rats which could account for the partial increase in CO and global AC and decrease in SVR that we observed in these animals. To investigate this phenomenon, we could study ovariectomized late pregnant rats in which case we would be certain that there would be no circulating relaxin.

6.2 EFFECTS OF RELAXIN ON ARTERIAL WALL STRUCTURE AND VASCULAR REMODELING

6.2.1 Relaxin-Induced Compositional Remodeling of the Vascular Wall

The increase in vascular gelatinase observed during pregnancy or after administration of recombinant human relaxin (rhRLX) to nonpregnant rats led us to consider that, in addition to reducing vascular smooth muscle tone, relaxin may also induce structural remodeling of the arterial wall. Vascular gelatinase activity has been implicated in vascular remodeling through degradation of extracellular matrix proteins such as collagen and elastin [68]. We postulated that both the reduction in smooth muscle tone and arterial remodeling could contribute to the increase in global AC *in vivo* during pregnancy, and after relaxin administration to nonpregnant rats. Accordingly, we examined the effects of relaxin on arterial collagen and elastin content. We found relaxin does induce compositional remodeling of small renal arteries by reducing relative collagen content. This finding is consistent with several other published reports implicating

relaxin's ability to antagonize the synthesis of or promote degradation of collagen. On the cellular level, rhRLX treatment has been shown to reduce the expression of collagen in human dermal fibroblasts and neonatal rat fibroblasts following stimulation with TGF-β1 [69, 70]. On the tissue level, rhRLX treatment has been shown to reduce collagen content in rodent models of renal, pulmonary, hepatic and cardiac fibrosis [69, 71-74]. Additionally, administration of rhRLX to hypoxic rats reduced accumulation of collagen in the main pulmonary artery [75]. Relaxin-deficient mice have also been shown to exhibit an accelerated, age-related increase in collagen content in the lung, heart, kidneys and skin [63-65, 76, 77]. These findings in $Rlx^{-/-}$ mice are consistent with our current work in which we found small renal arteries from $Rlx^{-/-}$ mice exhibit significantly increased levels of collagen compared to control counterparts. Furthermore, administration of rhRLX to older $Rlx^{-/-}$ mice significantly reversed the established fibrosis in lungs, kidneys and heart (reviewed in [76]).

Pregnancy has also been associated with compositional remodeling of the vascular wall. Mackey et al. reported that mesenteric arteries isolated from late pregnant rats are characterized by significantly reduced collagen content when compared to nonpregnant controls [12]. In addition, uterine arteries have been shown to exhibit a pregnancy-associated reduction in collagen content [7]. It is possible that endogenous, circulating relaxin plays a role in vascular wall compositional remodeling during pregnancy.

6.2.2 **Relaxin-Induced Geometric Remodeling of the Vascular Wall**

In addition to the relaxin-induced compositional remodeling, small renal arteries form rhRLX-treated and $Rlx^{+/+}$ mice, as well as rhRLX-treated rats, exhibited geometric remodeling of the vascular wall. Specifically, these arteries were characterized by a significant increase in

vascular wall area, as a result of smooth muscle cell hyperplasia, when compared to arteries from respective control animals. The increase in wall area may be a result of direct actions of relaxin on the vascular wall; although we do not currently have any evidence to support this conjecture. Geometric remodeling of the vascular wall has also been reported in pregnant animals. Osol and colleagues first reported that uterine radial arteries from late pregnant rats were characterized by a significant increase in vascular wall cross-sectional area when compared to those from nonpregnant rats [8]. In subsequent work they showed that vascular smooth muscle cells isolated from radial arteries were significantly elongated during late gestation and that the rate of proliferation of these cells and those from the main uterine artery was significantly increased. Accordingly, they concluded that smooth muscle cell hypertrophy and hyperplasia were underlying factors in the observed increase in vascular wall area of uterine arteries during gestation [11, 78]. In other studies, remodeling of the uterine artery (including increased vascular wall cross-sectional area resulting for smooth muscle cell hyperplasia) in psuedopregnant mice was comparable to that observed in normal pregnant mice. This finding indicated the presence of the fetus is not required for uterine artery remodeling during pregnancy and that maternal factors are most likely responsible for the changes in the vascular wall [79].

It is also likely the relaxin-mediated increase in wall area is secondary to the increase in blood flow observed during exogenous rhRLX administration or during pregnancy. Geometric remodeling of the vascular wall has also been reported in arteries during other physiological and experimentally induced conditions that result in a chronic increase in blood flow. Rat mesenteric arteries subjected to chronically elevated blood flow have been shown to exhibit a time-dependent increase in vascular wall area [80]. In another study using a similar animal model, mesenteric arteries subjected to chronically reduced blood flow were characterized by decreased

vascular wall area resulting from both the loss and reduction in size of smooth muscle cells [81]. Conversely, chronically elevated blood flow in similar arteries yielded increased wall area as result of increased smooth muscle cell proliferation [81]. It has been suggested that a chronic increase in blood flow results in an increase in wall shear stress, which leads to an elevation of the strain on arterial smooth muscle cells. This in turn can stimulate the expression of oncogenes and the production of growth factors which contribute to the hypertrophy of the vascular wall (reviewed in [82]).

To summarize, the exact mechanism through which relaxin elicits vascular wall geometric remodeling is not currently known. Relaxin, when exogenously administered, locally produced, or when circulating during pregnancy, may directly trigger geometric remodeling of the vascular wall through smooth muscle cell hyperplasia. On the other hand the relaxin-induced vascular wall geometric remodeling may be an indirect result of the relaxin-mediated increase in flow.

6.2.3 **Functional Relevance of Relaxin-Induced Vascular Wall Remodeling**

In order to determine the functional relevance of the relaxin-mediated vascular wall remodeling of small renal arteries, we examined the passive mechanical properties of these arteries. In these experiments, isolated small renal arteries were treated with papaverine and EGTA in order to eliminate vascular smooth muscle tone and enable us to quantify passive arterial compliance. Our results indicated that at any given midwall radius, circumferential wall stress of small renal arteries from relaxin-treated rats and mice was significantly reduced when compared to arteries from vehicle-infused counterparts. Similarly, small renal arteries from $Rlx^{+/+}$ mice were characterized by significantly lower circumferential wall stress for any given

midwall radius when compared to arteries from $Rlx^{-/-}$ mice. Of note, an increase in arterial compliance in small arteries, as we observed in small renal arteries, has been shown to significantly contribute to an overall increase in global arterial compliance [83]. Additionally, similar changes in the passive mechanics of mesenteric resistance arteries have been reported for late gestation in the rat [12]. Because vascular gelatinase activity plays a pivotal role in the remodeling of the extracellular matrix and also in the renal vasodilatory response to relaxin [25, 68], there are likely overlapping hormonal and cellular signaling mechanisms for the vasodilatory and vascular compliance changes during pregnancy and during rhRLX administration.

The increase in passive compliance of small renal arteries following relaxin treatment could be attributed to both the relaxin-mediated vascular wall compositional (reduced collagen content) and geometric (increased wall area) remodeling observed in these arteries. To determine the relative contributions of each type of remodeling, we examined the stiffness properties of the vascular wall using stress-strain analysis with the expectation that the structurally remodeled arteries from rhRLX-treated mice would exhibit reduced vascular wall stiffness. Contrary to our expectations, our initial analysis examining uniaxial (circumferential) wall stress-strain behavior showed that the relaxin-induced reduction in relative collagen content did not translate into reduced vessel wall stiffness. To ensure that we were not limited in our approach by characterizing arterial mechanical behavior in the circumferential direction only, we implemented a more physiologically relevant model of arterial mechanical behavior (i.e. a biaxial strain energy model). Using this model, we determined that vascular wall stiffness was not modified by relaxin under conditions of low circumferential and axial loads. However, at higher loads the relaxin-induced compositional remodeling became functionally relevant as the

arteries from the rhRLX-treated mice exhibited increasingly reduced vascular wall stiffness. Ultimately, the greatest reduction in vascular wall stiffness was observed at the highest loads. Interestingly, the difference in vascular wall stiffness between the arteries from the rhRLX-treated and control mice seems to be more dependent on circumferential rather than axial strain. These findings suggest the relaxin-induced decrease in collagen content of small renal arteries is functionally relevant only under conditions of high circumferential and, to a smaller degree, axial loads. Thus, under conditions of low circumferential and axial loads, the increased passive compliance observed in these arteries following relaxin treatment is primarily attributable to the relaxin-induced geometric remodeling.

There are several possible explanations as to why vascular wall stiffness is unchanged in small renal arteries from rhRLX-treated mice when subjected to low circumferential and axial loads, even though collagen content is significantly reduced in these arteries. First, it is possible that the magnitude of change in collagen content that we observed is not enough to elicit alterations in the passive vascular wall mechanical properties of these arteries. Second, passive vascular wall mechanical properties are not only determined by the relative content and mechanical properties of the individual load-bearing components of the vascular wall (i.e. collagen and elastin) but also by the way in which these components are architecturally arranged. Thus, overall collagen content may be significantly reduced in small renal arteries from rhRLX-treated mice but the architectural arrangement of collagen and elastin fibers may be unchanged. Of note, we do not currently have any data on the effects of relaxin on collagen and elastin fiber organization in the vascular wall. Although both of these scenarios are possible, we do not believe that they are likely.

Instead, our findings are more consistent with published works on the relative contributions of collagen and elastin on arterial passive mechanical properties. It is generally accepted that under conditions of low wall strain, elastin is the primary load-bearing component of the vascular wall and that as wall strain increases, collagen plays a more prominent role in supporting passive wall tension. To this end, Cox examined the passive mechanical properties of several different artery-types under *in-vitro* uniaxial (circumferential) loading conditions and reported that at low levels of circumferential strain corresponding to transmural pressures of up to 100 mmHg, only about 10% of collagen fibers support wall stress [84]. He reasoned that in addition to the ratio of collagen-to-elastin content and total connective tissue composition, arterial wall mechanics strongly depends on the differences in the recruitment of collagen fibers at different transmural pressures. Similar findings have been reported for dog aortae under *in vivo* conditions. Armentano et al. showed that significant participation of collagen fibers in vessel resistance to deformation occurs at mean aortic pressure of 118 mmHg and resistance to stretch at lower pressures is mainly supported by elastin fibers [85]. Finally, Dobrin and Canfield examined the passive biaxial mechanical behavior of dog carotid arteries following treatment with elastase or collagenase [86]. They showed that treatment with elastase significantly reduced circumferential and axial stress at low and high levels of biaxial strain indicating that elastin bears a portion of the distending load in both the circumferential and axial directions. Conversely, degradation of collagen had no significant effects on axial stress and reduced circumferential stress only when the arteries were pressurized by at least 60 mmHg. This indicates that collagen fibers are only load bearing in the circumferential direction and at higher levels of circumferential strain.

Combining these findings with our current work, we have shown that relaxin induces geometric remodeling of small renal arteries by increasing arterial wall area and compositional remodeling by reducing relative collagen content. Under conditions of low circumferential and axial loads, there are no significant differences in the vascular wall mechanical properties of small renal arteries isolated from rhRLX-treated mice compared to those from control mice. This is because under these conditions, elastin fibers are the primary load-bearing components of the vascular wall and relaxin does not elicit any changes in vascular elastin content. Under conditions of increasing biaxial loads (more particular increasing circumferential load), the reduced collagen content of small renal arteries from rhRLX-treated mice yields increasing lower levels of vascular wall stiffness compared to arteries from control mice.

Based on these observations, we began to investigate what the physiologic set points for circumferential and axial loads are. That is, we wanted know the magnitudes of biaxial strains for small renal arteries under normal physiologic loading conditions. Our preliminary data indicate that these arteries are subjected to low levels of circumferential and axial strains ($E_{\theta\theta}$: ~1.1 and E_{zz}: ~0.5) *in situ*. At these magnitudes of biaxial strains, we did not observe any difference in tissue strain energy between the rhRLX-treated and control small renal arteries (see **Figure 26**). Interestingly, previous work has shown that during pregnancy there is a significant increase in the volume of the kidney. Thus, it is quite likely that renal arteries during pregnancy are subjected to higher levels of stretch in axial direction, and perhaps even in the circumferential direction. It is also likely that similar increases in kidney volume and loading conditions of small renal arteries occur with relaxin infusion in nonpregnant animals. If these conjectures regarding increased circumferential and axial loads are true then our data indicate that the rhRLX-treated arteries will have reduced vascular wall stiffness compared to control arteries at

the same lading conditions. Thus, if rhRLX-treated small renal arteries were subjected to elevated levels of biaxial loads without compensatory remodeling of the vascular wall and reduced stiffness then these arteries would have had significantly increased wall stress. Thus, the relaxin-induced reduction in stiffness at high loads can be considered to be an adaptive response that guards against excessive rise in wall stress.

6.2.4 **Site-Specificity of the Effects of Relaxin on Systemic Arterial Circulation**

The relaxin-mediated arterial remodeling appears to be specific to small renal arteries. External iliac arteries isolated from rhRLX-treated and $Rlx^{+/+}$ mice did not exhibit alterations in wall area, smooth muscle cell density, or collagen content compared to the respective controls. Consequently, passive compliance was also unchanged in these arteries. We found similar results in isolated aortae in that relaxin treatment did not induce any significant alterations in smooth muscle cell density or collagen content in these arteries either (see **Appendix B**). Of note, the pregnancy-induced smooth muscle cell hyperplasia in uterine arteries in late pregnant rats was not observed in mesenteric arteries from the same rats [78]. Additionally, pseudopregnancy did not induce significant changes in wall area or smooth muscle cell characteristics in carotid arteries or abdominal and thoracic aortae [79]. There are a couple of possible explanations for this phenomenon. First, if the vascular remodeling observed following relaxin treatment and during pregnancy is secondary to the increase in blood flow, it is possible that certain artery beds are not subject to the same magnitude of increase in flow or, more importantly, increase in shear stress that occurs in the renal and uterine circulations. Consequently, the stimulus for vascular remodeling is not as potent in these artery beds following relaxin treatment or during pregnancy. However, if the relaxin induced vascular

remodeling is a direct effect of the hormone's actions on the vascular wall, it is also possible that the LGR7 receptor is more predominantly expressed by certain vascular beds than others. In fact, other work has suggested that small renal arteries from male mice may exhibit lower expression levels of the LGR7 receptor mRNA compared to female rats [52] and our current work suggests there is a difference in the temporal response to relaxin between male and female rats. It is just as likely that this difference in receptor expression or temporal response to relaxin between genders exist for different vascular beds.

6.2.5 **Unexpected Findings**

Because isolated renal arteries from rhRLX-treated mice and rats were characterized by increased passive compliance, we expected to observe similar alterations in the passive mechanical properties of arteries from midterm pregnant rats. However, there were no differences in the passive compliance or wall area of small renal and larger mesenteric arteries isolated from virgin and gravid rats; nor did the relaxin neutralizing or control antibodies impact arterial passive mechanics.

There are several potential explanations for the observed lack of relaxin's effects on vascular passive properties during this stage of pregnancy. First, rat relaxin is not as potent as human relaxin. Therefore, although circulating levels of rat relaxin during midterm pregnancy are sufficient to reduce arterial tone, they may be inadequate to affect vascular remodeling. Indeed, previous work has shown human relaxin is more potent than rat relaxin based on the isolated rat atria chronotropy bioassay [87]. Bearing this in mind, the increase in global AC observed in midterm pregnant rats appears to be primarily attributable to reduction in vascular smooth muscle tone and not to vascular remodeling. It should be noted that circulating levels of

relaxin are considerably higher during late gestation in the rat. Therefore, arteries isolated from late-pregnant rats may be more compliant. Indeed, previous reports indicated that renal and mesenteric arteries isolated from late-pregnant rats exhibit both increased passive compliance and reduced tone [12, 88]. Another possibility is that there are counter-regulatory factors circulating during pregnancy (versus the administration of rhRLX alone to nonpregnant rats) that offset the vascular remodeling properties of endogenous relaxin at least during midgestation.

7.0 TAKE HOME MESSAGES

On the whole animal level, relaxin increases cardiac output and global arterial compliance, and reduces systemic vascular resistance without any changes in mean arterial pressure in nonprengnant rats. Of note, we have also shown that relaxin exerts similar effects in hypertensive rat models (see **Appendix C**) [89]. Relaxin also mediates the cardiovascular adaptations to pregnancy in the gravid rat model. On the isolated artery level, relaxin induces vascular wall geometric and compositional remodeling in an artery-type-specific manner. Further, the relaxin-induced geometric remodeling of small renal arteries results in an increase in passive arterial compliance while the relaxin-induced compositional remodeling results in a reduction in vascular wall stiffness under high circumferential and axial loads.

Increased arterial stiffness is observed in many physiological (normal aging, post-menopausal state) and pathological (accelerated aging, chronic hypertension, diabetes, heart failure) conditions. Vascular stiffening results in modifications of systemic hemodynamics that negatively impact both the heart and the vessels. Based on its constellation of cardiovascular actions, we speculate that relaxin may prove to be a very useful therapeutic agent in improving vascular (stiffness and dilation) in the aforementioned cardiovascular states. Relaxin may be particularly useful in preeclampsia where cardiac output and global arterial compliance are reduced, and systemic vascular resistance and mean arterial pressure are increased [90], resulting in marked and selective organ hypo-perfusion. In this setting, relaxin administration may

improve maternal organ perfusion without unduly lowering MAP, thereby avoiding compromise of uterine blood flow. In fact, there may be a potential role for aberrant relaxin regulation in abnormal pregnancies such as preeclampsia wherein the cardiovascular adaptations to pregnancy are inadequate.

APPENDIX A

BIAXIAL TESTING SYSTEM FOR ISOLATED ARTERIES

An isobaric arteriograph system (Living Systems Instrumentation, Burlington, VT USA) was modified to enable us to make simultaneous measurement of pressure-diameter and force-length curves. The modified system consists of 3 major components: and vessel chamber with a micro cannula attached to a movable arm and a digital micrometer (**Figure 36**), a force transducer positioner (**Figure 37**), and a force transducer holder (**Figure 38**). SolidWorks engineering drawings of the individual components are illustrated below. **Figure 39** illustrates a working assembly of the entire system.

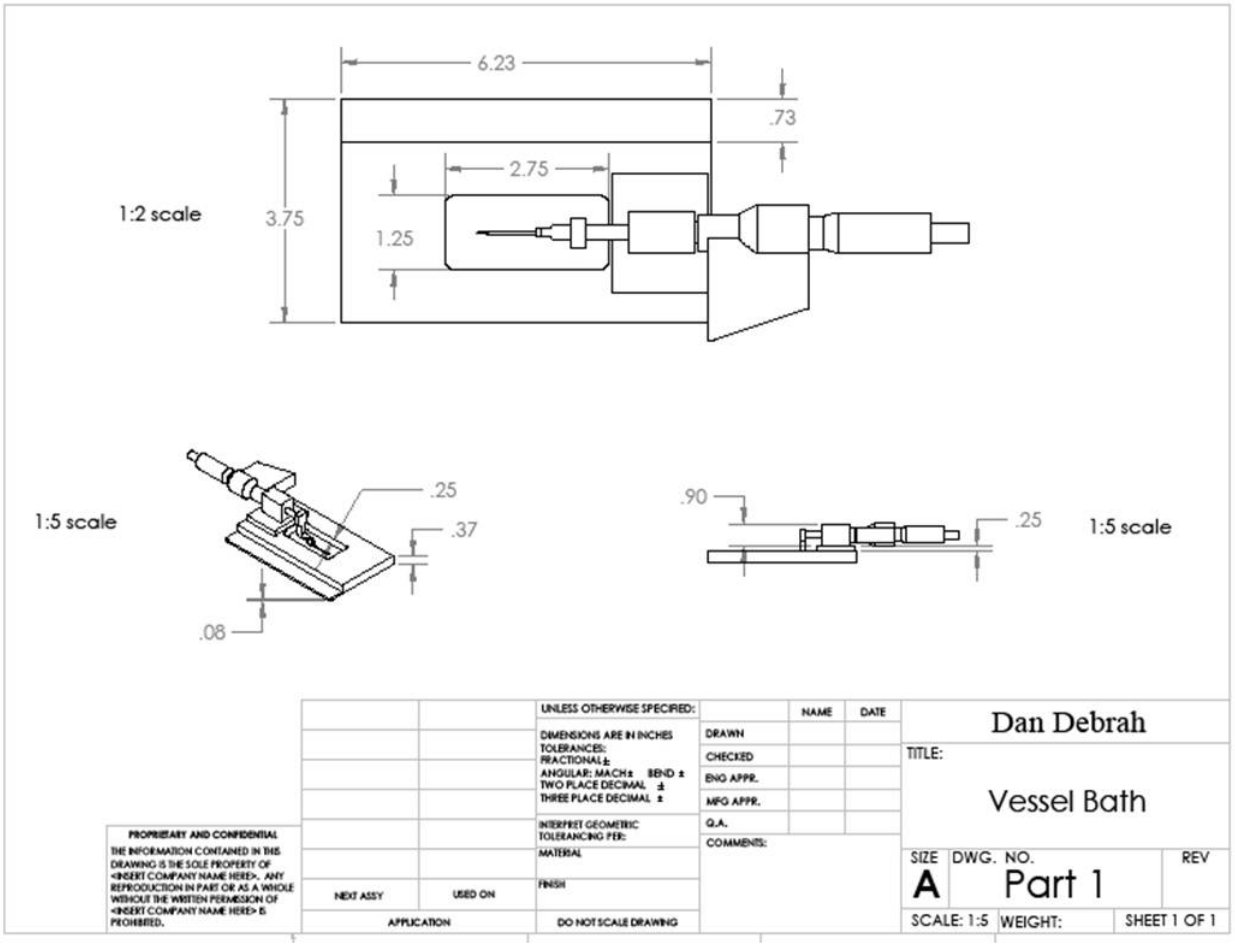

Figure 36. SolidWorks Schematic of Isolated Vessel Chamber.

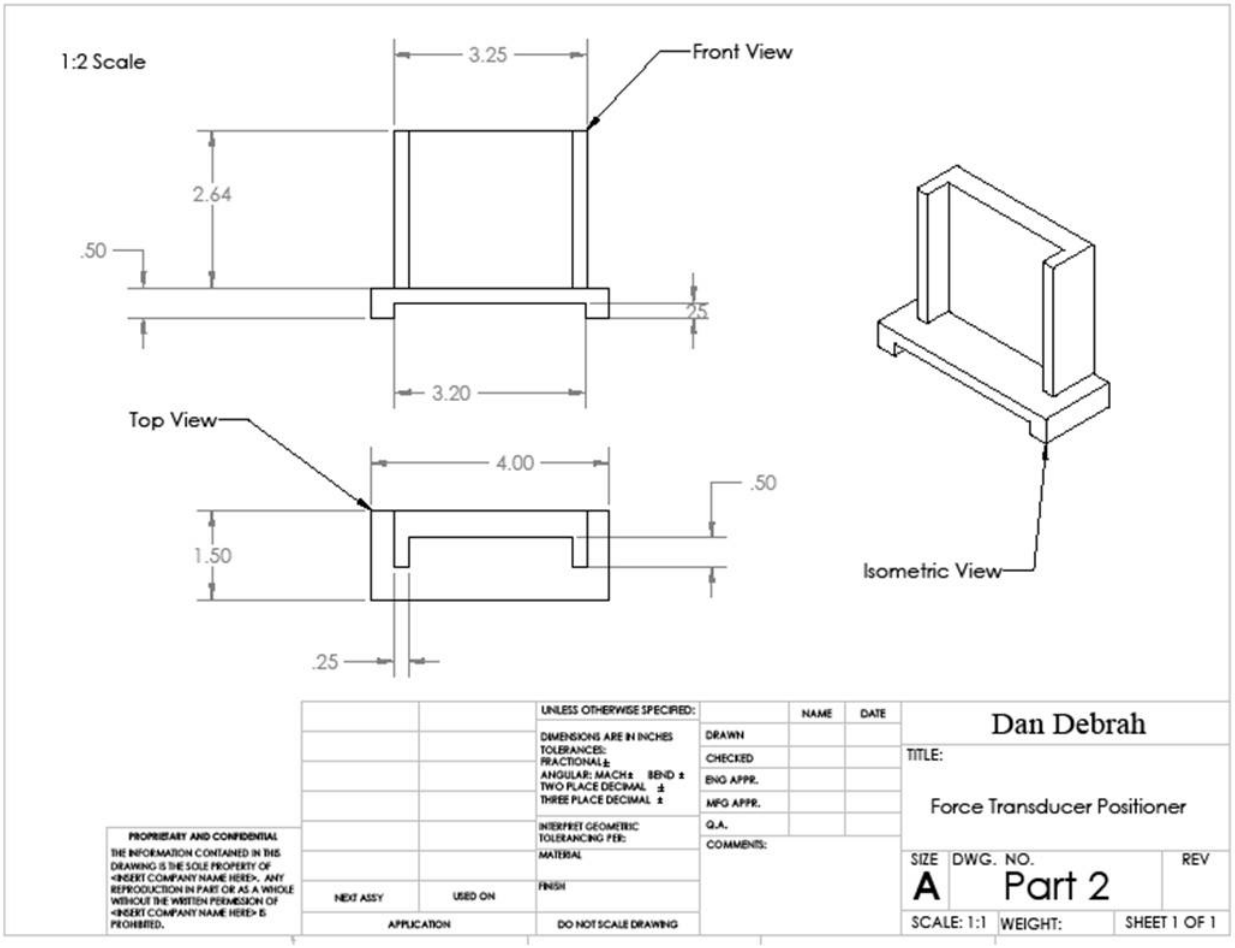

Figure 37. SolidWorks Schematic of Force Transducer Positioner.

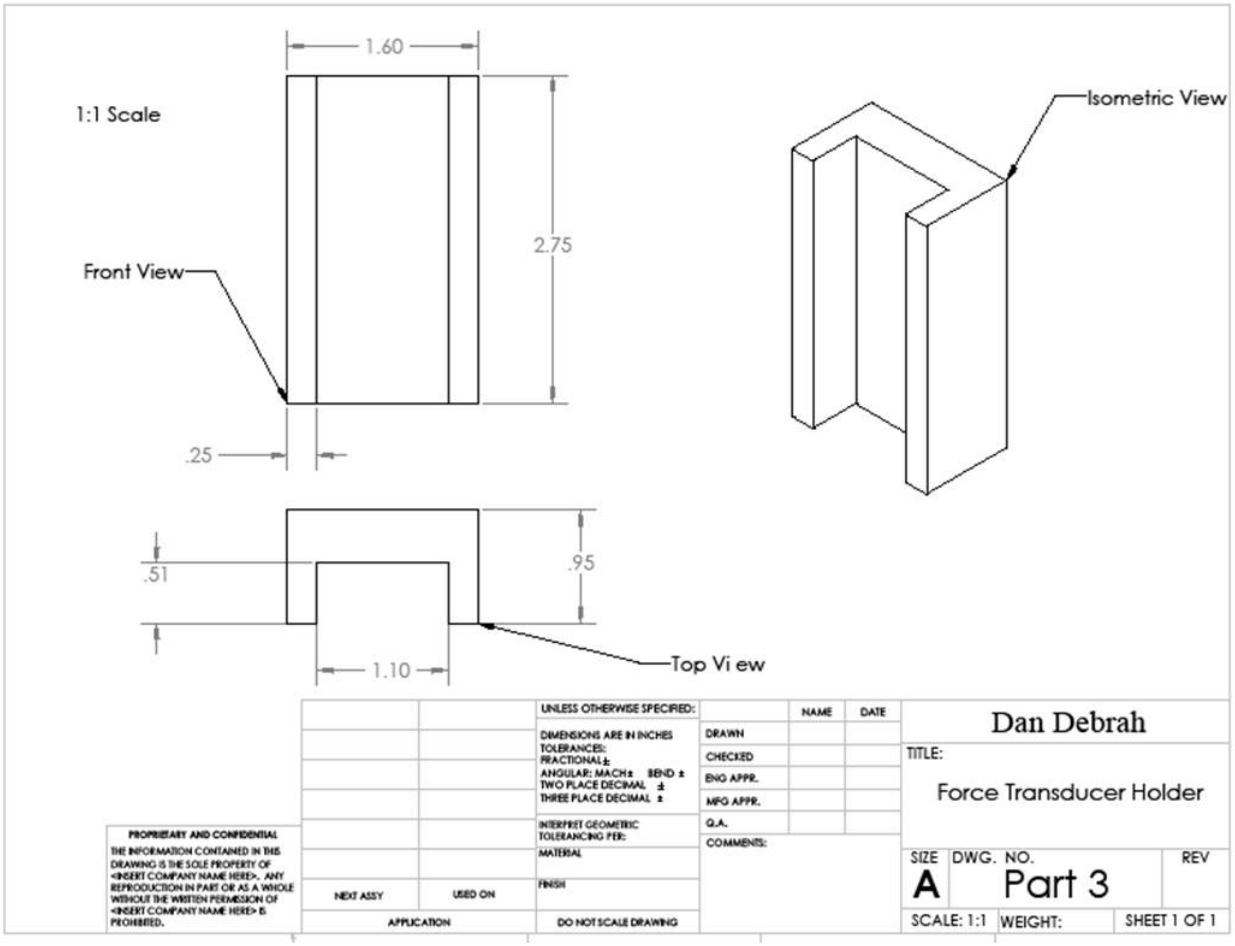

Figure 38. SolidWorks Schematic of Force Transducer Holder.

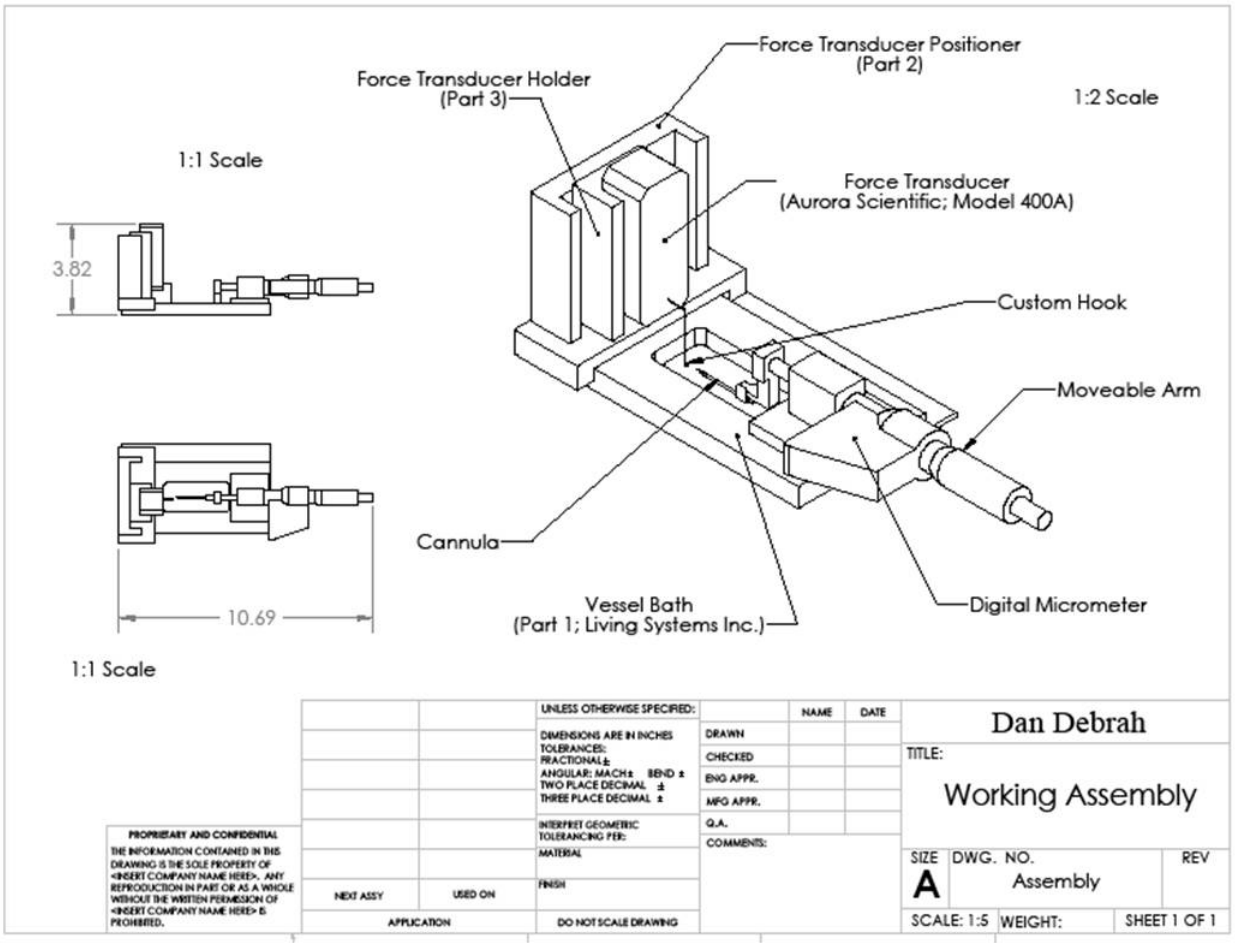

Figure 39. SolidWorks Schematic of Working Assembly Vascular Biaxial Testing System.

APPENDIX B

VASCULAR WALL EFFECTS OF RELAXIN ON ISOLATED AORTAE

B.1 PREAMBLE

Our work examining the effects of relaxin on vascular wall biochemical composition and smooth muscle cell (SMC) characteristics indicated that the vascular wall remodeling effects of relaxin were observed in small renal arteries and not external iliac arteries. This led us to consider the possibility that the vascular wall remodeling effects of relaxin were artery type specific. To begin to investigate this phenomenon, we examined the effects of relaxin on vascular wall collagen and elastin content as well as SMC density and size in aortae isolated from rhRLX-treated and control mice and $Rlx^{+/+}$ and $Rlx^{-/-}$ mice. Of note, due to their larger size we were unable to acquire any data on the vascular wall mechanical properties of these arteries (our mechanical testing apparatus for isolated arteries can only be used for small arteries).

B.2 SMOOTH MUSCLE CELL CHARACTERISTICS

Figure 40 illustrates SMC density in aortae isolated from rhRLX-treated, and vehicle-administered mice (Fig. 40A), as well as $Rlx^{+/+}$ and $Rlx^{-/-}$ mice (Fig. 40B). There was no significant difference in SMC density in aortae from rhRLX-treated mice compared to those from control mice (± vs ± cells/1000 μm^2; mean±SEM; P = NS). Similarly, SMC density in aortae from $Rlx^{-/-}$ mice was unchanged compared to those from $Rlx^{+/+}$ mice (± vs ± cells/1000 μm^2; P = NS).

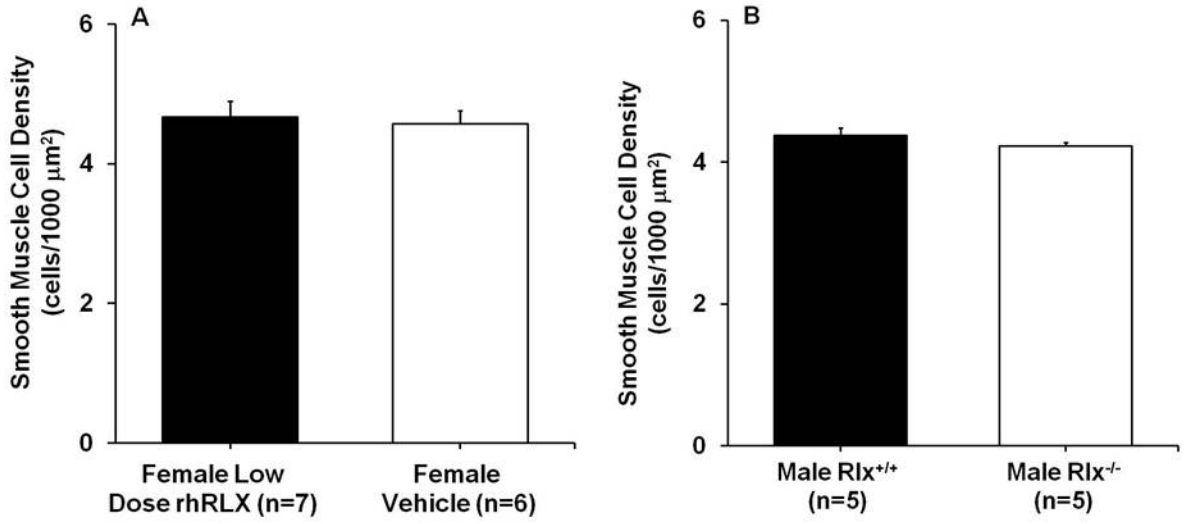

Figure 40. Smooth Muscle Cell Density of Aortae from *Female Mice* Administered Low Dose rhRLX, and *Male* $Rlx^{+/+}$ and $Rlx^{-/-}$ *mice*.

Average smooth muscle cell (SMC) density of aortae isolated from **(A)** mice treated with low dose rhRLX (1 μg/h) or vehicle for 5 days, and **(B)** $Rlx^{+/+}$ and $Rlx^{-/-}$ mice. Aortae were sectioned at 6 μm thickness and stained for smooth muscle actin. Smooth muscle cell density for each arterial cross-section was quantified as the ratio of number of SMC to arterial wall area. Representative SMC density of a given artery was computed as the average SMC density of 4-10 serial cross-sections of that artery. Data presented here are the composite average representative SMC density of each treatment group or genotype.

B.3 COLLAGEN AND ELASTIN CONTENT

Relative collagen content was quantified as the ratio of collagen concentration to total protein concentration and relative elastin content was quantified as the ratio of the mass of elastin to tissue dry weight (see **Section 4.5**). Similar to external iliac arteries, aortae isolated from rhRlx-treated mice did not exhibit a significant change in relative collagen content compared to those from control mice (± vs ± μg collagen/μg protein; mean±SEM; P = NS; **Figure 41A**). Additionally, elastin content was also unchanged in these arteries compared to those from control mice (± vs ± μg elastin/mg dry weight; **Figure 41B**).

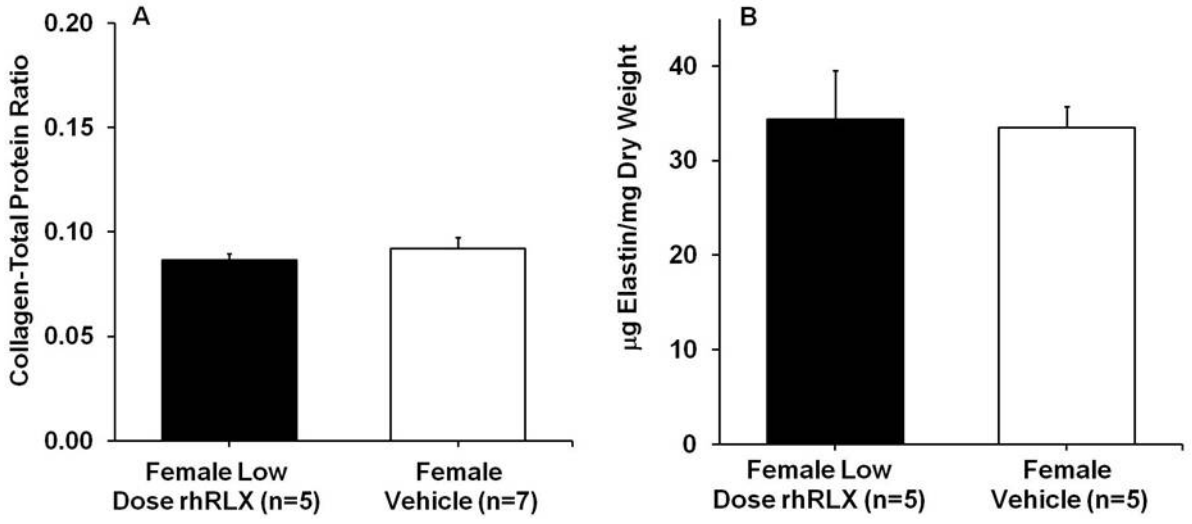

Figure 41. Relative Collagen and Elastin Content in Aortae from *Female Mice* Administered Low Dose rhRLX.

Relative collagen **(A)** and elastin **(B)** content of aortae isolated from mice treated with low dose rhRLX (1 μg/h) or vehicle for 5 days. Collagen and total protein concentrations were determined using the Sircol Collagen Assay and the Pierce BCA Protein Assay, respectively. Elastin amount was determined using the Fastin Elastin Assay. Data presented here represents relative collagen content expressed as the ratio of collagen to total protein concentration and relative elastin content expressed as the amount of elastin per tissue dry weight.

We observed comparable results in aortae isolated from $Rlx^{-/-}$ and $Rlx^{+/+}$ mice with the arteries from $Rlx^{-/-}$ mice not exhibiting any significant change collagen to total protein ratio compared to those from $Rlx^{+/+}$ mice (± vs ± μg collagen/μg protein; mean±SEM; P = NS; **Figure 42**). Due to the limited availability of samples, we were unable to assess elastin content in aortae from $Rlx^{+/+}$ mice. However, based on our other work, we do not anticipate there will be a relaxin-mediated alteration in elastin content in these arteries.

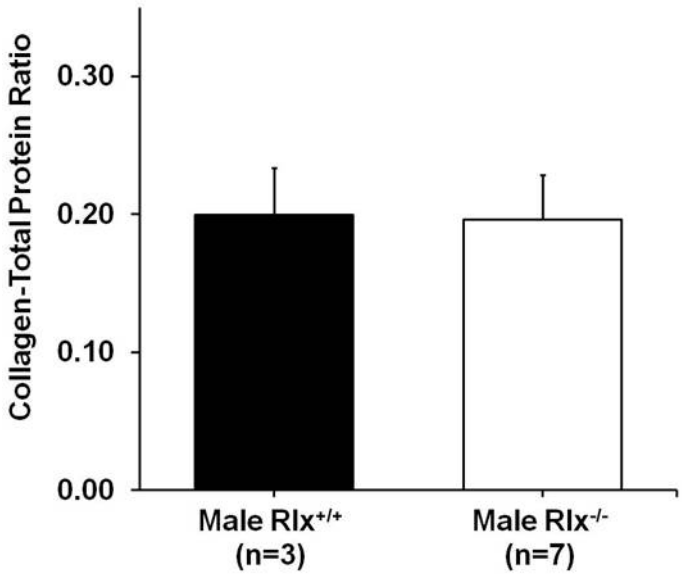

Figure 42. Relative Collagen Content in Aortae from *Male* $Rlx^{-/-}$ and *$Rlx^{+/+}$ mice*

Relative collagen content of aortae isolated from $Rlx^{+/+}$ and $Rlx^{-/-}$ mice. Collagen and total protein concentrations were determined using the Sircol Collagen Assay and the Pierce BCA Protein Assay, respectively. Data presented here represents relative collagen content expressed as the ratio of collagen to total protein concentration.

B.4 SUMMARY

To summarize, similar to external iliac arteries, administration of rhRLX to nonpregnant female mice did not yield any significant alterations in SMC density or arterial collagen and elastin content in aortae. Similar observations were made in aortae from $Rlx^{-/-}$ and $Rlx^{+/+}$ mice. We currently do not have any data on the effects of relaxin on vascular wall mechanical properties of aortae. However, we anticipate that there will be no relaxin-mediated alterations in this as well. This is further evidence suggesting that the vascular wall remodeling effects of relaxin are indeed artery type specific. Although we do not know the exact mechanism for the artery-type specificity of relaxin, there are several possible explanations for this phenomenon discussed above (see **Section 6.2.4**).

APPENDIX C

RELAXIN INCREASES CARDIAC OUTPUT AND REDUCES SYSEMIC ARTERIAL LOAD IN HYPERTENSIVE RATS

C.1 PREAMBLE

Although not directly related to the Specific Aims of the current work, we believe that relaxin's effects on systemic arterial load may be particularly beneficial in treating vascular disorders (discussed in **Section 7.0** above). Currently, the effects (both magnitude and temporal pattern) of relaxin on systemic hemodynamics and arterial properties in hypertensive animal models are not known. We have initiated a study to examine the cardiovascular effects of rhRLX in hypertensive rats using two models – Long-Evans rats chronically administered angiotensin II (AII) and spontaneously hypertensive rats (SHR). The details of this work are described below.

C.2 INTRODUCTION

Our work to date has revealed that relaxin acts outside the reproductive system and plays a role in regulating renal and cardiovascular function. Specifically, chronic administration of

recombinant human relaxin (rhRLX) to nonpregnant female and male normotensive rats, elicits a vasodilatory response resulting in increased cardiac output as well as reduced steady and pulsatile components of the arterial load [48, 50]. Furthermore, the magnitude of change in arterial load in response to relaxin treatment is dependent on the baseline value of arterial load [50]. That is, rats that exhibited higher systemic vascular resistance (SVR) or lower global arterial compliance (AC) at baseline responded more robustly to relaxin administration. Based on this observation, we reasoned that relaxin administration may be particularly effective in chronic hypertension in which arterial load is typically elevated. In fact, St-Louis et al. and Massicotte et al. [17, 18] showed that relaxin administration to female spontaneously hypertensive rats (SHR) caused a significant decrease in mean arterial pressure as early as 6 hours after the onset of relaxin infusion that persisted throughout the 5 days of relaxin infusion. However, these studies did not examine the effects of relaxin on other hemodynamic variables and arterial properties. Other studies have also reported that relaxin antagonizes the actions of angiotensin II (AII) in rats [16, 74]. Therefore, the primary goal of this study was to investigate the impact of rhRLX on systemic hemodynamics and arterial properties in two models of hypertension: rats made hypertensive by chronic administration of AII and SHR rats.

Relaxin-induced changes in systemic hemodynamics and arterial load properties were observed in normotensive rats at the earliest timepoint studied (3 days) and these changes persisted throughout the entire 7 days of rhRLX infusion [48, 50]. Other studies have shown that rhRLX vasodilates the renal circulation as early as 1-2 hours following the onset of intravenous infusion of the hormone [35]. Therefore, the second goal of the present study was to determine if the changes in systemic hemodynamics and arterial properties produced by relaxin would be

observed during short term (up to 6 hours) intravenous infusion of the hormone, especially in the hypertensive rats wherein arterial load is elevated at baseline.

C.3 METHODS

Animals

Long-Evans female rats (age: 12-14 weeks) were purchased from Harlan Sprague-Dawley (Frederick, Maryland USA) or Taconic (Germantown, NY USA). Male and female spontaneously hypertensive rats (age: 12-15 weeks) were purchased from Hilltop (Scottdale, Pennsylvania USA). They were provided PROLAB RMH 2000 diet containing 0.48% sodium (PME Feeds Inc., St. Louis, MO USA) and water *ad libitum* and were maintained on a 12:12-h light-dark cycle.

Instrumentation for Measurements in Conscious State: Surgical Procedure

The surgical procedure has been described previously in detail (see **Section 4.1.2**). Briefly, rats were anesthetized with 60 mg/kg ketamine i.m. and 21 mg/kg pentobarbital i.p. Ampicillin and atropine were given s.c. intraoperatively. The rats were then instrumented, using sterile technique, as follows: (i) a tygon catheter implanted in the right jugular vein with the tip lying at the junction of the anterior vena cava and right atrium, (ii) a thermodilution microprobe (22 cm long, F#1.5; Columbus Instruments, Columbus, OH USA) implanted in the abdominal aorta via the left femoral artery with the tip lying 1.0 cm below the left renal artery, and (iii) a mouse pressure catheter (TA11PA-C20, F#1.2; Data Science International, St. Paul, MN USA) implanted in the right carotid artery with the tip lying at the junction of the right carotid artery and aortic arch. For the acute administration of rhRLX, another tygon catheter was implanted in

the inferior vena cava via the left femoral vein such that the tip lay 1.0 cm below the left renal artery.

After instilling 0.05 ml of a heparin solution into the venous catheter(s) and plugging it with a straight pin, rats were given ampicillin by drinking water for 2 days (100 mg/50 ml with 2 tablespoons of dextrose). Terbutrol was given s.c. for post-operative analgesia.

Animal Models of Systemic Hypertension

Female Long-Evans rats 12-14 weeks of age, chronically administered AII via subcutaneous osmotic minipumps (60-120 ng/min) were used as one model of hypertension. Male spontaneous hypertensive rats 12-15 weeks of age were used as the second model of systemic hypertension.

Administration of Recombinant Human Relaxin (rhRLX)

The rhRLX (BAS, San Mateo, California USA) was provided as a 5.0 mg/ml solution in a buffer (20 mM sodium acetate, pH 5.0) and was diluted as necessary in the same buffer. For the acute infusion protocol, rhRLX was administered as an i.v. bolus over 3 min (2.0 μg/0.3 ml) followed by a continuous i.v. infusion for up to 6 hours at 4 μg/h. For chronic administration, one Alzet model 2001 osmotic minipump (Durect Corporation, Cupertino, CA USA) was inserted subcutaneously in the back of the animal under isoflurane anesthesia for rhRLX delivery up to 7 days at the dose of 4 μg/h.

Experimental Protocols

Acute administration of rhRLX to female normotensive rats **(Figure 43).** Five days after surgery, 4 to 7 baseline measurements of systemic hemodynamics were obtained over a 2 hour period followed by intravenous bolus (2.0 μg/0.3 ml) and continuous infusion of rhRLX at 4 μg/h for 4 hours. Systemic hemodynamics were assessed every hour.

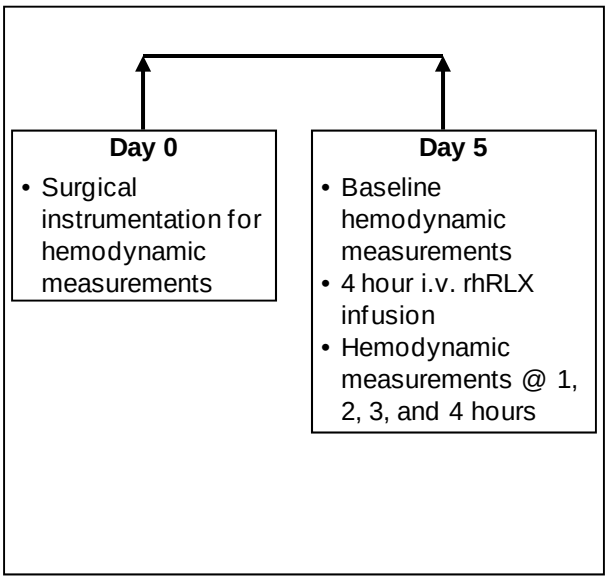

Figure 43. Timeline of Acute Administration of rhRLX to Normotensive Rats

Recombinant human relaxin was administered acutely, via i.v. infusion, to female normotensive rats over 4 hours. Measurements of systemic hemodynamics were made before and periodically during the 4 hour infusion period.

*Acute administration of rhRLX or vehicle to female, AII-treated rats (***Figure 44)**. Four to 7 control measurements of systemic hemodynamics were obtained over a 2 hour period prior to the administration of AII. Two days after initiating the AII infusion, 4 to 7 measurements of systemic hemodynamics were again obtained over a 2 hour period, followed by intravenous bolus (2.0 μg/0.3 ml) and continuous infusion of rhRLX at 4μg/h for 6 hours, or vehicle for rhRLX (20 mM sodium acetate, pH 5.0). Systemic hemodynamics were assessed every 2 hours during the 6-hour rhRLX or vehicle infusion. This protocol (i.e., acute infusion of rhRLX over a 6-hour period) was repeated 5 days after initiating the AII infusion.

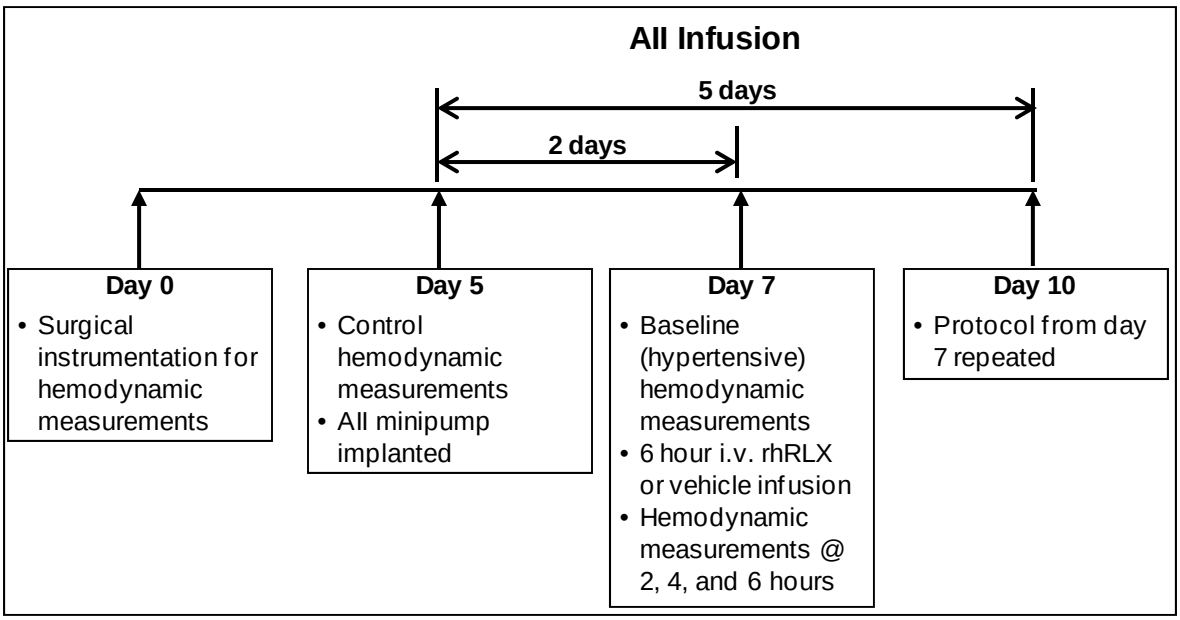

Figure 44. Timeline of Acute Administration of rhRLX to AII-Treated Rats

Female rats were chronically administered AII for 5 days. On days 2 and 5 following the initiation of AII infusion, rhRLX was administered acutely, via i.v. infusion, over 6 hours. Measurements of systemic hemodynamics were made before and after AII infusion prior to rhRLX infusion. Systemic hemodynamic measurements were made again during the 6 hour rhRLX infusion.

Acute and chronic administration of rhRLX to male spontaneously hypertensive rats **(Figure 45)**. For the acute administration protocol, 4 to 7 baseline measurements of systemic hemodynamics were obtained over a 2-hour period, 5 days after surgery followed by intravenous bolus (2.0 μg/0.3 ml) and continuous infusion of rhRLX (4 μg/h**)** for 6 hours. Systemic hemodynamics were assessed every 2 hours during the 6-hour rhRLX infusion. Following the 6-hour infusion, the rats were implanted with a subcutaneous osmotic minipump that delivered rhRLX for 7 days at the dose of 4 μg/h. Systemic hemodynamics were again measured 1, 4 and 6 days following implantation of the minipump.

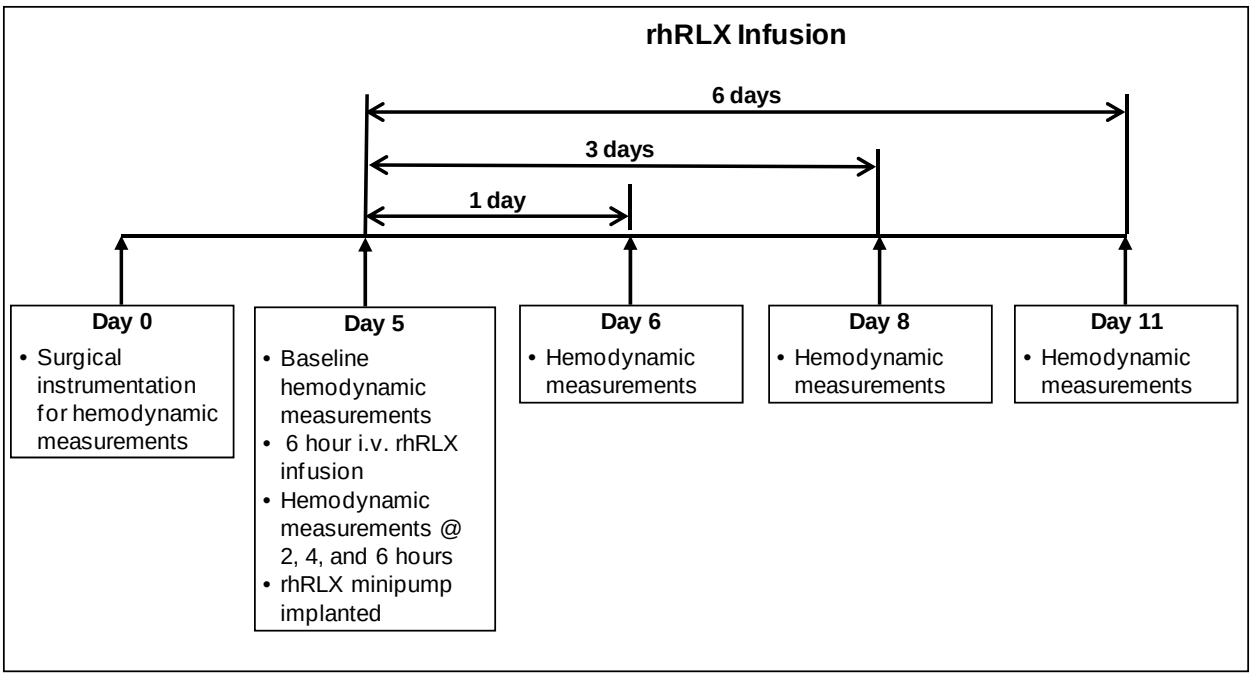

Figure 45. Timeline of Acute and Chronic Administration of rhRLX to SHR Rats

Male SHR rats were administered rhRLX acutely for 6 hours followed by chronic rhRLX administration for 7 days. Measurements of systemic hemodynamics were made before and during acute rhRLX infusion, and during chronic rhRLX infusion.

Postmortem Procedures

After completion of the measurement for the last time point of study, rats were anesthetized with 60 mg/kg pentobarbital i.v. Blood was obtained from the abdominal aorta for measurement of serum rhRLX levels. The position of the jugular catheter relative to the right atrium, the placement of the pressure catheter relative to the aortic arch, and the position of the thermocouple relative to the left renal artery were recorded.

Systemic Hemodynamics and Arterial Mechanical Properties

See **Section 4.1.5 – 4.1.8** for experimental procedures used.

Statistical Analysis

Data are presented as means ± SEM. One-factor repeated measures ANOVA was used to compare mean values at various time points during the administration of rhRLX to the baseline value. Two-factor ANOVA with repeated measures on both factors was used to compare mean values obtained during acute rhRLX infusion on days 2 and 5 following the initiation of AII infusion (Factor 1: different time points during acute rhRLX infusion; Factor 2: different AII infusion duration). If significant main effects were observed, pairwise comparisons between groups were performed using Fisher's LSD test. The Student's paired *t*-test was used to compare composite mean values during chronic rhRLX infusion with baseline values. $P<0.05$ was taken to be significant.

C.4 RESULTS

Portions of this work have been previously published elsewhere [89].

Acute administration of rhRLX to AII-treated rats. As detailed in Methods, each rat was administered rhRLX i.v. for a 6-hour period on days 2 and 5 after the initiation of the AII treatment. Because there was no statistically significant difference between days 2 and 5 for any of the systemic hemodynamics and arterial properties (by 2-factor repeated measure ANOVA), the results were averaged. Control values of HR, SV, CO and MAP prior to AII administration were 399±7 bpm, 0.34±0.02 ml, 135±6 ml/min, and 111±2 mmHg, respectively. Following treatment with AII (defined as the baseline condition for rhRLX treatment), HR, SV, CO and MAP were 367±14 bpm, 0.31±0.02 ml, 114±4 ml/min, and 138±6 mmHg, respectively. **Figure 46** illustrates the temporal patterns of changes in these hemodynamic variables (expressed as

percentages of baseline) in response to short-term i.v. infusion of rhRLX. Short-term rhRLX treatment resulted in a significant increase from baseline in CO within 2 hours after the initiation of the infusion. This increase in CO was due to increases in both SV and HR (Fig. 46). After 6 hours of rhRLX infusion, CO remained elevated (35±8%) above baseline, mainly due to the augmentation of SV to 26±6% above baseline. There was no statistically significant changes observed in MAP during the rhRLX infusion (Fig. 46).

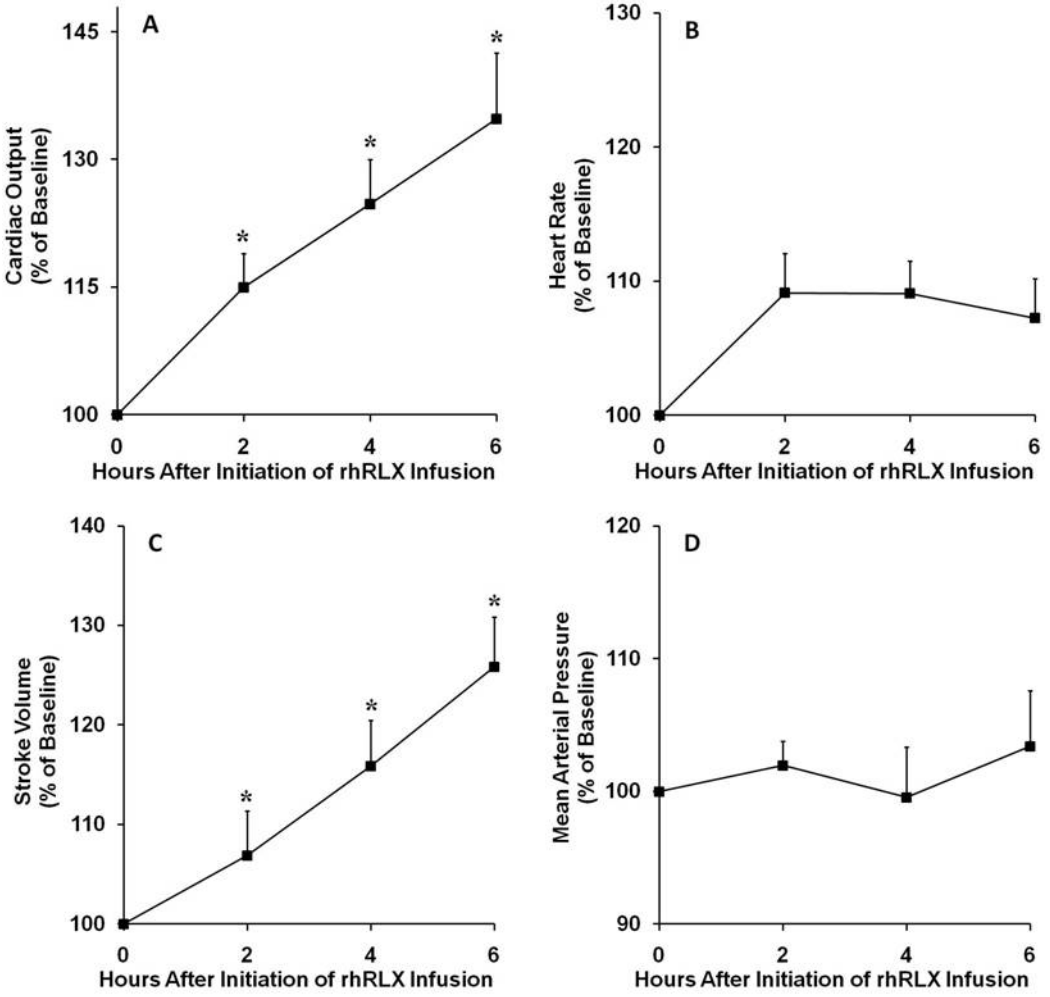

Figure 46. Temporal Pattern of Changes in Systemic Hemodynamics in AII-Treated Female Rats Administered Acute Low Dose rhRLX

Temporal changes in systemic hemodynamics in response to intravenous infusion of recombinant human relaxin (rhRLX) in female rats (n=7) chronically administered angiotensin II by osmotic minipump (60 ng/min) (see Methods for details). Rats were administered a 2 μg/0.3 ml bolus of rhRLX, followed by an infusion rates of 4 μg/h. Cardiac output **(A)**, heart rate **(B)**, stroke volume **(C)**, and mean arterial pressure **(D)** during rhRLX administration are presented as percentages of baseline. * $P<0.05$ *vs*. baseline (post-hoc Fisher's LSD).

Control value of SVR prior to AII administration was 49.9±2.1 mmHg·s/ml. Following treatment with AII (i.e., the baseline condition for rhRLX treatment), SVR increased to 74.6±3.9 mmHg·s/ml ($P<0.001$). **Figure 47** illustrates the temporal effects of acute i.v. infusion of rhRLX

on systemic arterial properties. There was a significant decrease from baseline in SVR within 2 hours following the onset of rhRLX infusion and global arterial compliance, as indicated by both measures (AC_{area} and SV/PP), was significantly increased within 4 hours.

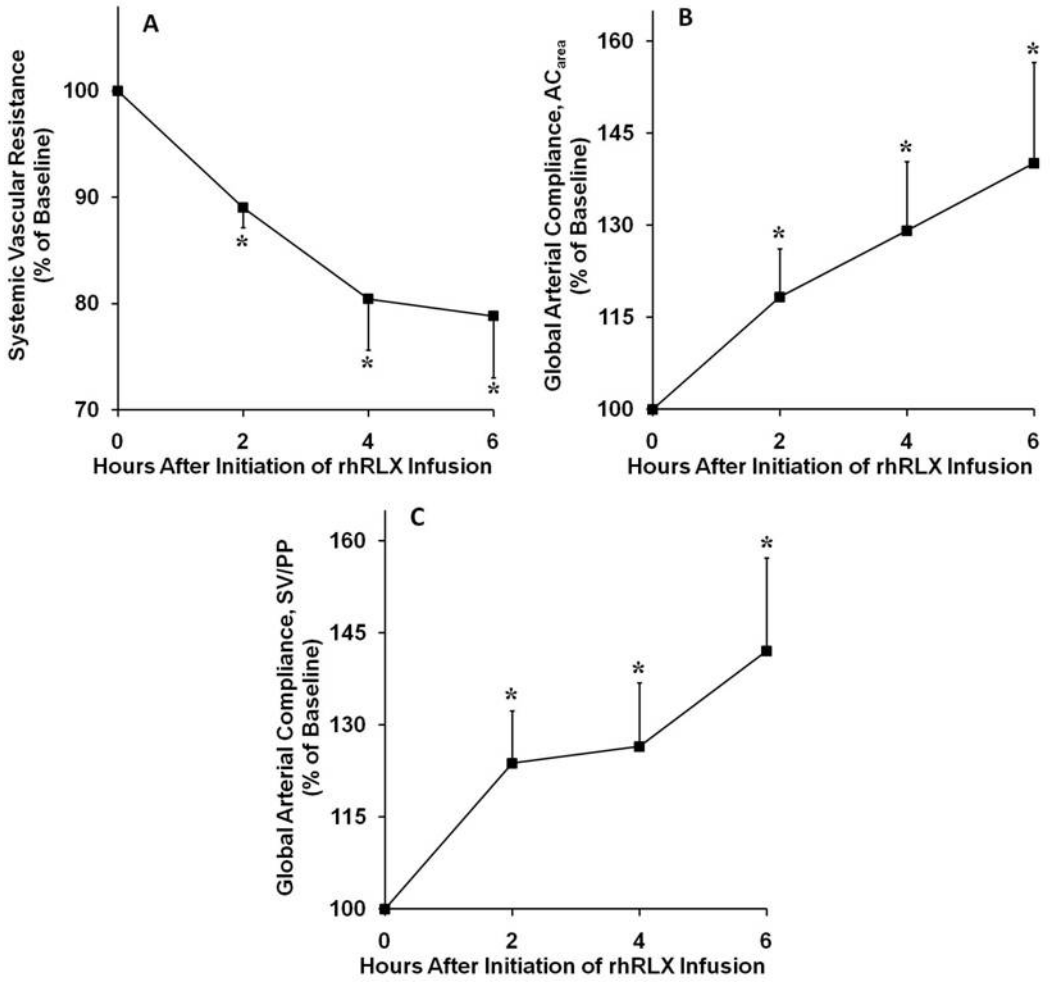

Figure 47. Temporal Pattern of Changes in Systemic Arterial Properties in AII-Treated Female Rats Administered Acute Low Dose rhRLX

Temporal changes in systemic arterial properties in response to intravenous infusion of recombinant human relaxin (rhRLX) in female rats (n=7) chronically administered angiotensin II by osmotic minipump (60 ng/min) (see Methods for details). Rats were administered a 2 μg/0.3 ml bolus of rhRLX, followed by an infusion rates of 4 μg/h. Systemic vascular resistance **(A)** and two measures of global arterial compliance AC_{area} **(A)**, and SV/PP **(C)** during rhRLX administration are presented as percentages of baseline. * $P<0.05$ *vs*. baseline (post-hoc Fisher's LSD).

As in our other work, we calculated a composite mean change from baseline for each variable by averaging values at all successive time points during the infusion of rhRLX that were characterized by a significant change from baseline but were not significantly different from each other. This yielded increases in CO and global arterial compliance of 24.9±3.9 and 34.3±12.6% from baseline, respectively and a decrease in SVR of 17.2±3.5% (all $P<0.05$ *vs.* baseline). The serum concentration of rhRLX measured in blood obtained after 6 hours of infusion was 26.0±0.6 ng/ml.

Three rats were subjected to the same protocol except they were administered the vehicle for rhRLX, rather than rhRLX. There were no significant changes from baseline in systemic hemodynamics or arterial properties during the 6-hour vehicle infusion (data not shown).

Acute administration of rhRLX to male spontaneously hypertensive rats. Baseline values of HR, SV, CO, and MAP were 385±13 bpm, 0.33±0.02 ml, 129±7 ml/min, and 175±7 mmHg, respectively. As detailed in Methods, systemic hemodynamics and arterial properties were assessed continuously during the 6-hour infusion of rhRLX. There were no statistically significant changes in the systemic hemodynamics or arterial properties among the data for various timepoints during the 6-hour infusion. Therefore, **figure 48** illustrates the combined mean change from baseline of the systemic hemodynamic variables measured over the 6-hour period. As compared to baseline, there was a slight, but statistically significant, increase in HR (Fig. 48B) which was offset by a small, but not statistically significant, decrease in SV (Fig. 48C), such that CO remained unchanged (Fig. 48A). Similarly, MAP was unchanged during the short term rhRLX infusion (Fig. 48D).

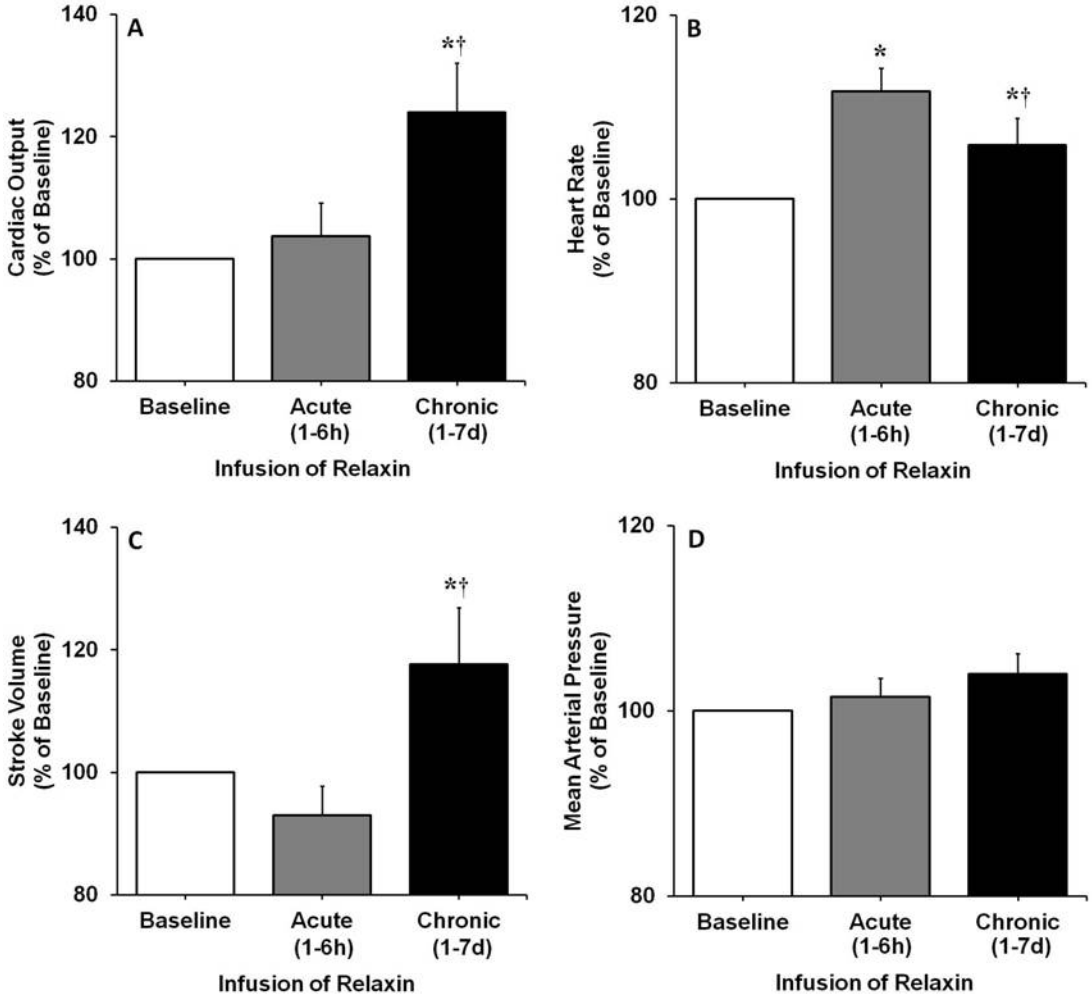

Figure 48. Temporal Pattern of Changes in Systemic Hemodynamics in Male SHR Rats Administered Chronic Low Dose rhRLX

Temporal changes in systemic hemodynamics in response to acute and chronic administration of rhRLX in male spontaneously hypertensive rats (n=7). For acute administration, rats were given an i.v. 2 μg/0.3 ml bolus of rhRLX, followed by an infusion rate of 4μg/h. For chronic administration, rhRLX was delivered by subcutaneous osmotic minipump at 4 μg/h. Cardiac output (**A**), heart rate (**B**), stroke volume (**C**), and mean arterial pressure (**D**) during rhRLX administration are presented as percentages of baseline. Bar graphs represent the combined mean change throughout the 6 hours of acute, or days 1, 4 and 6 of chronic rhRLX administration. * $P<0.05$ *vs*. baseline; † $P<0.05$ *vs*. short-term rhRLX-treated rats (post-hoc Fisher's LSD).

Baseline values of SVR, AC_{area}, and SV/PP were 83.7±5.6 mmHg·s/ml, 3.8±0.2 μl/mmHg, and 5.3±0.4 μl/mmHg, respectively. **Figure 49** illustrates the combined mean change

of the systemic arterial properties obtained during the 6-hour infusion of rhRLX. Short-term infusion of rhRLX did not yield any statistically significant changes.

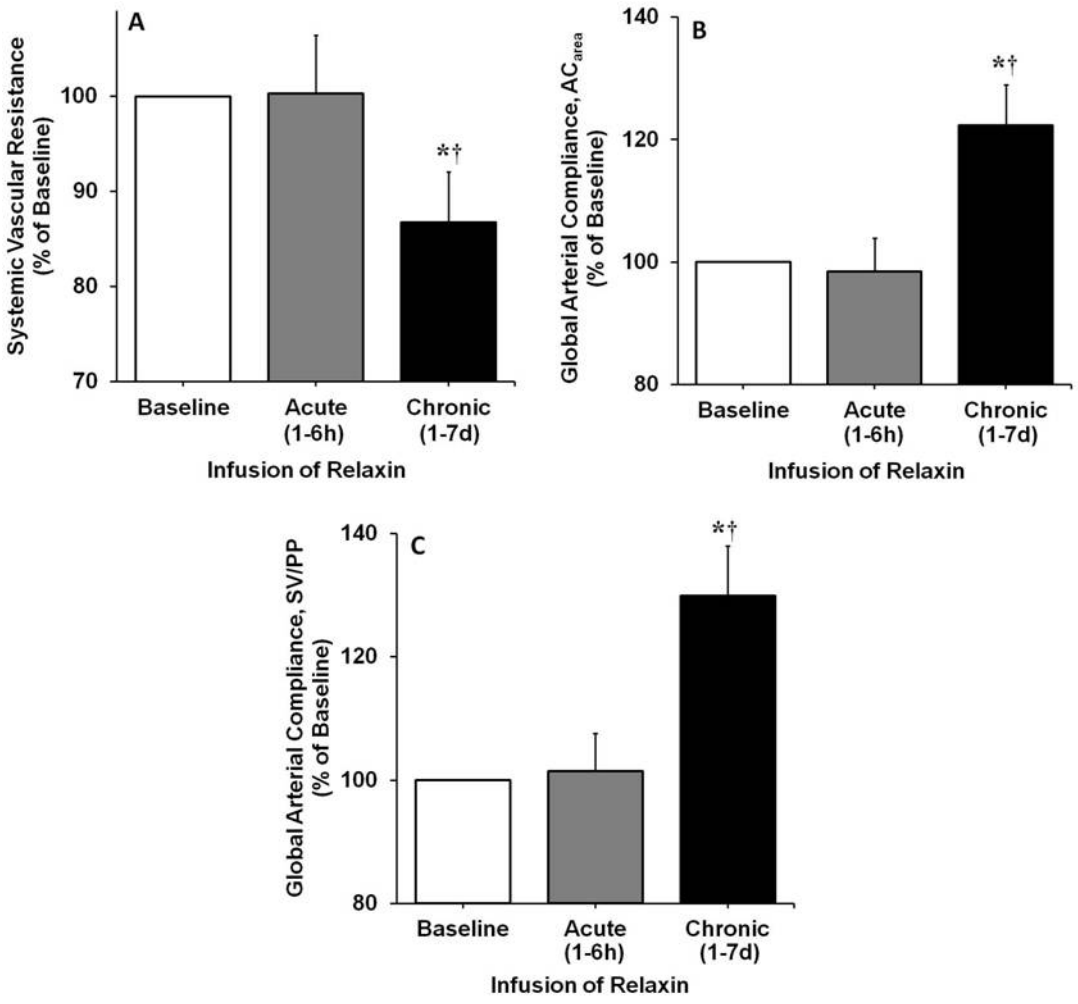

Figure 49. Temporal Pattern of Changes in Systemic Arterial Properties in Male SHR Rats Administered Chronic Low Dose rhRLX

Temporal changes in arterial properties in response to acute and chronic administration of rhRLX in male spontaneously hypertensive rats (n=7). For acute administration, rats were given an i.v. 2 μg/0.3 ml bolus of rhRLX, followed by an infusion rate of 4μg/h. For chronic administration, rhRLX was delivered by subcutaneous osmotic minipump at 4 μg/h. Systemic vascular resistance (**A**), and two measures of global arterial compliance AC_{area} (**B**), and SV/PP (**C**) during rhRLX administration are presented as percentages of baseline. Bar graphs represent the combined mean change throughout the 6 hours of acute, or days 1, 4 and 6 of chronic rhRLX administration. * $P<0.05$ *vs*. baseline; † $P<0.05$ *vs*. short-term rhRLX-treated rats (post-hoc Fisher's LSD).

Chronic administration of rhRLX to male spontaneously hypertensive rats. There were no statistically significant differences in systemic hemodynamics and arterial properties assessed at days 1, 4 and 6 of rhRLX administration by s.c. osmotic minipump. Therefore, combined mean changes of these variables obtained over the 6 day chronic infusion of rhRLX are illustrated in figures 41 and 42. Chronic rhRLX treatment resulted in a significant increase in HR compared to baseline (Fig. 48B). Similarly, SV was significantly increased from baseline (Fig. 48C). The increase in HR and SV resulted in a significant increase in CO (Fig. 48A). MAP was not significantly altered during the chronic rhRLX infusion (Fig. 48D). SVR was significantly reduced from baseline during the chronic rhRLX infusion (Fig. 49A) and both measures of global arterial compliance were significantly increased from baseline (Fig. 49B & 49C). The serum concentration of rhRLX measured in blood obtained after 7 days of infusion was 29.8±0.76 ng/ml.

Acute administration of rhRLX to female Long-Evans, normotensive rats (n=7). **Figure 50** illustrates the temporal changes in systemic hemodynamics in response to acute i.v. infusion of rhRLX in normotensive rats expressed as percentages of baseline. Baseline values of HR, SV, CO and MAP were 425±17 bpm, 0.30±0.01 ml, 129±7 ml/min, and 112±3 mmHg, respectively. During the 4-hour i.v. infusion of rhRLX, there were no significant changes from baseline in HR, SV, or CO (Fig. 50A-50C). There was a small (<10%), albeit significant increase in MAP 1 hour after the onset of rhRLX infusion and this increase persisted throughout the 4-hour infusion (Fig. 50D). Combining all the timepoints studied yielded overall changes of 4.4±2.9%, 2.3±2.6%, and 7.1±4.1% in HR, SV, and CO, respectively (all P=NS *vs.* baseline). Similarly, there was an overall increase of 9.8±3.0% in MAP (P<0.05 *vs.* baseline).

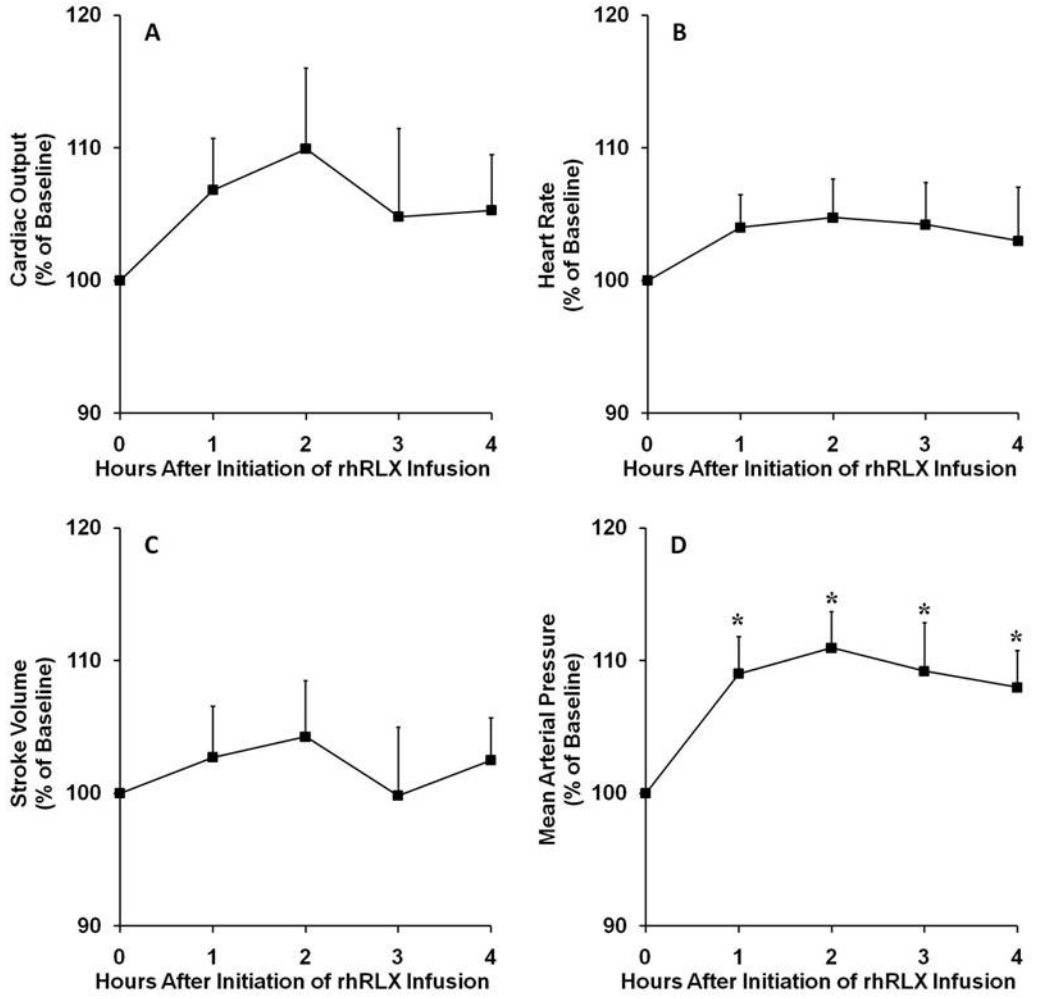

Figure 50. Temporal Pattern of Changes in Systemic Hemodynamics in Female Normotensive Rats Administered Low Dose rhRLX

Temporal changes in systemic hemodynamics in response to intravenous infusion of rhRLX in female Long Evans, normotensive rats. Rats were first administered a 2 μg/0.3 ml bolus of rhRLX over 3 min, followed by an infusion rate of 4 μg/h. Cardiac output **(A)**, heart rate **(B)**, stroke volume **(C)**, and mean arterial pressure **(D)** during rhRLX administration are presented as percentages of baseline. * $P<0.05$ *vs*. baseline (post-hoc Fisher's LSD).

The temporal responses of systemic arterial properties during acute i.v. infusion of rhRLX expressed as percentages of baseline are illustrated in **figure 51**. Baseline values of SVR, AC_{area}, and SV/PP were 53.1±3.2 mmHg·s/ml, 7.1±0.4 μl/mmHg, and 8.8±0.7 μl/mmHg,

respectively. Short-term infusion of rhRLX yielded no statistically significant changes from baseline in any systemic arterial properties. Because there were no statistically significant differences among various timepoints (1-4 hours) for any of the variables, data were combined for all timepoints studied. This yielded overall changes of 4.1±4.1%, -2.9± 2.9%, and 5.5±4.3% in SVR, AC_{area}, and SV/PP, respectively (all *P*=NS *vs.* baseline). The serum concentration of rhRLX measured in blood obtained after 4 hours of infusion was 13.4±3.5 ng/ml.

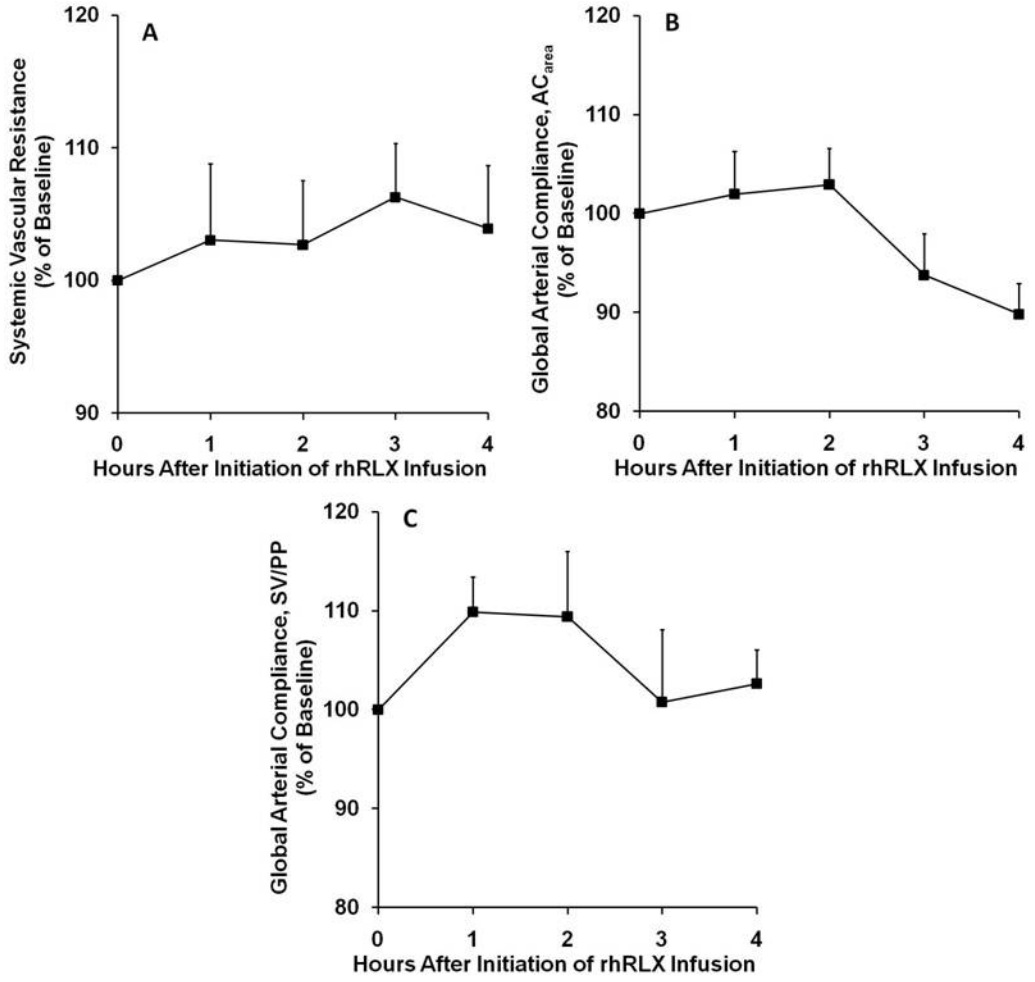

Figure 51. Temporal Pattern of Changes in Systemic Arterial Properties in Female Normotensive Rats Administered Low Dose rhRLX

Temporal changes in systemic arterial properties in response to intravenous infusion of rhRLX in female Long Evans, normotensive rats. Rats were first administered a 2 μg/0.3 ml bolus of rhRLX, followed by an infusion rate of 4 μg/h. Systemic vascular resistance **(A)** and two measures of global arterial compliance AC_{area} **(A)**, and SV/PP **(C)** during rhRLX administration are presented as percentages of baseline.

C.5 DISCUSSION

Major findings of the present study are as follows: (1) rhRLX reduces arterial load (a decrease in systemic vascular resistance and an increase in global arterial compliance) and increases cardiac output in hypertensive rats, without any effect on mean arterial pressure; (2) The temporal pattern of these changes are model-specific. While rats with AII-induced hypertension respond to rhRLX administration rapidly (within 2 hours), spontaneously hypertensive rats, like normotensive rats, respond more slowly (at least 1 day). To our knowledge, this investigation of relaxin on systemic hemodynamics and arterial properties in hypertensive animal models is unprecedented.

In other work, we reported that chronic administration of rhRLX to normotensive rats, elicits a systemic vasodilatory response that is observed as early as 3 days following the onset of rhRLX infusion (see **Section 5.1.3** and **Section 5.1.6**). In other work, rhRLX elicited a vasodilatory response in the renal circulation that is observed during both acute (within 1-2 hours) and chronic (2-5 days) administration of the hormone [16, 35]. In fact, the hormone mediates the renal circulatory (and osmoregulatory) changes of pregnancy in this species [23]. In the current study we did not observe a systemic vasodilatory response when the hormone was administered acutely to normotensive rats for 1 to 6 hours. This finding suggests that certain organ beds such as the kidneys are able to respond more quickly to the vasodilatory actions of relaxin[1]. Consistent with this concept is the observation that following preconstruction with phenylephrine, small renal, but not mesenteric or coronary arteries isolated from rats demonstrate an immediate relaxation response to rhRLX (Jackie Novak and Kirk P. Conrad, unpublished

[1] N.B. Because baseline renal blood flow (RBF) is only ~20% of CO, the expected increase in CO caused by a 20-40% increase in RBF by rhRLX is not readily detectable.

data, 2004). Furthermore, Fisher et al. reported that isolated human gluteal, but not pulmonary resistance arteries showed a rapid relaxation response to relaxin [91]. It is therefore possible that when administered *acutely*, relaxin preferentially vasodilates certain organ beds, and is ineffective in vasodilating others at least on a short term bases. Of note, acute i.v. infusion of rhRLX did result in a slight, but significant increase in MAP similar to previously reported observations [92].

Interestingly, rhRLX did elicit a rapid systemic vasodilatory response when acutely administered to rats with AII-mediated hypertension. In fact, the present work in hypertensive rats was spurned by our previous observation showing that normotensive rats with higher magnitudes of arterial load at baseline responded more robustly to chronic relaxin treatment. Rats with AII-mediated hypertension responded with an even greater increase in cardiac output and decrease in arterial load in a much shorter period of time than normotensive rats (*vide supra*). Pregnancy, and more specifically relaxin, has previously been shown to antagonize the vascular actions of AII. Conscious pregnant rats were less responsive to the renal and systemic vasoconstrictory effects of AII, both at mid- [27] and late-gestation [26, 93]. Chronic administration of relaxin to nonpregnant rats also attenuated AII-induced renal vasoconstriction [16]. Finally, Samuel et al. reported that relaxin reduced cardiac collagen synthesis and accumulation in myofibroblasts that had been stimulated with AII [74].

In contrast to AII-treated rats, spontaneously hypertensive rats did not respond to acute infusion of rhRLX. This finding was contrary to our expectations because recent reports demonstrated that AII contributes to hypertension in SHR rats through the angiotensin type 1 receptor [94, 95], and because relaxin has been shown to be a functional AII antagonist [16, 74]. The lack of response was not due to inadequate serum concentrations of rhRLX. In fact, the

circulating levels in all the studies in hypertensive rats were ~2X higher than normotensive animals. We do not have a ready explanation for why SHR rats did not respond acutely to rhRLX, however they did respond to chronic rhRLX administration. Based on our other work, the reduction in SVR and increase in global AC due to chronic rhRLX administration results from a reduction in vascular smooth muscle tone and remodeling of arterial extracellular matrix. Because relaxin possesses angiogenic attributes [20, 56], angiogenesis may also contribute to the changes in systemic hemodynamics and arterial properties.

In our work examining the effects of exogenous relaxin administration on systemic hemodynamics and arterial properties including the current study, we observed that the decline in SVR elicited by rhRLX is unaccompanied by a significant change in MAP. In fact, this situation resembles pregnancy in humans and other species where a profound reduction in SVR is associated with only a modest decline in MAP [5, 15, 34]. The decline in SVR is offset by a comparable rise in CO, thereby maintaining MAP. Four mechanisms may contribute to this reciprocal increase in CO during relaxin administration. First, relaxin is a positive chronotropic agent both *in vitro* and *in vivo* (at least in rats), an observation reported by us and several others [61, 96, 97]. Second, relaxin produces a positive inotropic effect in isolated ventricular tissue from rat and guinea pig heart [96-98]. Third, the fall in SVR and increase in arterial compliance reduce ventricular afterload, thereby abetting the increase in CO. Finally, because MAP does not fall, our studies suggest that relaxin is a pure arterial vasodilator, thus permitting venoconstriction and/or reduction in passive venous compliance that maintains the ventricular end diastolic volume or preload despite the decline in SVR. To our knowledge, there are no published studies on relaxin and the venous circulation. However, Edouard et al. conducted a longitudinal study examining venous behavior throughout normal pregnancy in women, and they

observed increased venous tone in the lower limb beginning in the first trimester that was strongly correlated with left ventricular diastolic diameter [99]. In summary, based on these previous findings and the present work, we speculate that relaxin may exert different actions in the venous and arterial circulations. Specifically, relaxin elicits a vasodilatory response in the arterial circulation, while augmenting venous tone either directly or indirectly (e.g., via potentiation of humoral venoconstriction or baroreflex mediated sympathetic tone). Consequently, the fall in SVR induced by relaxin is paralleled by an increase in CO and it is by this mechanism that MAP is maintained during relaxin administration.

Of note, other studies have reported that, contrary to what we observed in this investigation, MAP is significantly reduced in SHR rats in response to acute and chronic infusion of relaxin [17, 18]. These studies differed from the current investigation in that the animals used were female SHR rats. Therefore, to determine if female SHR rats show a different response to relaxin infusion than males, we obtained arterial pressure measurements before and during rhRLX infusion in 7 female SHR rats. (Note: Due to their small size (<210g), we only instrumented the animals with the mouse pressure catheter. In our experience, ligation of the femoral artery in small rats leads to hind limb ischemia.) Five days after the implantation of the mouse pressure catheter in the right carotid artery, the rats were briefly anaesthetized with isoflurane and implanted with an osmotic minipump that delivered rhRLX at 4 μg/h for 6 days. The serum level of rhRLX after 6 days of infusion was 28.6±2.16 ng/ml. Baseline values of HR and MAP were 405±2 bpm and 171±2 mmHg, respectively. When compared to baseline, HR was significantly increased during rhRLX infusion comparable to the male SHR rats. There was a small, but statistically significant decrease in MAP 6 hours following the infusion of rhRLX. However, MAP was not significantly different from baseline at any of the subsequent timepoints

studied. We attribute the small decrease in MAP at 6 hours to the hypotensive effects of isoflurane anesthesia. The hypotensive response to isoflurane anesthesia has been well documented in various strains of rats and SHR rats have been shown to be more sensitive in this regard [100, 101]. We do not have an immediate explanation for why we were unable to reproduce the results of St-Louis et al. and Massiochotte et al. [17, 18]; differences in surgical procedures and experimental approaches may contribute to this discrepancy.

APPENDIX D

DETAILED IMMUNOFLUORESCENCE PROTOCOLS

D.1 PREPARATION AND SECTIONING OF ISOLATED ARTERIES

After arteries are excised from the animal, they should be cleaned of all connective tissue then placed in 2% paraformaldehyde/PBS (fixing solution) in the fridge for ~4 hours. Arteries should then be rinsed with PBS and placed in 30% Sucrose/ PBS (cryoprotecting solution) for 24-48 hours in the fridge before being embedded in OCT.

To embed arteries in OCT molds, pour a small amount of OCT into a plastic embedding mold until it is half full and allow the OCT to settle for ~1 hour. Next, you must freeze isopentane over liquid nitrogen (LN). We found that this works best if you pour some LN into a large, wide container. Then pour some isopentane into a beaker and dunk the beaker into the LN. Wait for 2-5 min until isopentane starts to turn opaque. Have the plastic embedding mold with the OCT ready. Place the mold in the isopentane to freeze the OCT (shouldn't take more than a minute). Place the horizontally on top of the frozen OCT. Cut a small thin red string about the same length as the artery and place it next to the artery on top of the frozen OCT. We found that this was the only way to identify where the artery is after the OCT mold is frozen. This is especially important for small arteries. Pour OCT onto the mold and fill it to the top. Plunge the

mold into the isopentane bath for at least 30 sec or until OCT is completely frozen. Retrieve the mold, wrap in tin foil, label with permanent ink, and immediately store in a -80°C freezer until you are ready for sectioning. When necessary, transport molds on ice.

We found that small renal arteries were too small to embed individually in OCT. Therefore, we embedded the entire kidney. To do this, we gently removed the capsule and oriented the kidney so that the main renal artery faces upward. Then with a sharp razor, we made a cut in the horizontal plain a little less than halfway down the kidney. Then we placed both halves face-down in the OCT mold. The molds were frozen and stored the using the same techniques described above.

To section OCT blocks, fix sample block to the chuck with OCT media. Take several 6μm thick sections onto Superfrost Microscope Slides. We typically took at 15-20 sections per sample. Three-to-four sections were discarded in between each section that was stored. Slides can be stored at -80^{o}C until they are ready to be stained.

D.2 PROTOCOL FOR IMMUNOFLUORESCENCE STAINING OF ATERIAL CROSS-SECTIONS

This protocol was obtained from the Center for Biologic Imaging (CBI) website [102].

1. Rehydrate with 2 washes of 1xPBS.
2. 3 washes .5% BSA.
3. BLOCK with 2% BSA for 45 minutes.
4. 5 washes of .5% BSA.

5. Primary antibody for 60 minutes (prepared in .5% BSA, vortexed, and spun down for 5 minutes at 14000 RPM).
6. 5 washes of BSA.
7. Secondary antibody for 60 minutes (prepared in .5% BSA, vortexed, and spun down for 5 minutes at 14000 RPM).
8. 5 washes of .5% BSA.
9. 5 washes of PBS.
10. Hoescht stain for 30 seconds (prepared in de-ionized water at 1 mg/100 mL).
11. 3 washes with PBS.
12. Cover slip with gelvatol mounting medium [102] and refrigerate.
13. Slides must dry overnight and be stored at 4 C in the dark.

Note: Do not let tissue sections dry up, keep in liquid at all times until gelvatol step.

D.3 PROTOCOL FOR IMMUNOFLUORESCENCE STAINING OF CULTURED CELLS

This protocol was also obtained from the CBI website [102].

1. Wash off Media with 3 washes of 1xPBS
2. Fix in 2% paraformaldehyde for 15 minutes, made in PBS.
3. Permeabilize with 0.1% Triton X made in PBS solution for 15 min.
4. Rehydrate with 3 washes of PBS.
5. 5 washes of .5% BSA.
6. BLOCK with 2% BSA for 45 minutes.

7. 5 washes of .5% BSA.
8. Primary antibody in .5% BSA for 60 minutes (prepared in .5% BSA, vortexed, and spun down for 5 minutes at 14000 RPM).
9. 5 washes of .5% BSA.
10. Secondary antibody in .5% BSA for 60 minutes (prepared in .5% BSA, vortexed, and spun down for 5 minutes at 14000 RPM).
11. 5 washes of .5% BSA.
12. 5 washes of PBS.
13. Hoescht stain for 30 seconds.
14. 2 wash with PBS.
15. Cover slip with gelvatol and refrigerate.
16. Slides or coverslips must dry overnight at 4 C in the dark.

Note: Do not let cells dry up, keep in liquid at all times until gelvatol step.

APPENDIX E

COLLAGEN AND ELASTIN ASSAY PROTOCOLS

E.1 SIRCOL COLLAGEN ASSAY

This assay protocol was obtained from Dr. Rachelle Prantil-Baun.

Chemicals Needed:

1. Pepsin
2. 0.01N and 0.001N HCL
3. Sircol Collagen Assay Kit (Biocolor Ltd., Northern Ireland; purchased from Accurate Chemical Company; Catalog #: CLRS1111)

Supplies Needed:

1. Centrifuge Tubes
2. Vortex Genie
3. 15ml conical Tubes
4. 50 ml conical Tubes
5. Pipette tips (5µl, 20µl, 200µl, 1000µl)

6. Cuvettes and caps or 96 well plate

Equipment Needed:

1. Rocker Platform
2. Micro-centrifuge
3. Pipette guns of various accuracies
4. UV spectrophotometer or microplate reader

PROTOCOL:

Tissue Digestion:

1. Tissue should be cleaned of any extraneous tissue and weighed in its hydrated state.
2. Tissue is then freeze-dried for 4 hours (we used a lyophilizer for this purpose).
3. Weigh and record tissue dry weight.
4. Prepare 0.01 N and 0.001N HCL solutions and prepare pepsin-HCL solution (for digestion):
    a. Solution A: add 0.05 g of pepsin to 50 ml of 0.01N HCL solution and gently stir.
    b. Solution B: add 0.005 g of pepsin to 50 ml of 0.001N HCL solution and gently stir. This solution is used for smaller tissue samples; see Step 6 below.
    c. These solution needs to made fresh daily.
5. Mince tissue into small pieces and deposit into a microcentrifuge tube.
6. Add pepsin-HCL solution to the microcentrifuge tube:
    a. Add 100µl of pepsin-HCL Solution A for every 0.001g of tissue.

b. For smaller tissue add samples 1 ml of pepsin-HCL Solution B for every 0.001g of tissue.

7. Parafilm the centrifuge tubes and label.
8. Place on rocker platform in the refrigerator and allow to digest for 48 hours.

Assessment of Collagen:

1. Post-tissue digestion, vortex the solution and take 100 µl of the digested solution and place into a new microcentrifuge tube. Then take another 50 µl of the digested solution and place into a separate microcentrifuge tube and dilute with 50 µl of pepsin-HCL solution so that you have a solution of 1:2 digested tissue.
    a. Repeat the same process for another tube, but this time make a solution for 1:4 digested tissue.
    b. Repeat again for 1:8 digested tissue.
    c. Label each tube with the appropriate dilution.
2. Prepare collagen standards:

Table 11. Collagen Assay Standard Solutions

Volume of Stock Solution (0.5 mg/ml Collagen)	Volume of Dilutent (0.01N or 0.001N pepsin-HCL)	Final Collagen Concentration (µg/ml)
0 µl	100 µl	0 µg/ml
5 µl	95 µl	25 µg/ml
8 µl	92 µl	40 µg/ml
16 µl	84 µl	80 µg/ml
20 µl	80 µl	100 µg/ml
30 µl	70 µl	150 µg/ml

3. Add 1 ml of Sirius Red dye from assay kit to all centrifuge tubes (standards and diluted digested tissue).
4. Place all tubes on the rocking platform for 1 hour.
5. Spin down tubes using a microcentrifuge for 10 min at 10,000 RPM.
    a. Note: once spun down, tissue should be compacted enough so that it is not floating or mobile. If tissue is still floating, repeat step 5.
6. Pour out supernatant into a specimen cup, maintaining the precipitate at the bottom of the centrifuge tube and do your best to rid the tube of as much supernatant as possible. It is helpful to use a q-tip for this step.
7. Digest precipitate with 1 ml of Acetic Acid solution from assay kit.
8. Vortex each tube for ~30 seconds or until completely dissolved.
9. Pipette 3 200µl aliquots of each sample into separate wells of a 96 well plate.
10. Place plate into a microplate reader and read absorbance values anywhere from 530 nm to 570 nm. We obtained the best results reading at an absorbance of 560 nm.

Calculating Unknown Collagen Concentrations:

11. Plot absorbance vs. collagen standard concentration.
    a. This should be a linear curve (**Figure 52**).
12. Calculate collagen concentration based on best fit linear equation.

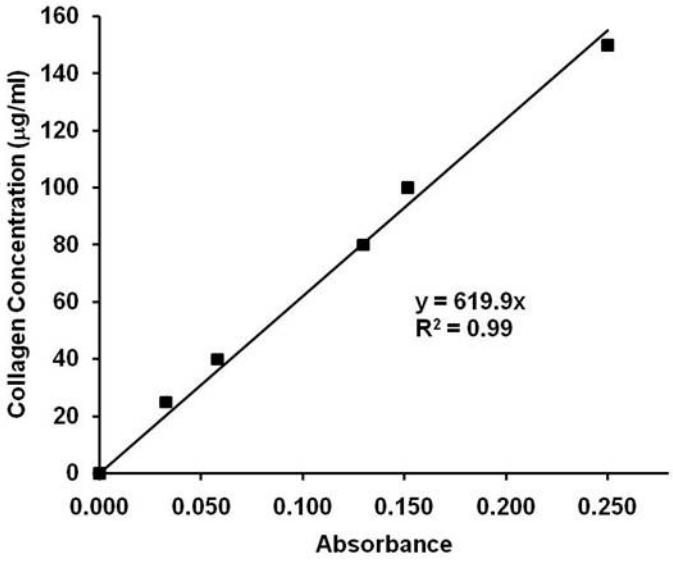

Figure 52. Sample Collagen Assay Standard Curve

Absorbance values were plotted *vs* known collagen concentrations. Experimental data were fitted to a linear equation (collagen concentration, y; absorbance, x). Best-fit constitutive parameters were then used to compute unknown collagen concentrations for a given absorbance.

E.2 FASTIN ELASTIN ASSAY

This assay protocol was obtained from Dr. Rachelle Prantil-Baun.

Chemicals Needed:

All the chemicals need are provided in the assay kit (Biocolor Ltd., Northern Ireland; purchased from Accurate Chemical Company; Catalog #: CLRF2000)

.

Supplies Needed:

1. Centrifuge Tubes
2. Vortex Genie

3. 15ml conical Tubes
4. 50 ml conical Tubes
5. Pipette tips (5µl, 20µl, 200µl, 1000µl)
6. Cuvettes and caps or 96 well plate
7. Microcon YM-3 Centrifugal Filter Unit (Millipore; Cat #:42403)

Equipment Needed:

1. Rocker Platform
2. Micro-centrifuge
3. Pipette guns of various accuracies
4. UV spectrophotometer or microplate reader

PROTOCOL:

1. Tissue should be cleaned of any extraneous tissue and weighed in its hydrated state.
2. Tissue is then freeze-dried overnight (we used a lyophilizer for this purpose).
3. Weigh and record tissue dry weight.
4. Put the entire artery (UNMINCED!) into a 1.5 mL microfuge tube. Add 20 volumes of 0.25 M oxalic acid (stock: 1.58 g oxalic acid + 50 ml de-ionized water).
    a. For example, if tissue dry weight is 0.1 g, then add 2 ml of 0.25 M oxalic acid.
5. Heat microfuge tube at 90^{o}C for 1 hour.
6. Chill tubes to room temperature quickly. Use an "ice water slurry".
7. Centrifuge the tubes at 3000 RPM at 4^{o}C for 10 minutes.
    a. Repeat this step until ALL of the tissue is compacted to the bottom.

8. Remove and save the supernatant. Label this supernatant, **E1**. *Keep in an ice bucket or in the refrigerator.*
9. To the pellet in Step 9, go back to Step 3 and add oxalic acid again.
    a. Add the same volume as original step.
10. Repeat the heating and centrifuging as in Steps 4 – 8. Label this supernatant, **E2**.

11. To this pellet from Step 10, repeat the oxalic acid extraction again as above. Call this supernatant **E3**.
12. Repeat the extraction a fourth time. Label the supernatant **E4**.
    a. For smaller tissue sample it might be necessary to repeat the extraction steps 5 or 6 times in order to ensure that there is a high yield of elastin.
13. Concentrate the acid extracts with a Microcon YM-3 Centrifugal Filter Unit.
    a. Add 500 µl of extract to filter and centrifuge at 14,000 RPM for 90 minutes.
    b. Repeat until entire volume of extract is filter.
    c. In order to retrieve elastin from filter, turn filter upside down in a separate centrifuge tubes and spin at 14,000 RPM for 10 min.
14. Add 1 ml of elastin precipitating reagent to each centrifuge tube.
    a. At this point you can combine all the extracts for each given sample by gently triturating elastin precipitating reagent in each centrifuge tube.
15. Place tubes in the fridge overnight.
16. After 24 hours, place extracts in a bath of ice in the fridge for ~30 minutes to ensure the tubes are at 0-4^{o}C.
17. Centrifuge tubes at 12,000 RPM at 4^{o}C for 10min.

18. During this time you should prepare elastin standards:
    a. Place 0µl, 5µl, 10µl, 20µl, 30µl, 40µl of elastin into separate tubes.
    b. Add 1ml of Fastin elastin dye reagent to each tube.
    c. Add 100µl of 90% ammounium sulfate solution.
19. After extracts have spun down, pour off the supernatant.
    a. Do this very well, b/c the trichloracetic acid in the precipitating agent binds to the elastin dye.
20. Add 1 ml of dye reagent to the extract tubes and 100ul of 90% ammonium sulfate.
21. Place extracts and standards on rocker (on slow x4) for 1 hour.
22. Centrifuge at 12,000 RPM for 10 minutes at room temperature.
23. Pour off supernatant.
24. Add 1 ml of destaining agent and vortex.
    a. Note: it is pretty tough to dissolve the solid so you might have to vortex several times.
25. Pipette 3 200µl aliquots of each sample into separate wells of a 96 well plate.
26. Place plate into a microplate reader and read absorbance values anywhere at close to 405 nm as possible. We obtained the best results reading at an absorbance of 450 nm.

Calculating Unknown Elastin Amounts:

27. Plot absorbance vs. mass of elastin.
    a. This should be a linear curve (**Figure 53**).
28. Calculate mass of elastin based on best fit linear equation.

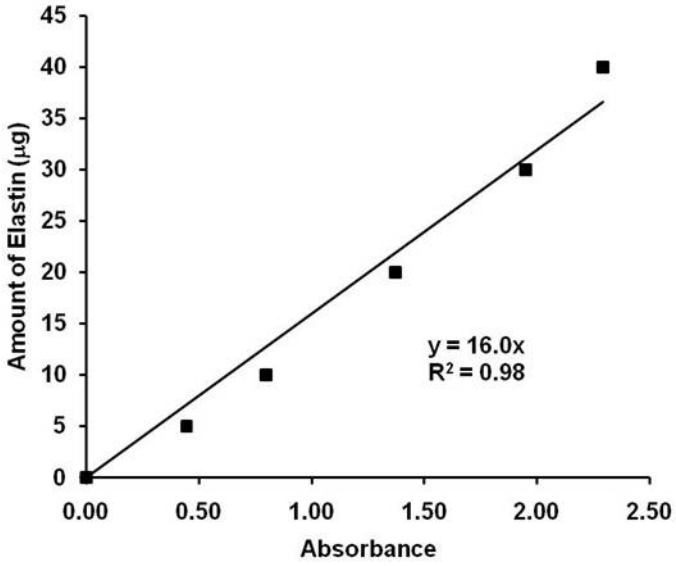

Figure 53. Sample Elastin Assay Standard Curve.

Absorbance values were plotted *vs* known elastin concentrations. Experimental data were fitted to a linear equation (elastin concentration, y; absorbance, x). Best-fit constitutive parameters were then used to compute unknown elastin concentrations for a given absorbance.

APPENDIX F

MATLAB PROGRAMS

F.1 ANALYSIS OF AORTIC PRESSURE WAVEFORMS AND CARDIAC OUTPUT MEASUREMENTS

This program is subdivided into several components which were assessed by a main program using callbacks. The main program is designed as a graphical user interface with several different handles that correspond to the various callbacks. The code for the main program is as follows:

```
clear
Fig=figure(1);
clf
set(Fig, 'Name', 'Global Arterial Compliance Analysis Program');
set(Fig,'menubar','none');


% handle1 defines the callback used to load pressure data
handle1 = uimenu('Label','Load');
handle1_1 = uimenu('Label','Load Data','callback','Load_Data','enable','on');
set(handle1_1,'parent',handle1);
set(handle1,'children',handle1_1);

% handle2 defines the callback used to pick a section of the pressure data to be analyzed
handle2 = uimenu('Label','Pick Section','callback','Pick_Section','enable','off');

% handle3 defines the callback used to select individual beats on the pressure waveform
handle3 = uimenu('Label','Select Beats','callback','Defn_Beats','enable','off');
```

```
% handle4 defines the callback used to plot individual beats of the pressure waveform
handle4 = uimenu('Label','Plot Beats','callback','Plot_Cycles','enable','off');

% handle5 defines the callback used to plot the average pressure waveform
handle5 = uimenu('Label',"Compute Ave Press Waveform','callback',' Compute_Mean_Cycle
','enable','off');

% handle6 defines the callback used to select the dicrotic notch on the average pressure waveform
handle6 = uimenu('Label','Pick DN','callback','Dicrotic_Notch','enable','off');

% handle7 defines the callback used to define the various user inputs
handle7 = uimenu('Label','User Inputs','enable','on');
handle7_1 = uimenu('Label','CO,'callback','User_Inputs','enable','on');
handle7_2 = uimenu('Label','Sampling Frequency','enable','on');
handle7_21 = uimenu('Label','View Current Sampling Frequency','callback','Enter_Freq','enable','on');
handle7_22 = uimenu('Label','Change Default Sampling Frequency','callback','Change Defaut
Freq','enable','on');
set(handle7_1,'parent',handle7);
set(handle7_2,'parent',handle7);
set(handle7,'children',[handle7_2 handle7_1]);
set(handle7_21,'parent',handle7_2);
set(handle7_22,'parent',handle7_2);
set(handle7_2,'children',[handle7_22 handle7_21]);

% handle8 defines the callback used to compute global AC
handle8 = uimenu('Label','Analyze!','callback','Compute_AC','enable','off');

% handle9 defines the callback used to save the results
handle9 = uimenu('Label','Save','enable','on');
handle9_1 = uimenu('Label','Save Results As...','callback','Save_Results_As','enable','off');
handle9_2 = uimenu('Label','Save Results','callback','Save_Results','enable','off');
handle9_3 = uimenu('Label','Save Figure','callback','Save_Figure','enable','off');
set(handle9_1,'parent',handle9);
set(handle9_2,'parent',handle9);
set(handle9_3,'parent',handle9);
set(handle9,'children',[handle9_3 handle9_2 handle9_1]);

% handle10 defines the callback close the program
handle10 = uimenu('Label','Exit','callback','close all');
```

The code for the "Load_Data" callback (handle1) is as follows:

```
%%  User selects file to load
[DataName,DataDirectory]=uigetfile('*.txt','Choose The Data File');
if exist(sprintf('%s%s',DataDirectory(1:end-1),DataDirectory(end))) = = 7 || ...
      exist(sprintf('%s%s',DataName(1:end-1),DataName(end))) = = 2
   cd(DataDirectory)
   data=textread(DataName);
```

```
    cd(ScriptDir);

%%  Load Pressure-Diameter data
    % Fill in time and pressure arrays
    time = data(:,1);
    pressure = data(:,2);

%%  Plot Data
    figure(1);
    hold off
    subplot('position',[.05,.7,.9,.25])
    plot(time, pressure);
    title(DataName);
    ylabel('Pressure (units)');
    xlabel('Time (sec)');

    set(handle2,'enable','on');
    set(handle3,'enable','on');
    set(handle7,'enable','on');
end
```

The code for the "Pick_Section" callback (handle2) is as follows:

```
%%  Plot Data
section='y';
while section=='y'
    figure(1);
    subplot('position',[.05,.7,.9,.25])
    plot(time, pressure);
    ylabel('Pressure (units)');
    xlabel('Time (sec)');
    title(DataName);
    ylabel('Pressure (mmHg)');

%%  Find and define a section selected by the user
    [x1,y1]=ginput(2);
    findpoint1=1;
    while abs(time(findpoint1,1)-x1(1,1)) > 0.01;
        findpoint1=findpoint1+1;
    end
    findpoint2=findpoint1+1;
    while abs(time(findpoint2,1)-x1(2,1)) > 0.01;
        findpoint2=findpoint2+1;
    end

%%  Plot the new sectoin
    subplot('position',[.05,.7,.9,.25])
    plot(time(findpoint1:findpoint2),pressure(findpoint1:findpoint2))
    title('Selected Section');
```

```
    ylabel('Pressure (units)');
    xlabel('Time (sec)');

    button = questdlg('Do you want to pick a different section?',...
        'Differnt Section','Yes','No','Yes');
    if strcmp(button,'Yes')
        section='y';
    elseif strcmp(button,'No')
        section='n';
    end

end

%%  Redefine variables to reflect the selected section
TempTime=time;
TempPressure=pressure;
clear time;
clear pressure;
time=TempTime(findpoint1:findpoint2);
pressure=TempPressure(findpoint1:findpoint2);
clear TempTime;
clear TempPressure;

%%  Enable relavant selections
set(handle1,'enable','on');
set(handle2,'enable','off');
set(handle3,'enable','on');
set(handle7,'enable','on');
set(handle10,'enable','on');
set(handle11,'enable','on');
```

The code for the "Defn_Beats" callback (handle3) is as follows:

```
%%  Re-plot the Data
subplot('position',[.05,.7,.9,.25])
plot(time, pressure)
title('Selected Section');
ylabel('Pressure (units)');
xlabel('Time (sec)');
hold on

%%  User Selects end-diastolic pressures for first two beats
if exist('man_select') == 0
    [x,y]=ginput(2);

    find_point2=1;
    count=0;
    longest=1;
```

```
%The purpose of the following section is to determine the length
%(period) of the longest beat.  This is needed in order to store
%the arrays corresponding to each beat in the same matrix.

%%  Identify first end-diastolic pressure
while count<length(x)-1
   count=count+1;
   find_point1=find_point2;
   if count==1
      while abs(time(find_point1,1)-x(count,1)) > 0.01;
         find_point1=find_point1+1;
      end
      temp1=pressure(find_point1:find_point1+80);
      [y1 z1]=min(temp1);
      find_point1Temp=find_point1+z1;
      if find_point1-5>0
         clear temp1;
         temp1=pressure(find_point1-5:find_point1+40);
         [y1 z1]=min(temp1);
         find_point1Temp=find_point1+z1-5;
      end
      if find_point1-10>0
         clear temp1;
         temp1=pressure(find_point1-10:find_point1+40);
         [y1 z1]=min(temp1);
         find_point1Temp=find_point1+z1-10;
      end
      if find_point1-20>0
         clear temp1;
         temp1=pressure(find_point1-20:find_point1+40);
         [y1 z1]=min(temp1);
         find_point1Temp=find_point1+z1-20;
      end
      if find_point1-40>0
         clear temp1;
         temp1=pressure(find_point1-40:find_point1+40);
         [y1 z1]=min(temp1);
         find_point1Temp=find_point1+z1-40;
      end
      find_point1=find_point1Temp;
   end

%%  Identify next end-diastolic pressure
   find_point2=find_point1+1;
   while abs(time(find_point2,1)-x(count+1,1)) > 0.01;
      find_point2=find_point2+1;
   end


   temp2=pressure(find_point2-40:find_point2);
   if find_point2+5<length(pressure)
```

```
            clear temp2;
            temp2=pressure(find_point2-40:find_point2+5);
        end
        if find_point2+10<length(pressure)
            clear temp2;
            temp2=pressure(find_point2-40:find_point2+10);
        end
        if find_point2+20<length(pressure)
            clear temp2;
            temp2=pressure(find_point2-40:find_point2+20);
        end
        if find_point2+40<length(pressure)
            clear temp2;
            temp2=pressure(find_point2-40:find_point2+40);
        end

        [y2 z2]=min(temp2);
        find_point2=find_point2+z2-40;
    end

%%  Use two selected EDPs to find other points
    TempPeriod=time(find_point2,1) - time(find_point1,1);  %Estimate Period
    TempFreq=1/(time(3)-time(2));       %Estimate Sample Frequency
    Nsamps=round(TempPeriod*TempFreq);  %Estimate Number of Samples
    SecLength=time(length(time))-x(1);  %Estimate The Length of the Section
    Nbeats=round(SecLength*TempFreq/Nsamps);  %Estimate Total Number of Beats

    for i=3:Nbeats
        if x(i-1) + TempPeriod <= time(length(time))
            x(i)=x(i-1) + TempPeriod;
        end
    end

%%  Identify first end-diastolic pressure
    longest=1;
    find_point2=1;
    count=0;
    while count<length(x)-1
        count=count+1;
        find_point1=find_point2;
        if count==1
            while abs(time(find_point1,1)-x(count,1)) > 0.01;
                find_point1=find_point1+1;
            end
            temp1=pressure(find_point1:find_point1+round(Nsamps/2));
            [y1 z1]=min(temp1);
            find_point1Temp=find_point1+z1;
            if find_point1-5>0
                clear temp1;
                temp1=pressure(find_point1-5:find_point1+round(Nsamps/2));
                [y1 z1]=min(temp1);
```

```
        find_point1Temp=find_point1+z1-5;
    end
    if find_point1-10>0
        clear temp1;
        temp1=pressure(find_point1-10:find_point1+round(Nsamps/2));
        [y1 z1]=min(temp1);
        find_point1Temp=find_point1+z1-10;
    end
    if find_point1-20>0
        clear temp1;
        temp1=pressure(find_point1-20:find_point1+round(Nsamps/2));
        [y1 z1]=min(temp1);
        find_point1Temp=find_point1+z1-20;
    end
    if find_point1-40>0
        clear temp1;
        temp1=pressure(find_point1-40:find_point1+round(Nsamps/2));
        [y1 z1]=min(temp1);
        find_point1Temp=find_point1+z1-40;
    end
    find_point1=find_point1Temp;
end

%%  Identify subsequent end-diastolic pressures
find_point2=find_point1+1;
while abs(time(find_point2,1)-x(count+1,1)) > 0.01;
    find_point2=find_point2+1;
end


temp2=pressure(find_point2-round(Nsamps/2):find_point2);
if find_point2+5<length(pressure)
    clear temp2;
    temp2=pressure(find_point2-round(Nsamps/2):find_point2+5);
end
if find_point2+10<length(pressure)
    clear temp2;
    temp2=pressure(find_point2-round(Nsamps/2):find_point2+10);
end
if find_point2+20<length(pressure)
    clear temp2;
    temp2=pressure(find_point2-round(Nsamps/2):find_point2+20);
end
if find_point2+40<length(pressure)
    clear temp2;
    temp2=pressure(find_point2-round(Nsamps/2):find_point2+40);
end
if find_point2+80<length(pressure)
    clear temp2;
    temp2=pressure(find_point2-round(Nsamps/2):find_point2+80);
end
```

```
        [y2 z2]=min(temp2);
        find_point2=find_point2+z2-round(Nsamps/2);

%%  Determine the length of the longest beat
        if length(pressure(find_point1:find_point2))>longest
            longest=length(pressure(find_point1:find_point2));
        end
        hold on

%%  Plot each EDP
        plot(time(find_point1,1),pressure(find_point1),'*r')
        plot(time(find_point2,1),pressure(find_point2),'*r')


        TimePoints(count)=time(find_point1);
        PressPoints(count)=pressure(find_point1);

        TimePoints(count+1)=time(find_point2);
        PressPoints(count+1)=pressure(find_point2);
    end

end
```

The code for the "Plot_Cycles" callback (handle4) is as follows:

```
%%  Create matrix to store each beat
cycles=zeros(longest,count);
newtime=zeros(longest,count);

%%  Identify first end-diastolic pressure
%Redefine each beat in order to store them
find_point2=1;
count=0;
while count<length(x)-1
    count=count+1;
    find_point1=find_point2;
    if count==1
        while abs(time(find_point1,1)-x(count,1)) > 0.01;
            find_point1=find_point1+1;
        end
        temp1=pressure(find_point1:find_point1+round(Nsamps/2));
        [y1 z1]=min(temp1);
        find_point1Temp=find_point1+z1;
        if find_point1-5>0
            clear temp1;
            temp1=pressure(find_point1-5:find_point1+round(Nsamps/2));
            [y1 z1]=min(temp1);
            find_point1Temp=find_point1+z1-5;
```

```
    end
    if find_point1-10>0
       clear temp1;
       temp1=pressure(find_point1-10:find_point1+round(Nsamps/2));
       [y1 z1]=min(temp1);
       find_point1Temp=find_point1+z1-10;
    end
    if find_point1-20>0
       clear temp1;
       temp1=pressure(find_point1-20:find_point1+round(Nsamps/2));
       [y1 z1]=min(temp1);
       find_point1Temp=find_point1+z1-20;
    end
    if find_point1-40>0
       clear temp1;
       temp1=pressure(find_point1-40:find_point1+round(Nsamps/2));
       [y1 z1]=min(temp1);
       find_point1Temp=find_point1+z1-40;
    end
    find_point1=find_point1Temp;
  end

%%  Identify subsequent end-diastolic pressures
  find_point2=find_point1+1;
  while abs(time(find_point2,1)-x(count+1,1)) > 0.01;
    find_point2=find_point2+1;
  end


  temp2=pressure(find_point2-round(Nsamps/2):find_point2);
  if find_point2+5<length(pressure)
    clear temp2;
    temp2=pressure(find_point2-round(Nsamps/2):find_point2+5);
  end
  if find_point2+10<length(pressure)
    clear temp2;
    temp2=pressure(find_point2-round(Nsamps/2):find_point2+10);
  end
  if find_point2+20<length(pressure)
    clear temp2;
    temp2=pressure(find_point2-round(Nsamps/2):find_point2+20);
  end
  if find_point2+40<length(pressure)
    clear temp2;
    temp2=pressure(find_point2-round(Nsamps/2):find_point2+40);
  end
  if find_point2+80<length(pressure)
    clear temp2;
    temp2=pressure(find_point2-round(Nsamps/2):find_point2+80);
  end
```

```
    [y2 z2]=min(temp2);
    find_point2=find_point2+z2-round(Nsamps/2);

%%  Store each beat in the cycles matrix
    new_cyc=pressure(find_point1:find_point2);
    cycles(1:find_point2-find_point1+1,count)=...
       pressure(find_point1:find_point2);
%%  Create new time array corresponding to new beats
    newtime(1:find_point2-find_point1+1,count)=(0:(1/Freq):((1/Freq)*(length(new_cyc)-1)))';

%%  Plot each beat
    subplot('position',[.08,.1,.4,.5])
    plot(newtime(1:find_point2-find_point1+1,count),cycles(1:find_point2-find_point1+1,count))
    title('Individual Beats');
    ylabel('Pressure (units)');
    xlabel('Time (sec)');
    hold on

    subplot('position',[.05,.7,.9,.25])%,'replace')
    plot(time, pressure)
    title('Selected Section');
    ylabel('Pressure (units)');
    xlabel('Time (sec)');
    hold on

    plot(time(find_point1:find_point2),pressure(find_point1:find_point2),'.r')

    pause on
    pause
end
subplot('position',[.05,.7,.9,.25])%,'replace');
plot(time, pressure)
hold on
plot(TimePoints,PressPoints,'*r')
title('Selected Section');
ylabel('Pressure (mmHg)');

%%  Enable relavant selections
set(handle1,'enable','on');
set(handle2,'enable','off');
set(handle3,'enable','off');
set(handle4,'enable','off');
set(handle5,'enable','on');
set(handle7,'enable','on');
set(handle10,'enable','on');
```

The code for the “Compute_Mean_Cycle” callback (handle5) is as follows:

```
%%  Replot pressure waveform without beat markers
```

```
subplot('position',[.05,.7,.9,.25])
plot(time, pressure)
hold on
title('Selected Section');
ylabel('Pressure (units)');
xlabel('Time (sec)');

%%  Plot each beat
for i=1:count
   cyc=1;
   while cycles(cyc,i)>0 & cyc<longest
      cyc=cyc+1;
   end
   cyc=cyc-1;

   subplot('position',[.08,.1,.4,.5])
   plot(newtime(1:cyc,i),cycles(1:cyc,i))
   ylabel('Pressure (units)');
   xlabel('Time (sec)');
   title('Individual Beats');
   hold on
end

%%  Determine the period (T) of each beat
for col=1:count
   cyc=1;
   while cycles(cyc,col)>0 & cyc<longest
      cyc=cyc+1;
   end
   cyc=cyc-1;
   T(col)=cyc/Freq;
end

%%  Calculate Average period
   Tavg=mean(T);

%%  Create new time array from which interpolation will done
   Ta=0:(1/Freq):Tavg;
   Ta=Ta';

%%  Interpolate & find new pressure array
for col=1:count
   cyc=1;
   while cycles(cyc,col)>0 & cyc<longest
      cyc=cyc+1;
   end
   cyc=cyc-1;

   Time=(0:(1/Freq):((cyc/Freq)-(1/Freq)))';
   x1=Time.*(Tavg/T(col));
   newpress(:,col)=interp1(x1,cycles(1:cyc,col),...
```

```
        Ta,'spline','extrap');
end
newpress=newpress(1:length(newpress)-5,:);
Ta=Ta(1:length(Ta)-5,:);

%%  Calculate the average pressure waveform
avgpress=mean(newpress');
avgpress_mean=mean(avgpress);
avgpress_min=min(avgpress);

%%  Calculate min, max and mean pressure from the average press waveform
avgpress_mean=mean(avgpress);
avgpress_min=min(avgpress);
avgpress_max=max(avgpress);

%%  Plot average pressure waveform

subplot('position',[.53,.1,.4,.5])
hold off
plot(Ta,avgpress)
ylabel('Pressure (mmHg)');
title('Average Beat (Scaled)');
xlabel('Time (sec)');
hold on

%%  Enable relavant selections
set(handle1,'enable','on');
set(handle2,'enable','off');
set(handle3,'enable','off');
set(handle4,'enable','off');
set(handle5,'enable','off');
set(handle6,'enable','on');
set(handle7,'enable','on');
set(handle10,'enable','on');
```

The code for the “Dicrotic_Notch” callback (handle6) is as follows:

```
%%  Enables user to select dicrotic notch
clear pressureone;
another='y';
while another=='y'
   hold off
   subplot('position',[.53,.1,.4,.5]);
   plot(Ta,avgpress)
   ylabel('Pressure (mmHg)');
   title('Average Beat (Scaled)');
   xlabel('Time (sec)');
   hold on
```

```
    [inc,incy] = ginput(1);
    find_point3=1;
    while abs(Ta(find_point3,1)-inc(1,1)) > 0.01;
        find_point3=find_point3+1;
    end
    incy=round(incy);
    pressureone = avgpress(find_point3);
    timeone = Ta(find_point3);
    plot(timeone,pressureone,'*r');

    button = questdlg('Do you want to pick a different DN?',...
        'Differnt DN','Yes','No','Yes');
    if strcmp(button,'Yes')
        another='y';
    elseif strcmp(button,'No')
        another='n';
    end
end

if exist('co') ~= 0
    set(handle8,'enable','on');
else
    set(handle8,'enable','off');
end

%%  Enable relavant selections
set(handle1,'enable','on');
set(handle2,'enable','off');
set(handle3,'enable','off');
set(handle4,'enable','off');
set(handle5,'enable','off');
set(handle6,'enable','on');
set(handle7,'enable','on');
set(handle10,'enable','on');
set(handle11,'enable','on');
```

The code for the “User_Inputs” callback (handle7) is as follows:

```
prompstr = {'Enther the CO ml/min'};
titlestr = 'User Inputs';
initstr = {'120'};
UserInpts = inputdlg(prompstr,titlestr,1,initstr);
co=str2num(UserInpts{1});
```

Finally, the code for the “Save_Results_As” callback (handle9) is as follows:

```
%%  Prompt User to Decide to Save to An Existing File or a New One
```

```
button = questdlg('Do You Want Add to An Exiting File or Save to A New File?',...
   'Save Output?','Existing File','New File','Existing File');
if strcmp(button,'Existing File')
   Adddata='A';
elseif strcmp(button,'New File')
   Adddata='N';
end

%%  Save Output File
if Adddata=='A'
   Results_Dir=sprintf('%s%s',ScriptDir(1:end-7),'Results');
   cd(Results_Dir);
   [ResFilename,FilePath] = uiputfile({'*.txt';'*.xls'},'Save As',DataName(1:length(DataName)-10));
   if ResFilename ~= 0

      %Save Results
      cd(FilePath);
      fid=fopen(ResFilename,'a');
      fprintf(fid,'%s %8.3f %8.3f %8.3f %8.3f %8.3f %8.3f %8.3f %8.3f %8.3f %8.3f %8.3f %8.3f
%8.3f \n',...
         DataName(1:length(DataName)-4), HR, co,avgpress_max, avgpress_min, avgpress_mean,...
         avgpress_max-avgpress_min, svr,ad, pressureone,...
         pressuretwo, compliance,pressdiff,sv,sv_pp*1000);
      fclose(fid);

      %Save Average Pressure Waveform
      AvePress_Dir=sprintf('%s%s',ScriptDir(1:end-7),'Ave Press Waveforms');
      cd(AvePress_Dir);
      fid2=fopen(sprintf('%s%s', DataName(1:end-4),'_AvePress.txt'),'w');
      fprintf(fid2,'%6.4f  %12.4f\n',[Ta avgpress']');
      fclose(fid2);
   end
elseif Adddata=='N'
   Results_Dir=sprintf('%s%s',ScriptDir(1:end-7),'Results');
   cd(Results_Dir);
   [ResFilename,FilePath] = uiputfile({'*.txt';'*.xls'},'Save As',DataName(1:length(DataName)-10));
   if ResFilename ~= 0

      %Save Results
      cd(FilePath);
      fid=fopen(ResFilename,'w');
      fprintf(fid,'%s %8.3f %8.3f %8.3f %8.3f %8.3f %8.3f %8.3f %8.3f %8.3f %8.3f %8.3f %8.3f
%8.3f \n',...
         DataName(1:length(DataName)-4), HR, co,avgpress_max, avgpress_min, avgpress_mean,...
         avgpress_max-avgpress_min, svr,ad, pressureone,...
         pressuretwo, compliance,pressdiff,sv, sv_pp*1000);
      fclose(fid);

      %Save Average Pressure Waveform
      AvePress_Dir=sprintf('%s%s',ScriptDir(1:end-7),'Ave Press Waveforms');
      cd(AvePress_Dir);
```

```
    fid2=fopen(sprintf('%s%s', DataName(1:end-4),'_AvePress.txt'),'w');
    fprintf(fid2,'%6.4f  %12.4f\n',[Ta avgpress']');
    fclose(fid2);
  end
end
```

F.2 ANALYSIS OF PRESSURE-DIAMETER AND FORCE-LENGTH DATA

Similar to the previous one (see **Appendix F.**1), this program is subdivided into several components which were assessed by a main program using callbacks. The main program was again designed as a graphical user interface with several different handles that correspond to the various callbacks. The code for the main program is as follows:

```
clear
Fig=figure(1);
clc
clf
set(Fig, 'Name', 'Isolated Artery Biaxial Analysis Program');
set(Fig,'menubar','none');
set(Fig, 'PaperOrientation', 'portrait')

% handle1 defines the callback used to load pressure-diameter and force-length data
handle1 = uimenu('Label','Load','enable','on');
handle1_1 = uimenu('Label','Load New Data','callback','Load_Data,'enable','on');
set(handle1_1,'parent',handle1);
set(handle1,'children',handle1_1);

% handle2 defines the callback used to compute 2nd Piola Kirchoff stresses
handle2 = uimenu('Label','Compute','enable','on');
handle2_1 = uimenu('Label','Piola-Kirchoff stresses','callback','PK_Stress,'enable','off');
set(handle2_1,'parent',handle2);
set(handle2,'children',handle2_1);

% handle3 defines the various callbacks used for curve fitting to different strain energy functions
handle3 = uimenu('Label','Fit Curve','enable','on');
handle3_1 = uimenu('Label','Polynomial','callback','Fit_Polynomial','enable','off');
handle3_2 = uimenu('Label','Exponential','callback','Fit_Exponential','enable','off');
handle3_3 = uimenu('Label','Mixed','callback','Fit_Mixed','enable','off');
set(handle3_1,'parent',handle3);
set(handle3_2,'parent',handle3);
set(handle3_3,'parent',handle3);
set(handle3,'children',[handle3_3 handle3_2 handle3_1]);
```

```
% handle4 defines the callbacks used to save results
handle4 = uimenu('Label','Save','enable','on');
handle4_1 = uimenu('Label','Save Coefficients','callback','SaveType=1;Save_Res','enable','off');
handle4_2 = uimenu('Label','Save Curves','callback','SaveType=2;Save_Res','enable','off');
handle4_3 = uimenu('Label','Save Figure','callback','SaveType=3;Save_Res','enable','on');
set(handle4_1,'parent',handle4);
set(handle4_2,'parent',handle4);
set(handle4_3,'parent',handle4);
set(handle4,'children',[handle4_3 handle4_2 handle4_1]);

% handle5 defines the callback close the program
handle5 = uimenu('Label','Exit','enable','on');
handle5_1 = uimenu('Label','EXIT!','callback','close all','enable','on');
set(handle5_1,'parent',handle5);
set(handle5,'children',handle5_1);
```

The code for the "Load_Data" callback (handle1) is as follows:

```
%%  User loads Pressure-Diameter data
[DataName,DataDirectory]=uigetfile('*.txt','Choose The Data File');
if exist(sprintf('%s%s',DataDirectory(1:end-1),DataDirectory(end))) = = 7

    cd(DataDirectory)
    data=textread(DataName);
    cd(ScriptDir)

%%  Assign variable names
    UnldDi = data(1,1);
    UnldDo = data(1,2);
    UnldL = data(1,3);
    [row col] = size(data);
    data=data(2:row,1:col);
    Press_mmHg = data(:,1);
    Press_Pa = data(:,2);
    Di = data(:,3);
    Do = data(:,4);
    Force_V=data(:,5);
    Length=data(:,6);

%%  Calculate Tmeasure, Ri, Ro, and Ai
    Ri = Di/2;
    Ro = Do/2;
    Tmeasured=Ro-Ri;
    Ai = pi*Ri.^2;

%%  Determine where each curve begins and calculate Am
    P0s=find(Press_mmHg==0);
    for i=1:length(P0s)
```

```
        T0s(i)=Tmeasured(P0s(i));
        Di0s(i)=Di(P0s(i));
        Am0s(i)=pi*T0s(i)*(T0s(i) + Di0s(i));
    end

%%  Calculate wall thickness for each measured Di based on Am
    j=0;
    for i=1:length(P0s)
        j=j+1;
        if i<length(P0s)
            Tcalculated(P0s(i):P0s(i+1)) = sqrt((Am0s(j) + Ai(P0s(i):P0s(i+1)))/pi)...
                - sqrt(Ai(P0s(i):P0s(i+1))/pi);
        elseif i==length(P0s)
            Tcalculated(P0s(i):length(Press_mmHg)) = sqrt((Am0s(j) + ...
                Ai(P0s(i):length(Press_mmHg)))/pi)...
                - sqrt(Ai(P0s(i):length(Press_mmHg))/pi);
        end
    end

%%  Prompt user to input the unloaded dimensions and conversion factor for force measurements
    prompt = {'Unloaded Inner Diameter (um)','Unloaded Outer Diameter (um)',...
        'Unloaded Length (mm)'};
    dlg_title ='Unloaded Dimensions';
    num_lines=1;
    def={num2str(UnldDi),num2str(UnldDo),num2str(UnldL)};
    inputvalues=inputdlg(prompt,dlg_title,num_lines,def);

%%  Assign variable names to unloaded dimensions
    UnldDi=str2num(inputvalues{1});
    UnldRi=UnldDi/2;
    UnldDo=str2num(inputvalues{2});
    UnldRo=UnldDo/2;
    UnldL=str2num(inputvalues{3});
    UnldT=UnldRo-UnldRi;
    ForceConv=load('DefForceConv.txt');
    Force_mN=Force_V*ForceConv;
    Force_N=Force_mN/1000;

%%  Calculate axial and circumferential stretch
    AxStr=Length/UnldL;
    CrcmStr=Di/UnldDi;

%%  Calculate axial and circumferential Cauchy stresses
    Crc_Cauch_Strs = Press_Pa.*(((UnldRo/1E6).*(CrcmStr.^2)./(UnldT/1E6))-1);
    Temp1 = (pi*UnldT/1E6);
    Temp2 = (2*UnldRo/1E6)-(UnldT/1E6);
    Temp3 = Crc_Cauch_Strs/2;
    Temp4 = Temp1*Temp2;
    Ax_Cauch_Strs = (Force_N/Temp4) + Temp3;

%% Plot pressure-diameter, force-length and stretch-stress relationships
```

```
hold off

TempLineProp={'-*r','-om','-xk','-+g','-vb','-pr','-hc','-dy',...
      '*r','om','xk','+g','vb','pr','hc','dy'};
for i=1:length(P0s)
   if i<length(P0s)
      subplot(2,2,1);
      plot(Press_mmHg(P0s(i):P0s(i+1)-1),Di(P0s(i):P0s(i+1)-1),TempLineProp{i})
      ylabel('Inner Diameter (um)')
      xlabel('Transmural Pressure (mmHg)')
      hold on

      subplot(2,2,3);
      plot(CrcmStr(P0s(i):P0s(i+1)-1),Crc_Cauch_Strs(P0s(i):P0s(i+1)-1)...
         ,TempLineProp{i})
      ylabel('Circumferential Cauchy Stress (Pa)')
      xlabel('Circumferential Stretch')
      hold on

      subplot(2,2,4);
      plot(CrcmStr(P0s(i):P0s(i+1)-1),Ax_Cauch_Strs(P0s(i):P0s(i+1)-1)...
         ,TempLineProp{i})
      ylabel('Axial Cauchy Stress (Pa)')
      xlabel('Circumferential Stretch')
      hold on
   elseif i==length(P0s)
      subplot(2,2,1);
      plot(Press_mmHg(P0s(i):length(Press_mmHg)),Di(P0s(i):length(Press_mmHg)),...
         TempLineProp{i})
      ylabel('Diameter (um)')
      xlabel('Transmural Pressure (mmHg)')
      hold on

      subplot(2,2,3);
      plot(CrcmStr(P0s(i):length(CrcmStr)),Crc_Cauch_Strs(P0s(i):length(CrcmStr)),...
         TempLineProp{i})
      ylabel('Circumferential Cauchy Stress (Pa)')
      xlabel('Circumferential Stretch')
      hold on

      subplot(2,2,4);
      plot(CrcmStr(P0s(i):length(CrcmStr)),Ax_Cauch_Strs(P0s(i):length(CrcmStr)),...
         TempLineProp{i})
      ylabel('Axial Cauchy Stress(Pa)')
      xlabel('Circumferential Stretch')
      hold on
   end
   TempPltLegnd1{i}=['\lambda','z  = ',num2str(AxStr(P0s(i)),'%.2f')];
end
subplot(2,2,1);
legend(TempPltLegnd1,'Location','SouthEast','FontSize',7)
```

```
    subplot(2,2,3);
    legend(TempPltLegnd1,'Location','NorthWest','FontSize',7)
    subplot(2,2,4);
    legend(TempPltLegnd1,'Location','NorthWest','FontSize',7)
    k=0;
    for f=0:(P0s(2)-P0s(1))-1
        i=1;
        k=k+1;
        for j=1:length(P0s)
            AxStrCrv(i,1)=AxStr(P0s(j)+f);
            AxStrCrv(i,2)=Force_mN(P0s(j)+f);
            AxStrCrv(i,3)=Ax_Cauch_Strs(P0s(j)+f);
            i=i+1;
        end
        subplot(2,2,2);
        plot(AxStrCrv(:,1),AxStrCrv(:,2),TempLineProp{k})
        ylabel('Axial Force (mN)')
        xlabel('Axial Stretch')
        hold on
        TempPltLegnd2{k}=[num2str(Press_mmHg(P0s(j)+f)),' mmHg'];
        legend(TempPltLegnd2,'Location','SouthEast','FontSize',7)
    end

%%  Label Figure
    FigLabel = uicontrol('Style','text','String',DataName(1:end-4),...
        'units','normalized','Position', [.415 .95 .2 .035],...
        'FontWeight','bold','FontSize',18,'BackgroundColor',[1 1 1]);

    set(handle2_1,'enable','on')
    set(handle3_1,'enable','on')
    set(handle3_2,'enable','on')
    set(handle3_3,'enable','on')
    set(handle3_4,'enable','on')
end
```

The code for the "PK_Stress" callback (handle2) is as follows:

```
delete(subplot(2,2,1))
delete(subplot(2,2,2))
delete(subplot(2,2,3))
delete(subplot(2,2,4))

%%  Calculate axial and circumferential 2nd Piola-Kirchoff stresses
Crc_PK_Strs = Crc_Cauch_Strs./(CrcmStr.^2);
Ax_PK_Strs = Ax_Cauch_Strs./(AxStr.^2);

%%  Calculate axial and circumferential Green-Lagrange Strains
Crc_GL_Str = ((CrcmStr.^2)-1)/2;
Ax_GL_Str = ((AxStr.^2)-1)/2;
```

```
%% Plot axial and circumferential 2nd Piola-Kirchoff stresses and stretch
TempLineProp={'-*r','-om','-xk','-+g','-vb','-pr','-hc','-dy'};
for i=1:length(P0s)
   if i<length(P0s)
      Plt1 = subplot('position',[.05,.13,.4,.7]);
      plot(Crc_GL_Str(P0s(i):P0s(i+1)-1),Crc_PK_Strs(P0s(i):P0s(i+1)-1)...
         ,TempLineProp{i})
      ylabel('Circumferential 2nd Piola-Kirchoff Stress (Pa)')
      xlabel('Circumferential Green-Lagrange Strain')
      hold on

   elseif i==length(P0s)
      Plt1 = subplot('position',[.05,.13,.4,.7]);
      plot(Crc_GL_Str(P0s(i):length(Crc_GL_Str)),...
         Crc_PK_Strs(P0s(i):length(Crc_GL_Str)),TempLineProp{i})
      ylabel('Circumferential 2nd Piola-Kirchoff Stress (Pa)')
      xlabel('Circumferential Green-Lagrange Strain')
      hold on

   end
   TempPltLegnd1{i}=['\lambda','z  = ',num2str(AxStr(P0s(i)),'%.2f')];
end
legend(TempPltLegnd1,'Location','NorthWest','FontSize',7)

for i=1:length(P0s)
   if i<length(P0s)
      Plt2 = subplot('position',[.55,.13,.4,.7]);
      plot(Crc_GL_Str(P0s(i):P0s(i+1)-1),Ax_PK_Strs(P0s(i):P0s(i+1)-1)...
         ,TempLineProp{i})
      ylabel('Axial 2nd Piola-Kirchoff Stress (Pa)')
      xlabel('Circumferential Green-Lagrange Strain')
      hold on

   elseif i==length(P0s)
      Plt2 = subplot('position',[.55,.13,.4,.7]);
      plot(Crc_GL_Str(P0s(i):length(Crc_GL_Str)),...
         Ax_PK_Strs(P0s(i):length(Crc_GL_Str)),TempLineProp{i})
      ylabel('Axial 2nd Piola-Kirchoff Stress (Pa)')
      xlabel('Circumferential Green-Lagrange Strain')
      hold on

   end
   TempPltLegnd1{i}=['\lambda','z  = ',num2str(AxStr(P0s(i)),'%.2f')];
end
legend(TempPltLegnd1,'Location','NorthWest','FontSize',7)

%%  Label Figure
delete(FigLabel)
FigLabel = uicontrol('Style','text','String',DataName(1:end-4),...
      'units','normalized','Position', [.415 .95 .2 .035],...
```

```
    'FontWeight','bold','FontSize',18,'BackgroundColor',[1 1 1]);
```

The code for the "Fit_Polynomial" callback (handle3_1) is as follows:

```
Redo='N';
%%  Calculate axial and circumferential 2nd Piola-Kirchoff stresses if
%%  necessary
if exist('PK_Run') == 0
   delete(subplot(2,2,1))
   delete(subplot(2,2,2))
   delete(subplot(2,2,3))
   delete(subplot(2,2,4))
   Crc_PK_Strs = Crc_Cauch_Strs./(CrcmStr.^2);
   Ax_PK_Strs = Ax_Cauch_Strs./(AxStr.^2);

%%  Calculate axial and circumferential Green-Lagrange Strains
   Crc_GL_Str = ((CrcmStr.^2)-1)/2;
   Ax_GL_Str = ((AxStr.^2)-1)/2;
end

%% Plot axial and circumferential 2nd Piola-Kirchoff stresses and Lagrange
%% Strains
subplot('position',[.05,.18,.4,.7])
hold off
subplot('position',[.55,.18,.4,.7])
hold off
TempLineProp={'*r','om','xk','+g','vb','pr','hc','dy'};
for i=1:length(P0s)
   if i<length(P0s)
      Plt1 = subplot('position',[.05,.13,.4,.7]);
      plot(Crc_GL_Str(P0s(i):P0s(i+1)-1),Crc_PK_Strs(P0s(i):P0s(i+1)-1)...
         ,TempLineProp{i})
      ylabel('Circumferential 2nd Piola-Kirchoff Stress (Pa)')
      xlabel('Circumferential Green-Lagrange Strain')
      hold on

   elseif i==length(P0s)
      Plt1 = subplot('position',[.05,.13,.4,.7]);
      plot(Crc_GL_Str(P0s(i):length(CrcmStr)),Crc_PK_Strs(P0s(i):length(CrcmStr)),...
         TempLineProp{i})
      ylabel('Circumferential 2nd Piola-Kirchoff Stress (Pa)')
      xlabel('Circumferential Green-Lagrange Strain')
      hold on
   end
end
legend(TempPltLegnd1,'Location','NorthWest','FontSize',7)

for i=1:length(P0s)
   if i<length(P0s)
```

```
        Plt2 = subplot('position',[.55,.13,.4,.7]);
        plot(Crc_GL_Str(P0s(i):P0s(i+1)-1),Ax_PK_Strs(P0s(i):P0s(i+1)-1)...
            ,TempLineProp{i})
        ylabel('Axial 2nd Piola-Kirchoff Stress (Pa)')
        xlabel('Circumferential Green-Lagrange Strain')
        hold on

    elseif i==length(P0s)
        Plt2 = subplot('position',[.55,.13,.4,.7]);
        plot(Crc_GL_Str(P0s(i):length(CrcmStr)),Ax_PK_Strs(P0s(i):length(CrcmStr)),...
            TempLineProp{i})
        ylabel('Axial 2nd Piola-Kirchoff Stress (Pa)')
        xlabel('Circumferential Green-Lagrange Strain')
        hold on

    end
    TempPltLegnd1{i}=['\lambda','z  = ',num2str(AxStr(P0s(i)),'%.2f')];
end
legend(TempPltLegnd1,'Location','NorthWest','FontSize',7)

%%  Prompt user to input the starting valuse of fit parameters
prompt = {'Enter an initial value for C1','Enter an initial value for C2',...
    'Enter an initial value for C3','Enter an initial value for C4',...
    'Enter an initial value for C5','Enter an initial value for C6',...
    'Enter an initial value for C7'};
dlg_title ='Input Given Parameters';
num_lines=1;
if exist('optivalues_Poly')==1
    for i=1:length(optivalues_Poly)
        def{i}=num2str(optivalues_Poly(i));
    end
else def={'34.2','-3.5','30.2','-5.8','22.0','11.1','-5.7'};
end

inputvalues_Poly=inputdlg(prompt,dlg_title,num_lines,def);
C1_Poly=str2num(inputvalues_Poly{1});
C2_Poly=str2num(inputvalues_Poly{2});
C3_Poly=str2num(inputvalues_Poly{3});
C4_Poly=str2num(inputvalues_Poly{4});
C5_Poly=str2num(inputvalues_Poly{5});
C6_Poly=str2num(inputvalues_Poly{6});
C7_Poly=str2num(inputvalues_Poly{7});

%%  Run optimization function
Iter_Count_Poly=0;
exitflag_Poly = 0;
while exitflag_Poly == 0 && Iter_Count_Poly < 50

    invalues_Poly = [C1_Poly C2_Poly C3_Poly ...
        C4_Poly C5_Poly C6_Poly C7_Poly];
    variables_Poly = [Crc_GL_Str Ax_GL_Str];
```

```
    CombStr_Poly = [Crc_PK_Strs;Ax_PK_Strs];

    [optivalues_Poly resnorm_Poly residuals_Poly exitflag_Poly ...
        Opti_Info_Poly lambda_Poly jacobian_Poly] = ...
        lsqcurvefit(@Optifun_Polynomial,invalues_Poly,...
        variables_Poly,CombStr_Poly);
    C1_Poly=optivalues_Poly(1);
    C2_Poly=optivalues_Poly(2);
    C3_Poly=optivalues_Poly(3);
    C4_Poly=optivalues_Poly(4);
    C5_Poly=optivalues_Poly(5);
    C6_Poly=optivalues_Poly(6);
    C7_Poly=optivalues_Poly(7);

    Iter_Count_Poly=Iter_Count_Poly+1;
end

%%  Calculate Predicted Stresses
Crc_Stress_Calc_Poly =(2*C1_Poly*Crc_GL_Str) + ...
    (C2_Poly*Ax_GL_Str) + 3*C4_Poly*(Crc_GL_Str.^2) + ...
    2*C5_Poly*(Crc_GL_Str.*Ax_GL_Str) + C6_Poly*(Ax_GL_Str.^2);

Ax_Stress_Calc_Poly =(C2_Poly*Crc_GL_Str) + ...
    (2*C3_Poly*Ax_GL_Str) +C5_Poly*(Crc_GL_Str.^2) + ...
    2*C6_Poly*(Crc_GL_Str.*Ax_GL_Str) + 3*C7_Poly*(Ax_GL_Str.^2);

%% Calculate R-squared values
TSS_Crc_Poly = sum((Crc_PK_Strs-mean(Crc_PK_Strs)).^2);
RSS_Crc_Poly = sum((Crc_PK_Strs-Crc_Stress_Calc_Poly).^2);
RSquared_Crc_Poly = (TSS_Crc_Poly - RSS_Crc_Poly)/TSS_Crc_Poly;

TSS_Ax_Poly = sum((Ax_PK_Strs-mean(Ax_PK_Strs)).^2);
RSS_Ax_Poly = sum((Ax_PK_Strs-Ax_Stress_Calc_Poly).^2);
RSquared_Ax_Poly = (TSS_Ax_Poly - RSS_Ax_Poly)/TSS_Ax_Poly;

%%  Calculate Predicted Stresses for Plotting
Crc_Str_Step_Poly = (max(Crc_GL_Str)-min(Crc_GL_Str))/100;
Plt_Crc_Str_Poly = min(Crc_GL_Str):Crc_Str_Step_Poly:max(Crc_GL_Str);
Plt_Crc_Str_Poly=Plt_Crc_Str_Poly';

for i=1:length(P0s)
    Plt_Crc_Stress_Poly(:,i) =(2*C1_Poly*Plt_Crc_Str_Poly) + ...
        (C2_Poly*Ax_GL_Str(P0s(i))) + 3*C4_Poly*(Plt_Crc_Str_Poly.^2) + ...
        2*C5_Poly*(Plt_Crc_Str_Poly*Ax_GL_Str(P0s(i))) ...
        + C6_Poly*(Ax_GL_Str(P0s(i))^2);

    Plt_Ax_Stress_Poly(:,i) =(C2_Poly*Plt_Crc_Str_Poly) + ...
        (2*C3_Poly*Ax_GL_Str(P0s(i))) + C5_Poly*(Plt_Crc_Str_Poly.^2) + ...
        2*C6_Poly*(Plt_Crc_Str_Poly*Ax_GL_Str(P0s(i))) + ...
        3*C7_Poly*(Ax_GL_Str(P0s(i))^2);
```

```
end

%% Plot Calculated axial and circumferential 2nd Piola-Kirchoff stresses
%%  and Lagrange strains
TempLineProp={'-r','-m','-k','-g','-b','-r','-c','-y'};
for i=1:length(P0s)
      subplot('position',[.05,.13,.4,.7])
      hold on
      plot(Plt_Crc_Str_Poly,Plt_Crc_Stress_Poly(:,i)...
         ,TempLineProp{i})
      ylabel('Circumferential 2nd Piola-Kirchoff Stress (Pa)')
      xlabel('Circumferential Green-Lagrange Strain')
end
legend(TempPltLegnd1,'Location','NorthWest','FontSize',7)

%% Display R-Squared value
TextPosition(1)=(max(Crc_GL_Str) - min(Crc_GL_Str))/15;
v=axis;
TextPosition(2)=v(3) + (v(4)-v(3))/2;
RSqDisp_Crc=sprintf('%s%s','R^2 = ',num2str(RSquared_Crc_Poly,'%.2f'));
RSqDisp_Crc_Hand=text(TextPosition(1),TextPosition(2),RSqDisp_Crc);
set(RSqDisp_Crc_Hand,'FontWeight','bold')

for i=1:length(P0s)
      Plt2 = subplot('position',[.55,.13,.4,.7]);
      plot(Plt_Crc_Str_Poly,Plt_Ax_Stress_Poly(:,i)...
         ,TempLineProp{i})
      ylabel('Axial 2nd Piola-Kirchoff Stress (Pa)')
      xlabel('Circumferential Green-Lagrange Strain')
      hold on
      TempPltLegnd1{i}=['\lambda','z  = ',num2str(AxStr(P0s(i)),'%.2f')];
end
legend(TempPltLegnd1,'Location','NorthWest','FontSize',7)

%% Display R-Squared value
TextPosition(1)=(max(Crc_GL_Str) - min(Crc_GL_Str))/15;
v=axis;
TextPosition(2)=v(3) + (v(4)-v(3))/2;
RSqDisp_Ax=sprintf('%s%s','R^2 = ',num2str(RSquared_Ax_Poly,'%.2f'));
RSqDisp_Ax_Hand=text(TextPosition(1),TextPosition(2),RSqDisp_Ax);
set(RSqDisp_Ax_Hand,'FontWeight','bold')

%%  Label Figure
delete(FigLabel)
TempLabel = sprintf('%s\n%s',DataName(1:end-4),'Polynomial Fit');
FigLabel = uicontrol('Style','text','String',TempLabel,...
      'units','normalized','Position', [.415 .9 .2 .065],...
      'FontWeight','bold','FontSize',14,'BackgroundColor',[1 1 1]);

%%  Alert user that max number of iterations reached
```

```
if Iter_Count_Poly > 1
   button = questdlg(sprintf('%s\n      %s%s%s',...
      'Maximum number of iterations reached!',...
      'Optimization ran ',num2str(Iter_Count_Poly),' times'),...
      'NOTE!!','Rerun','OK','Rerun');
   if strcmp(button,'Rerun')
      Redo='Y';
   elseif strcmp(button,'OK')
      Redo='N';
   end
end
if Redo == 'Y'
   Fit_Polynomial
end
```

The code for the "Fit_Exponential" callback (handle3_2) is as follows:

```
Redo='N';
%%  Calculate axial and circumferential 2nd Piola-Kirchoff stresses if
   %%  necessary
if exist('PK_Run') == 0
   delete(subplot(2,2,1))
   delete(subplot(2,2,2))
   delete(subplot(2,2,3))
   delete(subplot(2,2,4))
   Crc_PK_Strs = Crc_Cauch_Strs./(CrcmStr.^2);
   Ax_PK_Strs = Ax_Cauch_Strs./(AxStr.^2);

%%  Calculate axial and circumferential Green-Lagrange Strains
   Crc_GL_Str = ((CrcmStr.^2)-1)/2;
   Ax_GL_Str = ((AxStr.^2)-1)/2;
end

%% Plot axial and circumferential 2nd Piola-Kirchoff stresses and Lagrange
%% Strains
subplot('position',[.05,.55,.4,.4])
hold off
subplot('position',[.55,.55,.4,.4])
hold off
subplot('position',[.3,.06,.4,.4])
hold off
TempLineProp={'*r','om','xk','+g','vb','pr','hc','dy'};
for i=1:length(P0s)
   if i<length(P0s)
      Plt1 = subplot('position',[.05,.13,.4,.7]);
      plot(Crc_GL_Str(P0s(i):P0s(i+1)-1),Crc_PK_Strs(P0s(i):P0s(i+1)-1)...
         ,TempLineProp{i})
      ylabel('Circumferential 2nd Piola-Kirchoff Stress (Pa)')
      xlabel('Circumferential Green-Lagrange Strain')
```

```
        hold on

    elseif i==length(P0s)
        Plt1 = subplot('position',[.05,.13,.4,.7]);
        plot(Crc_GL_Str(P0s(i):length(CrcmStr)),Crc_PK_Strs(P0s(i):length(CrcmStr)),...
            TempLineProp{i})
        ylabel('Circumferential 2nd Piola-Kirchoff Stress (Pa)')
        xlabel('Circumferential Green-Lagrange Strain')
        hold on
    end
end
legend(TempPltLegnd1,'Location','NorthWest','FontSize',7)

for i=1:length(P0s)
    if i<length(P0s)
        Plt2 = subplot('position',[.55,.13,.4,.7]);
        plot(Crc_GL_Str(P0s(i):P0s(i+1)-1),Ax_PK_Strs(P0s(i):P0s(i+1)-1)...
            ,TempLineProp{i})
        ylabel('Axial 2nd Piola-Kirchoff Stress (Pa)')
        xlabel('Circumferential Green-Lagrange Strain')
        hold on

    elseif i==length(P0s)
        Plt2 = subplot('position',[.55,.13,.4,.7]);
        plot(Crc_GL_Str(P0s(i):length(CrcmStr)),Ax_PK_Strs(P0s(i):length(CrcmStr)),...
            TempLineProp{i})
        ylabel('Axial 2nd Piola-Kirchoff Stress (Pa)')
        xlabel('Circumferential Green-Lagrange Strain')
        hold on

    end
    TempPltLegnd1{i}=['\lambda','z  = ',num2str(AxStr(P0s(i)),'%.2f')];
end
legend(TempPltLegnd1,'Location','NorthWest','FontSize',7)

%%  Prompt user to input the starting values of fit parameters
prompt = {'Enter an initial value for C1','Enter an initial value for C2',...
    'Enter an initial value for C3','Enter an initial value for C4'};
dlg_title ='Input Starting Values';
num_lines=1;
if exist('optivalues_Exp')==1
    for i=1:length(optivalues_Exp)
        def{i}=num2str(optivalues_Exp(i));
    end
else def={'3776.056','0.209','0.175','0.148'};
end
kE=1;
inputvalues_Exp=inputdlg(prompt,dlg_title,num_lines,def);
C1_Exp=str2num(inputvalues_Exp{1});
C2_Exp=str2num(inputvalues_Exp{2});
C3_Exp=str2num(inputvalues_Exp{3});
```

```
C4_Exp=str2num(inputvalues_Exp{4});

%%  Run optimization function
Iter_Count_Exp=0;
exitflag_Exp = 0;
while exitflag_Exp == 0 && Iter_Count_Exp < 50

   invalues_Exp = [C1_Exp C2_Exp C3_Exp C4_Exp];
   variables_Exp = [Crc_GL_Str Ax_GL_Str];

   CombStr_Exp = [Crc_PK_Strs;Ax_PK_Strs];

   [optivalues_Exp resnorm_Exp residuals_Exp exitflag_Exp ...
      Opti_Info_Exp lambda_Exp jacobian_Exp] = ...
      lsqcurvefit(@Optifun_Exponential,invalues_Exp,...
      variables_Exp,CombStr_Exp);
   C1_Exp=optivalues_Exp(1);
   C2_Exp=optivalues_Exp(2);
   C3_Exp=optivalues_Exp(3);
   C4_Exp=optivalues_Exp(4);

   Iter_Count_Exp=Iter_Count_Exp+1;
end

%%  Calculate Predicted Stresses
Q_Calc = C2_Exp*(Crc_GL_Str.^2) + C3_Exp*(Ax_GL_Str.^2) + ...
   2*C4_Exp*(Crc_GL_Str.*Ax_GL_Str);

Crc_Stress_Calc_Exp = (C1_Exp*2*C2_Exp*Crc_GL_Str + ...
   C1_Exp*2*C4_Exp*Ax_GL_Str).*exp(Q_Calc);

Ax_Stress_Calc_Exp = (C1_Exp*2*C3_Exp*Ax_GL_Str + ...
   C1_Exp*2*C4_Exp*Crc_GL_Str).*exp(Q_Calc);

%% Calculate R-squared values
TSS_Crc_Exp = sum((Crc_PK_Strs-mean(Crc_PK_Strs)).^2);
RSS_Crc_Exp = sum((Crc_PK_Strs-Crc_Stress_Calc_Exp).^2);
RSquared_Crc_Exp = (TSS_Crc_Exp - RSS_Crc_Exp)/TSS_Crc_Exp;

TSS_Ax_Exp = sum((Ax_PK_Strs-mean(Ax_PK_Strs)).^2);
RSS_Ax_Exp = sum((Ax_PK_Strs-Ax_Stress_Calc_Exp).^2);
RSquared_Ax_Exp = (TSS_Ax_Exp - RSS_Ax_Exp)/TSS_Ax_Exp;

%%  Calculate Predicted Stresses for Plotting
Crc_Str_Step_Exp = (max(Crc_GL_Str)-min(Crc_GL_Str))/100;
Plt_Crc_Str_Exp = min(Crc_GL_Str):Crc_Str_Step_Exp:max(Crc_GL_Str);
Plt_Crc_Str_Exp=Plt_Crc_Str_Exp';

for i=1:length(P0s)
   Plt_Q_Calc(:,i) = C2_Exp*(Plt_Crc_Str_Exp.^2) + ...
      C3_Exp*(Ax_GL_Str(P0s(i))^2) + ...
```

```
        2*C4_Exp*(Plt_Crc_Str_Exp*Ax_GL_Str(P0s(i)));

    Plt_Crc_Stress_Exp(:,i) = (C1_Exp*2*C2_Exp*Plt_Crc_Str_Exp + ...
        C1_Exp*2*C4_Exp*Ax_GL_Str(P0s(i))).*exp(Plt_Q_Calc(:,i));

    Plt_Ax_Stress_Exp(:,i) = (C1_Exp*2*C3_Exp*Ax_GL_Str(P0s(i)) + ...
        C1_Exp*2*C4_Exp*Plt_Crc_Str_Exp).*exp(Plt_Q_Calc(:,i));
end


%% Plot Calculated axial and circumferential 2nd Piola-Kirchoff stresses
%%  and Lagrange strains

TempLineProp={'-r','-m','-k','-g','-b','-r','-c','-y'};
for i=1:length(P0s)
        subplot('position',[.05,.13,.4,.7])
        hold on
        plot(Plt_Crc_Str_Exp,Plt_Crc_Stress_Exp(:,i)...
            ,TempLineProp{i})
        ylabel('Circumferential 2nd Piola-Kirchoff Stress (Pa)')
        xlabel('Circumferential Green-Lagrange Strain')
end
legend(TempPltLegnd1,'Location','NorthWest','FontSize',7)

%% Display R-Squared value
TextPosition(1)=(max(Crc_GL_Str) - min(Crc_GL_Str))/15;
v=axis;
TextPosition(2)=v(3) + (v(4)-v(3))/2;
RSqDisp_Crc=sprintf('%s%s','R^2 = ',num2str(RSquared_Crc_Exp,'%.2f'));
RSqDisp_Crc_Hand=text(TextPosition(1),TextPosition(2),RSqDisp_Crc);
set(RSqDisp_Crc_Hand,'FontWeight','bold')

for i=1:length(P0s)
        Plt2 = subplot('position',[.55,.13,.4,.7]);
        plot(Plt_Crc_Str_Exp,Plt_Ax_Stress_Exp(:,i)...
            ,TempLineProp{i})
        ylabel('Axial 2nd Piola-Kirchoff Stress (Pa)')
        xlabel('Circumferential Green-Lagrange Strain')
        hold on
        TempPltLegnd1{i}=['\lambda','z  = ',num2str(AxStr(P0s(i)),'%.2f')];
end
legend(TempPltLegnd1,'Location','NorthWest','FontSize',7)

%% Display R-Squared value
TextPosition(1)=(max(Crc_GL_Str) - min(Crc_GL_Str))/15;
v=axis;
TextPosition(2)=v(3) + (v(4)-v(3))/2;
RSqDisp_Ax=sprintf('%s%s','R^2 = ',num2str(RSquared_Ax_Exp,'%.2f'));
RSqDisp_Ax_Hand=text(TextPosition(1),TextPosition(2),RSqDisp_Ax);
set(RSqDisp_Ax_Hand,'FontWeight','bold')
```

```
%%  Label Figure
delete(FigLabel)
TempLabel = sprintf('%s\n%s',DataName(1:end-4),'Exponential Fit');
FigLabel = uicontrol('Style','text','String',TempLabel,...
        'units','normalized','Position', [.415 .9 .2 .065],...
        'FontWeight','bold','FontSize',14,'BackgroundColor',[1 1 1]);

%%  Alert user that max number of iterations reached
if Iter_Count_Exp > 1
    button = questdlg(sprintf('%s\n      %s%s%s',...
        'Maximum number of iterations reached!',...
        'Optimization ran ',num2str(Iter_Count_Exp),' times'),...
        'NOTE!!','Rerun','OK','Rerun');
    if strcmp(button,'Rerun')
        Redo='Y';
    elseif strcmp(button,'OK')
        Redo='N';
    end
end
if Redo == 'Y'
    Fit_Exponential
end
Redo='N';
```

The code for the "Fit_Mixed" callback (handle3_3) is as follows:

```
Redo='N';
%%  Calculate axial and circumferential 2nd Piola-Kirchoff stresses if
%%  necessary
if exist('PK_Run') == 0
    delete(subplot(2,2,1))
    delete(subplot(2,2,2))
    delete(subplot(2,2,3))
    delete(subplot(2,2,4))
    Crc_PK_Strs = Crc_Cauch_Strs./(CrcmStr.^2);
    Ax_PK_Strs = Ax_Cauch_Strs./(AxStr.^2);

%%  Calculate axial and circumferential Green-Lagrange Strains
    Crc_GL_Str = ((CrcmStr.^2)-1)/2;
    Ax_GL_Str = ((AxStr.^2)-1)/2;
end

%% Plot axial and circumferential 2nd Piola-Kirchoff stresses and Lagrange
%% Strains
subplot('position',[.05,.18,.4,.7])
hold off
subplot('position',[.55,.18,.4,.7])
hold off
TempLineProp={'*r','om','xk','+g','vb','pr','hc','dy'};
```

```
for i=1:length(P0s)
   if i<length(P0s)
      Plt1 = subplot('position',[.05,.13,.4,.7]);
      plot(Crc_GL_Str(P0s(i):P0s(i+1)-1),Crc_PK_Strs(P0s(i):P0s(i+1)-1)...
         ,TempLineProp{i})
      ylabel('Circumferential 2nd Piola-Kirchoff Stress (Pa)')
      xlabel('Circumferential Green-Lagrange Strain')
      hold on

   elseif i==length(P0s)
      Plt1 = subplot('position',[.05,.13,.4,.7]);
      plot(Crc_GL_Str(P0s(i):length(CrcmStr)),Crc_PK_Strs(P0s(i):length(CrcmStr)),...
         TempLineProp{i})
      ylabel('Circumferential 2nd Piola-Kirchoff Stress (Pa)')
      xlabel('Circumferential Green-Lagrange Strain')
      hold on
   end
end
legend(TempPltLegnd1,'Location','NorthWest','FontSize',7)

for i=1:length(P0s)
   if i<length(P0s)
      Plt2 = subplot('position',[.55,.13,.4,.7]);
      plot(Crc_GL_Str(P0s(i):P0s(i+1)-1),Ax_PK_Strs(P0s(i):P0s(i+1)-1)...
         ,TempLineProp{i})
      ylabel('Axial 2nd Piola-Kirchoff Stress (Pa)')
      xlabel('Circumferential Green-Lagrange Strain')
      hold on

   elseif i==length(P0s)
      Plt2 = subplot('position',[.55,.13,.4,.7]);
      plot(Crc_GL_Str(P0s(i):length(CrcmStr)),Ax_PK_Strs(P0s(i):length(CrcmStr)),...
         TempLineProp{i})
      ylabel('Axial 2nd Piola-Kirchoff Stress (Pa)')
      xlabel('Circumferential Green-Lagrange Strain')
      hold on

   end
   TempPltLegnd1{i}=['\lambda','z  = ',num2str(AxStr(P0s(i)),'%.2f')];
end
legend(TempPltLegnd1,'Location','NorthWest','FontSize',7)

%%  Prompt user to input the starting valuse of fit parameters
prompt = {'Enter an initial value for C1','Enter an initial value for C2',...
   'Enter an initial value for C3','Enter an initial value for C4',...
   'Enter an initial value for C5','Enter an initial value for C6',...
   'Enter an initial value for C7'};
dlg_title ='Input Given Parameters';
num_lines=1;
if exist('optivalues_Mixed')==1
   for i=1:length(optivalues_Mixed)
```

```
        def{i}=num2str(optivalues_Mixed(i));
    end
else def={'1549','4430','3419','36','0.602','2.257','-0.815'};
end

inputvalues_Mixed=inputdlg(prompt,dlg_title,num_lines,def);
C1_Mixed=str2num(inputvalues_Mixed{1});
C2_Mixed=str2num(inputvalues_Mixed{2});
C3_Mixed=str2num(inputvalues_Mixed{3});
C4_Mixed=str2num(inputvalues_Mixed{4});
C5_Mixed=str2num(inputvalues_Mixed{5});
C6_Mixed=str2num(inputvalues_Mixed{6});
C7_Mixed=str2num(inputvalues_Mixed{7});

%%  Run optimization function
Iter_Count_Mixed=0;
exitflag_Mixed = 0;
while exitflag_Mixed == 0 && Iter_Count_Mixed < 50

    invalues_Mixed = [C1_Mixed C2_Mixed C3_Mixed ...
        C4_Mixed C5_Mixed C6_Mixed C7_Mixed];
    variables_Mixed = [Crc_GL_Str Ax_GL_Str];

    CombStr_Mixed = [Crc_PK_Strs;Ax_PK_Strs];

    [optivalues_Mixed resnorm_Mixed residuals_Mixed exitflag_Mixed ...
        Opti_Info_Mixed lambda_Mixed jacobian_Mixed] = ...
        lsqcurvefit(@Optifun_Mixed,invalues_Mixed,...
        variables_Mixed,CombStr_Mixed);
    C1_Mixed=optivalues_Mixed(1);
    C2_Mixed=optivalues_Mixed(2);
    C3_Mixed=optivalues_Mixed(3);
    C4_Mixed=optivalues_Mixed(4);
    C5_Mixed=optivalues_Mixed(5);
    C6_Mixed=optivalues_Mixed(6);
    C7_Mixed=optivalues_Mixed(7);

    Iter_Count_Mixed=Iter_Count_Mixed+1;
end

%%  Calculate Predicted Stresses
Q_Calc = C5_Mixed*(Crc_GL_Str.^2) + C6_Mixed*(Crc_GL_Str.*Ax_GL_Str) + ...
    C7_Mixed*(Ax_GL_Str.^2);

Crc_Stress_Calc_Mixed =(2*C1_Mixed*Crc_GL_Str) + (C2_Mixed*Ax_GL_Str) + ...
    (2*C4_Mixed*C5_Mixed*Crc_GL_Str + C4_Mixed*C6_Mixed*Ax_GL_Str).*exp(Q_Calc);

Ax_Stress_Calc_Mixed =(C2_Mixed*Crc_GL_Str) + (2*C3_Mixed*Ax_GL_Str) + ...
    (C4_Mixed*C6_Mixed*Crc_GL_Str + 2*C4_Mixed*C7_Mixed*Ax_GL_Str).*exp(Q_Calc);

%% Calculate R-squared values
```

```
TSS_Crc_Mixed = sum((Crc_PK_Strs-mean(Crc_PK_Strs)).^2);
RSS_Crc_Mixed = sum((Crc_PK_Strs-Crc_Stress_Calc_Mixed).^2);
RSquared_Crc_Mixed = (TSS_Crc_Mixed - RSS_Crc_Mixed)/TSS_Crc_Mixed;

TSS_Ax_Mixed = sum((Ax_PK_Strs-mean(Ax_PK_Strs)).^2);
RSS_Ax_Mixed = sum((Ax_PK_Strs-Ax_Stress_Calc_Mixed).^2);
RSquared_Ax_Mixed = (TSS_Ax_Mixed - RSS_Ax_Mixed)/TSS_Ax_Mixed;

%%  Calculate Predicted Stresses for Plotting
Crc_Str_Step_Mixed = (max(Crc_GL_Str)-min(Crc_GL_Str))/100;
Plt_Crc_Str_Mixed = min(Crc_GL_Str):Crc_Str_Step_Mixed:max(Crc_GL_Str);
Plt_Crc_Str_Mixed=Plt_Crc_Str_Mixed';

for i=1:length(P0s)
   Plt_Q_Calc(:,i) = C5_Mixed*(Plt_Crc_Str_Mixed.^2) +
C6_Mixed*(Plt_Crc_Str_Mixed.*Ax_GL_Str(P0s(i))) + ...
      C7_Mixed*(Ax_GL_Str(P0s(i)).^2);

   Plt_Crc_Stress_Mixed(:,i) = (2*C1_Mixed*Plt_Crc_Str_Mixed) + (C2_Mixed*Ax_GL_Str(P0s(i))) +
...
      (2*C4_Mixed*C5_Mixed*Plt_Crc_Str_Mixed +
C4_Mixed*C6_Mixed*Ax_GL_Str(P0s(i))).*exp(Plt_Q_Calc(:,i));

   Plt_Ax_Stress_Mixed(:,i) = (C2_Mixed*Plt_Crc_Str_Mixed) + (2*C3_Mixed*Ax_GL_Str(P0s(i))) +
...
      (C4_Mixed*C6_Mixed*Plt_Crc_Str_Mixed +
2*C4_Mixed*C7_Mixed*Ax_GL_Str(P0s(i))).*exp(Plt_Q_Calc(:,i));
end

%% Plot Calculated axial and circumferential 2nd Piola-Kirchoff stresses
%%  and Lagrange strains
 TempLineProp={'-r','-m','-k','-g','-b','-r','-c','-y'};
for i=1:length(P0s)
      subplot('position',[.05,.13,.4,.7])
      hold on
      plot(Plt_Crc_Str_Mixed,Plt_Crc_Stress_Mixed(:,i)...
         ,TempLineProp{i})
      ylabel('Circumferential 2nd Piola-Kirchoff Stress (Pa)')
      xlabel('Circumferential Green-Lagrange Strain')
end
legend(TempPltLegnd1,'Location','NorthWest','FontSize',7)

%% Display R-Squared value
TextPosition(1)=(max(Crc_GL_Str) - min(Crc_GL_Str))/15;
v=axis;
TextPosition(2)=v(3) + (v(4)-v(3))/2;
RSqDisp_Crc=sprintf('%s%s','R^2 = ',num2str(RSquared_Crc_Mixed,'%.2f'));
RSqDisp_Crc_Hand=text(TextPosition(1),TextPosition(2),RSqDisp_Crc);
set(RSqDisp_Crc_Hand,'FontWeight','bold')

for i=1:length(P0s)
```

```
%     if i<length(P0s)
        Plt2 = subplot('position',[.55,.13,.4,.7]);
        plot(Plt_Crc_Str_Mixed,Plt_Ax_Stress_Mixed(:,i)...
           ,TempLineProp{i})
        ylabel('Axial 2nd Piola-Kirchoff Stress (Pa)')
        xlabel('Circumferential Green-Lagrange Strain')
        hold on
        TempPltLegnd1{i}=['\lambda','z  = ',num2str(AxStr(P0s(i)),'%.2f')];
end
legend(TempPltLegnd1,'Location','NorthWest','FontSize',7)

%% Display R-Squared value
TextPosition(1)=(max(Crc_GL_Str) - min(Crc_GL_Str))/15;
v=axis;
TextPosition(2)=v(3) + (v(4)-v(3))/2;
RSqDisp_Ax=sprintf('%s%s','R^2 = ',num2str(RSquared_Ax_Mixed,'%.2f'));
RSqDisp_Ax_Hand=text(TextPosition(1),TextPosition(2),RSqDisp_Ax);
set(RSqDisp_Ax_Hand,'FontWeight','bold')

%%  Label Figure
delete(FigLabel)
TempLabel = sprintf('%s\n%s',DataName(1:end-4),'Mixed Fit');
FigLabel = uicontrol('Style','text','String',TempLabel,...
        'units','normalized','Position', [.415 .9 .2 .065],...
        'FontWeight','bold','FontSize',14,'BackgroundColor',[1 1 1]);

%%  Alert user that max number of iterations reached
if Iter_Count_Mixed > 1
    button = questdlg(sprintf('%s\n      %s%s%s',...
        'Maximum number of iterations reached!',...
        'Optimization ran ',num2str(Iter_Count_Mixed),' times'),...
        'NOTE!!','Rerun','OK','Rerun');
    if strcmp(button,'Rerun')
        Redo='Y';
    elseif strcmp(button,'OK')
        Redo='N';
    end
end
if Redo == 'Y'
    Fit_Mixed
end
```

The code for the polynomial optimization function (Optifun_Poly) is as follows:

```
function Comb_Stress_Poly = Optifun_Polynomial(invalues_Poly,variables_Poly)
global Comb_Stress_Poly
C1_Poly=invalues_Poly(1);
C2_Poly=invalues_Poly(2);
C3_Poly=invalues_Poly(3);
```

```
C4_Poly=invalues_Poly(4);
C5_Poly=invalues_Poly(5);
C6_Poly=invalues_Poly(6);
C7_Poly=invalues_Poly(7);

Crc_GL_Str=variables_Poly(:,1);
Ax_GL_Str=variables_Poly(:,2);


Crc_Stress_Poly =(2*C1_Poly*Crc_GL_Str) + ...
   (C2_Poly*Ax_GL_Str) + 3*C4_Poly*(Crc_GL_Str.^2) + ...
   2*C5_Poly*(Crc_GL_Str.*Ax_GL_Str) + C6_Poly*(Ax_GL_Str.^2);

Ax_Stress_Poly =(C2_Poly*Crc_GL_Str) + ...
   (2*C3_Poly*Ax_GL_Str) +C5_Poly*(Crc_GL_Str.^2) + ...
   2*C6_Poly*(Crc_GL_Str.*Ax_GL_Str) + 3*C7_Poly*(Ax_GL_Str.^2);

Comb_Stress_Poly = [Crc_Stress_Poly;Ax_Stress_Poly];
```

The code for the exponential optimization function (Optifun_Exponential) is as follows:

```
function Comb_Stress_Exp = Optifun_Exponential(invalues_Exp,variables_Exp)
global Comb_Stress_Exp
C1_Exp=invalues_Exp(1);
C2_Exp=invalues_Exp(2);
C3_Exp=invalues_Exp(3);
C4_Exp=invalues_Exp(4);

Crc_GL_Str=variables_Exp(:,1);
Ax_GL_Str=variables_Exp(:,2);

Q = C2_Exp*(Crc_GL_Str.^2) + C3_Exp*(Ax_GL_Str.^2) + ...
   2*C4_Exp*(Crc_GL_Str.*Ax_GL_Str);

Crc_Stress_Exp = (C1_Exp*2*C2_Exp*Crc_GL_Str + ...
   C1_Exp*2*C4_Exp*Ax_GL_Str).*exp(Q);

Ax_Stress_Exp = (C1_Exp*2*C3_Exp*Ax_GL_Str + ...
   C1_Exp*2*C4_Exp*Crc_GL_Str).*exp(Q);

Comb_Stress_Exp = [Crc_Stress_Exp;Ax_Stress_Exp];
```

The code for the mixed exponential-polynomial optimization function (Optifun_Mixed) is as follows:

```
function Comb_Stress_Mixed = Optifun_Mixed(invalues_Mixed,variables_Mixed)
global Comb_Stress_Mixed
```

```
C1_Mixed=invalues_Mixed(1);
C2_Mixed=invalues_Mixed(2);
C3_Mixed=invalues_Mixed(3);
C4_Mixed=invalues_Mixed(4);
C5_Mixed=invalues_Mixed(5);
C6_Mixed=invalues_Mixed(6);
C7_Mixed=invalues_Mixed(7);

Crc_GL_Str=variables_Mixed(:,1);
Ax_GL_Str=variables_Mixed(:,2);

Q = C5_Mixed*(Crc_GL_Str.^2) + C6_Mixed*(Crc_GL_Str.*Ax_GL_Str) + ...
   C7_Mixed*(Ax_GL_Str.^2);

Crc_Stress_Mixed =(2*C1_Mixed*Crc_GL_Str) + (C2_Mixed*Ax_GL_Str) + ...
   (2*C4_Mixed*C5_Mixed*Crc_GL_Str + C4_Mixed*C6_Mixed*Ax_GL_Str).*exp(Q);

Ax_Stress_Mixed =(C2_Mixed*Crc_GL_Str) + (2*C3_Mixed*Ax_GL_Str) + ...
   (C4_Mixed*C6_Mixed*Crc_GL_Str + 2*C4_Mixed*C7_Mixed*Ax_GL_Str).*exp(Q);

Comb_Stress_Mixed = [Crc_Stress_Mixed;Ax_Stress_Mixed];
```

The code for the “Save_Res” callback (handle4) is as follows:

```
ScriptDir=pwd;
Results_Dir=sprintf('%s%s',ScriptDir(1:end-7),'Results');
Figures_Dir=sprintf('%s%s',ScriptDir(1:end-7),'Saved Figures');

%%  Save Coefficients
if SaveType == 1
   if exist('C1_Exp')==1 || exist('C1_Poly')==1 || exist('C1_Mixed')==1

%%  Prompt User to Decide to Save to An Existing File or a New One
      button = questdlg('Do You Want to Add to An Exiting File or Save to A New File?',...
         'Save Output?','Existing File','New File','Existing File');
      if strcmp(button,'Existing File')
         Adddata='A';
      elseif strcmp(button,'New File')
         Adddata='N';
      end

%%  Save Coefficients
 %Append an existing file
      if Adddata=='A'
         cd(Results_Dir);
         [ResFilename,FilePath] = uiputfile({'*.txt';'*.xls'},'Save As',...
            sprintf('%s%s',DataName(1:end-4),'_Coefficients.txt'));
         if ResFilename ~= 0
            %Save coefficients for polynomial fit
```

```
            cd(FilePath);
            if exist('C1_Poly')== 1
               fid1=fopen(ResFilename,'a');
               fprintf(fid1,'%s\t %s\t %6.3f\t %6.3f\t %6.3f\t %6.3f\t %6.3f\t %6.3f\t %6.3f\t \n',...
                  DataName(1:end-4), 'Polynomial',C1_Poly, C2_Poly,C3_Poly,...
                  C4_Poly, C5_Poly, C6_Poly, C7_Poly);
               fclose(fid1);
            end

            %Save coefficients for exponential fit
            if exist('C1_Exp')== 1
               fid1=fopen(ResFilename,'a');
               fprintf(fid1,'%s\t %s\t %6.3f\t %6.3f\t %6.3f\t %6.3f\t %6.3f\t %6.3f\t %6.3f\t \n',...
                  DataName(1:end-4), 'Exponential',C1_Exp, C2_Exp, C3_Exp, C4_Exp, 0, 0, 0);
               fclose(fid1);
            end

            %Save coefficients for Choi exponential fit
            if exist('C1_ExpChoi')==1
               fid1=fopen(ResFilename,'a');
               fprintf(fid1,'%s\t %s\t %6.3f\t %6.3f\t %6.3f\t %6.3f\t %6.3f\t %6.3f\t %6.3f\t \n',...
                  DataName(1:end-4), 'Choi Exponential',C1_ExpChoi, C2_ExpChoi, C3_ExpChoi,
C4_ExpChoi, 0, 0, 0);
               fclose(fid1);
            end

            %Save coefficients for Mixed Model fit
            if exist('C1_Mixed')==1
               fid1=fopen(ResFilename,'a');
               fprintf(fid1,'%s\t %s\t %6.3f\t %6.3f\t %6.3f\t %6.3f\t %6.3f\t %6.3f\t %6.3f\t \n',...
                  DataName(1:end-4), 'Mixed Model',C1_Mixed, C2_Mixed, C3_Mixed, ...
                  C4_Mixed, C5_Mixed, C6_Mixed, C7_Mixed);
               fclose(fid1);
            end
         end
         cd(ScriptDir);

      %Save to a new file
      elseif Adddata=='N'
         cd(Results_Dir);
         [ResFilename,FilePath] = uiputfile({'*.txt';'*.xls'},'Save As',...
            sprintf('%s%s',DataName(1:end-4),'_Coefficients.txt'));
         if ResFilename ~= 0
            cd(FilePath);
            %Save column labels
            fid1=fopen(ResFilename,'w');
            fprintf(fid1,'%s\t %s\t %s\t %s\t %s\t %s\t %s\t %s\t %s\t \n',...
               'Vessel ID', 'Fit Type','C1', 'C2','C3', 'C4', 'C5', 'C6', 'C7');
             fclose(fid1);

            %Save coefficients for polynomial fit
```

```
            if exist('C1_Poly')== 1
               fid1=fopen(ResFilename,'a');
               fprintf(fid1,'%s\t %s\t %6.3f\t %6.3f\t %6.3f\t %6.3f\t %6.3f\t %6.3f\t %6.3f\t \n',...
                  DataName(1:end-4), 'Polynomial',C1_Poly, C2_Poly,C3_Poly,...
                  C4_Poly, C5_Poly, C6_Poly, C7_Poly);
                fclose(fid1);
            end

            %Save coefficients for exponential fit
            if exist('C1_Exp')== 1
               fid1=fopen(ResFilename,'a');
               fprintf(fid1,'%s\t %s\t %6.3f\t %6.3f\t %6.3f\t %6.3f\t %6.3f\t %6.3f\t %6.3f\t \n',...
                  DataName(1:end-4), 'Exponential',C1_Exp, C2_Exp, C3_Exp, C4_Exp, 0, 0, 0);
               fclose(fid1);
            end
            end

            %Save coefficients for Mixed Model fit
            if exist('C1_Mixed')==1
               fid1=fopen(ResFilename,'a');
               fprintf(fid1,'%s\t %s\t %6.3f\t %6.3f\t %6.3f\t %6.3f\t %6.3f\t %6.3f\t %6.3f\t \n',...
                  DataName(1:end-4), 'Mixed Model',C1_Mixed, C2_Mixed, C3_Mixed, ...
                  C4_Mixed, C5_Mixed, C6_Mixed, C7_Mixed);
               fclose(fid1);
            end
         end
         cd(ScriptDir);
      end
   elseif exist('C1_Exp')==0 && exist('C1_Poly')==0 && exist('C1_ExpChoi')==0
      msgbox(sprintf('%s\n%s',...
         'THERE ARE NO COEFFICIENTS TO BE SAVED!',...
         'PLEASE RUN OPTIMIZATION PROGRAM FIRST!'),...
         'ERROR!','warn');
      cd(ScriptDir);
   end
end

%%  Save Curves
if SaveType == 2
   clear Output2
   %Save Output
   cd(Results_Dir);
   [ResFilename,FilePath] = uiputfile({'*.txt';'*.xls'},'Save As',...
      sprintf('%s%s',DataName(1:end-4),'_Curves'));
   if ResFilename ~= 0
      cd(FilePath);

      %Create output array for curves
      Output=[Press_mmHg Di Do Force_mN Length CrcmStr AxStr Crc_Cauch_Strs ...
         Ax_Cauch_Strs Crc_PK_Strs Ax_PK_Strs Crc_GL_Str Ax_GL_Str];
```

```
        fid=fopen(ResFilename,'w');
        fprintf(fid,'%s\t %s\t %s\t %s\t %s\t %s\t %s\t %s\t %s\t %s\t %s\t %s\t \n',...
            'P(mmHg)', 'Di(um)','Do(um)', 'Force(mN)',...
            'Length(mm)', 'Strain(Circ)', 'Strain(Axial)',...
            'Cauch Stress(Circ)', 'Cauch Stress(Axial)',...
            'PK Stress(Circ)','PK Stress(Axial)',...
            'GL Strain(Circ)','GL Strain(Axial)');
        fprintf(fid,'%6.2f\t %6.2f\t %6.2f\t %6.2f\t %6.2f\t %6.2f\t %6.2f\t %6.2f\t %6.2f\t %6.2f\t
%6.2f\t %6.2f\t \n',...
            Output');
        fclose(fid);

        %Create output arrays for polynomial fit
        if exist('C1_Poly')== 1
            Output2=[Plt_Crc_Str_Poly Plt_Crc_Stress_Poly Plt_Ax_Stress_Poly];
        end

        %Create output array for exponential fit only
        if exist('C1_Exp')== 1
            Exp_Array =[Plt_Crc_Str_Exp Plt_Crc_Stress_Exp Plt_Ax_Stress_Exp];
            Arr_Size = size(Exp_Array);
            Arr_Size = Arr_Size(2);
            Output2(:,end+1:end+Arr_Size) = Exp_Array;
        end

        %Create output array for Mixed Model fit only
        if exist('C1_Mixed')== 1
            Mixed_Array =[Plt_Crc_Str_Mixed Plt_Crc_Stress_Mixed Plt_Ax_Stress_Mixed];
            Arr_Size = size(Mixed_Array);
            Arr_Size = Arr_Size(2);
            Output2(:,end+1:end+Arr_Size) = Mixed_Array;
        end

        %Save File
        row=size(Output2);
        row=row(2);
        Fmt='%6.2f\t ';
        for i=2:row
            Fmt=sprintf('%s%s',Fmt,'%6.2f\t ');
            if i==row
                Fmt=sprintf('%s%s',Fmt,'\n');
            end
        end

        fid_2=fopen(sprintf('%s%s',ResFilename(1:end-11),'_Predicted.txt'),'w');
        fprintf(fid_2,Fmt,Output2');
        fclose(fid_2);
    end
    cd(ScriptDir);
end
```

BIBLIOGRAPHY

1. **Shroff SG** 1998 Pulsatie arterial load and cardiovascular function: fact, fiction, and wishful thinking. *Ther Res* 19:59-66.

2. **Liu Z, Brin KP, and Yin FC** 1986 Estimation of total arterial compliance: an improved method and evaluation of current methods. *Am J Physiol* 251(3 Pt 2):H588-600.

3. **Franklin SS** 2004 Pulse pressure as a risk factor. *Clin Exp Hypertens* 26(7-8):645-52.

4. **Wilcox CS** 2002 Reactive oxygen species: roles in blood pressure and kidney function. *Curr Hypertens Rep* 4(2):160-6.

5. **McLaughlin M, Roberts, J.M.**, Hemodynamic changes, in Chesley's Hypertensive Disorders in Pregnancy, Lindheimer MD, Roberts, J.M., Cunningham, F.G., Editor. 1999 Appletom & Lange: Stamford, CT. p. 69-102.

6. **Poppas A, Shroff SG, Korcarz CE, Hibbard JU, Berger DS, Lindheimer MD, and Lang RM** 1997 Serial assessment of the cardiovascular system in normal pregnancy. Role of arterial compliance and pulsatile arterial load. *Circulation* 95(10):2407-15.

7. **Griendling KK, Fuller EO, and Cox RH** 1985 Pregnancy-induced changes in sheep uterine and carotid arteries. *Am J Physiol* 248(5 Pt 2):H658-65.

8. **Osol G and Cipolla M** 1993 Pregnancy-induced changes in the three-dimensional mechanical properties of pressurized rat uteroplacental (radial) arteries. *Am J Obstet Gynecol* 168(1 Pt 1):268-74.

9. **Page KL, Celia G, Leddy G, Taatjes DJ, and Osol G** 2002 Structural remodeling of rat uterine veins in pregnancy. *Am J Obstet Gynecol* 187(6):1647-52.

10. **Bird IM, Zhang L, and Magness RR** 2003 Possible mechanisms underlying pregnancy-induced changes in uterine artery endothelial function. *Am J Physiol Regul Integr Comp Physiol* 284(2):R245-58.

11. **Hammer ES and Cipolla MJ** 2005 Arterial wall hyperplasia is increased in placental compared with myoendometrial radial uterine arteries from late-pregnant rats. *Am J Obstet Gynecol* 192(1):302-8.

12. **Mackey K, Meyer MC, Stirewalt WS, Starcher BC, and McLaughlin MK** 1992 Composition and mechanics of mesenteric resistance arteries from pregnant rats. *Am J Physiol* 263(1 Pt 2):R2-8.

13. **Hart MV, Rowles JR, Hohimer AR, Morton MJ, and Hosenpud JD** 1984 Hemodynamics in the guinea pig after anesthetization with ketamine/xylazine. *Am J Vet Res* 45(11):2328-30.

14. **Davis LE, Hohimer AR, Giraud GD, Paul MS, and Morton MJ** 1989 Vascular pressure-volume relationships in pregnant and estrogen-treated guinea pigs. *Am J Physiol* 257(5 Pt 2):R1205-11.

15. **Slangen BF, Out IC, Verkeste CM, and Peeters LL** 1996 Hemodynamic changes in early pregnancy in chronically instrumented, conscious rats. *Am J Physiol* 270(5 Pt 2):H1779-84.

16. **Danielson LA, Sherwood OD, and Conrad KP** 1999 Relaxin is a potent renal vasodilator in conscious rats. *J Clin Invest* 103(4):525-33.

17. **St-Louis J and Massicotte G** 1985 Chronic decrease of blood pressure by rat relaxin in spontaneously hypertensive rats. *Life Sci* 37(14):1351-7.

18. **Massicotte G, Parent A, and St-Louis J** 1989 Blunted responses to vasoconstrictors in mesenteric vasculature but not in portal vein of spontaneously hypertensive rats treated with relaxin. *Proc Soc Exp Biol Med* 190(3):254-9.

19. **Bani-Sacchi T, Bigazzi M, Bani D, Mannaioni PF, and Masini E** 1995 Relaxin-induced increased coronary flow through stimulation of nitric oxide production. *Br J Pharmacol* 116(1):1589-94.

20. **Conrad KP and Novak J** 2004 Emerging role of relaxin in renal and cardiovascular function. *Am J Physiol Regul Integr Comp Physiol* 287(2):R250-61.

21. **Sherwood OD** 2004 Relaxin's physiological roles and other diverse actions. *Endocr Rev* 25(2):205-34.

22. **Conrad KP, Lindheimer, M.D.**, Renal and Cardiovascular Alterations, in Chesley's Hypertensive Disorders in Pregnancy, Lindheimer MD, Roberts, J.M., Cunningham, F.G., Editor. 1999 Appletom & Lange: Stamford, CT. p. 263-326.

23. **Novak J, Danielson LA, Kerchner LJ, Sherwood OD, Ramirez RJ, Moalli PA, and Conrad KP** 2001 Relaxin is essential for renal vasodilation during pregnancy in conscious rats. *J Clin Invest* 107(11):1469-75.

24. **Danielson LA, Kercher LJ, and Conrad KP** 2000 Impact of gender and endothelin on renal vasodilation and hyperfiltration induced by relaxin in conscious rats. *Am J Physiol Regul Integr Comp Physiol* 279(4):R1298-304.

25. **Jeyabalan A, Novak J, Danielson LA, Kerchner LJ, Opett SL, and Conrad KP** 2003 Essential role for vascular gelatinase activity in relaxin-induced renal vasodilation, hyperfiltration, and reduced myogenic reactivity of small arteries. *Circ Res* 93(12):1249-57.

26. **Conrad KP and Colpoys MC** 1986 Evidence against the hypothesis that prostaglandins are the vasodepressor agents of pregnancy. Serial studies in chronically instrumented, conscious rats. *J Clin Invest* 77(1):236-45.

27. **Danielson LA and Conrad KP** 1995 Acute blockade of nitric oxide synthase inhibits renal vasodilation and hyperfiltration during pregnancy in chronically instrumented conscious rats. *J Clin Invest* 96(1):482-90.

28. **Novak J, Ramirez RJ, Gandley RE, Sherwood OD, and Conrad KP** 2002 Myogenic reactivity is reduced in small renal arteries isolated from relaxin-treated rats. *Am J Physiol Regul Integr Comp Physiol* 283(2):R349-55.

29. **Gandley RE, Conrad KP, and McLaughlin MK** 2001 Endothelin and nitric oxide mediate reduced myogenic reactivity of small renal arteries from pregnant rats. *Am J Physiol Regul Integr Comp Physiol* 280(1):R1-7.

30. **Conrad KP, Gandley RE, Ogawa T, Nakanishi S, and Danielson LA** 1999 Endothelin mediates renal vasodilation and hyperfiltration during pregnancy in chronically instrumented conscious rats. *Am J Physiol* 276(5 Pt 2):F767-76.

31. **Fernandez-Patron C, Radomski MW, and Davidge ST** 2000 Role of matrix metalloproteinase-2 in thrombin-induced vasorelaxation of rat mesenteric arteries. *Am J Physiol Heart Circ Physiol* 278(5):H1473-9.

32. **Fernandez-Patron C, Radomski MW, and Davidge ST** 1999 Vascular matrix metalloproteinase-2 cleaves big endothelin-1 yielding a novel vasoconstrictor. *Circ Res* 85(10):906-11.

33. **Jeyabalan A, Shroff SG, Novak J, and Conrad KP** 2007 The vascular actions of relaxin. *Adv Exp Med Biol* 612:65-87.

34. **Gilson GJ, Mosher MD, and Conrad KP** 1992 Systemic hemodynamics and oxygen transport during pregnancy in chronically instrumented, conscious rats. *Am J Physiol* 263(6 Pt 2):H1911-8.

35. **Danielson LA and Conrad KP** 2003 Time course and dose response of relaxin-mediated renal vasodilation, hyperfiltration, and changes in plasma osmolality in conscious rats. *J Appl Physiol* 95(4):1509-14.

36. **Osborn JW, Jr., Barber BJ, Quillen EW, Jr., Abram RJ, and Cowley AW, Jr.** 1986 Chronic measurement of cardiac output in unanesthetized rats using miniature thermocouples. *Am J Physiol* 251(6 Pt 2):H1365-72.

37. **Mills PA, Huetteman DA, Brockway BP, Zwiers LM, Gelsema AJ, Schwartz RS, and Kramer K** 2000 A new method for measurement of blood pressure, heart rate, and activity in the mouse by radiotelemetry. *J Appl Physiol* 88(5):1537-44.

38. **Burattini R, Fioretti S, and Jetto L** 1985 A simple algorithm for defining the mean cardiac cycle of aortic flow and pressure during steady state. *Comput Biomed Res* 18(4):303-12.

39. **Chemla D, Hebert JL, Coirault C, Zamani K, Suard I, Colin P, and Lecarpentier Y** 1998 Total arterial compliance estimated by stroke volume-to-aortic pulse pressure ratio in humans. *Am J Physiol* 274(2 Pt 2):H500-5.

40. **Guico-Lamm ML, Voss EW, Jr., and Sherwood OD** 1988 Monoclonal antibodies specific for rat relaxin. I. Production and characterization of monoclonal antibodies that neutralize rat relaxin's bioactivity in vivo. *Endocrinology* 123(5):2472-8.

41. **Hwang JJ, Shanks RD, and Sherwood OD** 1989 Monoclonal antibodies specific for rat relaxin. IV. Passive immunization with monoclonal antibodies during the antepartum period reduces cervical growth and extensibility, disrupts birth, and reduces pup survival in intact rats. *Endocrinology* 125(1):260-6.

42. **Cholley BP, Lang RM, Korcarz CE, and Shroff SG** 2001 Smooth muscle relaxation and local hydraulic impedance properties of the aorta. *J Appl Physiol* 90(6):2427-38.

43. **Schulze-Bauer CA, Morth C, and Holzapfel GA** 2003 Passive biaxial mechanical response of aged human iliac arteries. *J Biomech Eng* 125(3):395-406.

44. **Vaishnav RN, Young JT, Janicki JS, and Patel DJ** 1972 Nonlinear anisotropic elastic properties of the canine aorta. *Biophys J* 12(8):1008-27.

45. **Fung YC, Fronek K, and Patitucci P** 1979 Pseudoelasticity of arteries and the choice of its mathematical expression. *Am J Physiol* 237(5):H620-31.

46. **Demiray H, Weizsacker HW, and Pascale K** 1986 A mechanical model for passive behaviour of rats' carotid artery. *Biomed Tech (Berl)* 31(3):46-52.

47. **Ratkowsky D**, Nonlinear regression modeling: a unified practical approach. 1983, New York: Marcel Dekker.

48. **Conrad KP, Debrah DO, Novak J, Danielson LA, and Shroff SG** 2004 Relaxin modifies systemic arterial resistance and compliance in conscious, nonpregnant rats. *Endocrinology* 145(7):3289-96.

49. **Conrad KP and Russ RD** 1992 Augmentation of baroreflex-mediated bradycardia in conscious pregnant rats. *Am J Physiol* 262(3 Pt 2):R472-7.

50. **Debrah DO, Conrad KP, Danielson LA, and Shroff SG** 2005 Effects of relaxin on systemic arterial hemodynamics and mechanical properties in conscious rats: sex dependency and dose response. *J Appl Physiol* 98(3):1013-20.

51. **Debrah DO, Novak J, Matthews JE, Ramirez RJ, Shroff SG, and Conrad KP** 2006 Relaxin is essential for systemic vasodilation and increased global arterial compliance during early pregnancy in conscious rats. *Endocrinology* 147(11):5126-31.

52. **Novak J, Parry LJ, Matthews JE, Kerchner LJ, Indovina K, Hanley-Yanez K, Doty KD, Debrah DO, Shroff SG, and Conrad KP** 2006 Evidence for local relaxin ligand-receptor expression and function in arteries. *Faseb J* 20(13):2352-62.

53. **Sacks MS and Chuong CJ** 1998 Orthotropic mechanical properties of chemically treated bovine pericardium. *Ann Biomed Eng* 26(5):892-902.

54. **Robson SC, Hunter S, Boys RJ, and Dunlop W** 1989 Serial study of factors influencing changes in cardiac output during human pregnancy. *Am J Physiol* 256(4 Pt 2):H1060-5.

55. **Slangen BF, van Ingen Schenau DS, van Gorp AW, De Mey JG, and Peeters LL** 1997 Aortic distensibility and compliance in conscious pregnant rats. *Am J Physiol* 272(3 Pt 2):H1260-5.

56. **Unemori EN, Lewis M, Constant J, Arnold G, Grove BH, Normand J, Deshpande U, Salles A, Pickford LB, Erikson ME, Hunt TK, and Huang X** 2000 Relaxin induces vascular endothelial growth factor expression and angiogenesis selectively at wound sites. *Wound Repair Regen* 8(5):361-70.

57. **Puyraimond A, Fridman R, Lemesle M, Arbeille B, and Menashi S** 2001 MMP-2 colocalizes with caveolae on the surface of endothelial cells. *Exp Cell Res* 262(1):28-36.

58. **Goligorsky MS, Budzikowski AS, Tsukahara H, and Noiri E** 1999 Co-operation between endothelin and nitric oxide in promoting endothelial cell migration and angiogenesis. *Clin Exp Pharmacol Physiol* 26(3):269-71.

59. **Hasan KM, Manyonda IT, Ng FS, Singer DR, and Antonios TF** 2002 Skin capillary density changes in normal pregnancy and pre-eclampsia. *J Hypertens* 20(12):2439-43.

60. **Hsu SY, Nakabayashi K, Nishi S, Kumagai J, Kudo M, Sherwood OD, and Hsueh AJ** 2002 Activation of orphan receptors by the hormone relaxin. *Science* 295(5555):671-4.

61. **Kakouris H, Eddie LW, and Summers RJ** 1992 Cardiac effects of relaxin in rats. *Lancet* 339(8801):1076-8.

62. **Smith MC, Danielson LA, Conrad KP, and Davison JM** 2006 Influence of recombinant human relaxin on renal hemodynamics in healthy volunteers. *J Am Soc Nephrol* 17(11):3192-7.

63. **Du XJ, Samuel CS, Gao XM, Zhao L, Parry LJ, and Tregear GW** 2003 Increased myocardial collagen and ventricular diastolic dysfunction in relaxin deficient mice: a gender-specific phenotype. *Cardiovasc Res* 57(2):395-404.

64. **Samuel CS, Zhao C, Bond CP, Hewitson TD, Amento EP, and Summers RJ** 2004 Relaxin-1-deficient mice develop an age-related progression of renal fibrosis. *Kidney Int* 65(6):2054-64.

65. **Samuel CS, Zhao C, Yang Q, Wang H, Tian H, Tregear GW, and Amento EP** 2005 The relaxin gene knockout mouse: a model of progressive scleroderma. *J Invest Dermatol* 125(4):692-9.

66. **Keyes L, Rodman DM, Curran-Everett D, Morris K, and Moore LG** 1998 Effect of K+ATP channel inhibition on total and regional vascular resistance in guinea pig pregnancy. *Am J Physiol* 275(2 Pt 2):H680-8.

67. **Meyer MC, Brayden JE, and McLaughlin MK** 1993 Characteristics of vascular smooth muscle in the maternal resistance circulation during pregnancy in the rat. *Am J Obstet Gynecol* 169(6):1510-6.

68. **Kuzuya M and Iguchi A** 2003 Role of matrix metalloproteinases in vascular remodeling. *J Atheroscler Thromb* 10(5):275-82.

69. **McGuane JT and Parry LJ** 2005 Relaxin and the extracellular matrix: molecular mechanisms of action and implications for cardiovascular disease. *Expert Rev Mol Med* 7(21):1-18.

70. **Unemori EN and Amento EP** 1990 Relaxin modulates synthesis and secretion of procollagenase and collagen by human dermal fibroblasts. *J Biol Chem* 265(18):10681-5.

71. **Garber SL, Mirochnik Y, Brecklin CS, Unemori EN, Singh AK, Slobodskoy L, Grove BH, Arruda JA, and Dunea G** 2001 Relaxin decreases renal interstitial fibrosis and slows progression of renal disease. *Kidney Int* 59(3):876-82.

72. **Unemori EN, Pickford LB, Salles AL, Piercy CE, Grove BH, Erikson ME, and Amento EP** 1996 Relaxin induces an extracellular matrix-degrading phenotype in human lung fibroblasts in vitro and inhibits lung fibrosis in a murine model in vivo. *J Clin Invest* 98(12):2739-45.

73. **Williams EJ, Benyon RC, Trim N, Hadwin R, Grove BH, Arthur MJ, Unemori EN, and Iredale JP** 2001 Relaxin inhibits effective collagen deposition by cultured hepatic stellate cells and decreases rat liver fibrosis in vivo. *Gut* 49(4):577-83.

74. **Samuel CS, Unemori EN, Mookerjee I, Bathgate RA, Layfield SL, Mak J, Tregear GW, and Du XJ** 2004 Relaxin modulates cardiac fibroblast proliferation, differentiation, and collagen production and reverses cardiac fibrosis in vivo. *Endocrinology* 145(9):4125-33.

75. **Tozzi CA, Poiani GJ, McHugh NA, Shakarjian MP, Grove BH, Samuel CS, Unemori EN, and Riley DJ** 2005 Recombinant human relaxin reduces hypoxic pulmonary hypertension in the rat. *Pulm Pharmacol Ther* 18(5):346-53.

76. **Samuel CS** 2005 Relaxin: antifibrotic properties and effects in models of disease. *Clin Med Res* 3(4):241-9.

77. **Samuel CS, Zhao C, Bathgate RA, Bond CP, Burton MD, Parry LJ, Summers RJ, Tang ML, Amento EP, and Tregear GW** 2003 Relaxin deficiency in mice is associated with an age-related progression of pulmonary fibrosis. *Faseb J* 17(1):121-3.

78. **Cipolla M and Osol G** 1994 Hypertrophic and hyperplastic effects of pregnancy on the rat uterine arterial wall. *Am J Obstet Gynecol* 171(3):805-11.

79. **van der Heijden OW, Essers YP, Spaanderman ME, De Mey JG, van Eys GJ, and Peeters LL** 2005 Uterine artery remodeling in pseudopregnancy is comparable to that in early pregnancy. *Biol Reprod* 73(6):1289-93.

80. **Tulis DA, Unthank JL, and Prewitt RL** 1998 Flow-induced arterial remodeling in rat mesenteric vasculature. *Am J Physiol* 274(3 Pt 2):H874-82.

81. **Buus CL, Pourageaud F, Fazzi GE, Janssen G, Mulvany MJ, and De Mey JG** 2001 Smooth muscle cell changes during flow-related remodeling of rat mesenteric resistance arteries. *Circ Res* 89(2):180-6.

82. **De Mey JG, Schiffers PM, Hilgers RH, and Sanders MM** 2005 Toward functional genomics of flow-induced outward remodeling of resistance arteries. *Am J Physiol Heart Circ Physiol* 288(3):H1022-7.

83. **Shroff SG, Berger DS, Korcarz C, Lang RM, Marcus RH, and Miller DE** 1995 Physiological relevance of T-tube model parameters with emphasis on arterial compliances. *Am J Physiol* 269(1 Pt 2):H365-74.

84. **Cox RH** 1978 Passive mechanics and connective tissue composition of canine arteries. *Am J Physiol* 234(5):H533-41.

85. **Armentano RL, Levenson J, Barra JG, Fischer EI, Breitbart GJ, Pichel RH, and Simon A** 1991 Assessment of elastin and collagen contribution to aortic elasticity in conscious dogs. *Am J Physiol* 260(6 Pt 2):H1870-7.

86. **Dobrin PB and Canfield TR** 1984 Elastase, collagenase, and the biaxial elastic properties of dog carotid artery. *Am J Physiol* 247(1 Pt 2):H124-31.

87. **Tan YY, Wade JD, Tregear GW, and Summers RJ** 1998 Comparison of relaxin receptors in rat isolated atria and uterus by use of synthetic and native relaxin analogues. *Br J Pharmacol* 123(4):762-70.

88. **Gandley RE, Griggs KC, Conrad KP, and McLaughlin MK** 1997 Intrinsic tone and passive mechanics of isolated renal arteries from virgin and late-pregnant rats. *Am J Physiol* 273(1 Pt 2):R22-7.

89. **Debrah DO, Conrad KP, Jeyabalan A, Danielson LA, and Shroff SG** 2005 Relaxin increases cardiac output and reduces systemic arterial load in hypertensive rats. *Hypertension* 46(4):745-50.

90. **Hibbard JU, Korcarz CE, Nendaz GG, Lindheimer MD, Lang RM, and Shroff SG** 2005 The arterial system in pre-eclampsia and chronic hypertension with superimposed pre-eclampsia. *Bjog* 112(7):897-903.

91. **Fisher C, MacLean M, Morecroft I, Seed A, Johnston F, Hillier C, and McMurray J** 2002 Is the pregnancy hormone relaxin also a vasodilator peptide secreted by the heart? *Circulation* 106(3):292-5.

92. **Parry LJ, Wilson BC, Poterski RS, and Summerlee AJ** 1998 The cardiovascular effects of porcine relaxin in Brattleboro rats. *Endocrine* 8(3):317-22.

93. **Novak J, Reckelhoff J, Bumgarner L, Cockrell K, Kassab S, and Granger JP** 1997 Reduced sensitivity of the renal circulation to angiotensin II in pregnant rats. *Hypertension* 30(3 Pt 2):580-4.

94. **Duke LM, Evans RG, and Widdop RE** 2005 AT2 receptors contribute to acute blood pressure-lowering and vasodilator effects of AT1 receptor antagonism in conscious normotensive but not hypertensive rats. *Am J Physiol Heart Circ Physiol* 288(5):H2289-97.

95. **Barber MN, Sampey DB, and Widdop RE** 1999 AT(2) receptor stimulation enhances antihypertensive effect of AT(1) receptor antagonist in hypertensive rats. *Hypertension* 34(5):1112-6.

96. **Coulson CC, Thorp JM, Jr., Mayer DC, and Cefalo RC** 1996 Central hemodynamic effects of recombinant human relaxin in the isolated, perfused rat heart model. *Obstet Gynecol* 87(4):610-2.

97. **Kompa AR, Samuel CS, and Summers RJ** 2002 Inotropic responses to human gene 2 (B29) relaxin in a rat model of myocardial infarction (MI): effect of pertussis toxin. *Br J Pharmacol* 137(5):710-8.

98. **Masini E, Bani D, Bello MG, Bigazzi M, Mannaioni PF, and Sacchi TB** 1997 Relaxin counteracts myocardial damage induced by ischemia-reperfusion in isolated guinea pig hearts: evidence for an involvement of nitric oxide. *Endocrinology* 138(11):4713-20.

99. **Edouard DA, Pannier BM, London GM, Cuche JL, and Safar ME** 1998 Venous and arterial behavior during normal pregnancy. *Am J Physiol* 274(5 Pt 2):H1605-12.

100. **Cole DJ, Marcantonio S, and Drummond JC** 1990 Anesthetic requirement of isoflurane is reduced in spontaneously hypertensive and Wistar-Kyoto rats. *Lab Anim Sci* 40(5):506-9.

101. **Seyde WC, Durieux ME, and Longnecker DE** 1987 The hemodynamic response to isoflurane is altered in genetically hypertensive (SHR), as compared with normotensive (WKY), rats. *Anesthesiology* 66(6):798-804.

102. CBI. Center for Biologic Imaging; Protocols. [cited May 2008]; http://www.cbi.pitt.edu/protocols/index.html].